The University Of Sheffield.

Investigating the roles of blood flow and cell signalling pathways during zebrafish vascular remodelling

Yan Chen

A thesis submitted in partial fulfilment of the requirements for the degree of Doctor of Philosophy

The University of Sheffield

Faculty of Medicine, Dentistry & Health

Department of Infection, Immunity & Cardiovascular Disease

September 2020

Table of Contents

List of Tables

List of Figures

List of abbreviations

AA	Aortic Arch
AJ	Adherens Junction
aPKC	Atypical Protein Kinase C
ANG	Angiopoietin
AVM	Arteriovenous Malformation
BMP	Bone Morphogenic Protein
CVP	Caudal Vein Plexus
DA	Dorsal Aorta
DLAV	Dorsal Longitudinal Anastomotic Vessel
EC	Endothelial Cell
ECM	Extracellular Matrix
ENG	Endoglin
ERK	Extracellular signal-Regulated Kinase
GPCR	G Protein-Coupled Receptor
HHT	Hereditary Haemorrhagic Telangiectasia
HPV	Hepatic Vessel
HUVEC	Human Umbilical Vein Endothelial Cell
ICV	Inter-Connecting Vessel
ISV	Intersegmental Vessel
JBL	Junction-Based Lamellipodia

JNK	c-Jun-N-terminal Kinase
MAPK	Mitogen-Activated Protein Kinase
MMP	Matrix Metalloproteinase
MTOC	Microtubule-Organisation Centre
NO	Nitric Oxide
NRARP	Notch-Regulated Ankyrin Repeat Protein
PAH	Pulmonary Arterial Hypertension
PCV	Posterior Cardinal Vein
PDGF	Platelet-Derived Growth Factor
PL	Parachordal Line
PLC-γ	Phospholipase C-gamma
PV	Pancreatic Vessel
RTK	Receptor Tyrosine Kinase
SA	Segmental Artery
Shh	Sonic hedgehog
SIA	Supra-Intestinal Artery
SIV	Sub-Intestinal Vein
SIVP	Sub-Intestinal Vein Plexus
SV	Segmental Vein
TGF-β	transforming growth factor-β
VEGF	Vascular Endothelial Growth Factor
WNT	

List of publications

Abstracts generated from the thesis and presented in conferences:

1. 14th International Zebrafish Conference, China, June 2019 and in the Northern Vascular Biology Forum, Sheffield, December 2019 (awarded best PhD poster presentation).

Endothelial cells (ECs) detect physical cues exerted by blood flow and convert these into molecular signals which induce cellular adaptations. Dysregulation of EC responses to flow induced haemodynamic forces are thought to underlie many cardiovascular diseases including atherosclerosis. However, the mechanisms by which ECs sense mechanical forces to generate a complex vascular network is incompletely understood. We hypothesise that blood flow is essential for appropriate vascular patterning by refining local molecular signals and that by exploiting a vascular plexus, the sub intestinal vein plexus (SIVP) which undergoes flow dependent remodelling in zebrafish, and shows genetic conservation with mammals, we will identify these signals and mechanisms.

In the absence of blood flow, the zebrafish SIV exhibits increased leading SIVP sprouts which fail to regress. ECs migrate ventrally during SIVP formation, and blood flow instructs their migration towards ventral and lateral direction, while the majority of ECs only migrate ventrally in the absence of flow. Both VEGF and BMP receptors are expressed in the SIVP, however, VEGF signaling is required for leading sprout regression under low flow but not with normal flow. Interestingly, inhibition of BMP signaling results in increased leading sprout number and enlarged SIV caliber, suggesting that BMP signaling is required for cell migration and cell shape change during vascular remodelling. Collectively this suggests blood flow mediated haemodynamic force is required for developmental vascular remodelling potentially via induction of VEGF- and Bmp- mediated vessel regression.

2. Annual Conference of British Society for Developmental Biology (BSDB), Warwick, April 2018.

Endothelial cells (ECs) detect physical cues exerted by blood flow and convert these into molecular signals which induce cellular adaptations. Dysregulation

of EC responses to flow induced haemodynamic forces are thought to underlie many cardiovascular diseases including atherosclerosis. However, the mechanisms by which ECs sense mechanical forces to generate a complex vascular network is incompletely understood. We hypothesise that blood flow is essential for appropriate vascular patterning by refining local molecular signals and that by exploiting a vascular plexus, the sub intestinal vein (SIV), which undergoes flow dependent remodelling in zebrafish, and shows genetic conservation with mammals, we will identify these signals and mechanisms.

In the absence of blood flow, the zebrafish SIV exhibits increased leading SIV sprouts which fail to regress and in which total number of ECs was increased. Blood flow provides directionality during collective EC migration in the forming SIV, and lack of blood flow leads to more cells migrating ventrally and fewer cells migrating laterally. Elevated VEGF signalling overrides flow dependent SIV regression, whereas Notch signalling is dispensable for SIV remodeling. Interestingly, expression of VEGF receptors and Bmp receptors are increased in the absence of blood flow Collectively, this suggests blood flow mediated haemodynamic force is required for developmental vascular remodelling potentially via induction of VEGF and Bmp mediated vessel regression.

3. LifeCourse Conference, Sheffield, April 2018 (awarded best PhD poster presentation).

Endothelial cells (ECs) are able to detect physical cues exerted by the blood flow and convert them into molecular signals which induce cellular adaptations. Dysregulation of EC responses to flow-induced haemodynamic forces are thought to underlie many cardiovascular diseases. During development, embryos without blood flow only form a primitive vascular network without hierarchical branching of arteries, veins and capillaries. While the effects of haemodynamic force on ECs have been extensively studied in vitro and in mature vascular systems, the fundamental mechanisms by which ECs sense the physical forces of blood flow to integrate downstream signalling pathways and co-ordinate embryonic vascular remodelling in vivo are incompletely understood.

We have employed the zebrafish sub-intestinal vein (SIV) as a model to investigate haemodynamic force-dependent vascular remodelling. In the absence of blood flow, embryos exhibit increased EC number and frequency of leading SIV sprouts which fail to regress. We have found that blood flow acts as a permanent switch over a long developmental time window to induce vessel regression within the SIV. Interestingly, embryos with reduced shear stress exhibit normal SIV development and remodelling. Elevated VEGF signalling

overrides flow dependent vessel regression in the SIV and blood flow suppresses expression of a VEGF decoy receptor sflt1. Notch signalling is dispensable for SIV remodelling. Collectively, our data suggest that blood flow-mediated haemodynamic force is required to initiate developmental vascular remodelling and this may occur via induction of VEGF-mediated vessel regression within the SIV.

Papers published with me as a co-author during my course:

1. Cher Farrugia, Graham P Stafford, Jan Potempa, Robert N Wilkinson,**Yan Chen**, Craig Murdoch, Magdalena Widziolek. (2020). Mechanisms of vascular damage by systemic dissemination of the oral pathogen Porphyromonas gingivalis. *The FEBS Journal. 2020, 1-17.*

2. Aaron M. Savage, Sathishkumar Kurusamy, **Yan Chen**, Zhen Jiang, Karishma Chhabria, Ryan B. MacDonald, Hyejeong R. Kim, Heather L. Wilson, Fredericus J. M. van Eeden, Angel L. Armesilla, Timothy J. A. Chico & Robert N. Wilkinson. (2019). *tmem3* is essential for VEGF-mediated endothelial calcium oscillations and angiogenesis. *Nature Communications* 2019,10, 732

3. Moore C, Richens JL, Hough Y,Ucanok D, Malla S, Sang F, **Chen Y**, Elworthy S, Wilkinson RN, Gering M.(2018). Gfi1aa and Gfi1b set the pace for primitive erythroblast differentiation from hemangioblasts in the zebrafish embryo. *Blood Advances*. 2018;2(20):2589-2606.

Abstract

During vertebrate embryonic development, vascular networks adapt to the increasing demand of growing tissues by sprouting angiogenesis and vascular remodelling. These processes involve connection of blind-ended angiogenic sprouts to form a tubular vessel and pruning of redundant blood vessels, which leads to a more haemodynamically efficient vascular network. While much is known about angiogenic sprouting, little is known about vessel remodelling at the cellular and molecular levels. Most blood vessels develop from existing vessels which are patent with stable blood flow, and dysregulation of endothelial cell (EC) responses to flow induced haemodynamic forces are thought to underlie many cardiovascular diseases including atherosclerosis. Therefore, my thesis focuses on the sub-intestinal vein plexus (SIVP) which is a vascular plexus that undergoes blood-flow dependent remodelling in the zebrafish embryo.

In this thesis, I investigate the role of blood flow on vascular remodelling by directly comparing the morphological differences and EC behaviour during SIVP remodelling in the presence and absence of flow. I demonstrate that the absence of flow leads to general morphological alterations in the SIVP, including increased number of leading sprouts as well as increased EC number within the sprouts. Using time-lapse imaging I found that the majority of the leading sprouts in the SIVP undergo sprout regression in the presence of flow rather than anastomosis during remodelling. Analysis of individual EC migratory

trajectories reveals that accumulation of ECs in the leading sprouts in the absence of flow is due to disrupted cell rearrangement, rather than cell proliferation. Sprout regression is regulated by coordinated rearrangement of ECs within the vessel lumen and the non-perfused leading sprouts, mediated by directed EC polarisation and migration against blood flow. The lack of flow disrupts these directed cellular behaviours and leads to defects of vascular remodelling. Taken together, these studies provide a clear view of cellular behaviour that underlies vessel remodelling and the role of blood flow acted on individual ECs during development.

I have also analysed the functions of vascular endothelial growth factor (VEGF) and bone morphogenetic protein (BMP) signalling and their potential interactions with blood flow during SIVP remodelling. I found that elevated VEGF signalling overrides flow-dependent sprout regression, whereas inhibition of BMP signalling results in ectopic leading sprouts in the presence or absence of flow. Inhibition of *vegfr3*/*flt4* under low flow conditions also increases sprout number but reduces vessel diameter. These studies indicate vessel regression is controlled by a complex regulatory network which involves molecular signals and physical cues exerted by blood flow during vascular remodelling.

Chapter 1 Introduction

1.1 The clinical importance of angiogenic remodelling

The cardiovascular system is the first organ to form in vertebrate embryos and is responsible for the transport of nutrient, oxygen and waste throughout the embryo. The cardiovascular system is comprised of blood vessels of different sizes and shapes which form a highly branched circulatory network to meet the demands of every tissue of the body. The circulation initiates in the beating heart which pumps blood to large arteries, through arterioles and finally reaches the capillary beds where metabolic exchange takes place. Blood flow returns from capillaries through venules and veins into the heart. The oxygen-depleted blood then goes from the heart to the lung for re-oxygenation of the blood and returns back to the heart to start next cycle of circulation (Herbert and Stainier, 2011).

The inner most layer of all blood vessels is comprised of endothelial cells (ECs) which are in direct contact with blood flow and form the barrier to fluid filtration and gas exchange. During embryonic development, the first blood vessels arise via vasculogenesis, the *de novo* formation of blood vessels from endothelial precursors termed angioblasts. Following this, ECs migrate to generate new blood vessels from existing ones, which gives rise to a branched vascular network that undergoes pruning and regression to form a more hierarchical structure. This process is termed angiogenesis (Adams and Alitalo, 2007; Herbert and Stainier, 2011).

Angiogenesis occurs in developing embryos as well as in adults when the ECs are activated in the context of wound healing or diseased regions.

Whilst much has been learned about early steps in angiogenesis such as sprouting and lumen formation, we still know relatively little about how a primary vasculature which may have excess vessels remodels into a haemodynamically efficient network. The issue of optimal vessel density via remodelling is of particular importance as it reduces the resistance for blood delivery and increases the efficiency of metabolic exchange (Garcia and Larina, 2014; Jones, 2011; Lucitti *et al.*, 2007). Understanding the mechanisms underlying vascular remodelling also helps to develop better therapies in the context of tumour angiogenesis. The tumour vasculature is disorganised and immature with limited pruning and regression. Although the original idea of starving the tumour by solely targeting pro-angiogenic signalling (mainly vascular endothelial growth factor, VEGF) has not been successful in clinical trials of certain tumours, the combination of anti-angiogenesis treatment with systemic chemotherapy has proven to be an effective strategy. The reason behind the phenomenon is proposed that inhibition of VEGF signalling may prune away the most immature and poorly perfused vessels and bring the tumour vasculature to a normally perfused network that allows the delivery of cytotoxic agents to the tumour (Huang *et al.*, 2013). Further improvement of the therapeutic efficacy will require a better understanding of vascular remodelling.

A key issue common to both embryonic and adult vessel remodelling is how ECs sense flow and determine the fate of a vessel to remodel, with its need for a continuing requirement of vessel integrity and permeability. Dysfunction of EC sensing and adaptation leads to serious cardiovascular diseases such as atherosclerosis (Baeyens *et al.*, 2016a; Chatzizisis *et al.*, 2007; Souilhol *et al.*, 2020; Yurdagul *et al.*, 2016).

Atherosclerosis is a disease characterised by build-up of lipids and chronic inflammation of the cells along the inner wall of arteries, leading to pathologic remodelling of the vessel and formation of plaques. Although atherosclerosis is highly associated with systemic risk factors (e.g. hypercholesterolemia and old age), studies have established that plaque development also involves local cues such as blood flow. Atherosclerotic plaques predominantly occur at sites with low or disturbed flow which alters EC behaviour by inducing excessive EC proliferation, apoptosis, and inflammation; while high pulsatile laminar flow induces vessel stabilisation and dilation (Warboys *et al.*, 2011; Yurdagul *et al.*, 2016). Recent studies using unbiased genome-wide approaches to compare expression profiles at regions of low or high blood flow has revealed multiple signalling and transcriptional programmes that contribute to endothelial pathophysiology and atherosclerosis. Interestingly, many of these signalling pathways have been shown to regulate angiogenesis during embryonic development, implying the conserved roles of the genes in both developmental and

pathological settings (reviewed in Souilhol *et al.,* 2020). This also highlights the beneficial impacts of developmental studies on identification of new therapeutic targets for treatment of cardiovascular diseases.

Although the outcomes of angiogenic sprouting (generation of more vessels) and remodelling (reduction of vascular complexity) differ, they share common cellular behaviours such as cell proliferation and migration. Therefore, to place vascular remodelling in context, it helps to outline the current understanding of vessel formation and the model systems used to study angiogenesis.

1.2 Model systems employed to study angiogenesis

A variety of model systems have been established to study angiogenesis and the effects of molecules on the process under physiological or pathological conditions. Generally, these systems can be classified as *in vitro* or *in vivo* assays. Depending on their accessibility and availability, researchers favour different models for specific research questions. *In vitro* studies often provide efficient and insightful results with relatively low cost and easy access of cell culture. However, the trade-off is that the experimental conditions vary between studies, leading to discrepancies. In addition, *in vitro* assays are not currently able to accurately mimic the microenvironment that ECs experience in a living organism. By contrast, *in vivo* models provide more accurate simulation of the

living microenvironment and therefore potentially more reliable assessments of the angiogenic process. Importantly, despite their anatomical differences, vertebrates exhibit many aspects of common genetic control of angiogenesis during development, which allows comparison and potential application to humans. Some drawbacks associated with *in vivo* approaches are the relatively high cost and maintenance, the often-time-consuming nature of the experimental approaches and challenges in imaging at the cellular level. But still, *in vivo* assays are indispensable and should be considered as final confirmation of *in vitro* results. Evaluation of the angiogenesis assays has been recently reviewed in Simons *et al.* (2015) and Stryker *et al.* (2019), and therefore this section provides an overview of the animal models with a focus on zebrafish which is the model used in this thesis.

Quail and Chick embryos

The chick embryo chorioallantoic membrane (CAM) is an extraembryonic membrane that is present in the fertilized eggs of all avian species. It contains a dense capillary network which is favoured for studies of morphogenetic aspect of angiogenesis and assessments of pro- and anti-angiogenic molecules (Ribatti, 2010). Recent improvement of gene editing techniques has advanced the establishment of transgenic lines to study the vasculogenesis of aortae and sprouting behaviour of ECs in the avian embryos (Sato and Lansford, 2013; Sid and Schusser, 2018), although more specific reporters are needed for further insights in angiogenesis at cellular level.

Mouse models

A variety of transgenic mice containing various floxed genes and tissue-specific Cre drivers, as well as industrial-available specific antibodies, enable researchers to customise their own genetic toolkits. Favoured mouse models for studying developmental angiogenesis include retina, cornea, and xenografts. The murine ocular system allows easy observation of angiogenic sprouting, remodelling and maturation of the vessels. Manipulation of the genome has uncovered many signalling pathways that are important for vessel formation (Liu *et al.*, 2017). The eye vasculatures are obtained from mouse with desired background and the tissues are often fixed for later analysis. Therefore, this system is *ex vivo* with a lack of flow, although progress has been made using *in silico* simulation of flow (Franco *et al.*, 2016, 2015). Other vascular beds such as the extraembryonic yolk sac (Udan *et al.*, 2013) and cranial vessels (Burrell et al 2013) have also been utilised.

Zebrafish

The zebrafish has proved to be an excellent model for studying angiogenesis *in vivo* for a variety of reasons. First of all, zebrafish produce hundreds of embryos per week *ex utero*, making this an effective model for large-scale screening for angiogenic drugs. Zebrafish embryos are small, which permits survival for seven days without blood circulation due to passive diffusion of oxygen (Stainier *et al.*, 1995), they develop rapidly (heartbeat begins at 22 hours post fertilisation) and are optically translucent. This allows

experimental and genetic manipulation of the cardiovascular system and live observation of development over time using a microscope. In addition, recent genetic engineering techniques enables generation of tissue- or even organelle-specific transgenic lines (Kwon *et al.*, 2016; Lawson and Weinstein, 2002a). These characteristics, combined with the use of high-resolution microscopy (e.g. confocal or light-sheet microscopy), have helped us to scrutinise the development of vessels at cellular level (Figure 1.1A).

Many vascular beds have been utilised to study angiogenesis in zebrafish including the intersegmental vessels (ISVs) (reviewed in Siekmann *et al.*, 2013), the caudal vein plexus (CVP) (Karthik *et al.*, 2018; Wakayama *et al.*, 2015; Wiley *et al.*, 2011), the cranial vessels (Chen *et al.*, 2012; Kimura *et al.*, 2015; Lenard *et al.*, 2013), and more recently the sub-intestinal vein plexus (SIVP) (Goi and Childs, 2016; Hen *et al.*, 2015; Koenig *et al.*, 2016; Lenard *et al.*, 2015). These studies have largely advanced our understanding of endothelial cell migration, cell polarity, and cellular interaction during angiogenesis.

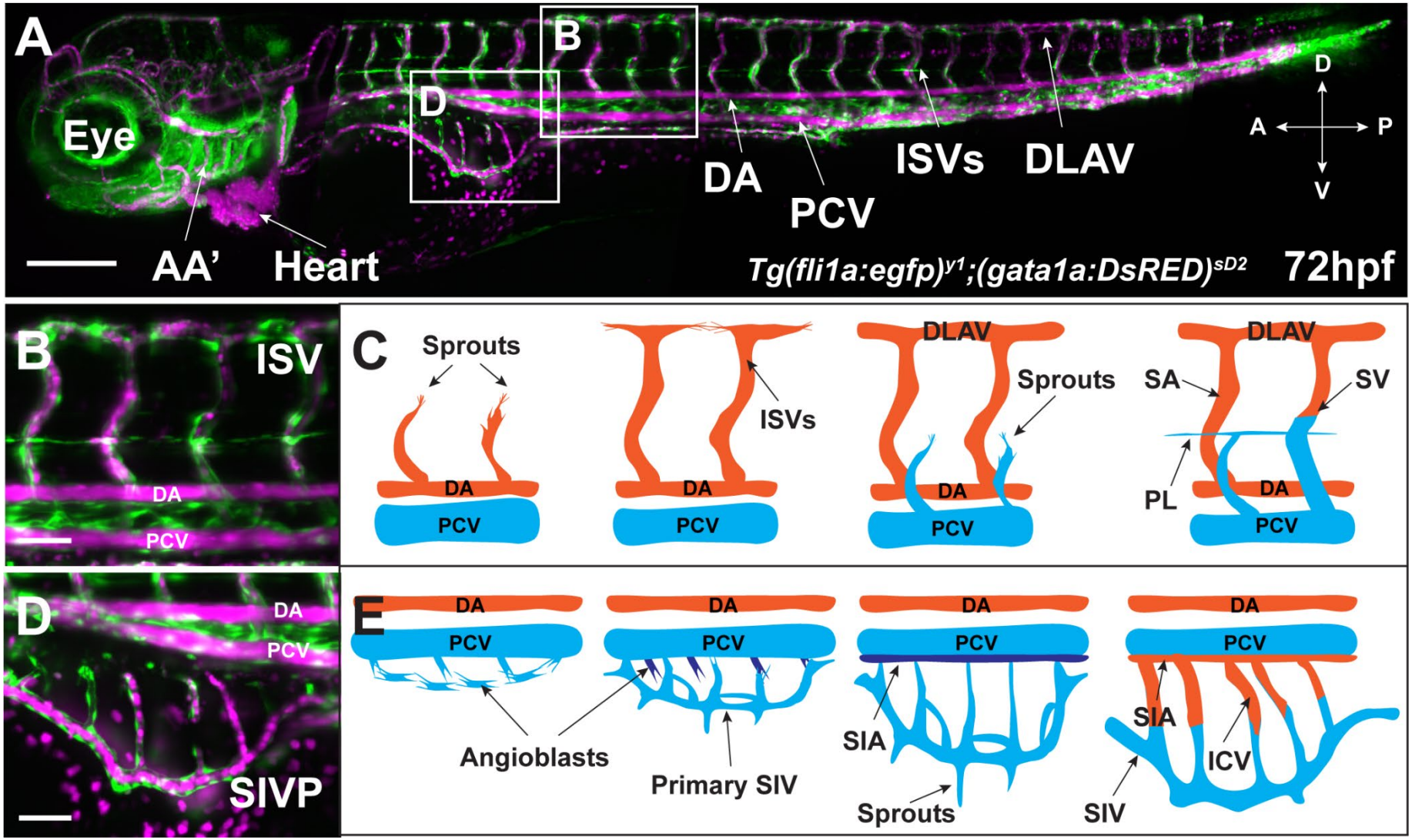
A
Eye
AA'
Heart
B
D
DA
PCV
ISVs
DLAV
D
A
P
V
Tg(fli1a:egfp)y1;(gata1a:DsRED)sD2
72hpf
B
ISV
DA
PCV
C
Sprouts
ISVs
DLAV
Sprouts
SA
SV
PL
D
DA
PCV
SIVP
E
Angioblasts
Primary SIV
SIA
Sprouts
SIA
ICV
SIV

Figure 1.1 The development of ISV and SIV in the zebrafish

(**A**) Lateral view of a 72hpf wildtype zebrafish from *Tg(fli1a:egfp)^{y1};(gata1a:DsRED)^{sD2}*, showing endothelial cells in GFP (green) and erythrocytes in DsRED (false-coloured in magenta). Scale bar: 200μm. (**B**) Enlarged area from A to show the ISVs. Scale bar: 50μm. (**C**) Schematic illustration of the suggested process of ISV formation at 1-2dpf. Sprouts derived from the DA migrate dorsally to form the ISVs and DLAV. Sprouts from the PCV fuse to the existing ISVs to remodel them into SVs or lymphatics. (**D**) Enlarged area from A to show the SIVP. Scale bar: 50μm. (**E**) Schematic illustration of the suggested process of SIVP formation at 1-3dpf. Sprouts from the PCV migrate ventrally to form the primary SIV. ECs of the SIV also migrate dorsally to form the ICVs (branches) and connect with the SIA. The anterior part of the SIV is connected and contributed to the liver (left side) or the pancreatic (right side) vasculature (see texts). AA', aortic arch; DA, dorsal aorta; PCV, posterior cardinal vein; ISV, intersegmental vessel; DLAV, dorsal longitudinal anastomosing vessel; SIVP, sub-intestinal vein plexus; SA, segmental artery; SV, segmental vein; PL, parachordal lines; SIA, supra-intestinal artery; ICV, inter-connecting vessel; SIV, sub-intestinal vein. Orange colour denotes the arterial blood and blue the venous blood. Orientation: D, dorsal; V, ventral; A, anterior; P, posterior.

1.2.1.2 The development of zebrafish ISVs

Many of the studies on vascular development in zebrafish have focused on the formation of ISVs, due to their simple yet stereotypical patterning (Figure 1.1B &C). The two main axial vessels, the dorsal aorta (DA) and posterior cardinal vein (PCV), develop via vasculogenesis which will be described in more detail in section 1.3.1.1. The ISVs then sprout bilaterally from the dorsal wall of the DA, anterior to each somite boundary from approximately 22 hours post fertilisation (hpf) (Isogai *et al.*, 2001). These ISVs have an arterial origin, therefore are also termed segmental arteries (SAs). The parallel SA branches migrate dorsally and anastomose at the top of the neural tube into the dorsal longitudinal anastomotic vessel (DLAV). At around 30-32hpf after the onset of flow within the DA and PCV, a second wave of angiogenic sprouting starts from the PCV. These sprouts either connect to existing SAs, remodelling them into venous ISVs (termed segmental veins, SVs) or sprout to the level of the horizontal myoseptum to contribute to lymphatic structures, which further migrate along the SAs and the DLAV to form a functional trunk lymphatic network (Geudens *et al.*, 2019; Isogai *et al.*, 2003; Yaniv *et al.*, 2006). Although the order of SAs and SVs along the trunk is not fixed, the ISVs show a balanced number of arteries and veins at approximate 1:1 ratio (Bussmann *et al.*, 2010; Geudens *et al.*, 2019). The stereotypical sprouting and regular patterning of the ISVs are very attractive for angiogenesis studies, and many cellular and

molecular mechanisms underlying the process have been discovered, which will be introduced in more detail in following sections.

1.2.1.3 The zebrafish SIVP as an emerging model to study vascular development

Despite the morphological advantages of ISVs, some of the characteristics of the vessels are unique, making it difficult to extrapolate the findings to other vascular beds. Firstly, when the tip of the ISV sprout reaches the roof of the trunk, it migrates anteriorly and/or posteriorly to fuse with other cells, giving it a 'T-shape' (Figure 1.1C), which is not observed in other vessels in the zebrafish (Betz *et al.*, 2016) or in the mouse retina (Gerhardt *et al.*, 2003). Secondly, the ISVs are constrained by the physical barrier of the somites, and rarely generate or prune additional branches after secondary angiogenesis. This hyper-stereotypical pattern is less comparable to other less tightly constrained plexuses, such as the mouse retina or yolk sac vessels. Thirdly, distinct signalling pathways are employed in angiogenic sprouting from the DA and PCV; while the former is dependent on the VEGFs (Covassin *et al.*, 2009), the latter is regulated by bone morphogenetic protein (BMP) to form the CVP in the tail region (Wiley *et al.*, 2011), indicating ECs use distinct molecular mechanisms in various vascular beds. Therefore, it is necessary to explore different vessel types to fully understand the mechanistic regulation of angiogenesis.

The origin and development of the SIVP

The zebrafish sub-intestinal vein plexus has recently emerged as an alternative model to study not only the cellular mechanism of the vascular remodelling in response to flow (Lenard *et al.*, 2015) but also the molecular regulations of an organ-specific plexus from a venous origin (Goi and Childs, 2016; Hen *et al.*, 2015; Koenig *et al.*, 2016; Nicenboim *et al.*, 2015). The SIVP is a vascular network that originally absorbs nutrients from the yolk, distributes these via blood to the developing embryo, and later vascularises the digestive system in the larva and adult fish. The murine equivalent of the embryonic SIVP are the vitelline veins which connect the embryo with the extraembryonic circulation in the yolk sac (Goi and Childs, 2016). The SIVP in the developing embryo comprises the supra-intestinal artery (SIA), left- and right- sub-intestinal vein (SIV) located bilaterally on the yolk-sac, and inter-connecting vessels (ICVs) that branch between the SIA and SIV (see Figure 1.1D &E). Little was known about the early development of the SIVP until the first vascular anatomical atlas was published using confocal angiography (Isogai *et al.*, 2001). The zebrafish atlas suggests that the SIVP begins to form at 2.5 days post fertilisation (dpf) and achieves its basket-like shape at approximately 3dpf. The SIA was believed to originate from the anterior mesenteric artery (AMA) as an extension of the dorsal aorta (Isogai *et al.*, 2001). However, with the help of high-resolution real-time imaging techniques, the SIVP was more recently confirmed to sprout from the floor of PCV (Goi and Childs, 2016; Hen *et al.*,

2015; Koenig *et al.*, 2016; Nicenboim *et al.*, 2015).

Angioblasts from the PCV sprout at approximately 30hpf and coalesce to form a primitive SIV (Hen *et al.*, 2015). Although the ECs sprout from an existing vessel, the PCV, they do not retain connections to the PCV as in standard sprouting angiogenesis; rather, they follow a path that is similar to vasculogenesis in which angioblasts form a *de novo* vessel (Koenig *et al.*, 2016). Therefore, the sprouting mechanism of the SIVP is probably a combination of vasculogenesis and angiogenesis. The primitive SIVP subsequently expands bilaterally over the surface of the yolk ball. Meanwhile, ECs from the primary SIV migrate dorsally to form branches and the SIA. How the SIA is formed is currently under debate due to imaging difficulties since it is located deep in the tissue between the embryo trunk and the yolk sac. It has been suggested that the SIA is populated by ECs which migrate dorsally from the SIV at approximately 40hpf (Hen *et al.*, 2015) or by a secondary wave of sprouting from the PCV at later stages around 42-56hpf (Koenig *et al.*, 2016). Nonetheless, the whole plexus arises from a venous origin and the SIA gradually obtains its arterial identity as indicated by expression of a Notch reporter by 72hpf (Koenig *et al.*, 2016). The anterior part of the PCV, along with the anterior part of the SIV, give rise to hepatic vessels (HPV, left side of the embryo) and pancreatic vessels (PV, right side) (Hen *et al.*, 2015).

Studies using the SIVP as a model

The SIVP has been a popular platform for pro- or anti-angiogenesis drug

screening (Chan *et al.*, 2012; Kuo *et al.*, 2011; Nicoli *et al.*, 2009; Raghunath *et al.*, 2009; Zanin *et al.*, 2019; Zhang, J. *et al.*, 2018) and tumour xenograft (Nicoli *et al.*, 2007; Nicoli and Presta, 2007). However, recent findings on the molecular basis of the SIVP formation have revealed that the plexus is more sensitive to certain signalling pathways such as VEGF and BMP, but does not respond to others including Sonic hedgehog (Shh) and platelet-derived growth factor (PDGF) signalling (Goi and Childs, 2016). Therefore, care must be taken when interpreting the studies using the SIVP as a model for drug screening or tumour xenograft. Thus, it is essential to further investigate the molecular basis of the SIVP to facilitate establishment of better assays.

The SIVP is also an excellent model to study flow-dependent cellular behaviours during vessel remodelling. Several types of vessel remodelling have been reported to occur during SIVP remodelling, including cross-branch pruning (Lenard *et al.*, 2015), collateral fusion (Lenard *et al.*, 2015), and leading sprout retraction (Hen *et al.*, 2015). Researchers have discovered the cellular mechanism of cross-branch pruning (Lenard *et al.*, 2015) which will be described in more detail in section 1.3.1.4, while the mechanisms of collateral fusion and sprout retraction are still unknown.

The leading migratory endothelial sprouts of the SIVP (Figure 1.1), rather than consisting of a single tip cell as frequently seen in the ISVs, contain a pair of ECs which retract into the main plexus together during remodelling (Hen *et al.*, 2015). Current studies on angiogenesis focus mostly on the sprouts that

eventually connect with each other or with a patent vessel (see section 1.3.1.3), however, how the ‘loose-end’ sprouts are remodelled and whether blood flow contributes to the process remain poorly understood. We therefore seek to understand the cellular and molecular mechanisms underlying the leading sprout regression in the SIVP.

1.3 Morphogenetic and molecular control of blood vessel formation

1.3.1.1 Vasculogenesis

Blood vessel formation via vasculogenesis occurs both intra- and extra-embryonically in vertebrates. The sources of endothelial and haematopoietic precursors include the embryonic mesoderm, as well as extraembryonic yolk sac, allantois and placenta (Patel-Hett and D’Amore, 2011). Within the extraembryonic yolk sac, precursor cells from the mesoderm migrate and aggregate into clusters called blood islands, which the outer cells differentiate into ECs that line the vascular lumen and the inner cells differentiate into erythrocytes (Hartenstein, 2006). In addition, it has been suggested that both endothelial and haemopoietic progenitor cells arise from a common precursor called a haemangioblast (Lacaud and Kouskoff, 2017). Similarly, in the embryo proper, angioblasts from the posterior lateral mesoderm (PLM) migrate towards the midline and arrange into a cord-like structure by embryonic day (E) 7.0 in mice (Drake, 2003), by the 10-somite stage in zebrafish (Gering and Patient,

2005), and by 1-somite stage in avian (Flamme and Breier, 2002). The cords subsequently separate and lumenise to form the DA and the PCV (Patel-Hett and D'Amore, 2011).

How the angioblasts are specified from other mesodermal cells remains elusive. The *cloche* gene has been identified as a master regulator for EC and haematopoietic development (Stainier *et al.*, 1996). In zebrafish, *cloche* mutants display defective development of ECs and blood cells, while also exhibit increased cardiomyocyte numbers (Stainier *et al.*, 1996). Cloche was recently identified as *npas4l*, which is transiently expressed in endothelial and haematopoietic precursors, prior to the expression of early endothelial and haematopoietic lineage markers *etv2* and *scl/tal1*, respectively (Reischauer *et al.*, 2016). Whether the function of *npas4l* is conserved in other species needs further investigation. The migration of angioblasts towards the midline initiates with *gridlock/hey2* (Notch signalling) expressing arterial precursors (Quillien *et al.*, 2014; Zhong *et al.*, 2000), followed by venous precursors 3 hours later (Jin *et al.*, 2005; Kohli *et al.*, 2013). *etv2* has also been shown to regulate angioblast migration to the midline (Sumanas and Lin, 2006).

Additional cues for angioblast migration come from the somites. VEGF was long believed to have a primary role in both angioblasts and EC migration and proliferation (Herbert and Stainier, 2011). Shh signalling controls VEGFA expression, which acts as a chemoattractant to induce angioblast migration (Lawson *et al.*, 2002; Shalaby *et al.*, 1995). However, in zebrafish, *vegfaa*

mutants do not exhibit defective vasculogenesis, and reveals VEGFA signalling is probably associated to the proliferation rather than migration of angioblasts (Rossi *et al.*, 2016). Instead, *elabela*, which is expressed in notochord cells, is the midline attractant for the migration of angioblasts which express Apelin receptor (*aplnr*) (Helker *et al.*, 2015).

Following midline migration of angioblasts, these cells separate and form the DA and the PCV. In zebrafish, the specification of arterial-venous fates of the primary vascular chord has been suggested to depend on the interaction of VEGF and Notch signalling pathways. Shh derived from the notochord activates the *vegfa* expression in the somites. The Vegfa binds to Vegf receptor 2, Vegfr2 (Kdrl in zebrafish), and upregulates Notch and downstream EphrinB2a, resulting in arterial differentiation in a subset of angioblasts (Lawson *et al.*, 2002; Lawson and Weinstein, 2002b). Loss of Shh signalling abrogates arterial differentiation but can be rescued by addition of VEGF. However, interestingly, Shh signalling can bypass VEGF to induce arterial differentiation via calcitonin receptor-like A (*Calcrla*), indicating a complex interplay between VEGF and Shh signalling during DA formation (Wilkinson *et al.*, 2012). The expression of *Efnb2a* is restricted to the dorsal-most angioblasts in the vascular cord while the ventral ones express *Ephb4a* which leads to ventral migration of the cells and formation of the PCV (Ellertsdóttir *et al.*, 2010; Herbert *et al.*, 2009).

1.3.1.2 **Angiogenesis**

Angiogenesis describes the generation of new blood vessels from pre-existing ones. The branching process is approached either by tip-cell driven formation of new vessels (i.e. sprouting angiogenesis), or by splitting an existing vessel into two (intussusceptive angiogenesis). Intussusception is mainly reported in mammals (Makanya *et al.*, 2009), although recently it has been demonstrated in the zebrafish CVP (Karthik *et al.*, 2018). Intussusception is characterised by the formation of intraluminal 'pillars' that diagonally split a vessel into two smaller vessels, and is driven by haemodynamic forces (Karthik *et al.*, 2018; Makanya *et al.*, 2009). The mechanism controlling intussusception during angiogenesis is poorly understood and less relevant to the aim of this thesis, therefore I refrain from introducing it in detail. The term 'angiogenesis' in the following sections refers to sprouting angiogenesis. The formation of blood vessels via angiogenesis is a multi-step event that includes 1) ECs sprout from the parent vessel and connection of the sprouts to form a tube; 2) formation of lumen in the newly formed tube; 3) optimisation of the vascular network via vascular remodelling; 4) recruitment of other cells types to form mature and stabilised vessels. Although the process has been divided into several steps for presentational clarity, in reality, the development of the vessel is a dynamic process and the steps may interlink. For example, lumen formation can occur during sprout elongation, or the regressing sprout breaks and re-connects to the vessel several times before detachment (Lenard *et al.*, 2015).

1.3.1.3 Sprouting

1.3.1.3.1 Angiogenic guidance and tip cell selection

Upon angiogenic stimulus, a subset of ECs is selected to sprout from the existing vessels, these cells are termed tip cells which guide the sprout. They are followed by a few cells termed stalk cells, which retain contact with the parent vessel and migrate collectively as the base of the sprout. The critical regulators of angiogenic sprouting is the VEGF signalling pathway and along with Notch signalling provides guidance for sprouts to migrate (reviewed in Siekmann *et al.*, 2013). ECs also respond to different angiogenic stimuli based on their vascular context. For example, in zebrafish, the formation of the CVP is BMP dependent (Wiley *et al.*, 2011). CXC-motif chemokine ligand 12 (Cxcl12) and its receptor Cxcr4, in addition to VEGF, are required for sprouting and anastomosis of hindbrain central arteries (Bussmann *et al.*, 2011; Fujita *et al.*, 2011). Additionally, blood flow has been found to control the location of sprouting and to direct elongation in quail embryos (Ghaffari *et al.*, 2015). Repulsive signals such as type 3 semaphorins (*sema3*) are expressed in zebrafish somites, which bind to their receptor PlexinD1 in the ECs, to repel sprouts from the somites boundaries and therefore guide proper patterning of the ISVs (Torres-Vázquez *et al.*, 2004).

How a tip cell is specified and guided to sprout has been extensively studied and many vascular regulators have been discovered (reviewed in

Herbert and Stainier, 2011). The balance between VEGF and Notch signalling is critical to control the behaviour of angiogenic sprouts. Diffusing VEGF-A binds to VEGFR2 located on the membrane of the ECs, leading to activation of the ECs and formation of filopodial extensions (Gerhardt *et al.*, 2003). To ensure that only a few ECs are selected, the first activated cells suppress their neighbours from sensing the VEGF-A signal, which is achieved by interacting with Notch signalling. Both tip cell and stalk cells express Delta-like-4 (Dll4) (ligand) and Notch (receptor) (Hasan *et al.*, 2017; Hellström *et al.*, 2007; Lobov *et al.*, 2007). In tip cells, VEGFR signalling is high, increasing Dll4 signalling which activates Notch on the adjacent membrane of the stalk cells. Notch downregulates VEGFR expression and thus desensitises stalk cells to VEGF-A (Hellström *et al.*, 2007; Lobov *et al.*, 2007). By contrast, lower levels of Dll4 signalling in stalk cells results in decreased Notch signalling in the tip cells and in turn increases VEGFR signalling, making the tip cell more angiogenic (Leslie *et al.*, 2007; Siekmann and Lawson, 2007).

ECs display dynamic calcium (Ca^{2+}) oscillations when budding from the DA in zebrafish and only the tip cells that sprout out maintain active Ca^{2+} signalling, revealing a dynamic tip cell selection event indicated by Ca^{2+} activities (Yokota *et al.*, 2015). Stalk cells were also found to show Ca^{2+} oscillations as they follow the tip cells during sprouting (Yokota *et al.*, 2015). These Ca^{2+} oscillations were found to be dependent on VEGF signalling (Yokota *et al.*, 2015) and downstream transmembrane protein 33 (Tmem33) to

regulate Notch signalling and Erk phosphorylation (Savage *et al.*, 2019). In addition to Ca^{2+} oscillations, the cell cycle may also be a useful indicator for tip cell selection. It has been shown that ECs that emerge from the DA are mainly in the S/G2/M phase and undergo cell division shortly after sprouting (Fukuhara *et al.*, 2014). Asymmetric division of ECs may enforce the tip/stalk cell hierarchy, with tip daughter cells having more cytoplasm and higher Erk activity than stalk daughter cell (Costa *et al.*, 2016).

Another important negative regulator of VEGF signalling during angiogenesis is the VEGF receptor 1 (VEGFR1, also called FLT1). Stalk cell secrete a soluble isoform of VEGFR1 (sVEGFR1), which binds to VEGFA with a higher affinity than VEGFR2 but possesses weak kinase activity (Park *et al.*, 1994). Therefore, sVEGFR1 secreted from the stalk cells functions as a sink for VEGFA. Deletions of VEGFR1 or sVEGFR1 in mouse and zebrafish show hyper-sprouting phenotypes (Chappell *et al.*, 2009; Krueger *et al.*, 2011). Furthermore, Notch induces the transcription of VEGFR1 to inhibit VEGF-A induced vascularisation (Funahashi *et al.*, 2010).

It is important to note that the first tip cell is not always the ‘winner’ since both tip and stalk cells compete for the tip position (Jakobsson *et al.*, 2010). Fluctuations in VEGFR2 signalling mediated by Notch and VEGFR1 leads to the ‘shuffling’ of the tip/stalk position (Funahashi *et al.*, 2010; Jakobsson *et al.*, 2010; Siekmann *et al.*, 2013). Moreover, the binary scenario of VEGF/Notch crosstalk implies the result of only one EC at the tip of the sprout, which is

usually the case in the ISVs. However, recent studies have reported two or more filopodia-extending ECs at the tip of the sprout and cannot be explained by transient tip/stalk ‘shuffling’. Multicellular sprouts have been observed in various sprout assays including human umbilical vein endothelial cells (HUVECs), mouse retina, and mouse embryonic back vessels (Pelton *et al.*, 2014), as well as in the zebrafish SIVP (Hen *et al.*, 2015), suggesting additional signalling pathways are involved in the tip cell selection.

In summary, upon angiogenic stimulation of VEGF and other stimuli, ECs initiate invasive sprouting behaviour. Negative regulators including Notch and VEGFR1 are required for proper sprouting and tip/stalk cell identity (Figure 1.2A).

1.3.1.3.2 **Sprout elongation**

After the initial formation of a sprout, the sprout elongates, which is supported by coordinated cell migration and proliferation of both tip and stalk cells (Figure 1.2B). The newly generated cells act as ‘building blocks’ for sustained elongation of the sprout (Gerhardt *et al.*, 2003). In addition to the frequency of cell proliferation, the coordinated alignment of the daughter cells is also important for sprout elongation since it determines whether an endothelial tube becomes wider or longer (Zeng *et al.*, 2007).

A well-orchestrated teamplay is required to keep the cells ‘in line’. The plane of EC division is mostly perpendicular to the long axis of the growing

sprout, elongating the length of the sprout. In addition, this process is influenced by VEGF signalling such that *Flt1*$^{-/-}$ mutant vessels exhibit randomised orientation of EC divisions (Zeng *et al.*, 2007). The migratory competition of tip/stalk cells during collective migration also contributes to the elongation of the sprouts (Arima *et al.*, 2011). It has been suggested that the heterogenous expression of VEGF and Notch in tip/stalk cells is important for directed sprouting (Ubezio *et al.*, 2016). By contrast, high levels of VEGF initiate the tip cell phenotype simultaneously, which leads to subsequent simultaneous activation of Notch inhibition, converting all tip cells into stalk cells (Ubezio *et al.*, 2016). The synchronisation of the Dll4-Notch signalling breaks the lateral inhibition and induce transition from sprouting to clustering of cells that increases sprout diameter (Ubezio *et al.*, 2016). Recent studies using zebrafish also found that cell elongation and rearrangement are important for sprout elongation. Cell elongation is dependent on shape changes of stalk cells, in which vascular endothelial cadherin (VE-cad, also known as Cdh5) transmits cytoskeletal forces via actin polymerisation at cell junctions and drives EC elongation (Sauteur *et al.*, 2014). Interestingly, ablation of tip cells does not impair migration and connection of the sprout to the DLAV, indicating that the tip cell does not apply a major pulling force on the sprout (Sauteur *et al.*, 2014). Instead, ECs use each other as migratory substrates to crawl over one another, resulting in cell migration and rearrangement and subsequent sprout/tube elongation (Paatero *et al.*, 2018). At cellular junctions, a transient junction-

based lamellipodia-like protrusion, namely JBL, is formed and serves as an anchor for intracellular actomyosin contractions (Paatero *et al.*, 2018).

1.3.1.3.3 **Anastomosis**

Anastomosis describes the connection of two blind-ended sprouts (head-to-head) or the fusion of one sprout to a pre-existing vessel (head-to-side) (reviewed in Betz *et al.*, 2016). The zebrafish ISVs are a typical type of 'head-to-head' anastomosis. When the ISVs reach the top of the trunk, each 'T-shaped' vessel contains two blind-ended sprouts which connect to its neighbouring sprouts and form the DLAV (see Figure 1.1C). The filopodia from each tip cell contact each other and form a stable connection which is called an apical membrane initiation site (AMIS) (Betz *et al.*, 2016; Bryant *et al.*, 2010). The stabilisation of the AMIS is dependent on deposition of adherens junction (AJ) proteins such as VE-cad at the site (Lenard *et al.*, 2013). The single connection point then opens up as a ring where the two tip cells overlap to increase their mutual surface (Blum *et al.*, 2008; Herwig *et al.*, 2011; Lenard *et al.*, 2013). The overlapping surface supports cell polarisation and formation of the apical membrane which is a hallmark of lumen formation. It has also been suggested that macrophages facilitate the connection of the two tip cells by acting as a 'bridge' for their filopodial contacts and stabilisation in mouse (Fantin *et al.*, 2010).

The elongated sprouts can contain partial lumens via different mechanisms

(see following section 1.1.1.1) and therefore anastomosis and lumen formation are tightly linked (Figure 1.2C). Following the formation of junctional rings, ECs extend the partial lumens to form a unicellular lumen, underlying a mechanism termed type I anastomosis, or migrate over each other to form a multicellular tube via type II anastomosis (reviewed in Betz *et al.*, 2016).

Type I anastomosis (see Figure 1.2D) occurs where a lumen is present in the sprout and involves rapid insertion of luminal space from the stalk cell to the connected tip cells. The formation of apical membrane in the tip cells quickly expands and connects at the mutual site, leading to a continuous intracellular lumen through these cells. This is a characteristic of type I anastomosis that the two interacting tip cells with transcellular lumens connect and lead to the formation of a unicellular tube. The unicellular tube eventually converts into a multicellular vessel via coordinated cell rearrangement involving complex junctional transformation and cell splitting, a unique mechanism of which EC cytoplasm splits to allow adjacent junctional rings to elongate and connect, resulting in formation of cell-cell junctions between three ECs (Lenard *et al.*, 2013).

By contrast, type II anastomosis (see Figure 1.2E) occurs in the absence of a lumen in the stalk cells. Similarly, after the formation of AMIS, the two tip cells crawl over each other and establish apical membrane at the mutual surface. Without the force of blood pressure, the ECs first rearrange to form a multicellular tube. During this rearrangement, isolated luminal pockets are

observed within the cells, which fuse to form larger luminal space that later enlarges to facilitate blood flow (Herwig *et al.*, 2011). Multicellular tubes allow maintenance of blood flow during cell division within the tube while EC division in unicellular tubes leads to collapse of lumen and temporal cessation of blood flow (Aydogan *et al.*, 2015). The formation of a mature multicellular tube relies on active EC rearrangement via elongation of initial junctional rings. The lamellipodia-like protrusions, JBL, are enriched in VE-cad and F-actin and provides adhesive support for ZO1-positive junctions to move forward and establish new junctions (Paatero *et al.*, 2018). In this way, the two connected ECs can crawl over each other by a ratchet-like mechanism (Paatero *et al.*, 2018).

'Head-to-side' anastomosis is observed in zebrafish cranial vessels (Kochhan *et al.*, 2013; Lenard *et al.*, 2013), although morphologically different from anastomosis of two tip cells, it shares some common features, such as the formation of AMIS and the rapid insertion of apical membrane (Betz *et al.*, 2016; Lenard *et al.*, 2013), and resembles type I anastomosis (Lenard *et al.*, 2013).

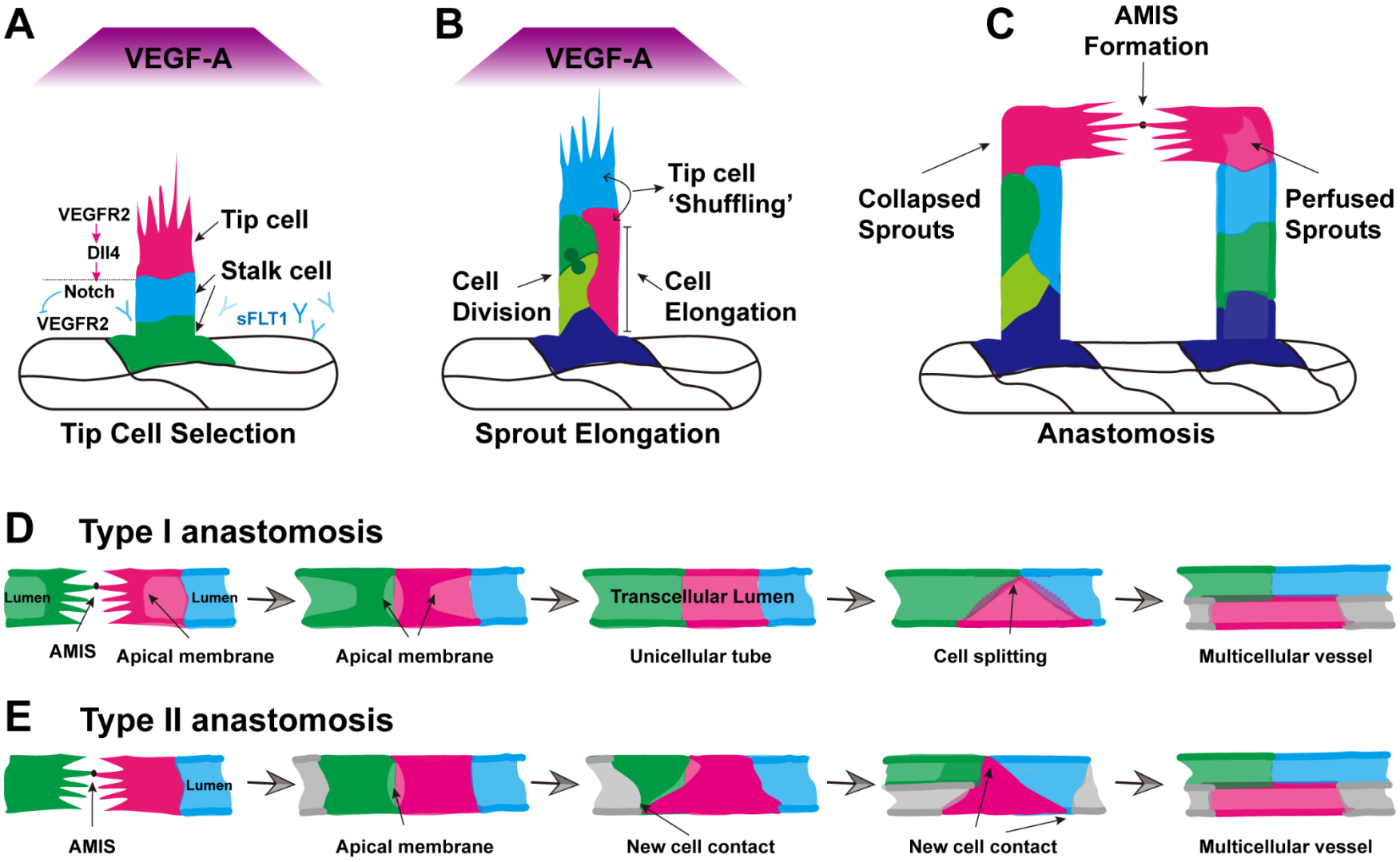
A
VEGF-A
VEGFR2
Dll4
Notch
VEGFR2
Tip cell
Stalk cell
sFLT1
Tip Cell Selection
B
VEGF-A
Tip cell
'Shuffling'
Cell
Division
Cell
Elongation
Sprout Elongation
C
AMIS
Formation
Collapsed
Sprouts
Perfused
Sprouts
Anastomosis
D
Type I anastomosis
Lumen
Lumen
AMIS
Apical membrane
Apical membrane
Transcellular Lumen
Unicellular tube
Cell splitting
Multicellular vessel
E
Type II anastomosis
Lumen
AMIS
Apical membrane
New cell contact
New cell contact
Multicellular vessel

Figure 1.2 The cycle of angiogenic sprouting

(**A**) Tip cell selection. Upon exposure to VEGF-A, ECs expressed higher VEGFR2 sprout from a multi-cellular vessel; Notch and VEGFR1 ensures a single EC is selected to guide the sprout (magenta, tip cell).

(**B**) Tip/stalk competition and sprout elongation. The tip cell that are rich in filopodia has strong motility and leads the way. Fluctuations of VEGFR2 expression in the ECs leads to competition of the tip cell position. The outgrowth of the sprout is supported by cell proliferation and cell elongation.

(**C**) Anastomosis of the two blind-ended sprouts. Filopodia in the two tip cells form a stable connection termed apical membrane initiation site (AMIS) which initiates the formation of the apical membrane at the mutual surface. The migrating sprouts can be collapsed or partially lumenised, which leads to two modes of anastomosis.

(**D**) Type I anastomosis. The process initiates in two partially lumenised sprouts. The AMIS expands into a junctional ring in which the membranes are apically polarised, creating a luminal pocket. The luminal pocket then fuses with the apical membrane that pushed by blood pressure from stalk cells to the base of the tip cells. The membrane fusion generates a unicellular tube with transcellular lumen. Subsequent conversion from a unicellular to a multicellular tube involves cell rearrangement and cell splitting.

(**E**) Type II anastomosis. The process occurs in non-lumenised sprouts. After formation of AMIS, the ECs elongate and rearrange, leading to new cell contacts. Further cell rearrangement leads to a multicellular vessel.

1.1.1.1 Lumen formation

The formation of a vascular lumen is critical for a vessel to be functional. During this process, ECs develop apical-basal polarity, and rapidly respond to physical forces exerted by blood flow without additional support from mural cells. Due to its nature and the absence of specific markers, the lumen is often recognised as a space delineated by a lack of signal surrounded by fluorescently labelled membrane or cytoplasm of ECs. This indirect analysis leads to debates on the contributions of small structures such as vacuoles or membrane blebbing. Several cellular mechanisms have been proposed on how a lumen is initiated and these are classified differently based on their cellular behaviour or cell membrane structures. Here, I group them as intra- and extra-cellular lumen formation mechanisms.

1.3.1.3.4 Intracellular lumen formation

Intracellular lumen formation refers to a hollow space enclosed by a single EC which results from vacuole fusion or transcellular membrane invagination. The primary ISVs sprouts before the onset of blood flow in the DA, and to explain the luminal space within the sprout, the vacuole fusion model was proposed by Kamei *et al.,* (2006) (Figure 1.3A1). In this process, ECs take up solutes from extracellular space to form vacuoles which coalesce intracellularly and connect with neighbouring vacuoles, leading to an interconnected luminal space (Kamei *et al.*, 2006). The observation of small vesicles within the ISVs

was also reported in a recent study using high resolution live imaging (Yu *et al.*, 2015). Moreover, intercellular deposition of vacuoles was also observed, which is formed by exocytosis of vacuoles (Blum *et al.*, 2008; Wang *et al.*, 2010), resembling cord hollowing (a mechanism of extracellular lumen formation), suggesting that different mechanisms are used even within the same vascular bed.

ECs also generate transcellular lumens via membrane invagination (Figure 1.3A2) which refers to apical membrane pushed by blood pressure from the stalk cell (connecting to a patent vessel) to the tip cell (Herwig *et al.*, 2011; Lenard *et al.*, 2013). It was first described in unicellular tubes of elongating sprout (see type I anastomosis in Figure 1.2 (Lenard *et al.*, 2013), while more recently it has also been reported in multicellular lumens which is actually more frequently observed in angiogenic sprouts (Gebala *et al.*, 2016). The expansion of the membrane invagination may be supported by inverse blebbing of the apical membrane (Gebala *et al.*, 2016); however, the authors also argued that no vacuoles were observed in their transgenic reporter lines, again challenging the view of vacuole fusion mechanisms.

1.3.1.3.5 **Extracellular lumen formation**

Extracellular lumen formation (also known as cord hollowing) refers to the generation of a luminal space between paired ECs via electrostatic repulsion, cell rearrangement or disposition of vacuoles (Figure 1.3B). During the process,

the ECs first form a tight cord-like structure via adherens junctions. Subsequently, ECs become polarised and at the apical membrane side a luminal compartment appears between the contacted cells.

The initiation of apical membrane separation is dependent on VE-cad, which localises Cdc42 and Podocalyxin 2, a member of CD34-sialomucins, via recruitment of apical polarity related protein Par3 (Strilić *et al.*, 2010, 2009). Disposition of the CD34 complex at the cell-cell contact site induces negatively charged electrostatic repulsion for the initiation of lumen opening (Strilić *et al.*, 2010, 2009). Subsequently, VE-cads re-locates laterally to induce cell shape changes and further expansion of the lumen (Strilić *et al.*, 2010). The lumen opening is proposed to be triggered by VEGFR2 mediated signalling (Strilić *et al.*, 2009). An alternative initiation of extracellular lumen is via intracellular vacuoles that fuse with the plasma membrane and exocytose to the extracellular luminal spaces (Yu *et al.*, 2015). ECs then undergo cell rearrangement and shape change to give rise to a multicellular tube via JBL (Paatero *et al.*, 2018; Schuermann *et al.*, 2014).

In addition to the above mechanisms of lumen formation, a poorly understood process called lumen ensheathment has been reported in the zebrafish common cardinal vein (CCV). It has been described as collective migration of ECs migrating as a sheet along the routes of the blood flow, and eventually enclose the entire lumen (Helker *et al.*, 2013).

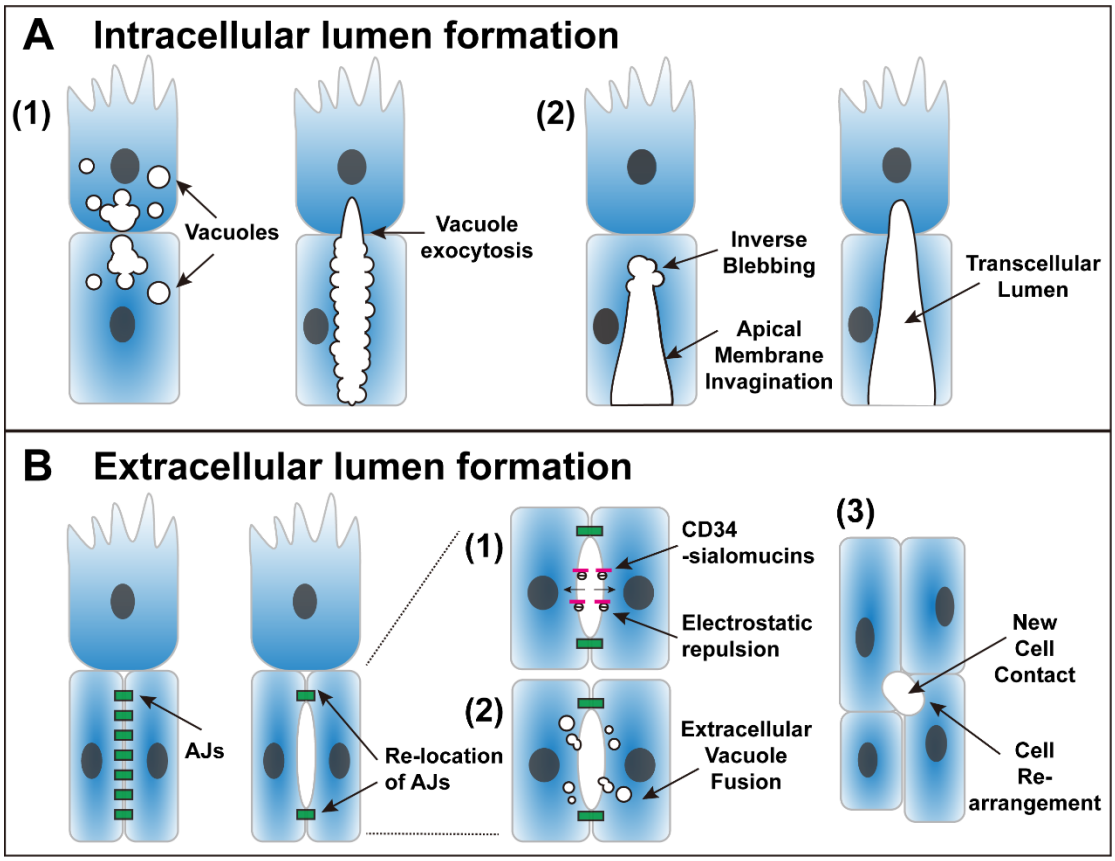

Figure 1.3 Mechanisms of blood vessel lumen formation

(**A**) Intracellular lumen formation refers to luminal space within a single EC. It can be sub-divided into two mechanisms: (1) vacuoles coalesce intracellularly and fuse with neighbouring vacuoles via exocytosis; (2) blood pressure-dependent invagination pushes the apical membrane from the stalk cell to tip cell. The inverse blebbing at the front of the membrane may also facilitate its directed expansion.

(**B**) Extracellular lumen formation involves formation of adherens junctions between the contact surface of the ECs. The AJs subsequently relocate their position to the periphery side of the cells to allow a luminal space to take place between the cells. The initiation of apical membrane separation occurs via electrostatic repulsion mediated by CD34-sialomucins (1), extracellular vacuole fusion (2), or cell rearrangement (3).

1.3.1.4 Vascular remodelling

After the establishment of a primary vascular network, blood vessels undergo remodelling to balance haemodynamic and metabolic needs. The remodelling events include adjustments in vessel diameters and retraction of redundant branches via selected vessel pruning or massive regression of the vasculature. Recent studies have revealed the morphogenic control of vessel pruning in cross-branches using zebrafish (Lenard *et al.*, 2015, 2013). There are certain parallels between angiogenic sprouting and remodelling. While generation of new vessels include cell proliferation and filopodial connection, remodelling involves trimming of unwanted vessels via apoptosis and cell migration away from the pruning vessel (anastomosis 'in reverse') (reviewed in Betz *et al.*, 2016).

1.3.1.4.1 Apoptosis-mediated remodelling

Apoptosis-mediated regression occurs in physiological processes that experience drastic metabolic changes, for example, the regression of mammary gland vessels (Andres and Djonov, 2010) or pathological models such as retinopathy of prematurity models, and tumour angiogenesis upon VEGF manipulation (Korn and Augustin, 2015). In developing embryos, programmed cell death has also been observed in the cranial vessels in zebrafish (Kochhan *et al.*, 2013) and ocular vasculatures in mice (Franco *et al.*, 2015; Lobov *et al.*, 2005). It has been suggested that apoptosis is the primary

mechanism preferred in large plexi, providing an efficient method to clear an entire vasculature. However, a recent study also reported that EC apoptosis in addition to cell migration contributes to branch pruning of the zebrafish brain vessels (Zhang, Y. *et al.*, 2018), suggesting that blood vessels may use different mechanisms simultaneously for remodelling.

1.3.1.4.2 **Cell migration-mediated remodelling**

Apoptosis-independent recycling of ECs from unnecessary vascular segments is more commonly observed in smaller vessels of various animal models, including mouse/rat retina and vitelline vessels, chick yolk sac, and zebrafish eyes and ISVs (Chen *et al.*, 2012; Franco *et al.*, 2015; Hughes and Chan-Ling, 2000; Kochhan *et al.*, 2013; le Noble *et al.*, 2004; Lobov *et al.*, 2011; Phng *et al.*, 2009). The trimming process is mostly observed in branches across two main vessels, or loop-forming segments, in a process termed vessel pruning.

Vessel pruning is mediated by ECs migrating away from the site of pruning to the stable vessels. The lateral migration of the ECs is highly dependent on blood flow which could be a driver of pruning selection (Chen *et al.*, 2012). Furthermore, it was shown that the lack of blood flow *per se* does not cause pruning, but rather the different flow patterns in juxtaposed branches trigger the pruning of the cross-branch (Franco *et al.*, 2015; Kochhan *et al.*, 2013). Blood flow regulates the directed migration of ECs by influencing their axial polarity

indicated by Golgi and nucleus (Franco *et al.*, 2015). It has been shown *in vitro* and *in vivo* that Golgi locates in front of the nucleus as a polarisation cue during cell migration and that the degree of polarisation is positively correlated with the flow magnitude (Franco *et al.*, 2015; Kwon *et al.*, 2016; Martin *et al.*, 2018). In response to local difference of flow, ECs of a cross-branch experiencing slower flow or low shear stress are more likely to polarize and migrate towards high shear stress segments (Franco *et al.*, 2015)

Recent studies using the zebrafish SIVP and ISV to understand blood vessel remodelling have revealed that once a particular vessel was selected for pruning, two modes of cell behaviour may occur depending on the perfusion of the vessel (Lenard *et al.*, 2015) (Figure 1.4).

Similar to type I anastomosis but in a reverse mode, type I pruning happens when the vessel remained perfused, in a process which converted a multicellular tube into a unicellular tube (Figure 1.4A). The last linking cell undergoes ‘self-fusion’ in which a cell wraps itself around the lumen. While cell splitting during anastomosis occurs via generation of new junctions within a single EC, cell self-fusion terminates the cell boundaries and form a seamless transcellular lumen (Lenard *et al.*, 2015; Yu *et al.*, 2015). At the final stage, the transcellular lumen collapses and the cell detaches from the vessel at the contralateral side. The connection of the last cell to the vessel often breaks and re-connects several times before it finally retracts (Lenard *et al.*, 2015). Type II pruning occurs in multicellular vessels that initially collapse, then transform into

a unicellular tube via cell rearrangement, which eventually resolves to the parent vessel (Figure 1.4B). The authors further point out that flow is required for vessel regression since the pruning events were significantly decreased in the absence of flow (Lenard *et al.*, 2015).

In contrast to vessel pruning in which ECs migrate away from the regressing branch, ECs that comprise a vascular loop can migrate towards each other and close the loop, which is termed collateral fusion (Udan *et al.*, 2013). Collateral fusion has been reported in the mouse extraembryonic yolk sac (Udan *et al.*, 2013) and zebrafish SIVP (Lenard *et al.*, 2015). The fusion of the loops leads to a larger vessel since the ECs are re-used and rearranged via migration.

In addition to lumenised branches, leading sprouts at the migration front have also been found to regress in the zebrafish SIVP (see section 1.2.1.3). The retraction of the paired tip cells have been suggested to be migration-driven (Hen *et al.*, 2015). However, the cellular and molecular mechanisms underlying the process remain unclear and is a major focus of this thesis.

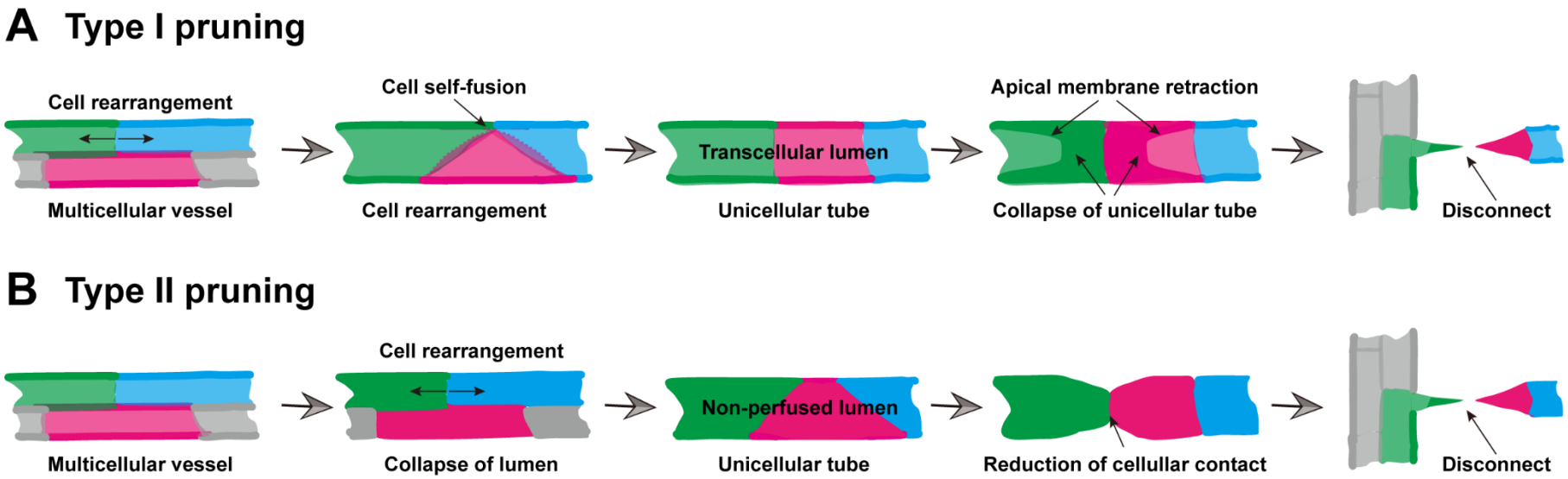

Figure 1.4 The cellular mechanisms of vessel pruning

(**A**) Type I pruning. The process occurs in lumenised vessels. ECs rearrange and migrate away from each other, and the remaining cells form a unicellular tube via cell self-fusion. Cell self-fusion describes an EC wraps itself around the lumen and seals its boundaries into a seamless transcellular tube. The lumen then collapses, and the last two cells detach their contacts and migrate into the recipient vessels.

(**B**) Type II pruning. The process involves firstly the collapse of lumen in the multicellular vessel. Subsequently, the ECs rearrange and migrate to for a unicellular tube, followed by reduction and eventually disconnection of cellular contacts.

1.3.1.5 **Maturation and stabilisation**

The last step of angiogenesis is the maturation and stabilisation of blood vessels, which enables the vessels to be resistant to the changes in blood flow. During the process, various supporting mural cells (including vascular smooth muscle cells (vSMCs) and pericytes) and extracellular matrix (ECM) elements are recruited. The existence and functions of mural cells have been reported in zebrafish using various transgenic lines (Chen *et al.*, 2017; Seiler *et al.*, 2010; Stratman *et al.*, 2017; Whitesell *et al.*, 2014). The recruitment of pericytes is regulated by PDGF signalling pathway that is secreted from ECs, serving as an attractant for pericytes. In turn, mural cells secrete angiopoietins which bind to endothelial receptors Tie1 and Tie2 to support vascular maturation and stabilisation (reviewed in Gaengel *et al.*, 2009).

1.3.1.6 **Molecular control of blood vessel formation**

From the above introduction of angiogenesis, we know that ECs share common cellular behaviours during steps of sprouting and remodelling, including cell migration, cell shape change, and cell rearrangements. However, we still know relatively little about the molecular basis underlying these behaviours. Most studies have focused on the sprouting aspect of angiogenesis in which the principle factor is VEGF, while the remodelling aspect is less well understood. Low VEGF signalling leads to EC apoptosis and cessation of blood

flow, resulting in vessel regression (reviewed in Korn and Augustin, 2015). In addition, BMP signalling is emerging as an important pathway in vascular remodelling in response to blood flow.

1.3.1.7 **VEGF signalling**

VEGF-A, originally identified as vascular permeability factor (VPF) (Senger *et al.*, 1990), is the principal master regulator in angiogenesis. VEGF-A is the best-characterised member of a family of homodimeric glycoproteins that includes placental growth factor (PIGF) and VEGF-B, -C, -D, -E (Viral), and -F (found in snake toxin). VEGFs are broadly expressed and play important roles in various organs, such as the central nervous system, kidney, and liver, in addition to their best-characterised functions in vasculature (Herbert and Stainier, 2011; Simons *et al.*, 2016). The biological function of VEGFs is predicated upon binding to three receptor tyrosine kinases (RTKs), VEGFR1-3, that are typically localised on the surface of ECs (Ferrara and Davis-Smyth, 1997). Similarly, zebrafish also have multiple Vegf ligands (Vegf-aa, -ab, -b, -c, -d, -e, -f and PIGF) and receptors (Vegfr-1/Flt1, Vegfr2/Kdrl-kdr, and Vegfr3/Flt4). A partial genome duplication in zebrafish has resulted in two orthologues of *VEGFA* in zebrafish, *vegfaa* and *vegfab* (Bahary *et al.*, 2007). There are also two homologs of *VEGFR2*, namely *Kdr/Kdrb* and *Kdrl/Flk1/Kdra/Vegfr4* (Bussmann *et al.*, 2008; Covassin *et al.*, 2006a).

VEGF-A has a number of different isoforms following alternative splicing of

its precursor mRNA (VEGF-A-121, -145, 165, -183, -189, -206) and VEGF-A-165 is the most abundantly expressed in human (Robinson and Stringer, 2001). In zebrafish, $Vegfa_{165}$ and $Vegfa_{121}$ are the dominant forms expressed (Liang *et al.*, 2001). Vegfa primarily binds to Kdr/Kdrl to activate downstream Ca^{2+} oscillation, phospholipase C-gamma (PLC-γ) and the mitogen-activated protein kinase (MAPK)/extracellular signal-regulated kinase (ERK) signalling, leading to pro-angiogenic effects (Savage *et al.*, 2019; Shin *et al.*, 2016a; Takahashi *et al.*, 2001; Yokota *et al.*, 2015). Mutation- or morpholino-induced defects in either level of the ligand (Bahary *et al.*, 2007; Koenig *et al.*, 2016), the receptors (Covassin *et al.*, 2006b; Habeck *et al.*, 2002) or the downstream effectors (Covassin *et al.*, 2009; Savage *et al.*, 2019; Shin *et al.*, 2016a) causes defective sprout induction and outgrowth or defective arterial specification of ECs.

As has been described previously, Flt1 acts as a decoy receptor for Vegfa to limit its pro-angiogenic output. Knockdown of *flt1* leads to increased tip cell number and hyperbranching of arterial ISVs, as well as reduced expression of Notch receptors (Krueger *et al.*, 2011). Zebrafish neuronal *flt1* mutants exhibit similar phenotypes with increased angiogenesis in which ectopic sprouts emanate from venous ISVs. Interestingly, the ectopic hyper-sprouting in *flt1* mutants can be rescued by inhibition of blood flow (Wild *et al.*, 2017).

Although Vegfc-Vegfr3 (Flt4) signalling has been best studied during lymphatic formation, it is also required for the secondary sprouting of veins and lymphatics during ISV formation. Vegfc can also bind to Kdr and Kdrl to

influence the formation of segmental arteries (Covassin *et al.*, 2006b). Moreover, *flt4* is suppressed by *dll4* in SAs to regulate arterio-venous differentiation of ISVs (Hogan *et al.*, 2009b).

The scenario of VEGF regulation becomes more complicated as studies explore its functions during different aspects of angiogenesis in various vascular beds. For example, Vegfd binds to Flt4 in zebrafish trunk but binds to Kdr in the head to regulate lymphatic development (Vogrin *et al.*, 2019). The interaction between receptors or co-receptors may also reveal a different level of VEGF regulation. Although VEGF receptors generally form homodimers, the existence of VEGFR2/VEGFR3 and VEGFR1/VEGFR3 heterodimers has been suggested and R2-R3 heterodimers induced by VEGFA or VEGFC might positively regulate angiogenic sprouting (reviewed in Simons *et al.*, 2016). Neuropilin-1 (NRP1) has been shown to be a co-receptor for VEGF-A in mice (Mukouyama *et al.*, 2005) and zebrafish (Lee *et al.*, 2002), and it facilitates intracellular trafficking of VEGFR2 to induce ERK1/2 activation (Lanahan *et al.*, 2013).

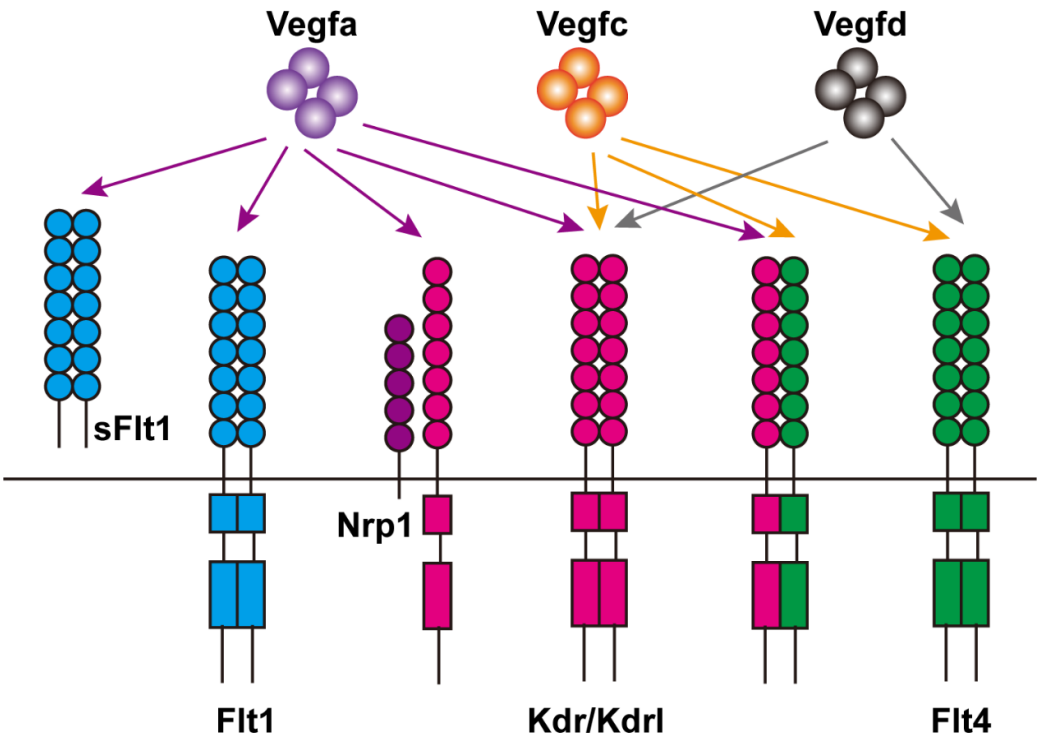

Figure 1.5 VEGF ligand-receptor interactions

Different ligand-receptor interactions occur in different contexts. Both isoforms of Flt1 (soluble and membrane-bound) are considered as decoy receptors for Vegfa to limit angiogenesis. Kdr/Kdrl transduce the main angiogenic signals, promoting EC migration, proliferation and vessel permeability. Nrp1 is a coreceptor for Vegfa. Kdr and Flt4 can form heterodimers. Vegfc-Flt4 signalling controls venous and lymphatic formation. Vegfd can also bind to Flt4 or Kdr based on context.

1.3.1.8 **BMP signalling**

BMPs are members of the transforming growth factor-β (TGF-β) superfamily and were first identified in extracts from bone matrix that induces ectopic bone formation when implanted subcutaneously in rats (Wozney *et al.*, 1988). It is now known that BMPs play important roles in nearly all vertebrate organs and have emerged as fundamental signals in regulation of vascular formation and function. BMP signalling not only plays important roles in

endothelial specification and venous differentiation during embryonic development, but also promotes angiogenesis and senses flow shear stress in adult vasculature (reviewed in Dyer *et al.*, 2014; Franco and Gerhardt, 2016; and García de Vinuesa *et al.*, 2016). It is also directly linked to several vascular disorders including pulmonary arterial hypertension (PAH) and hereditary haemorrhagic telangiectasia (HHT) (reviewed in Lowery and de Caestecker, 2010 and Wang *et al.*, 2014). Based on sequence similarity and affinities for receptors, the BMP ligands are divided into subgroups, among which BMP2/4 and BMP9/10 subgroups are best studied in vascular biology. BMPs can signal through canonical and non-canonical pathways (Figure 1.6A). In canonical BMP signalling, BMPs bind to two dimers of type I (ALK1, ALK2, ALK3, and ALK6) and type II receptors (BMMPR2, ActRIIA, ActRIIB). The ligand-receptor association initiates phosphorylation of the receptor-regulated SMADs (R-SMADs). These phosphorylated R-SMADs bind to SMAD4 to form a complex which re-locates into the nucleus and activates transcription of target genes, leading to cellular adaptations. The non-canonical pathway of BMPs on the other hand is less well-understood. It has been found to affect PI3K/Akt, PKC, various MAPK kinases (ERK, p38 and JNK) and others, without recruiting R-SMADs (Zhang, 2009) (Figure 1.6A), therefore this pathway is also termed the non-SMAD pathway. Nonetheless, the function of endothelial BMP signalling is context dependent and varies amongst different endothelial cell types, for example, whether these are exposed to flow *in vitro*, and when it interacts with

other pathways, such as VEGF, Notch, and Wnt signalling (reviewed in de Vinuesa *et al.*, 2016).

1.3.1.8.1 **The BMP2/4 subgroup**

The BMP2/4 ligands typically bind to ALK3/ALK6 and BMPR2, activating downstream SMAD1/5/8 (Figure 1.6B). BMP2/4 signalling has been demonstrated to be pro-angiogenic, by promoting proliferation, cell migration and tube formation (De Jesus Perez *et al.*, 2009; Finkenzeller *et al.*, 2012; Suzuki *et al.*, 2008). In pulmonary artery endothelial cells, BMP2 associates with Wnt signalling which interacts with β-catenin or RhoA-Rac1 to drive proliferation or migration, respectively (De Jesus Perez *et al.*, 2009), although it induces cell migration and invasion without affecting proliferation in HUVECs (Finkenzeller *et al.*, 2012). In the zebrafish caudal vein plexus, Bmp2b along with its receptors Bmpr2a and Bmpr2b, promotes venous sprouting (via R-SMADs) and sprout elongation (via ERKs) (Wiley *et al.*, 2011). BMP4 promotes EC proliferation and migration via stimulation of VEGFA-VEGFR2 and ANG1-TIE2 signalling (Suzuki *et al.*, 2008). However, overexpression of BMP4 has also been reported to inhibit tube formation via downregulation of VEGF and matrix metalloproteinase (MMP9) in laser-induced choroidal neovascularisation (Xu *et al.*, 2012). In addition, BMP4 infusion in the mouse causes hypertension due to impaired EC-dependent vasorelaxation in aortic rings (Miriyala *et al.*, 2006). These studies highlight the importance of context in BMP function and

its role in venous specification.

1.3.1.8.2 **The BMP9/10 subgroup**

BMP9/10 binds to ALK1 and BMPR2 with high affinity (Brown *et al.*, 2005). The BMP9/10-ALK1 pathway generally induces anti-angiogenic effects and promotes vessel quiescence (de Vinuesa *et al.*, 2016; Lowery and de Caestecker, 2010) (Figure 1.6B), although it also activates VEGF and Tie2 signalling to induce EC proliferation and tube formation (Nolan-Stevaux *et al.*, 2012; Suzuki *et al.*, 2010). BMP9 and 10 are mainly produced by liver and heart, respectively (Miller *et al.*, 2000; Neuhaus *et al.*, 1999), and BMP9 has also been detected in the blood circulation (David *et al.*, 2008). While deletion of *Bmp10* leads to embryonic death because of cardiac and vascular defects, *Bmp9*-deficient mice are viable (Chen *et al.*, 2004, 2013; Ricard *et al.*, 2012). However, neutralising BMP10 with antibodies in *Bmp9* mutants causes hyper-branching of the retina vasculature, suggesting an overlapping role in the two BMP ligands (Chen *et al.*, 2013; Ricard *et al.*, 2012). *Alk1* knockout mice die at midgestation due to excessive fusion of capillaries (arteriovenous malformation, AVM) and hyperdilation of large vessels (Oh *et al.*, 2000). The role of BMP9/10-ALK1 signalling has also been demonstrated in zebrafish: *alk1* morphants or mutants exhibit enlarged cranial arteries and severe AVMs (Corti *et al.*, 2011; Rochon *et al.*, 2016); *bmp10* and *bmp10-like* double morphants have similar but milder vascular defects as in *alk1* morphants (Laux *et al.*, 2013); and *bmp9* morphants

show impaired venous remodelling in the CVP (Wooderchak-Donahue *et al.*, 2013). Interestingly, Alk1 is activated by both blood flow and circulating Bmp10 in zebrafish, leading to restriction of arterial diameter at the onset of flow (Laux *et al.*, 2013). These studies suggested an important role of the BMP9/10-ALK1 pathway in vascular remodelling and stabilisation.

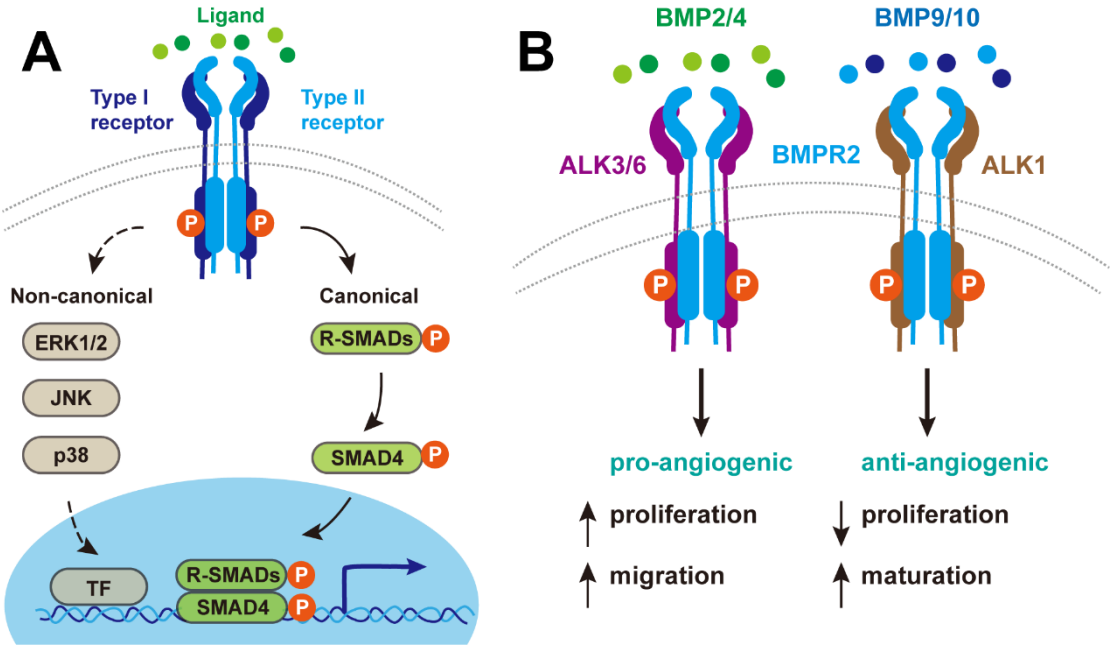

Figure 1.6 BMP signalling pathways in vasculature

(**A**) BMPs signal through the canonical, SMAD-dependent pathway, or various non-canonical pathways. In the canonical pathway, BMP ligands bind to type I and type II receptor and activates SMAD cascade. Phosphorylated R-SMADs (SMAD1/5/8) associates with the co-SMAD (SMAD4) to form a complex which induces transcription of target genes. Various non-canonical pathways, including MAPK signalling, also regulate gene expression. ERK, extracellular signal-regulated kinase; JNK, c-Jun-N-terminal kinase; TF, transcription factor. (**B**) BMP2/4 induces pro-angiogenic effects via binding to ALK3/6 and BMRP2, to promote EC proliferation and migration. BMP9/10 associates with ALK1 and BMPR2 to induce anti-angiogenic effects via inhibiting EC proliferation and promoting vessel maturation.

1.3.1.9 **Notch and WNT signalling**

In contrast to the pro-angiogenic regulation of VEGF, Dll4/Notch signalling is usually considered as anti-angiogenic (see review Korn & Augustin 2015). Loss of Notch signalling results in hyper-sprouting and an increase in the number of tip cells in all vascular beds examined so far (reviewed in Siekmann *et al.*, 2013). Notch is also tightly linked to arterial specification, as Notch promotes arterial identity and is absent in venous ISVs (Quillien *et al.*, 2014). In addition, Notch also plays important roles in vascular remodelling. Oxygen induced Dll4/Notch shifts the expression of vasoactive genes to vasoconstrictive ones, inducing vessel occlusion and EC apoptosis (Lobov *et al.*, 2011). Notch interacts with WNT signalling via Notch-regulated ankyrin repeat protein (NRARP), a negative regulator of Notch. Loss of *Nrarp* results in increased vessel regression due to a decrease in Wnt-induced stalk cell proliferation (Phng *et al.*, 2009). These studies confirm the involvement of Notch in vascular remodelling and its potential role as a switch for vessel pruning.

Canonical WNT/β-catenin signalling has been suggested to promote vascular remodelling in certain contexts. *β-catenin* gain-of-function upregulates Notch signalling which induces increased lumen, remodelling, branching and arteriovenous specification defects. Angiopoetin-2 (ANG2) induces vessel regression while ANG1 promotes EC survival, mediated by crosstalk with *Wnt7b* expression in macrophages (Rao *et al.*, 2007).

Non-canonical WNT signalling is also involved in vessel pruning and

regression by regulating ECs survival and apoptosis (Korn *et al.*, 2014). Of particular interest, flow-induced cell migration/rearrangements are responsible for vessel pruning, via regulation of non-canonical WNT signalling on EC polarity (Franco *et al.*, 2016). In primitive vasculature, non-canonical WNT signalling stabilizes ECs movements and keeps vessels open under low flow conditions; when exposed to higher shear stress levels, additional signalling pathways are activated and this overcomes the stable threshold set by WNT signalling; as a result, ECs polarise and migrate against the direction of flow, leading to vessel pruning (Franco *et al.*, 2016).

1.4 Collective cell migration and mechanotransduction

1.4.1.1 Collective cell migration during angiogenesis

Although morphologically different, ECs share common behavioural changes during sprouting and remodelling, including cell proliferation, establishment of polarity, and cell migration. Cells can either migrate individually, namely single-cell migration, or as multicellular units, termed collective migration. The migratory behaviours described above, either during sprouting where tip cells and stalk cells within a sprout coordinate to invade avascular tissues or during remodelling where they rearrange to prune a branch, are typical of collective cell migration (Khalil and Friedl, 2010). Collectively migrating cells impose additional constraints such as differentiation of leader

and follower cells (tip and stalk cells in the context of angiogenesis), maintaining connectivity and force transmission with neighbouring cells and organising multicellular polarity (Haeger *et al.*, 2015). However, it is important to note that current knowledge of collective cell migration is mostly gained from 2D or 3D *in vitro* data. The mechanisms controlling angiogenic collective migration *in vivo* are only started to be investigated and has been mostly focused on angiogenic sprouting (see following sections). The mechanisms underlying collective migration during remodelling are largely unknown.

Formation of filopodia and front-rear polarity

The tip cells at the leading edge determine the direction and efficiency of collective cell migration. A hallmark of tip cells is their intrinsic bipolarity of which the front end enriches with filopodia and lamellipodia and the rear region engages with stalk cells (Figure 1.7). The bipolarity is mediated by localised activation of members of the Rho family of small GTPases, including Rac1, Cdc42, and RhoA (Ladwein and Rottner, 2008). In cell sheets, generally, Cdc42 and Rac1 are stimulated at the front of the leader cells, leading to Arp2/3 activation which then promotes rapid and dynamic polymerisation of actin and formation of filopodia/lamellipodia (Goley and Welch, 2006). Cdc42 also regulates the localisation of microtubule-organisation centre (MTOC) and the Golgi apparatus. Their localisation in front of the nucleus is a hallmark of cell polarisation (Lizama and Zovein, 2013). It has been shown in mice recently that the front-rear polarity of tip cells is regulated by the adaptor proteins NCK1/2

and CDC42 downstream of VEGFR2 activation (Dubrac *et al.*, 2016; Laviña *et al.*, 2018). CAMSAP2, which binds to non-centrosomal MT, is required for Golgi-mediated EC polarisation and positively regulates venous ISV sprouting in zebrafish (Martin *et al.*, 2018). During zebrafish CVP formation, BMP induces formation of EC filopodia and migration via Arhgef9b-mediated activation of Cdc42 and Formin-like 3 (Fmnl3) (Wakayama *et al.*, 2015). Rac1 can also induce Aurora A kinase phosphorylation which leads to polarised orientation of microtubules (Braun *et al.*, 2014). These localised actin and microtubule cytoskeletons, combined with dynamic dis- or re-assembly of integrin-based contacts with extracellular matrix (ECM), facilitates the forward movement of the cells. RhoA, in contrast, locates at the rear end of the moving cell and promotes actomyosin-dependent contraction of the cell body and retraction of the cell rear (Lizama and Zovein, 2013). Interestingly, although Rac1 and Rho genes are shown to be critical for EC migration *in vitro*, deletion of these genes *in vivo* only shows mild defects. *Rac1* EC-specific KO display slightly delayed EC migration and RhoA is dispensable for physiological angiogenesis in mouse retinal vessels, suggesting additional signals and alternative compensatory mechanisms are present in the *in vivo* setting (Nohata *et al.*, 2016; Zahra *et al.*, 2019).

Sensing of stimuli by tip cells is commonly believed to occur via filopodial or lamellipodial extension (Gerhardt *et al.*, 2003). However, recently filopodia were found to be dispensable for directed EC migration in ISVs, although their

presence increases the migration efficiency of the vessels (Phng *et al.*, 2013). In contrast, filopodia in BMP-dependent CVP formation is essential for proper venous sprouting (Wakayama *et al.*, 2015). The difference has been proposed to result from the ability of the tip cells to form lamellipodia. VEGF can activate both Cdc42 and Rac1, which promotes the formation of filopodia and lamellipodia, respectively, while BMP can only stimulate Cdc42. Therefore ECs fail to migrate in the absence of filopodia in the CVP while the migration can continue in the ISV via formation of lamellipodia (Wakayama *et al.*, 2015).

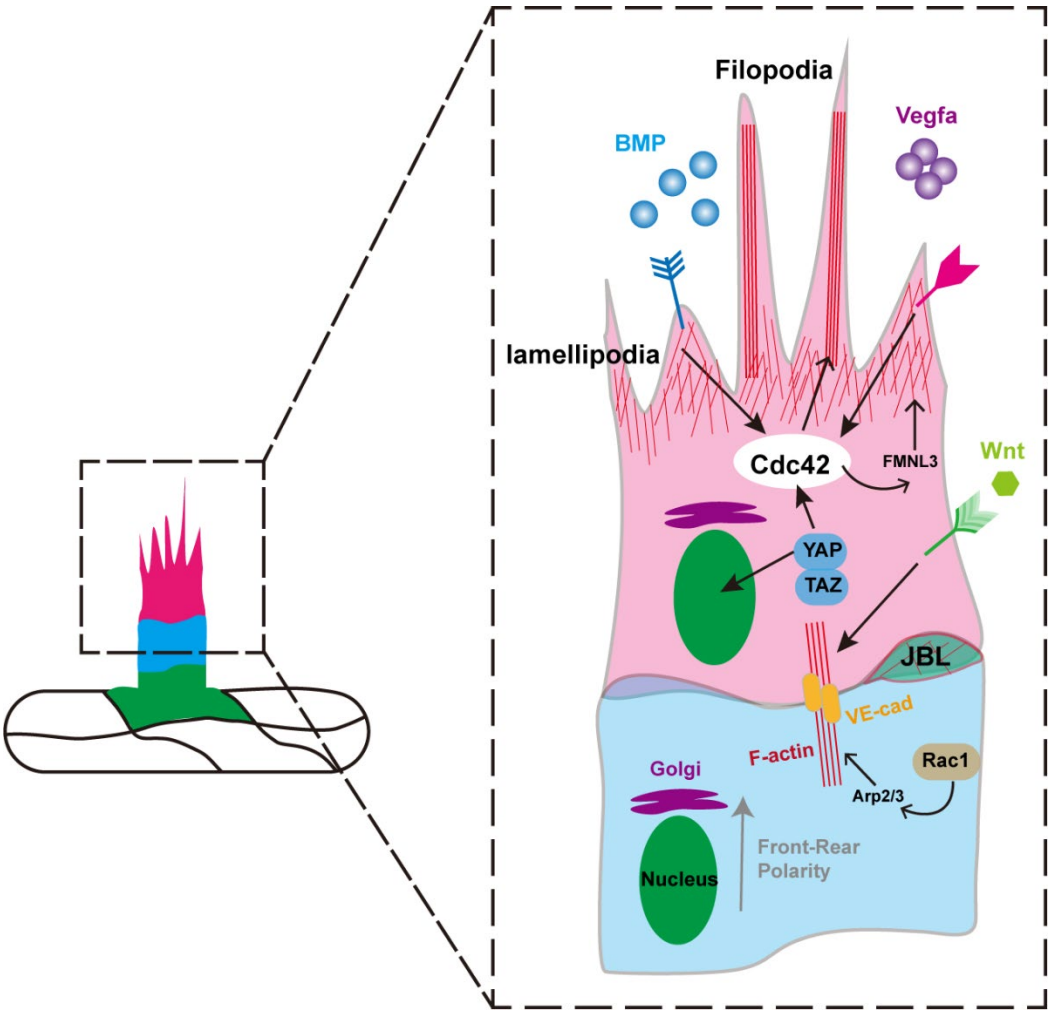

Figure 1.7 Formation of filopodia and cell polarity during collective cell migration

Schematic illustration of a migrating sprout with a tip cell (pink) and a stalk cell (blue). VEGF and BMP signalling pathways are critical for activation of Rho family members, such as Cdc42 and Rac1, which trigger formins Fmnl3 and Arp2/3 respectively, to induce formation of filipodia and lamellipodia. Cdc42 also regulates location of Golgi during cell polarisation. Wnt signalling pathways also regulate cell polarity and enhance intercellular force transmission and collective cell migration via recruitment of vinculin to adherens junctions (cadherin fingers, see text). Junction-based lamellipodia (JBL) are important for junctional stability and EC migration.

Force transmission during collective cell migration

Leader cells are linked with follower cells via tight junctions and adherens junctions (for example, VE-cads). In cell sheets, polarised VE-cadherin-rich membrane protrusions (termed cadherin fingers), which leader cells extend from their rear and follower cells engulf at their front, resulting in asymmetric recruitment of curvature-selective regulators to bias collective cell migration towards leading cell direction (Hayer *et al.*, 2016). Followers can also directly participate in generation of traction forces by forming basal membrane protrusions (‘cryptic lamellipodia’) that interact with underlying substrate and generate motility (Farooqui and Fenteany, 2005). Oscillating lamellipodia-like protrusions, JAIL and JBL, are also proposed to regulate coordinated EC movements during angiogenic sprouting and anastomosis *in vivo* (Cao *et al.*, 2017; Paatero *et al.*, 2018). It has also been shown that WNT5A, through ROR2, activates CDC42 at cell junctions, which stabilises vinculin binding to α-catenin, leading to efficient coordination of collective migration (Carvalho *et al.*, 2019). Low non-canonical Wnt signalling weakens adherens junctions and therefore impairs force transmission and collective migration in sprouting angiogenesis (Carvalho *et al.*, 2019). Moreover, focal adhesion protein DLC1, which expression is dependent on YAP and TAZ, is required for cell polarisation and contractility in directed collective migration (Van Der Stoel *et al.*, 2020).

Apical-basal polarity and axial polarity

The widely accepted model of angiogenic sprouting consist of a single tip

cell at the leading front of the sprout, as frequently observed in ISVs. However, vessel sprouts composed of multiple tip cells have also been reported in distinct vascular beds (Hen *et al.*, 2015; Pelton *et al.*, 2014). These cells overlap with each other and form a longitudinal cell-cell border where apicobasal polarity proteins such as PODXL (apical) and β1-integrin (basal) are detected (Pelton *et al.*, 2014). The apical polarised border is considered to be a site of lumen formation, presumably via a cord-hollowing mechanism. Loss of atypical protein kinase C (aPKC) disrupts the EC overlapping and lumen formation in the sprouts (Pelton *et al.*, 2014).

Upon the onset of blood flow, ECs also establish axial polarity which is indicated by the position of nucleus and Golgi complex (Kwon *et al.*, 2016). In quiescent vessels, ECs polarise against flow, with Golgi positioning upstream of the nucleus. When the flow profile changes, the balance of axial polarisation breaks and ECs establish front-rear polarity and undergo migration, resulting in vessel pruning (Franco *et al.*, 2016). Blood flow is a key regulator of cell behaviour during angiogenic sprouting and remodelling and will be described in detail in the following sections.

1.4.1.2 **Haemodynamic forces in blood vessels**

1.4.1.3 **Haemodynamic forces and mechanoreceptors**

Prior to the onset of blood flow, vessel development is mainly regulated by molecules in the local environment (auto- or paracrine factors); while upon the

onset of flow, mechanical forces and endocrine factors also regulate the behaviour of ECs. These mechanical forces include shear stress, which is the frictional force exerted by the flowing blood, and circumferential stress, which is perpendicular to the vessel wall and is exerted by blood pressure. Shear stress is proportional to the flow rate and blood viscosity and is inversely proportional to the vessel diameter (Jones *et al.*, 2006).

The direct role of haemodynamic forces at early stages of vascular development are still highly debated as it is difficult to distinguish the EC response to physical forces or to the solutes carried by the blood flow, such as oxygen and growth factors. However, it is becoming clear through *in vitro* analysis that shear stress is a critical physical factor in the regulation of EC function. A variety of candidate mechanoreceptors or structures have been identified, including ion channels, G proteins and G protein-coupled receptors (GPCRs), ECM receptors (e.g. integrins), endothelial glycocalyx, primary cilia, caveolae, cell-cell adhesion junction proteins and BMPRs (reviewed in Ando and Yamamoto, 2013; Chen *et al.*, 2016). Flow-mediated activation of mechanoreceptors in ECs leads to cellular adaptations through a process termed mechanotransduction.

In addition to blood velocity, shear stress is also dependent on blood viscosity, which is related to the number of red blood cells (RBCs) within the circulation. Mouse embryos without circuiting RBCs exhibit drastically reduced vascular remodelling, but could be rescued by injection of a viscous plant starch

which restored blood viscosity (Lucitti *et al.*, 2007). It has also been shown in the zebrafish that abrogation of circulating erythrocytes decreases the primary cilia deflection levels in response to flow and results in reduced formation of vascular loops (Goetz *et al.*, 2014). Reduced blood viscosity also impairs the coverage of vascular mural cells (vMC) (Chen *et al.*, 2017). These studies suggest that the mechanical forces are necessary and sufficient for vascular remodelling.

PECAM1/VE-cad/VEGFR complex

Platelet endothelial cell adhesion molecule-1 (PECAM1), an adhesion molecule, and VE-cad are specifically localized to cell-cell junctions. Along with VEGFR2, these form a flow-sensing complex that is important for ECs to transform physical cues into biochemical response (Coon *et al.*, 2015). PECAM1 may act as a direct mechanosensor or be activated by upstream force-mediated by the cytoskeleton. Tension on PECAM1 triggers ligand-independent transactivation of VEGFR2 (Tzima *et al.*, 2005). VE-cad at the junctions may function as a scaffolding platform, which facilitates activation of VEGFR2-mediated downstream cascades, such as Nitric oxide (NO) production and activation of integrins (Conway *et al.*, 2013; Coon *et al.*, 2015). The adherens complex is also responsible for EC planar polarisation, with the Golgi apparatus and MTOC positioned upstream of the nucleus in response to flow (Tzima *et al.*, 2005).

Recent studies also identified VEGFR3 as a new element comprising the

PECAM1-VE-cadherin-VEGFRs complex (Baeyens *et al.*, 2015). In addition, the levels of VEGFR3 may provide a set point of shear stress, at which within a certain range vascular vessels are quiescent and stabilised whereas outside this range remodelling is triggered (Baeyens *et al.*, 2015). In comparison to ECs, lymphatic ECs possess a higher level of VEGFR3 which leads to a lower set point of shear stress needed for cell orientation; inhibition of VEGFR3 in lymphatic cells increases the set point. Deficiency in VEGFR3/Flt4 in mouse and zebrafish reduces the diameter of the aorta consistent with flow-dependent remodelling (Baeyens *et al.*, 2015; Coon *et al.*, 2015).

BMP receptors

BMPRs have been shown to function as mechanosensors in different contexts. Oscillatory flow activates BMPR2 which then induces BMPR1B-integrin association, leading to SMAD1/5 phosphorylation *in vitro* and *in vivo*. In this context, SMAD activation results in EC proliferation (Zhou *et al.*, 2012). *alk1* is regulated by blood flow in zebrafish cranial vessels (Laux *et al.*, 2013). It has also been shown that blood flow sensitises the response of EC to BMP9, in which the concentration of BMP9 is 17-fold lower in the presence of flow than that without to induce similar response in HUVECs (Baeyens *et al.*, 2016b). Interestingly, the sensitisation may result from flow-dependent association of ALK1 and its co-receptor Endoglin (ENG) (Baeyens *et al.*, 2016b). Knockdown of either ALK1 or ENG drives AVM formation at the region with high flow and leads to failure in mural cell recruitment in the mouse retina (Baeyens *et al.*,

2016b). This suggests that BMP signalling promotes endothelial quiescence in response to flow. In addition, *alk1*-deficient ECs in zebrafish fail to migrate against blood flow, leading to AVM formations, suggesting the important roles of Alk1 signalling in flow sensing and vascular remodelling are conserved from mammals (Rochon *et al.*, 2016).

EC nucleus

It has been shown that the endothelial nucleus can act as a mechanoreceptor in response to flow. The bulge of the nucleus is pushed by the hydrodynamic drag from flowing blood and the acto-myosin cytoskeleton which is attached to the nuclear envelope, rearranges the position of the nucleus, therefore inducing EC polarisation (Tkachenko *et al.*, 2013). Moreover, the nuclei elongate and align against flow direction in order to minimise the total force experienced (Hazel and Pedley, 2000).

1.4.1.4 **Blood flow dependent signalling pathways in vascular remodelling**

In section 1.3.1.4, I have introduced the role of blood flow in cellular behaviours during vascular remodelling, including regulation of EC polarisation and cell migration from low-flow towards high-flow regions (Figure 1.8A) (Chen *et al.*, 2012; Franco *et al.*, 2016; Kochhan *et al.*, 2013; Kwon *et al.*, 2016; Lenard *et al.*, 2015). This section will focus on flow-mediated molecular signalling pathways that are involved in vascular remodelling and their functions in

different cellular behaviours.

EC polarisation and migration

Several genes and pathways have been shown to regulate EC polarisation. In zebrafish, the Golgi localisation of ECs requires the Apelin receptor (APLNR or APJ), a G-protein coupled receptor and arterial ECs generally display higher degree of polarisation than venous ECs in response to flow (Kwon *et al.*, 2016) (see Figure 1.8B). EC-specific inducible *Par-3* deleted mice exhibit compromised EC axial polarity in a flow-rate-dependent manner without affecting apical-basal polarity (Hikita *et al.*, 2018). Moreover, vascular inflammatory responses are increased upon *Par3* loss-of-function (Hikita *et al.*, 2018). In developing coronary arteries, the expression of Dachshund homolog 1 (DACH1) depends on flow intensity (Chang *et al.*, 2017). Low flow promotes high expression of DACH1-mediated EC migration against flow and its expression is inhibited under high flow in mature arteries (Chang *et al.*, 2017). Overexpression of *Dach1* promotes EC polarisation and migration, which can be reversed upon CXCL12/CXCR4 inhibition (Chang *et al.*, 2017), suggesting that *Cxcl12* is a downstream effector which is known to be involved in EC migration against flow during artery formation (Xu *et al.*, 2014).

It is becoming clear that different cell types display preferential response to a range of shear stress (Baeyens *et al.*, 2015). This selectivity or sensitivity to shear stress is proposed to be regulated by the level of VEGFR3 being expressed in ECs, by tuning the sensitivity of the shear stress sensor

PECAM1/VE-cad (see 1.4.1.3) (Baeyens *et al.*, 2015). Non-canonical Wnt signalling, Wnt5a and Wnt11, has also been suggested to regulate EC sensitivity to flow (Franco *et al.*, 2016). However, loss of Wnt signalling does not alter flow sensing genes but disrupts EC polarisation and migration-driven pruning in vessels, suggesting that Wnt acts downstream of flow sensing machinery and more signalling pathways are involved to directly modulate flow sensing (Franco *et al.*, 2015).

Cell-cell junctions

Blood can also regulate vascular homeostasis by promoting cell-cell junctional stability and actomyosin contractility (Figure 1.7 & Figure 1.8B). Loss of the G protein-coupled S1P receptor-1 (S1P1) leads to increased EC sprouting and formation of ectopic branches, which is correlated with disinhibition of VEGF signalling (Gaengel *et al.*, 2012). S1P1 is induced by laminar shear stress and enhances stabilisation of adherens junctions (Jung *et al.*, 2012). The Hippo signalling transcription factors, YES-associated protein (YAP) and transcriptional coactivator with PDZ-binding motif (TAZ), are key regulators during angiogenesis. During sprouting, YAP and TAZ, in response to mechanistic stretch (rather than blood flow), promote EC proliferation and cell rearrangement by increasing VE-cad turnover and formation of junction associated intermediate lamellipodia (Neto *et al.*, 2018). Importantly, YAP and TAZ strongly inhibit BMP signalling, suggesting integration of mechanical stimuli with biochemical signalling in ECs (Neto *et al.*, 2018). In zebrafish ECs,

transcriptional activity and localisation of Yap1 from cytoplasm to nucleus in response to flow have been observed (Nakajima *et al.*, 2017). It has also been shown in cultured human ECs that shear stress enhances nuclear import of YAP by increasing the number of F-actin bundles in the cytoplasm that associate with angiomotin (AMOT) which in turn release YAP to the nucleus (Nakajima *et al.*, 2017).

EC proliferation and apoptosis

EC proliferation is critical during early angiogenesis since it supports the expansion of vessels by providing newly generated cells. However, how blood flow regulates EC proliferation during angiogenesis is unclear, because it is difficult to distinguish proliferation mediated by flow and natural development. Our current knowledge of EC proliferation in response to flow is mainly from *in vitro* cultured cells exposed to different patterns of flow. At straight regions of blood vessels, ECs are exposed to uniform laminar shear stress while regions near vessel curvatures, ECs experience oscillatory low shear stress (reviewed in Souilhol *et al.*, 2020). High laminar shear stress (LSS) promotes EC quiescence and low proliferation rate by activating p53 and cyclin-dependent kinase inhibitor 1 (p21) which leads to endothelial cell cycle arrest (Akimoto *et al.*, 2000; Lin *et al.*, 2000). LSS also suppresses EC apoptosis via activation of the PI3K/Akt survival pathway (Dimmeler *et al.*, 1998). By contrast, disturbed flow increases inflammatory gene expression and enhances apoptosis and proliferation of ECs, leading to increased EC turnover (Hansson and Schwartz,

1983; Sakao *et al.*, 2005; Tardy *et al.*, 1997). Recent studies identify YAP as an important regulator of EC proliferation in response to flow in cultured ECs. YAP translocation to the nucleus is activated by disturbed flow and therefore triggers EC proliferation (Wang, K. C. *et al.*, 2016; Wang, L. *et al.*, 2016). However, in zebrafish, Yap1 is involved in the maintenance of the DLAV and central arteries upon onset of flow (Nakajima *et al.*, 2017). Future studies are needed to understand the different mechanisms *in vitro* and *in vivo*.

Vessel diameter

Vessel remodelling also involves altering vessel diameter in response to flow (Figure 1.8C). Enlargement of vessel diameter can be achieved by EC proliferation (Zeng *et al.*, 2007), migration of ECs from neighbouring vessels (Rochon *et al.*, 2016; Udan *et al.*, 2013) and changes of cell shape/size (Sugden *et al.*, 2017). Recent studies have started to uncover the signalling pathways that are involved in regulation of vessel calibre and these highlight the role of BMP signalling during this process (see 1.3.1.8). Loss of *alk1* leads to aberrantly enlarged arteries and formation of flow-dependent AVMs due to defects in EC migration (Rochon *et al.*, 2016). Similarly, *endoglin* mutant zebrafish display an enlarged DA at 3dpf when normally its calibre should reduce (Sugden *et al.*, 2017). This is due to a failure of ECs to change their shapes. How physical cues are transduced to these receptors and what controls cell shape downstream remains unknown. Deletion of downstream effector *Smad4* also causes an increase of coronary artery diameter upon the

initiation of flow, which coincides with SMAD1/5/8 activation (Poduri *et al.*, 2017). Increased EC proliferation is observed in these Smad4-deficient arteries while *in vitro* observations also reveal defects in cell migration against the flow direction (Poduri *et al.*, 2017). Deletion of VEGFR3 in mice and zebrafish leads to decreased artery diameter, because reduced expression of VEGFR3 elevates the threshold of shear stress and thus the vessel narrows to increase the shear stress to compensate (Baeyens *et al.*, 2015). It is important to note that these findings are derived from arteries and whether different signalling pathways are employed in veins during vessel diameter regulation remains unknown.

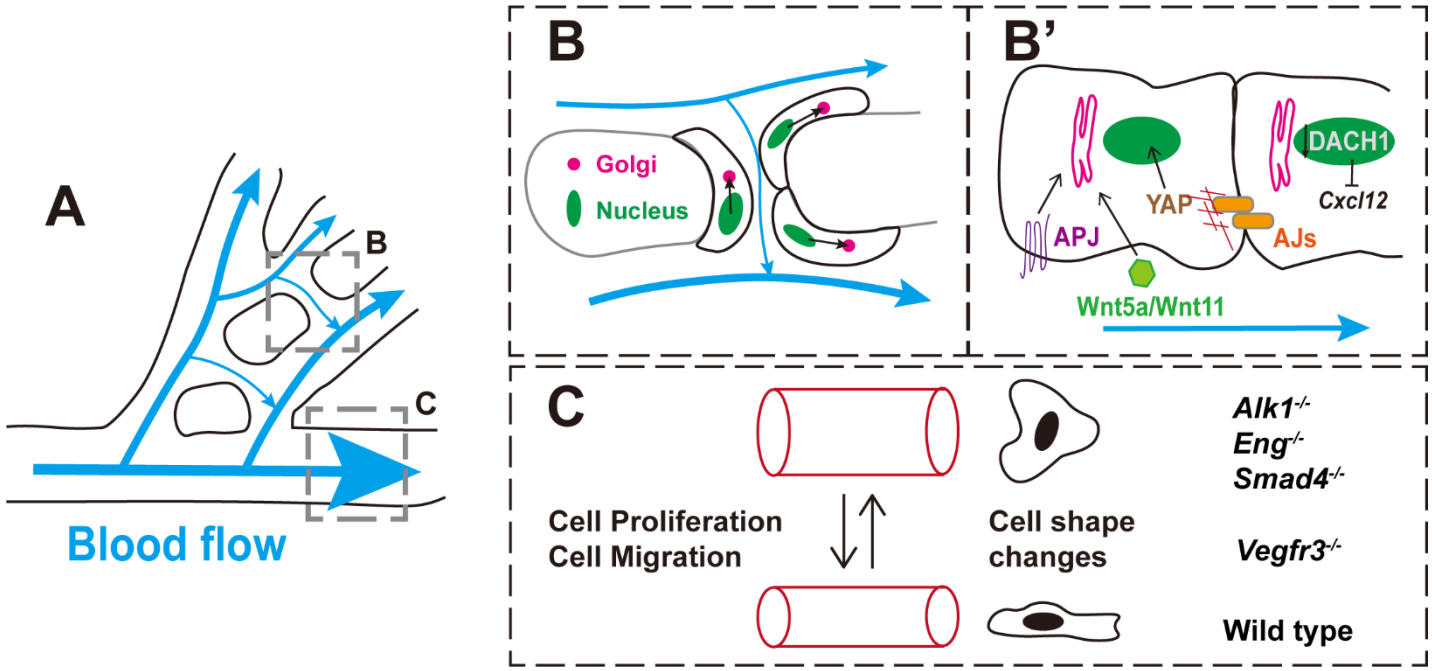

Figure 1.8 Flow-mediated endothelial cell behaviours during vascular remodelling

(**A**) Schematic illustration of a vascular plexus with various flow directions and intensities, which are indicated by blue arrows of different thickness. (**B**) Vessel pruning at a cross branch. The asymmetric shear stress between juxtaposed vessels leads to the migration of ECs away from low-flow to high-flow vessels. ECs display front-rear polarity which is indicated by the position of Golgi and nucleus. (**B'**) Regulators involved in flow-mediated front-rear polarity. Wnt5a and Wnt11 and APLNR (APJ) regulate EC polarisation against flow. High flow induces translocation of YAP to the nucleus and reduces the expression of DACH1 to stabilise cell junctions and blood vessels. (**C**) Arteries adjust their diameter in response to flow. Arteries can increase the diameter via cell proliferation and migration or decrease via cell shape changes. Deficiency in BMP signalling results in enlarged vessels due to defects in cell migration (*Alk1*$^{-/-}$), proliferation (*Smad4*$^{-/-}$), or cell shape changes (*Eng*$^{-/-}$). Loss of *Vegfr3* leads to reduction of vessel calibre.

In this chapter, I described the cellular and molecular mechanisms that are involved during angiogenesis and emphasised flow-mediated cellular behaviours in all steps of vascular morphogenesis. ECs share common behaviours such as cell polarisation and migration during sprouting and remodelling yet display reverse outcomes, suggesting different modes of EC behaviour during angiogenesis. Which biochemical and mechanical signals influence the mode of EC behaviours during sprouting and remodelling? How do ECs respond if blood flow is inhibited *in vivo*? In addition, other cellular behaviours, such as proliferation and shape changes, how do they contribute to vascular remodelling in response to flow? Answering these questions could help us to better understand the mechanisms underlying angiogenesis and to develop better therapies for cardiovascular diseases.

1.5 Hypothesis and Aims of the thesis

During embryonic development and in diseased vascular region, ECs share common cellular behaviours and signalling pathways in response to flow, including VEGF and BMP signalling and their functions in cell proliferation and migration. I aim to elucidate the importance of blood flow-induced forces in vascular remodelling *in vivo* using the zebrafish SIVP as a model. Therefore I hypothesise that…

Blood flow is essential for appropriate vascular patterning by refining local molecular signals including VEGF and BMP signalling pathways.

In the following chapters, I will address the following questions:

1. Does blood flow control EC proliferation during vascular remodelling?

2. Whether blood flow affects EC migration in a venous plexus and if so, how does it regulate this at both the whole plexus and single cell level?

3. How does a migrating sprout regress into the main plexus without compromising vascular integrity?

4. Are VEGF and BMP signalling required for SIVP remodelling and how do they instruct the associated cellular changes in the presence or absence of flow?

Chapter 2 Materials & Methods

2.1 Materials

2.1.1.1 Fish lines

Fish Line	Function	Reference
AB, London wildtype	Wild Type	European Zebrafish Resource Centre
Nacre (*mitfa*)	melanophore development defects	(Elworthy *et al.*, 2003)
Tg(fli1a:GFP)^{y1}	Endothelial GFP	(Lawson and Weinstein, 2002a)
Tg(gata1a:DsRED)^{sD2}	Erythroid cell RFP	(Traver *et al.*, 2003)
Tg(fli1a:lifeact-mClover)^{SH467}	Endothelial actin GFP	(Savage *et al.*, 2019)
Tg(fli1a:AC-tagRFP)^{SH511}	Endothelial actin RFP	(Savage *et al.*, 2019)
Tg(fli1a:nls-mCherry)^{SH550}	Endothelial nucleus RFP	Unpublished, Dr R. Wilkinson
Tg(-0.8flt1:enhRFP)^{hu5333}	Arterial EC RFP	(Bussmann *et al.*, 2010)
Tg(bre:egfp)^{pt510}	BMP responsive elemement GFP	(Laux *et al.*, 2011)
Tg(flk1:EGFP-NLS)^{zf109}	Endothelial nucleus GFP	(Blum *et al.*, 2008)
Tg(fli1:nls-EGFP)^{SH549}	Endothelial nucleus GFP	This thesis
Tg(fli1a:golgi-tagRFP);(cryaa:CFP)^{SH529}	Endothelial Golgi RFP	This thesis
Tg(fli1a:pecam1-EGFP)^{SH524}	Endothelial cell junction GFP	This thesis
Tg(hs70l:bmp4-v2a-GFP);(cryaa:CFP)^{SH600}	Expression of *bmp4-v2a-GFP* under heat-shock	This thesis
Tg(hs70l:bmpr2b-v2a-GFP);(cryaa:CFP)^{SH601}	Expression of *bmpr2b-v2a-GFP* under heat-shock	This thesis

Table 2.1 Fish lines

2.1.1.2 Buffer & Solutions

All chemicals were from Sigma-Aldrich®, unless otherwise stated. All

solutions were prepared with autoclaved MilliQ™ and were sterilised by filtration or autoclaving where appropriate.

Solutions and buffers	Ingredients
1X E3 Medium	0.17mM KCl; 5mM NaCl; 0.33mM $CaCl_2$; 0.33mM $MgSO_4$; Diluted from 10X E3 stock with 2 drops of methylene blue per litre.
1X TAE	40mM Tris-Cl, 20mM Acetate and 1mM EDTA
20X SSC (saline sodium citrate)	0.3M Na_3Citrate; 3M NaCl.
1% agarose gel	1% agarose gel in 1X TAE buffer containing 0.2-0.5µg/mL ethidium bromide or 10µl of SYBR Green per 100ml of gel.
4% paraformaldehyde (PFA)	2g paraformaldehyde per 50ml 1X PBS (4%, store at 4°C)
0.5M EDTA	For 500mL stock: 93.06g disodium EDTA in MilliQ water, pH:8.0
BCL buffer III	100mM Tris-Cl pH9.5; 50mM $MgCl_2$; 100mM NaCl; 0.1% Tween 20
Bleaching Solution	0.5X SSC; 5% Deionised Formamide; 1% H_2O_2; top up with dH_2O
Hybridization Buffer (Hybe+/+)	50% Deionised Formamide; 5X SSC; 9.2mM Citric acid; 0.1% Tween 20; tRNA (0.5mg/mL); Heparin (50mg/mL), store at -20°C
Hybridization Buffer (Hybe-/-)	50% Deionised Formamide; 5X SSC; 9.2mM Citric acid; 0.1% Tween 20, store at -20°C
Immuno B-buffer	PBST; 1% BSA; 10% goat serum; 0.8% Triton X-100
Immuno I-buffer	PBST; 1% BSA; 1% goat serum; 0.8% Triton X-100
LB	10g bactotryptone; 5g bactoyeast; 10g NaCl to 1 litre with dH_2O; pH7.0
LB agar	LB containing 15g bactoagar per litre
Maleic acid buffer (MAB)	For 500mL stock: 5.8g maleic acid, 1.5M NaCl, pH: 7.5,
MAB Blocking reagent (for *in situ*)	MAB containing 2% block reagent (from Roche)
Morpholino	1mM stock solution (~8µg/µl): 300nmol MO were dissolved in 300µl dH_2O. Sealed with parafilm and stored at room temperature.
Phosphate buffered solution (PBS)	Made up from the 10X stock (from Thermo Fisher); 150mM Phosphate buffer, pH7.2;

	0.85% NaCl.
PBST	1xPBS; 0.1% Tween 20.
PBS-T (for immuno)	PBST; 1% Triton X-100
PBS-TS (for immuno)	PBST; 10% goat serum; 1% Triton X-100
Pronase	20mg/mL stock pronase
Proteinase K	10µg/mL proteinase K in PBST
TE buffer	10mM Tris-Cl pH8.0; 1mM EDTA
Tricaine (MS222)	Stock: 4g Tricaine in 1L dH_2O (pH7, adjusted with NaOH or 1M Tris pH9); 1X working solution: 4.2ml tricaine stock in 100ml water

Table 2.2 Solutions and Buffers

2.1.1.3 Antibiotics

Antibiotic	Stock concentration	Working concentration
Ampicillin	50 mg/ml	60 µg/ml
Carbenicillin	100 mg/ml	50 µg/ml
Kanamycin	10 mg/ml	50 µg/ml
Streptomycin	10 mg/ml	50 µg/ml
Chloramphenicol	34 mg/ml	12.5 µg/ml

Table 2.3 Antibiotics

2.1.1.4 Antibodies

Name	1st or 2nd	Host species	Unit	Source	Usage
Anti-Digoxigenin-AP Fab	2nd	sheep	150U	Roche	*in situ*
pSMAD1/5 (Ser463/465)	1st	Rabbit	100µl	Cell Signalling Technology	Immuno-staining
Alexa Fluor 488	2nd	Goat anti-Rabbit	2mg/ml	Invitrogen	Immuno-staining

*1st: primary antibody; 2nd: secondary antibody

Table 2.4 Antibodies

2.1.1.5 Chemical inhibitors

AV951, DAPT, and DMH1 were dissolved in Dimethyl sulfoxide (DMSO, Sigma-Aldrich).

Compounds	Source	Function
DMSO	Sigma-Aldrich	Organic Solvent
AV951	Selleckchem (S1207)	VEGF receptor inhibitor
DAPT	Sigma-Aldrich (D4952)	Gamma secretase inhibitor- impairs Notch signalling
DMH1	Sigma-Aldrich (D8946)	BMP type I receptor inhibitor

Table 2.5 Chemical inhibitors

2.1.1.6 Morpholinos

MOs were all from Gene Tools, LLC. The working solutions see 2.2.1.19.

MO	Sequence	Blocking site	Reference
Standard Control	5'-CCTCTTACCTCAGTTACAATTTATA-3'	No target	Gene Tools, LLC
tnnt2a	5'-CATGTTTGCTCTGATCTGACACGCA-3'	TB*	(Sehnert *et al.*, 2002)
flt4	5'-CTCTTCATTTCCAGGTTTCAAGTCC-3'	TB	(Hogan *et al.*, 2009b)
gata1	5'-CTGCAAGTGTAGTATTGAAGATGTC-3'	TB	(Galloway *et al.*, 2005)
alk1	5'-ATCGGTTTCACTCACCAACACACTC-3'	SB**	(Rochon *et al.*, 2016)
bmp10	5'-AAAAGTGATTTCTGCTACCAGCCAT-3'	TB	(Laux *et al.*, 2013)
bmp10-like	5'-GCAGCAGAGAATCAGCCATGACTGC-3'	TB	(Laux *et al.*, 2013)

* Translation Blocking & ** Splice Blocking

Table 2.6 Morpholino sequence

2.1.1.7 Plasmids

2.1.1.1 Plasmids for probes

All plasmids are Ampicillin/Carbenicillin resistant.

Probe	Restriction Site	Antisense polymerase	Reference	Made by
alk1	SacII	SP6	(Roman *et al.*, 2002)	R. Wilkinson
alk3a	EcoRI	T7	(Monteiro *et al.*, 2008)	R. Wilkinson
alk3b (bmpr1ab)	PCR probe	T7	(Neal *et al.*, 2017)	Y. Chen
alk6a	EcoRI	SP6	(Monteiro *et al.*, 2008)	R. Wilkinson
alk8	EcoRI	T7	(Monteiro *et al.*, 2008)	R. Wilkinson
bmp2b	EcoRI	T3	(Kishimoto *et al.*, 1997)	R. Wilkinson
bmp4	EcoRI	T3	(Kishimoto *et al.*, 1997)	R. Wilkinson
bmp7	HindIII	T7	(Dick *et al.*, 2000)	R. Wilkinson
bmpr2a	BamHI	T7	(Monteiro *et al.*, 2008)	R. Wilkinson
bmpr2b	NotI	Sp6	(Monteiro *et al.*, 2008)	R. Wilkinson
cdh5	PCR probe	T7	(Larson *et al.*, 2004)	R. Wilkinson
flt4	EcoRI	T7	(Thompson *et al.*, 1998)	R. Wilkinson
mflt1	SacII	SP6	(Krueger *et al.*, 2011)	Y. Chen
sflt1	PstI	T7	(Krueger *et al.*, 2011)	Y. Chen
vegfaa	XbaI	T7	N/A	R. Wilkinson
vegfc	EcoRI	T7	(Hogan *et al.*, 2009a)	R. Wilkinson

Table 2.7 Probes for *in situ* hybridisation

2.1.1.2 Plasmids for mRNA expression

The following plasmids are used for *in vitro* transcription of mRNA (2.2.1.12). Stored at -80°C and thawed before use.

mRNA	Restriction Site	Sense polymerase	Reference	Made by
vegfaa$_{165}$	NotI	SP6	(Lawson *et al.*, 2002)	Y.Chen
vegfc	NotI	SP6	(Hogan *et al.*, 2009a)	Y.Chen
mTurquoise2	NotI	SP6	R. Wilkinson Lab	Y.Chen
Tol2 transposase	NotI	SP6	(Kwan *et al.*, 2007)	Y.Chen

Table 2.8 Plasmids for mRNA expression

2.1.1.3 Plasmids for Gateway® cloning

Name	Insert	Size	Reference	#
p5E-fli1a	2kb chimeric fli1ep enhancer/promoter fragment; drives endothelial expression	4.6kb	(Villefranc *et al.*, 2007)	3
p5E-hsp70l	1.5 kb hsp70l promoter for heat-shock induction	4.2kb	(Kwan *et al.*, 2007)	334
pME-golgi-tagRFP	894 bp fragments containing a cDNA of human B4GALT1 fused to RFP	3.4kb	This thesis, Y.Chen	330
pME-nlsEGFP	nuclear-localized EGFP	3.3kb	(Kwan *et al.*, 2007)	56
pME-bmp4	*bmp4* full length mRNA	3.7kb	This thesis, Y. Chen	332
pME-bmpr2b	bmpr2b full length mRNA	5.9kb	This thesis, Y. Chen	335
p3E-polyA	SV40 late polyA signal	2.8kb	(Kwan *et al.*, 2007)	80
p3E-v2a-EGFP	V2A fusion with EGFP	3.7kb	Unpublished, R. Wilkinson	52
pDestTol2pA2	pDestTol2pA with ~2 kb extraneous sequence removed	5.9kb	(Kwan *et al.*, 2007)	10

pDestTol2cryCFP	destination vector with CFP driven by *aA-crystallin* promoter	7.3kb	(Hamilton *et al.*, 2020)	120
pDONR221	middle donor vector; attP1-P2 flanking chlor/ccdB cassette	4.8kb	Invitrogen	N/A
pCS2FA-transposase	for *in vitro* transcription of capped Tol2 transposase mRNA plus polyA signal (2kb)	6kb	(Kwan *et al.*, 2007)	9

# indicates the stock number in Wilkinson lab.

Table 2.9 Plasmids for Gateway® cloning

2.1.1.4 Primers & cDNA geneblocks®

All primers were synthesised by Integrated DNA Technologies™ (IDT). Primers were resuspended with dH_2O at stock concentration of 100µM. The Golgi cDNA gene block was resuspended in TE pH8 at 20ng/µl and incubated at 55°C for 20s. Stored at -20°C.

Primer name	Primer sequence
B4GALt1-tagRFPattb1F	5’-GGGGACAAGTTTGTACAAAAAAGCAGGCTTCATGAGGCTTCGGGAGCCG -3’
B4GALt1-tagRFPattb2R	5’-GGGGACCACTTTGTACAAGAAAGCTGGGTCTCAATTAAGTTTGTGCCC -3’
Zbmp4-F	5’- ATGATTCTTGGTAATCGAATGC -3’
Zbmp4-R	5’- GCGGCAGCCACACCCCTC -3’
Zbmp4-attB1F	5’-GGGGACAAGTTTGTACAAAAAAGCAGGCTTCATGATTCCTGGTAATCGAATGC -3’
Zbmp4-attb2R	5’-GGGGACCACTTTGTACAAGAAAGCTGGGTCGCGGCAGCCACACCCCTC -3’
Bmpr1ab-F (alk3b)	5’- TGTCATGTAGCACTCTCTGC -3’
Bmpr1ab-T7-R (alk3b)	5’- TAATACGACTCACTATAGGGTGAGCTGCAATTCGGTGGCC -3’
Bmpr2bclaI-F	5’- ATCGATATGAGAGTGCGGATCCTAAACC -3’
Bmpr2blongxh	5’ -

ol (no stop) (for repairing)	CTCGAGCAGGCAGGTCATATCTGGAGGATCGGAGGTCAGAGTAGCT GTTGCTGTTCCTCCGCCGACCAAAAACACGGCGATGCTGGACTTTG ATTGG - 3’
Bmpr2b sequencing primers	F1: 5’ - TGGCGGTAAATGGCCCGCGATGGCT -3’ F2: 5’ -GAATGGCACCTACAGATTCTGCTGCTGC -3’ F3: 5’ -TCACTGACCAGAGGACTGGCCTATCTG -3’ F4: 5’ -TCACTGACCAGAGGACTGGCCTATCTG -3’ F5.5: 5’ -GTGCTGGAGTGGTCGTAGTA -3’ F6: 5’ -GAAGACCAGAGCGGCCAAACTCACT -3’
Golgi cDNA block (B4Galt1 1-60TagRFP)	5’ - ATGAGGCTTCGGGAGCCGCTCCTGAGCGGCAGCGCCGCGATGCCAG GCGCGTCCCTACAGCGGGCCTGCCGCCTGCTCGTGGCCGTCTGCGC TCTGCACCTTGGCGTCACCCTCGTTTACTACCTGGCTGGCCGCGAC CTGAGCCGCCTGCCCCAACTGGTCGGAGTCTCCACACCGCTGATGG TGTCTAAGGGCGAAGAGCTGATTAAGGAGAACATGCACATGAAGCT GTACATGGAGGGCACCGTGAACAACCACCACTTCAAGTGCACATCC GAGGGCGAAGGCAAGCCCTACGAGGGCACCCAGACCATGAGAATCA AGGTGGTCGAGGGCGGCCCTCTCCCCTTCGCCTTCGACATCCTGGC TACCAGCTTCATGTACGGCAGCAGAACCTTCATCAACCACACCCAG GGCATCCCCGACTTCTTTAAGCAGTCCTTCCCTGAGGGCTTCACAT GGGAGAGAGTCACCACATACGAAGACGGGGGCGTGCTGACCGCTAC CCAGGACACCAGCCTCCAGGACGGCTGCCTCATCTACAACGTCAAG ATCAGAGGGGTGAACTTCCCATCCAACGGCCCTGTGATGCAGAAGA AAACACTCGGCTGGGAGGCCAACACCGAGATGCTGTACCCCGCTGA CGGCGGCCTGGAAGGCAGAAGCGACATGGCCCTGAAGCTCGTGGGC GGGGGCCACCTGATCTGCAACTTCAAGACCACATACAGATCCAAGA AACCCGCTAAGAACCTCAAGATGCCCGGCGTCTACTATGTGGACCA CAGACTGGAAAGAATCAAGGAGGCCGACAAAGAGACCTACGTCGAG CAGCACGAGGTGGCTGTGGCCAGATACTGCGACCTCCCTAGCAAAC TGGGGCACAAACTTAATTGA – 3’

Table 2.10 Primers

2.2 Methods

2.2.1.1 Molecular biology protocols

2.2.1.2 Gateway® Cloning

The Multi-Site Gateway® cloning technique (Invitrogen) allows rapid generation of modular transgene constructs for microinjection in zebrafish.

Three entry vectors (5' entry, middle entry, and 3' entry) and a destination vector were required to make up the final transgene construct via recombination (Figure 2.1). In this thesis, 5' entry vector usually contains promoter sequence (e.g. *fli1a* promoter), middle entry vector contains target genes with or without fused fluorophore (e.g. *golgi-tagRFP*), and 3' entry vector contains fluorophore and/or SV40 late polyA tail. To generate an entry vector (all pMEs in this thesis), target gene cassette was cloned into donor vector to generate an entry vector via BP reaction (2.2.1.2.1). Target gene fragment could also be ligated into an empty donor vector (i.e. pME-MCS) using the same restriction enzyme sites, to generate an entry vector (2.2.1.2.2).Different entry vectors were subsequently assembled into any destination vector via LR reaction.

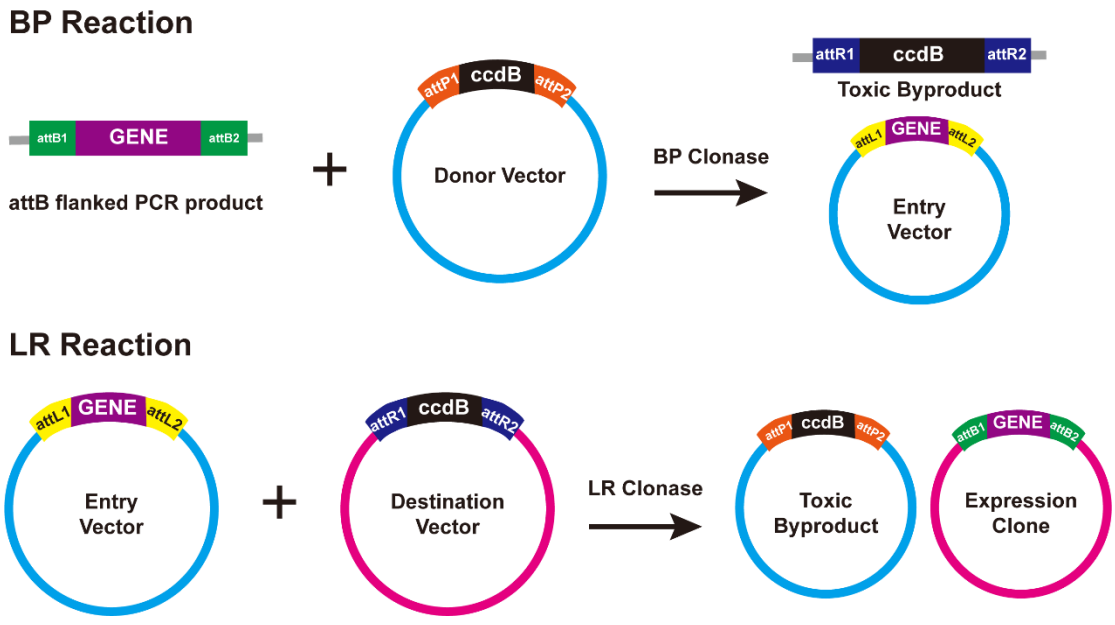

Figure 2.1 Gateway® Cloning to generate expression clone

Schematics show the principle of Gateway® cloning. The BP reaction creates an attL-flanked entry clone and the LR reaction creates an expression clone for generation of transgenic line.

2.2.1.2.1 Generation of entry vector via BP reaction

To generate an entry vector with desired gene fragment (pME vector in this thesis), attB1 and attB2 sites were added to the 5' and 3' end of the gene fragment, using primers containing attB sites (Table 2.10) and Phusion® PCR amplification (2.2.1.4). The PCR products were then purified via gel extraction (2.2.1.7). The attB-flanked gene fragment was cloned into a donor vector (pDONR221) containing attP recombination sites via BP reaction. An equimolar amount of the appropriate pDONR221 and purified PCR product (commonly 50-100 femtomoles) are combined with 6µl TE buffer Ph8.0 and 2µl BP Clonase II enzyme mix in a final volume of 10µl. The reaction was incubated at 25°C overnight. Following the BP reaction, a resultant pME vector was generated.

2.2.1.2.2 Generation of entry vector via ligation

In the case of construct pME-bmpr2b, the full length *bmpr2b* element was excised from a pGemT-easy vector via restriction enzyme sites, and was ligated into a middle entry vector (pME-CS2) containing multiple cloning sites from pCS2+ which was also digested with the same enzymes (see 2.2.1.19.5). To determine whether the insert has been successfully ligated into the plasmid and whether this was positioned in correct orientation, the plasmid was diagnostically digested with restriction enzymes (see 2.2.1.19.5). Cutting sites flanking either site of the insert were used to determine the existence of the insert, and sites that cut within the target gene and created two bands of distinct

sizes were used to determine orientation of the insert (see 2.2.1.19.5).

2.2.1.2.3 Generation of transgene construct via LR reaction

Sequencing of target genes within the newly generated entry vector were performed prior to LR reaction. All entry clones (5', middle, and 3') and destination vectors were diluted to 20 femtomoles, prior to addition to a 10µl reaction mix. Equimolar amounts of entry vectors and destination vector are combined with 4µl TE buffer Ph8.0 and 2µl LR Clonase II Plus enzyme mix in a final volume of 10µl. The reaction was incubated at 25°C overnight.

2.2.1.2.4 Transformation and selection of clones

Following the BP or LR reaction, the reaction mix was transformed into chemically competent cells to amplify plasmids (see 2.2.1.9). Entry clones are kanamycin-resistant and destination vectors are ampicillin-resistant. Therefore, BP reaction were plated onto kanamycin plates and LR reactions onto ampicillin plates. Single clones (usually 6 clones) were picked and grown in LB broth containing appropriate antibiotics. Translucent clones could be observed in plates from LR reaction (this does not apply to BP reaction) and these ones usually had higher rates of successful recombination than opaque colonies. Plasmids were then purified from the competent cells and confirmed by restriction enzyme digestion and/or sequencing.

2.2.1.2.5 **Assembling sequences of transgene plasmids**

To generate a circular graphic map of the transgene plasmid, application 'ApE' (A plasmid Editor, by M. Wayne Davis) was used. To perform *in silico* assembly, the three entry clones and the destination clone were opened in ApE, and the Tool>Recombination Tool was selected, followed by selection of 'Multi-site LR reaction (4-1-2-3)'. The resulting predicted gene map was employed to select restriction enzyme sites.

2.2.1.3 **Whole embryo RNA extraction**

Approximately 100 staged embryos were selected for making RNA stocks for RT-PCR. Embryos were homogenised in 1 ml Trizol® solution by pipetting up and down for approximately 1 minute and incubated at RT for 5 minutes. 200µl of chloroform was added and mixed by shaking the tube several times before spinning at 12,000g, 4°C for 15 minutes. The upper aqueous phase was removed to a fresh tube and 500µl isopropanol was added and mixed. Samples were incubated for at RT for 10 minutes and spun again at 13,300 RPM, 4°C for 15 minutes. Supernatant was gently removed without dislodging the pellet, which was then washed with 500µl of 75% ethanol and centrifuged at 13,300RPM, 4°C for 5 minutes. Solutions were removed and pellets were then resuspended in 100µl MiliQ for RNA stocks.

2.2.1.4 **RT-PCR**

RT-PCR was performed to generate the *bmp4* full length coding sequence for pME or amplification of *in situ* probes, The SuperScript™III One-Step RT-PCR System from Invitrogen was used for RT-PCR, which was performed according to manufacturer's guidelines. RNA template was generated from AB embryos at 26hpf, using RNA extraction (2.2.1.3). The PCR products were run on a 1% gel with SYBR Green. Bands with desired size were excised and purified via gel extraction.

2.2.1.5 **Phusion® PCR**

To generate *golgi-tagRFP* and *bmpr2b* elements for PME, Phusion® (NEB) PCR was performed, which was ideal for long amplicons. Primers used were listed in Table 2.10. The Phusion® PCR was performed according to manufacturer's guidelines. The template DNA of *golgi-tagRFP* was a synthesised gene block and 10ng of which was added in a 20µl reaction. To repair the C-terminal of *bmpr2b*, a long reverse primer containing the missing sequence was used (Table 2.10). The *bmpr2b* plasmid (without C-terminal) was used as template (20ng per reaction). Since the repair primers were long, 3% DMSO was added to denature long/complex primers and reduce their annealing temperature. The PCR products were run on a 1% gel with SYBR Green (Invitrogen). Bands with desired size were excised and purified via gel extraction.

2.2.1.6 Gel electrophoresis

PCR samples were loaded in 1X loading buffer alongside suitable DNA ladders (100bp or 1kb DNA ladders, NEB). Samples were visualised by electrophoresis on 1% agarose gel (Table 2.2) containing ethidium bromide or SYBR Green (Invitrogen), running at 120V until gels were resolved.

2.2.1.7 Gel extraction and PCR purification

Gel extraction was performed to extract target DNA bands. Selected DNA bands were excised using a clean scalpel and transferred to a pre-weighed 2ml tube. The excised gel pieces in the tube were weighed again to determine the volume of solutions needed to dissolve the gels. QIAquick® Gel Extraction Kit (QIAGEN) was used to extract samples in agarose gels and performed as per manufacturer guidelines.

When gel extraction was unnecessary, PCR purification was carried out using QIAquick® PCR Purification Kit according to manufacturer's instructions.

2.2.1.8 DNA ligation

DNA ligation favoured a insert:vector molar ratio at 3:1. The appropriate amount of PCR product (insert) to include in the ligation reaction was calculated as (ng of vector * kb size of insert) / (kb size of vector) * 3 = ng of insert. A 20µl reaction was set up containing 1µl T4 ligase, 2µl 10X T4 ligase buffer, appropriate amount of vector and insert, and topped up with MilliQ water. T4

ligase and buffer were obtained from pGEM®-T Easy vector system. Ligation was performed at 4°C overnight.

2.2.1.9 Transformation of competent cells

50µl competent *Escherichia coli* (*E. coli*) cells were thawed on ice for 10mins before addition of 1-3µL plasmid sample or ligation mix. The mixture was incubated on ice for 30 minutes followed by a 30 second heat shock at 42°C. The reaction mix was then immediately put on ice for 5 minutes. Subsequently, 950µl of LB broth was added into mixture directly with gentle mixing. The culture was then incubated in shaking for at least 1 hour before plating out on LB agar plates, which contained appropriate antibiotics. LB agar plates were incubated overnight at 37°C.

Single colonies were picked using a sterile wooden toothpick which was then placed into a bottle of 6ml LB broth for mini culture. For midi culture, 1ml of mini culture was added to a beaker of 100ml LB. The LB broth contained appropriate antibiotics and the cultures were incubated overnight at 37°C, shaking.

2.2.1.10 Mini and midi prep isolation of plasmid DNA

Plasmid DNA was isolated from cultures using a QIAprep Spin Mini Kit (QIAGEN) for minipreps or using a NucleoBond® Xtra Midi Kit (Machery-Nagel) for midipreps, as per manufacturer's guidelines. The concentrations of purified

plasmids were tested using NanoDrop™.

2.2.1.11 *In situ* hybridisation probe synthesis

Probes were made either by transcription from plasmids or synthesis from PCR. Antisense RNAs for *in situ* hybridisation were transcribed from linear plasmid templates (2.2.1.13), using T3, T7 and SP6 RNA polymerases (Table 2.7). 1µg of linearised plasmid or PCR product was used along with 2µl DIG-UTP labelling mix (Roch), 4µl 5X transcription buffer (Promega), 0.5µl RNAse inhibitor (Promega) and 1µl of appropriate polymerase (Promega). The reaction was made up to 20µl with dH_2O.The transcription reaction was incubated at 37°C for 2 hours.

Following transcription, 1µl of reaction was removed to a new tube and saved for later gel electrophoresis. Linearised plasmid template was removed by digestion with DNase I (NEB) for 15 minutes in 37°C water bath. Pre- and Post- DNase I digestion RNA were checked on 1% gel to confirm digestion of DNA template. Subsequent to successful removal of template, reaction was stopped by addition of 1µl of 0.5M EDTA and 80µl MilliQ water into the mixture.

Labelled probe was precipitated with 33µl of 10M NH_4Ac and 350µl of ice cold 100% ethanol at -20°C for at least 2 hours. The reaction was then centrifuged for 30 minutes at 4°C, followed by removal of supernatant and 70% ethanol wash by centrifugation for 15 minutes at 4°C. The resultant pellet was air dried and resuspended in 20µl MilliQ and stored at -20°C. A post-

precipitation sample was run on 1% gel to estimate quantity and integrity of the RNA probe.

In situ probes from PCR templates were generated via RT-PCR amplification (2.2.1.4), followed by gel extraction (2.2.1.7) and transcription as described above.

2.2.1.12 *In vitro* synthesis of mRNA for injection

Full length mRNA for injection was synthesised using plasmid templates (Table 2.8). Plasmids were linearised via enzyme digestion (see 2.2.1.13) and purified via precipitation. Transcription was performed using mMESSAGE mMachine™ Transcription Kit (Invitrogen) as per manufacturer's guidelines. Following transcription, 1µl of reaction was removed and 1µl DNase I was added to digest DNA template. Pre- and post-DNaseI-treated mRNA were analysed via gel electrophoresis to assay for successful transcription and template removal. Recovery of the RNA was performed using Phenol extraction method. 115µl MilliQ and 15µl Ammonium Acetate Stop Solution (provided by the transcription kit) were added into the mixture. Equal volumes (150µl) of acidic phenol/chloroform (Invitrogen) were added and the tubes were vortexed before centrifugation at 13,300rpm for 5 minutes. The upper, aqueous phase containing the RNA was collected and subsequently re-extracted as above with one volume of chloroform. RNA was precipitated by adding one volume of isopropanol. The mixture was vortexed thoroughly and then chilled at -20°C for

15mins, followed by 15-minute centrifugation at maximum speed to pellet the RNA. The resultant pellet was air dried and resuspended with 20µl MilliQ. 1µl of the RNA was run on a 1% gel to estimate quantity and integrity (a certain amount of RNA would be lost after phenol extraction). The exact concentration of the RNA was tested using NanoDrop™. The mRNA was then aliquoted to small amount and stored at -80°C for future use.

2.2.1.13 Restriction enzyme digestion

All enzymes and digestion buffers used in this thesis were from New England Biolabs (NEB). Restriction enzyme digestion was set up as per manufacturer guidelines. Generally, 5µl of miniprep was used in a 50µl digestion reaction. For plasmid linearization (for *in situ* probe or full-length mRNA), 10µg of plasmid was used. The volume of the plasmid should be less than 25% of total reaction volume. If the digested plasmids were needed for other experiments, restriction enzymes were removed via Phenol/Chloroform extraction and precipitation (2.2.1.14).

2.2.1.14 Phenol/Chloroform extraction of DNA

To remove restriction enzymes, the digestion reaction was made up to 400µl with MilliQ. DNA was then extracted by adding 400µl of phenol: chloroform: Isoamylalcohol (25:24:1), followed by vortexing and centrifugation for 5 minutes at 4°C. The supernatant was removed to a new tube prior to

addition of 400µl chloroform:isoamylalcohol (24:1), followed by vortexing and centrifugation for 5 minutes at 4°C. The supernatant was again removed to a new tube and 40µl of 3M sodium acetate (pH5.2) and 1ml of 100% ethanol were added, followed by vortexing and incubation for 30mins at -20°C. Samples were centrifuged at 13,300 rpm and 4°C for 30 minutes. After centrifugation, the supernatant was removed, and the DNA pellet was washed with 70% ethanol and centrifuged for 5 minutes at maximum speed. The pellet was then air dried and resuspended in 20µl MilliQ.

2.2.1.15 Determination of DNA and RNA concentrations

The concentrations of DNA and RNA solutions were tested using a Thermo Scientific™ NanoDrop™ to monitor their UV absorption at 260nm. Purity was measured as a ratio of corrected absorbance at 260nm to 280nm (~1.8 for DNA and ~2.0 for RNA).

2.2.1.16 Determination of morpholino concentration

Determination of morpholino concentration was performed as recommended in the Gene Tools protocol (by Dan Arbogast). The concentrations of morpholinos were calculated using Thermo Scientific™ NanoDrop™ to monitor their UV absorption at 265nm. 5 µl of the Morpholino solution was diluted into 95 µl of 0.1 N HCl (20X dilution) and NanoDrop™ was blanked with the same diluent. Parameters of NanoDrop™ software were set

as follows: sample type-other, λ at 265nm, constant = MW * 1000 / Molar Abs (provided in product information sheet). To calculate the concentration of the original morpholino solution, the reading in the NanoDrop™ was multiplied by the dilution factor of 20X. To calculate the millimolar concentration of the morpholino solution, divide the concentration by MW: (ng/µl) / MW = mM.

2.2.1.17 Zebrafish protocols

2.2.1.18 Fish maintenance

Adult fish were maintained according to Home office guidelines. A cycle of 14-hour light and 10-hour dark was given and fish were housed at a constant temperature of 28.5°C. Breeding was performed either by pair mating or marbling (group-laying). Zebrafish embryos younger than 5.2 dpf were kept in petri dishes, with numbers not exceeding 100 per plate and were kept in 28.5°C incubator. All zebrafish experiments were approved by the Home Office and were conducted according to the stipulations set out in project licence 70/8388.

2.2.1.19 Generation of transgenic lines

Constructs used to generate transgenic lines in this thesis were made by Gateway® cloning (2.2.1.2).

2.2.1.19.1 **Endothelial Golgi reporter line *Tg(fli1a:golgi-tagRFP); (cryaa:CFP)^{SH529}***

The synthesized *golgi-tagRFP* gene fragment contains a cDNA encoding amino acids 1–60 of the human β-1, 4-galactosyltransferase1 (B4GALT1) (Kwon *et al.*, 2016), which is mainly localised to the *trans* Golgi network (Cole *et al.*, 1996), and was fused to tagRFP fluorescent protein. *attB* sites were added to the gene fragment via Phusion® PCR using primers B4GALt1-tagRFPattb1F and B4GALt1-tagRFPattb2R (Table 2.10) and subsequently cloned into a middle entry vector via BP reaction (2.2.1.2.1). Gateway® cloning was performed to combine a 5' entry vector containing the *fli1a* promoter and a 3' entry vector containing a polyA sequence (Table 2.9). Since the Golgi is small and RFP expression would be difficult to detect using a stereo-fluorescent microscope, these entry vectors were cloned into a destination vector containing *cryaa:CFP* element which act as a dominant transgene marker and drives zebrafish CFP in lens under *aA-crystallin* promoter (Berger and Currie, 2013). The *fli1a:golgi-tagRFP;cryaa:CFP* plasmid (#331 in Wilkinson database) along with *Tol2* mRNA were injected into *Tg(flk1:EGFP-NLS)^{zf109}* or *Tg(fli1:nls-GFP)^{SH549}* embryos which expressed green endothelial nuclei.

Embryos were sorted for blue eye under fluorescent microscope and the *cryaa:CFP*+ ones were moved to light-sheet microscope to sort for red fluorescent expression adjacent to GFP+ nuclei (Figure 2.2). Potential founders were outcrossed for the next generation (F1) to establish stable transmission

of target genes. The desired F1 embryos were raised and this transgenic line was designated *Tg(fli1a:golgi-tagRFP); (cryaa:CFP)*^{SH529}.

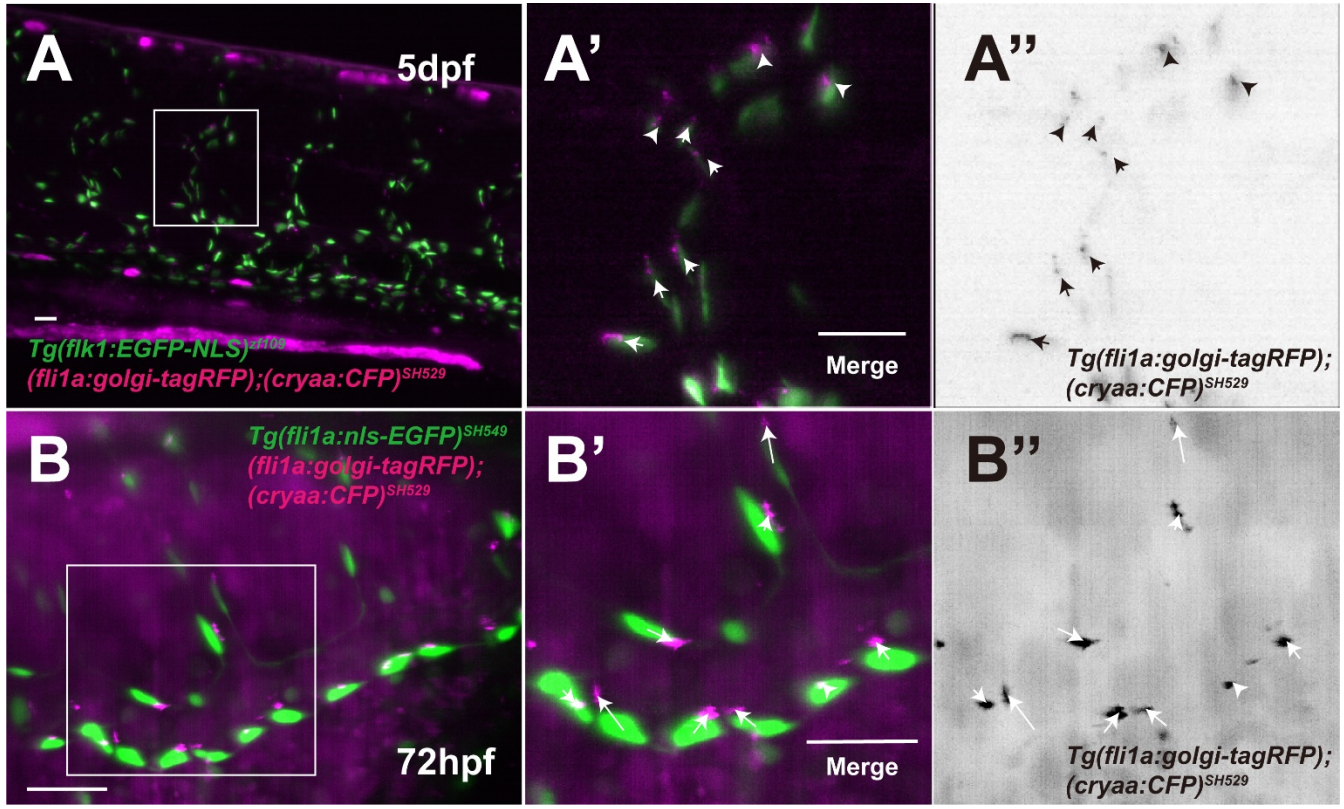

Figure 2.2 *Tg(fli1a:golgi-tagRFP); (cryaa:CFP)^{SH529}* labels endothelial Golgi apparatus.

Tg(fli1a:golgi-tagRFP);(cryaa:CFP)^{SH529} embryos display endothelial RFP fluorescence at 5dpf in the ISVs (**A**) or at 72hpf in the SIVP (**B**). A' and A'' are enlarged from A. B' and B'' are enlarged from B. Arrows indicate directions from nucleus to Golgi apparatus. GFP+ endothelial nuclei are driven by either *flk1* (A) or *fli1a* promoter (B). Scale bar: 20μm.

2.2.1.19.2 **Endothelial nucleus reporter line *Tg(fli1a:nls-EGFP)^{SH549}***

The endothelial nucleus reporter line *Tg(flk1:EGFP-NLS)^{zf109}* displayed very low expression in the SIVP, therefore it was necessary to generate an endothelial nucleus line with a stronger promoter that drives expression in the SIVP, for example *fli1a*. Gateway® entry vectors to make *fli1a: nls-EGFP* were present and ready to use in the lab, including p5E-fli1a, pME-nlsEGFP, and p3E-polyA (Table 2.9). The *fli1a:nls-EGFP* plasmid (#338 in Wilkinson database) along with *Tol2* mRNA were injected in Nacre embryos. Embryos expressing *fli1a:nls-EGFP* were raised and F1 progeny was designated *Tg(fli1a:nls-EGFP)^{SH549}* (Figure 2.3).

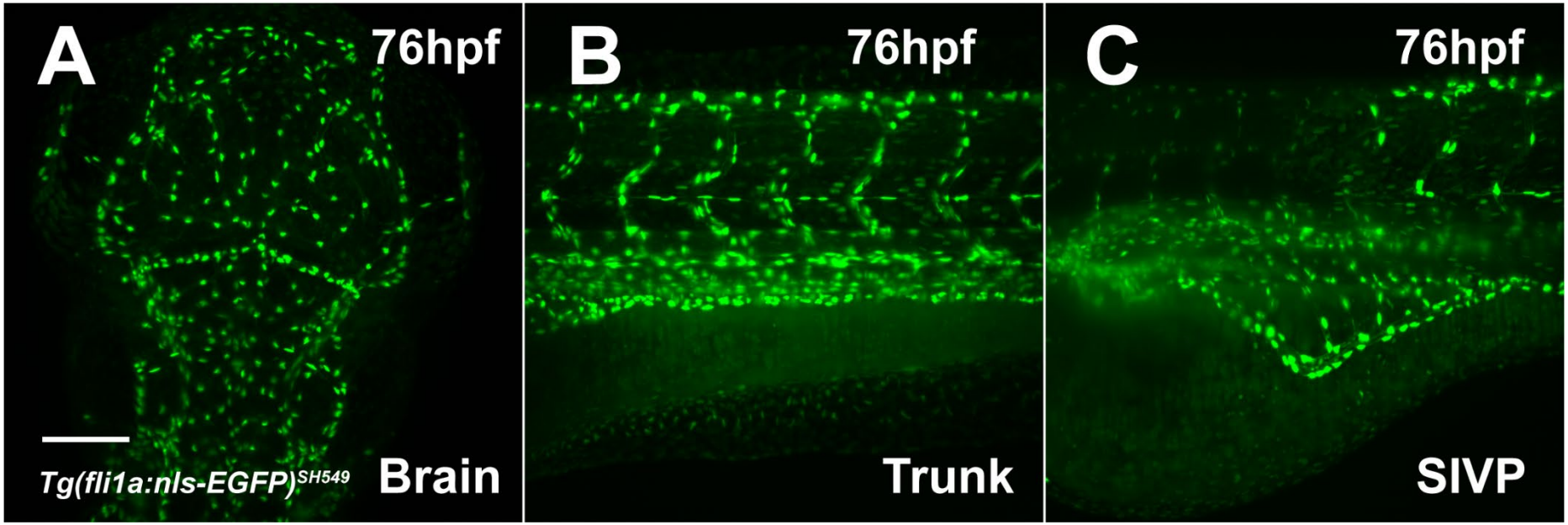

Figure 2.3 The novel transgenic line *Tg(fli1a:nls-EGFP)^{SH549}* labels the endothelial nucleus.

Tg(fli1a:nls-EGFP)^{SH549} embryo displays endothelial EGFP fluorescence at 76hpf in the blood vessels of brain (**A**), trunk (**B**), and the SIVP (**C**). Scale bar: 100μm.

2.2.1.19.3 **Endothelial cell junction reporter line *Tg(fli1a:PECAM1-EGFP)^{SH524}***

The *fli1:PECAM1-eGFP* plasmid (#328 in Wilkinson database) was kindly provided by Mochizuki's lab (Ando *et al.*, 2016) and was injected along with *Tol2* mRNA into *nacre* zebrafish. Embryos which exhibited ring-like expression at intercellular junctions were sorted and raised. Potential founders were raised and out crossed to produce F1 progeny. Although this line displayed clear intercellular junctional expression in ECs of the ISVs, the expression within the SIVP was optically obscured by the background autofluorescence of the yolk ball, while the expression of *pecam1-EGFP* was relatively weak, even when laser power was set as high as 60% (Figure 2.4B). Therefore, this line was not used to investigate EC junctional behaviour in the SIVP in this thesis.

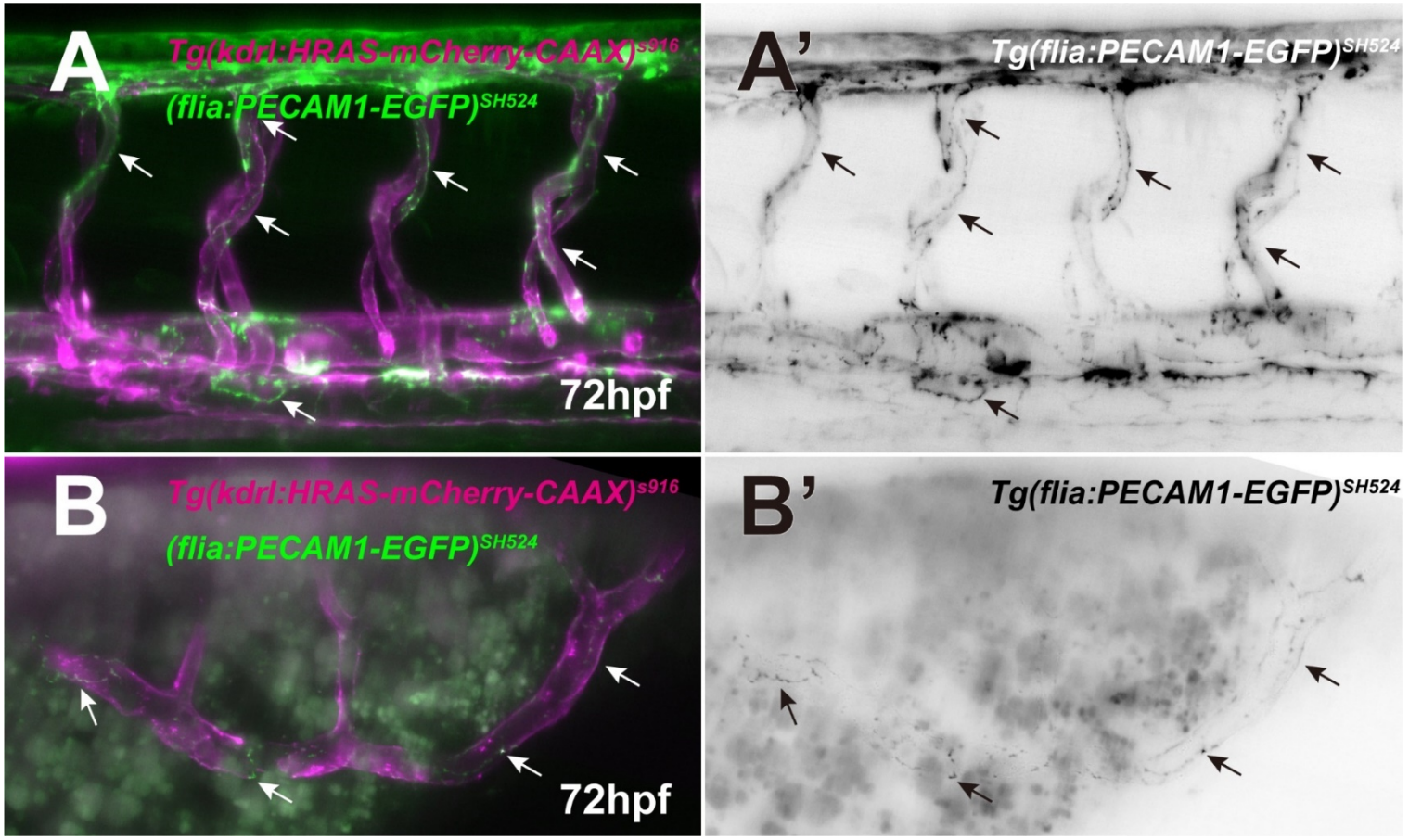

Figure 2.4 *Tg(fli1a:PECAM1-EGFP)^{SH524}* labels endothelial PECAM1 at cell junctions.

Tg(fli1a:pecam1-EGFP)^{SH524} embryo display endothelial EGFP fluorescence at 72hpf in the ISVs (**A**) and the SIVP (**B**). Arrows indicate ring-like regions of high PECAM1 density, in regions likely to be cell boundaries. *Tg(kdrl:HRAS-mCherry-CAAX)^{s916}* labels endothelial membrane in RFP.

2.2.1.19.4 **Generation of a line for conditional activation of *bmp4, Tg(hs70l:bmp4-v2a-GFP); (cryaa:CFP)^{SH600}***

Full length *bmp4* mRNA was generated via RT-PCR using primers Zbmp4-attB1F and Zbmp4-attB2R (Table 2.10) and cloned into middle entry vectors. The heat shock promoter *hsp70l* was inserted in 5' entry vector (Kwan *et al.*, 2007) to drive *bmp4* expression conditionally. *GFP* was fused to *bmp4* as an indicator of successful expression of *bmp4* under heat shock, and was separated by a 'self-cleaving' viral 2A (v2a) site (Szymczak *et al.*, 2004) to avoid potential interference from GFP during Bmp4 protein folding. For easy sorting and raising of embryos without performing heat shock, these entry vectors were assembled via Gateway® cloning into a destination vector containing *cryaa:CFP* element to generate blue eyes. The construct *hsp70l:bmp4-v2a-GFP;cryaa:CFP* (#333 in Wilkinson database) was injected along with *Tol2* mRNA in Nacre embryos. Blue-eyed founders were raised and out crossed to obtain F1 progenies. To characterise effectiveness of the transgene induction, a portion of the embryos from the same cross were heat shocked to determine GFP expression, followed by fixation and *in situ* hybridisation of *bmp4* mRNA. Heat-shock of embryos at dome stage led to mortality of the embryos before 24hpf. Embryos heat-shocked at 24hpf or 48hpf exhibited GFP+ expression in somites. The remaining embryos whose siblings showed GFP+ expression and increased *bmp4* expression by *in situ* (Figure5.9E) were raised, and the line

was designated *Tg(hs70l:bmp4-v2a-GFP); (cryaa:CFP)*^{SH600}.

2.2.1.19.5 Generation of a line for conditional activation of *bmpr2b*, *Tg(hs70l:bmpr2b-v2a-GFP); (cryaa:CFP)*^{SH601}

The *bmpr2b* expressing plasmid was kindly provided by Rui Monteiro's lab (Monteiro *et al.*, 2008). The plasmid was sequenced (primers see Table 2.10) and displayed a small missing piece of C-terminal sequence, therefore it was repaired via Phusion® PCR with primers, Bmpr2bclaI-F and Bmpr2blongxhoI (no stop), containing the missing sequence as well as restriction sites (ClaI & XhoI) (Table 2.10). The repaired full length *bmpr2b* (3216bp) was incubated in the presence of Taq polymerase at 72°C (A-tailing) and ligated into pGemT-easy vector. The ligated vector was amplified via transformation of competent *E. coli* cells. The *bmpr2b*-pGemT vector (#336 in Wilkinson database) was digested with ClaI, XhoI and PvuI (this would only cut within the vector, to distinguish ~3kb bmrp2b and ~3kb vector) enzymes to separate *bmpr2b* full length sequence from the vector. pME and PCS2+ vectors were digested with ClaI and XhoI enzymes, followed by T4 ligation of *bmpr2b* to generate pME-bmpr2b (#335) for transgenesis and PCS2-bmpr2b (#339) for mRNA expression, respectively. Subsequently, the ligated pME-bmpr2b plasmid was amplified via miniprep culture and was again extracted from *E. coli* cells. To determine whether *bmpr2b* was successfully inserted into pME, the plasmid was cut with XhoI and ClaI and run on a gel to visualise the existence of bmpr2b

band. To determine the orientation of the inserted *bmpr2b*, the plasmid was also digested with ClaI and SacI which cuts asymmetrically in the plasmid.

The correctly oriented pME-bmpr2b was sequenced, and a clone with verified sequence of full length *bmpr2b* was recombined with p5E-hsp70l and p3E-v2a-EGFP into pDestTol2cryCFP vector. The final product was injected along with *Tol2* mRNA into Nacre embryos. Blue-eyed founders were raised and out crossed to obtain F1 progenies. To characterise the transgenic line, a portion of the embryos from the same cross was heat shocked to determine GFP expression and phenotype of *bmrp2b* overexpression. The remaining embryos whose siblings showed GFP^{+} expression and ectopic ISVs (Figure5.8C) were raised, and the line was designated *Tg(hs70l:bmp4-v2a-GFP); (cryaa:CFP)*^{SH600}.

2.2.1.20 Morpholino, mRNA and plasmid injections

Protocol was adapted from (Rosen *et al.*, 2009). Individual adult pairs were mated and separated by a divider which would be removed before injection to ensure accurate timing of fertilisation. Freshly laid embryos were immediately transferred to injection apparatus once collected and were sorted against a glass slide in a petri dish. Morpholinos (Table 2.6) or capped mRNA (Table 2.8) were loaded in the needle using Microloader tips (Eppendorf). The capillary needle was then broken at the tip with forceps and connected to injector (Pneumatic PicoPumps PV820). The injection pressure was adjusted, and the

liquid drops were measured using Graticules Optics® covered with mineral oil (Sigma), to a volume of 0.5nl (=0.1mm). Embryos were injected in the yolk sac/ the embryonic cell prior to/at one-cell stage and allowed to develop in the 28.5°C incubator. Each corresponding experiment was repeated at least three times (i.e. freshly made-up injection solutions at three different days) and each repeat had approximately 100 embryos for each group. The following table (Table 2.11) displays the working solutions used in microinjection.

Molecule	**Stock conc.**	**Injection solution**	**Final Mass/ embryo**
***control* MO**	1mM	Follow experimental group	
***tnnt2a* MO**	1mM	10X dilution, inj. 1nl	~0.8ng
***flt4* MO**	1mM	10X dilution, inj. 1nl	~0.8ng
***gata1* MO**	1mM	10X dilution, inj. 1nl	~0.8ng
***tnnt2a* + *flt4* MO**		5X dilution each, combined equal volume & inj. 1nl	~0.8ng each
***gata1* + *flt4* MO**		5X dilution each, combined equal volume & inj. 1nl	~0.8ng each
***alk1* MO**	1mM	3.3X dilution, inj. 1nl	~2.5ng
***bmp10* MO**	2mM	Co-inject: 4µl bmp10 stock + 1µl bmp10-l stock, inj. 1nl	~14ng
***bmp10-like* MO**	2mM		~3ng
***mTQ2* mRNA**	~1µg/µl*	Follow experimental group	
***vegfaa*$_{165}$ mRNA**	~1µg/µl	200ng/µl, inj. 1nl	200pg
***vegfc* mRNA**	~1µg/µl	400ng/µl, inj. 1nl	400pg
Gateway® plasmid	200ng/µl	Co-inject mix 2.5µl plasmid + 2.5µl *Tol2* mRNA, inj. 0.5nl & 1nl	50-100pg
***Tol2* mRNA**	200ng/ul		50-100pg

*concentration of mRNA varies between transcription reactions

Table 2.11 Preparation of working solutions for microinjection

2.2.1.21 Embryo dechorionation

Embryos (>24hpf) were either dechorionated with forceps or chemically with Pronase (in large batches of embryos). For protease dechorionation 1ml

of Pronase stock solution (20mg/ml) was added to 9ml of 1x E3 containing the embryos and incubated for 10-15 minutes until the first few embryos broke free from the chorion. Thereafter, the solution was washed off by changing E3 three times, and the remaining chorions were removed by gently pipetting the embryos up and down or using forceps.

2.2.1.22 Drug treatment

Chemical inhibitors were diluted into working concentration in 10ml of E3 and added to a 6-well plate for each group accordingly. Twenty dechorionised embryos (e.g. *control* or *tnnt2a* morphants) were placed in each well and incubated in the solution containing the compound for an appropriate time. All drug treatments have been repeated for at least three times.

Molecules	Stock concentration	Working concentration	Incubation time
DMSO	Stock	Identical volume as inhibitor used	Identical time as inhibitor treatment
AV951	10mM	25nM	48-72hpf
DAPT	10mM	100μM	24-72hpf
DMH1	10mM	25μM	24-72hpf; 24-48hpf; 48-72hpf
Tricaine	4g/L	4X (16.8%, v/v)	48-72hpf

Table 2.12 Concentration and incubation time of drug treatment

2.2.1.23 Fixation and dehydration of embryos

Prior to *in situ* hybridisation or immunostaining, embryos were selected under different conditions (e.g. *control* or *tnnt2a* morphants) at different developmental stages based on experimental needs. Selected embryos were

then dechorionised and fixed with 4% PFA overnight at 4°C or 3 hours at room temperature. Following fixation, embryos were dehydrated by washing sequentially into methanol in PBST (25%, 50%, 75% and 100% methanol:PBST) with 5 minute intervals, and were stored at -20°C at least overnight before use.

2.2.1.24 Whole mount RNA *in situ* hybridisation

Whole mount *in situ* hybridisation was performed as described previously (Wilkinson *et al.*, 2012). See corresponding figure legends for the experimental repeats.

Day 1

Approximately twenty embryos were used per group and placed in 1.5ml Eppendorf tube. Embryos were rehydrated with sequential washes from methanol (75%, 50%, and 25% methanol:PBST) to 100% PBST. Embryos at 2-3dpf were treated with 10µg/ml Proteinase K for 25-30 minutes. The reaction was stopped by washing embryos with glycine (2mg/ml, in PBST) twice and embryos were fixed again with 4% PFA for 20mins. Following this, embryos were pre-hybridised with 50% Hybe$^{+/+}$: 50% PBST for 5 minutes and then incubated with Hybe$^{+/+}$ at 65°C for at least 1 hour. The pre-hybridisation solution was then replaced with Hybe$^{+/+}$ containing a 1:200 diluted probe required and left overnight at 65°C.

Day 2

Hybe$^{+/+}$ containing probe was removed from the tubes and stored at -20°C,

which can be re-used up to 6 times. Embryos then went through a series of washes from Hybe$^{-/-}$ to 2X SSC solution (100%, 75%, 50%, 25% Hybe$^{-/-}$:2X SSC and 100% 2X SSC) at 65°C with 10 min interval between each wash. Embryos then were washed 4 times with 0.2X SSC at 65°C, using 15-minute wash steps. Following this, embryos underwent a second wash series from 0.2X SSC to MABtw (75%, 50%, 25% 0.2X SSC:MABtw and 100% MABtw). This series of washes was performed at RT with 5-minute intervals. Embryos were then washed into 2% MAB Blocking Reagent at RT for at least an hour, with gentle shaking. Blocking reagent was then replaced with 2% blocking containing anti-Digoxigenin antibody (1:5000, Table 2.4) and embryos were incubated at 4°C with gentle agitation overnight.

Day 3

Embryos were taken from 4°C to RT for further incubation with antibody, for an hour with gentle rocking. Background antibodies were then removed by washing embryos 8 times with MABtw for 15 minutes each step. Following this, embryos were washed with BCL III buffer 3 times for 5 minutes each step prior to incubation of BM Purple^{TM} (Roche) which was 1:1 mixed with BCL III buffer (Table 2.2). The staining process was developing in the dark (covered with foil) and was monitored from time to time to ensure desired staining was reached. The staining was stopped once the colour was developed by washing embryos with BCL III buffer 3 times with 5-minute interval. Embryos in comparison were stained under the same conditions and for the same period of time.

Pigmentation of embryos were removed by incubating in bleaching solution (Table 2.2) for 1-2 hours depending on developmental stages. Bleaching solution was washed away with PBST, 3 times for 5 minutes each step. Embryos were re-fixed with 4% PFA at room temperature for 3 hours followed by 3 washes with PBST for 5 minutes each step. To facilitate imaging and long-term storage, embryos were transferred into 80% glycerol (in PBST). Embryos were stored at RT in the dark.

2.2.1.25 Whole mount immunostaining

Whole mount immunostaining was adapted from (Inoue and Wittbrodt, 2011). Fixed embryos were rehydrated with 1X PBST for 10 minutes three times. For pSMAD1/5 staining, embryos were then incubated in 1mM Tris-HCl at pH9.0 for 5 minutes, followed by heating at 70°C for 15 min. Depending on different antibodies, 1X PBST pH7 or 1mM citrate pH6 (instead of Tris-HCL) might be used prior to the heating step. After heating, embryos were directly washed in 1X PBST for 10 minutes twice and then washed in MilliQ for 5 minutes twice. To enhance tissue permeabilization, embryos were treated with acetone (pre-chilled) for 20 minutes at -20°C. Subsequently, embryos were washed with MilliQ for 5 minutes twice and then six times with 1X PBST (5 minutes each). Embryos were then incubated in blocking buffer (B-buffer, Table 2.2) for 3 hours at 4°C. After blocking, embryos were incubated with the respective primary antibodies (pSmad1/5, 1:500) in the incubation buffer (I-

buffer, Table 2.2) at 4°C for three days with gentle agitation.

To remove residual primary antibody, embryos were sequentially washed with PBS-TS three times with 1-hour interval, followed with PBS-T twice with 10-minute interval, and again with PBS-TS twice with 1-hour interval. The embryos were incubated with secondary antibodies (Alexa Fluor 488, 1:500) in the dark for two and half days, and then washed three times with PBS-TS with 1-hour interval and with 1X PBST twice with 1-hour interval. To take pictures, embryos were embedded in 1% low-melting agarose and imaged using light-sheet microscopy. Experimental repeat number for normal embryos (or 'controls') was two, for drug-treated or heat-shocked embryos was one, with approximately twenty embryos each group.

2.2.1.26 Heat shock induction

Staged embryos (at 24hpf and 48hpf) were placed into a 96-well plate individually in each well and covered with adequate E3 medium. The plate was then added to a PCR machine set at desired temperature. *Tg(hs70l:bmp4-v2a-GFP);(cryaa:CFP)*^{SH600} was heated at 37°C for 30 minutes and rested at 28°C for 30 minutes, and the cycle was repeated twice (1.5 hour heat shock in total). *Tg(hs70l:bmpr2b-v2a-GFP); (cryaa:CFP)*^{SH601} was heated at 38°C for 1 hour. After heat shock, embryos were returned to petri dishes and placed at 28.5°C incubator. Prior to imaging, embryos were sorted based on blue eyes (*cryaa:CFP*) and GFP expression in the somites. All heat-shocked experiments

have been repeated over three times.

2.2.1.27 Microscopy

2.2.1.28 Light microscopy

Day-to-day examination of embryos was performed using Leica M165FC, M125C, or Leica DFC. Embryos stained following *in situ* hybridisation were imaged using a Leica DFC microscope and analysed using Leica Application Suite software (LAS v4.3.0).

2.2.1.29 Fluorescent microscopy

Embryos were anaesthetised using tricaine prior to fluorescent sorting and imaging. A Leica DFC microscope and LAS v4.3.0 software or a Zeiss AXIO Zoom V16 and Zen Blue software were used.

2.2.1.30 Light-sheet microscopy

Embryos were anaesthetised and immobilised using 1% Low melting point agarose (Thermo Scientific™). Embryos were mounted in a glass capillary and held in place by agarose. The capillary was then placed within the imaging chamber of Z.1 Light Sheet (Zeiss) microscopy. The chamber contained a mixture of E3 and 1X tricaine, to ensure embryos remained anaesthetised throughout imaging. The temperature in the chamber was set at 28.5 °C. Prior to imaging, agarose containing the embryos was gently pushed out of the

capillary and suspended in front of the camera. Images were acquired using ZEN Black software (Zeiss).

Generally, laser intensity was set at 0.5-20% and exposure time at 7.5-30ms depending on the transgene imaged. The same settings were applied on control and experimental embryos throughout the imaging process. To record 3D images, the step size in z-directions was set as 1μm for objectives with magnification of 20X unless otherwise stated. For time-lapse imaging, interval time was set at 5 minutes for Movie 1 (blood flow) and Movie 9 (AC-tagRFP), and 10 minutes for Movie 3 (sprouts over time) and Movie 4 & Movie 5 (cell tracking data).

2.2.1.31 Quantification and statistical analysis

2.2.1.32 Quantification of general morphology of the SIVP

2.2.1.32.1 Embryo positioning during still imaging

The SIVP develops on the surface of the yolk ball and its appearance is largely affected by the curvature of the yolk. To reduce visual artefacts and to gain meaningful comparisons, the potential systematic variables were carefully controlled, by positioning embryos at similar angle to avoid distortion caused by the nature of yolk ball. Anatomical landmarks, such as the angle of left and right DLAVs and the angle between middle cerebral vein (MCeV) and eyeball, were used to ensure the region of interest was comparable in different embryos.

Each experimental condition, including tricaine-treated, morpholino injected, and CRISPR/Cas9 injected embryos, was repeated for three times.

2.2.1.32.2 Image pre-processing and quantification

Still images acquired from light-sheet microscopy were exported as Tagged Image File Format (TIFF). TIFF images were then loaded into Fiji (ImageJ) for processing. The scale of the images was transformed from pixel size to μm (values gained from light-sheet scale). Images were rotated to position the zebrafish head towards left and ISVs towards up. The DA and PCV were positioned horizontally (0°). All RFP/mCherry channels of images in this thesis were false coloured in magenta for better presentation.

The parameters used to represent SIVP morphology, including area, length, vascular loops, sprout number and EC number (Figure 3.2), were quantified in a region as wide as 5 somites. The length of the SIVP was measured as the vertical distance from the SIA to the most ventral part of the SIV. Images in both GFP (EC cytosol) and RFP (nuclei) were used to ensure the RFP dots quantified were within the SIVP.

2.2.1.33 Cell trajectory analysis

2.2.1.33.1 Acquisition and pre-processing of time-lapse images

For one experimental repeat of cell trajectory analysis, one *control* and one

tnnt2a morphant were mounted in the same agarose and positioned as close as possible without interfering with each other. These two embryos were imaged at the same time to ensure phenotypes were captured in the same developmental stages. Time-lapse images were exported as a series of TIFF files. TIFF images were then loaded into Fiji (ImageJ) for processing. The number of experimental repeats has been stated in corresponding figure legends. The scale of the images was transformed from pixel size to μm (values gained from light-sheet scale). Image stacks were aligned using a plugin in Fiji, namely Linear Stack Alignment with SIFT (Lowe, 2004). The algorithm was run with the following parameters: 1.6px Gaussian blur, 10 steps per scale, octave, 64px minimum image size, 1920px single plane field of view, 15 feature descriptors, 8 orientation bins, 0.98 closest/next ratio, 3px maximum alignment error (global alignment with 10px), 0.05 inlier ratio, rigid transform and without interpolation. The aligned stacks were saved as a new TIFF file for future use.

2.2.1.33.2 **Acquisition of cell tracks**

After stack alignment, the stacks were down sampled to make interval time at 30 minutes. The RFP channel displaying endothelial nuclei of the SIVP was saved as a separate TIFF file. The endothelial cells in the RFP channel were labelled and tracked in a semi-automated manner using TrackMate Plugin, implemented in Fiji (Tinevez *et al.*, 2017). The algorithm was run with the following parameters: LoG detector, estimated blob diameter at 10μm, enabled

median filter and sub-pixel localization, 0.05 initial thresholding, HyperStack Displayer, X and Y filter were used to discard cells outside the SIVP, LAP Tracker, gap closing and track segment splitting were allowed, no filter was used for tracks. In display options panel, TrackScheme was used to manually correct cell tracks, including adding missing tracks, rearranging mis-connected tracks between adjacent cells and deleting tracks of non-endothelial cells. Once all tracks were correctly labelled, three Excel files were exported by clicking Analysis, including Track statistics, Links in tracks statistics (referred as links file), and Spots in tracks statistics (referred as spots file). Every individual EC traced was represented as an individual track (including daughter cells) which was given a distinct ID number. The links of a given cell at two consecutive time points were listed in links file. The statistics of every cell at every timepoint were listed in spots file, including x and y coordinates, time frame, and colour. These data were analysed by custom-made MATLAB scripts.

2.2.1.33.3 **Analysis of cell tracks using MATLAB scripts**

Two MATLAB scripts were created and used for cell trajectory analysis in this thesis, including ‘script 1 track analysis’ and ‘script 2 direction analysis’. These scripts are available on GitHub with following link: https://github.com/yanc0913/SIVP_cell_tracking.

To run the script 1, cell tracking files (links file and spots file, 2.2.1.33.2) of one experiment were required for input. Users were asked to type in input file

names as well as an output file name. The output file includes values analysed from the cell trajectory, including track distance, track displacement, distance/displacement ratio (tortuosity index), migration velocity as well as track and step delta x and delta y (see Figure 3.7). These results were all output in an Excel file with several spreadsheets. Noted that the script was run for a single experimental repeat at a time, therefore users would need to change file names accordingly for different repeats.

Script 2 helped to analyse cell migration direction in every step (see Figure 3.6), providing scatter plots of cell steps in one *control* and one *tnnt2a* repeat, generating a polar histogram of cell migration steps (including all *control* or *tnnt2a* repeats), as well as the values of the polar histogram. This script included two sections, the first was to analyse an individual experimental repeat and generate the values of polar histogram in an Excel file. To run this section, values of step delta x and delta y were required, which were obtained from script 1. Users were asked to type in input and output file names, as well as column locations in the output spread sheet for data to be written in. The second section was run for scatter plots and polar histogram plots. The output data from the two scripts were imported in GraphPad Prism 8 to plot figures and run statistical tests.

2.2.1.33.4 **Calculation of distance, displacement & velocity**

One cell at position 1 (x_1 and y_1) migrates to its next position 2 (x_2 and y_2) in a time range (from t_1 to t_2). This was described as a 'step' in this thesis (Figure 3.6A). Step delta x (Δx) and delta y (Δy) were calculated as x_2-x_1 and y_2-y_1, respectively. The distance of the step (equals to displacement in this case) was calculated as $\sqrt{\Delta x^2 + \Delta y^2}$. Similarly, track displacement was calculated from track delta X (ΔX) and track delta Y (ΔY) which were obtained by the last position of the cell subtracting the initial position in a track. Track distance was the sum of step displacements. Migration velocity was calculated as step displacement divided by time interval (30 minutes in this thesis), and the mean velocity at a certain time range was the average of each velocity in that range.

2.2.1.33.5 **Angle of each cell migration step**

Migration direction of each step was calculated using atan2 function in MATLAB, which computed the four-quadrant inverse tangent (arctangent) of delta y and delta x. The output values from this function was theta (θ) in radians, which were then plotted in polar histogram (also known as rose chart). The polar histogram function generated a histogram plot in polar coordinates by sorting the theta values into equally spaced bins (angles). The numbers in each bin were normalised to the total number of values. The height of each bar was the relative number of observations.

2.2.1.33.6 **EC rearrangement**

At the beginning of cell tracking (~56hpf), ECs were colour labelled as tip cell (magenta), SIV cell (blue), and branch cell (orange), depending on their initial positions (Figure 3.5). At the end of observation (~72hpf), their positions were evaluated again to see whether the ECs moved to a different subset (e.g. a blue cell initially located in the SIV ended up in the branches, recorded as one rearrangement event). The number of ECs at initial or ending position and the events of EC rearrangement were manually recorded.

2.2.1.34 **Statistical analysis**

Statistical analysis and graphic plotting were performed using GraphPad Prism 8. All statistical analysis was described in figure legends, including paired/unpaired t-test, ordinary One-way ANOVA, and two-way ANOVA. All error bars display the mean and standard deviation in the figures. P values, unless exact value is listed, are as follows: *=<0.05, **=<0.01, ***=<0.001, ****=<0.0001.

Chapter 3 The role of blood flow in coordinating vascular remodelling of the sub-intestinal vein

3.1 Introduction

Despite the importance of vessel remodelling for early development, little is known about how remodelling of the vasculature occurs. Although mechanisms of apoptosis and flow-dependent cell migration have been proposed to regulate vessel remodelling, cellular and molecular understanding of how these might happen are still conspicuously lacking. Recent studies employed the SIVP as a novel pruning model in zebrafish and have revealed interesting cellular behaviours during branch pruning using this model (Lenard *et al.*, 2015 and introduction 1.3.1.4.2). Variation in the timing of lumen collapse led to two types of vascular pruning and the event of branch pruning was reduced in *tnnt2a* morphants which had no flow (Lenard *et al.*, 2015), suggesting that flow is required for branch pruning. Moreover, vascular pruning involves extensive rearrangement of ECs (Lenard *et al.*, 2015).

Other vessel remodelling behaviours have also been observed including sprout retraction during which leading sprouts at the migration front of the SIVP do not fuse with another sprout and would eventually retract into the main vessel (Hen *et al.*, 2015). This process was speculated as being driven by migration of the ECs within the sprout (Hen *et al.*, 2015). However, how such migratory behaviour is regulated and whether blood flow is required in the process remains unknown. Given that blood flow plays an important role in branch pruning, it is reasonable to speculate that flow may regulate the retraction of these sprouts. While no apoptotic cells were observed during

branch pruning (Lenard *et al.*, 2015), proliferation occurred in both leading and trailing cells to support the expansion of the plexus (Goi and Childs, 2016; Lenard *et al.*, 2015). Whether blood flow regulates cell apoptosis and proliferation during SIVP remodelling is also unknown.

Hypothesis

Blood flow is required for vascular remodelling via EC migration.

Aims

1. To determine the migratory behaviour of ECs during remodelling and whether blood flow affects these behaviours.

2. To investigate whether blood flow regulates EC proliferation and/or apoptosis during vascular remodelling.

In this chapter, I present the essential role of blood flow in vascular regression of the leading sprouts. I demonstrate that the absence of flow leads to general morphological alterations in the SIVP, including increased number of leading sprouts as well as increased EC number within the sprouts. Using time-lapse imaging and analysis of individual EC migratory trajectory, I show that accumulation of ECs in the leading sprouts is due to disrupted cell rearrangement in the absence of flow, rather than cell proliferation. Sprout regression is regulated by coordinated rearrangement of ECs on the luminal

surface and the non-perfused leading sprouts, mediated by directed EC polarisation and migration against blood flow. Taken together, these studies provide a clear view of cellular behaviour that underlies vessel remodelling and the role of blood flow on individual ECs during development.

3.2 Blood flow perfuses the SIVP in an anterior-to-posterior manner.

How blood flow perfuses the SIVP is still unknown so far. Central to investigating how blood flow contributes to the regulation of SIVP development, I sought to determine the timing and pattern of perfusion within the SIVP.

Tg(fli1a:egfp)^{y1};(gata1a:dsRED)^{sD2} were employed to label endothelial cells with GFP and red blood cells with DsRED which was pseudo-coloured in magenta. The SIVP emerges from the PCV at around 30hpf (Goi and Childs, 2016; Hen *et al.*, 2015; Koenig *et al.*, 2016; Nicenboim *et al.*, 2015), and expands ventrally over the surface of the yolk. From pilot studies I observed that blood flow was not present before 48hpf in the SIVP, therefore embryos were imaged from approximately 53hpf, when only a primary SIVP was formed and no RBCs were detected within the plexus (Figure 3.1A). Embryos were imaged for approximate 19 hours.

Still images of the flow pattern in the SIVP were obtained from time-lapse video which was presented in Appendix Movie 1. Before the onset of blood flow, a primitive SIVP with vascular loops was observed at the anterior part of the plexus (Figure 3.1A, green arrow) while at the posterior angiogenic sprouts started to coalesce (Figure 3.1A, green arrow head). This was in line with previous reports that sprouting and looping of the SIVP happened in an anterior-to-posterior manner (Koenig *et al.*, 2016). Blood flow started at 55hpf when a stream of RBCs was detected at the most anterior part of the SIVP while

the rest of the plexus remained free of flow (Figure 3.1B &B'). The path of RBCs flowing within the SIA was clearly detectable by 56hpf (Figure 3.1C', magenta arrow), running through vertical branches and pooling in the SIV (Figure 3.1C', blue arrow), after which it returned to the heart via the hepatic portal vein (HPV). Over time, blood flow progressed towards the posterior plexus such that by 60hpf, approximately 75% of the SIVP was perfused (Figure 3.1D &D') and by 70hpf, the whole plexus was perfused by blood flow (Figure 3.1E &E'). Interestingly, although blood flow drained into the SIV, no RBCs were observed within the leading sprouts which connected with the ventral SIV (see Movie 2). The sprouts remained free of RBCs during the whole process of remodelling until these retracted into the main plexus (Figure 3.1C'', D'' &E', arrows).

In summary, these data indicate that blood flow perfuses the SIVP in an anterior-to-posterior manner (Figure 3.1F, light & dark magenta lines) and that leading sprouts are non-perfused by RBCs during remodelling (Figure 3.1F, square).

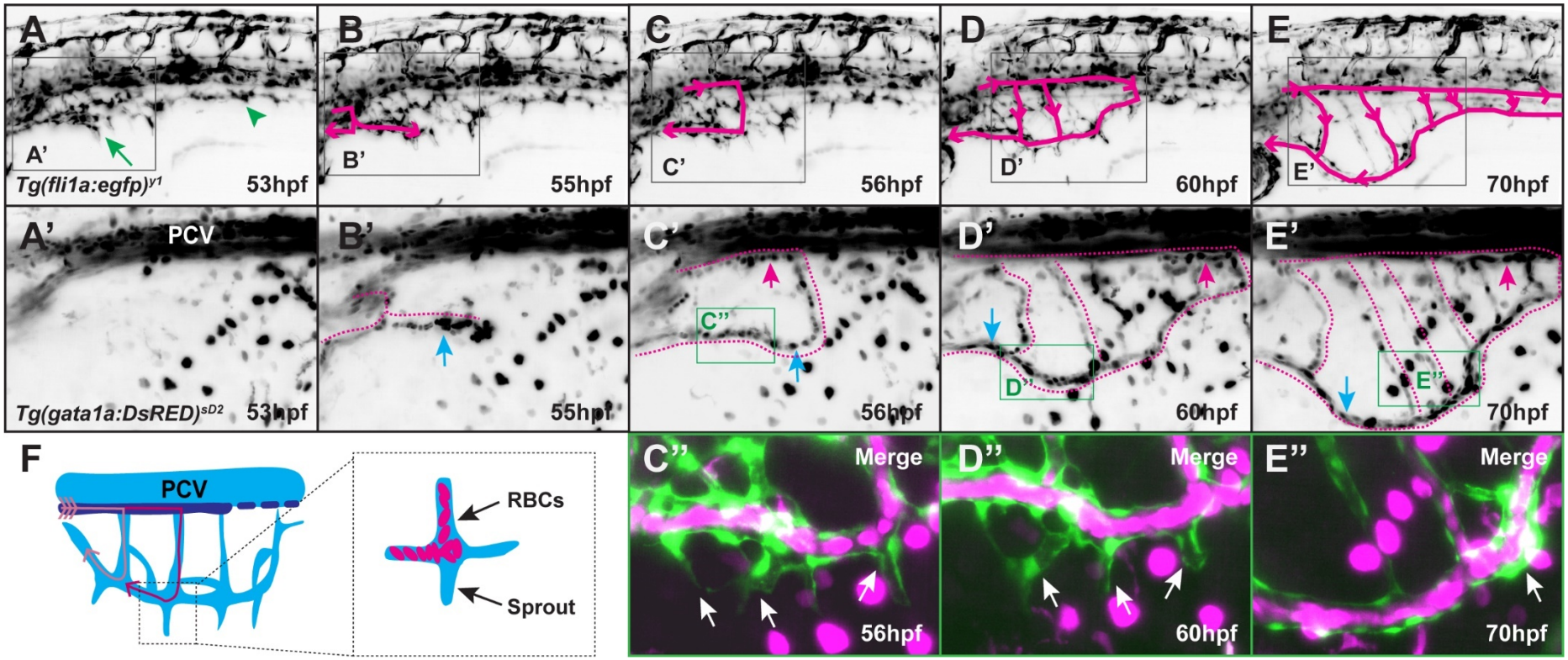

Figure 3.1 Blood flow perfuses the SIVP in an anterior-posterior manner.

(**A-E**) Still images from a time-lapse video (Movie 1) showing the pattern of blood flow perfusion in the SIVP. *Tg(fli1a:egfp)*^{y1} was used to label endothelial cells and *Tg(gata1a:DsRED)*^{sD2} label red blood cells, as an indicator of blood flow in the zebrafish. Area in grey square in **A-E** is enlarged in **A'-E'** in which RFP channel is shown. Blood flow is absent in the SIVP (**A&A'**) until 55hpf when RBCs are pushed into the anterior part of the SIVP (**B&B'**). Blood starts to flow at around 56hpf in the anterior plexus (**C&C"**) and continues to perfuse more posteriorly as the SIV developing over time (**D-E&D'-E'**). Blood flows from the SIA (**C'-E'**, magenta arrows) which connects with upstream anterior mesenteric artery (AMA), through the branches, and drains into the SIV (**C' -E'**, blue arrows) which collects all the blood to the hepatic portal vein (HPV). Area in green square in **C'-E'** is enlarged in **C"-E"** to show that the leading sprouts are free of RBC flow. See Movie 2. (**F**) Schematics show the blood flow pattern during SIVP development.

3.3 Absence of blood flow disrupts SIVP morphology and alters distribution of ECs.

To determine the effects of flow on SIVP morphogenesis, embryos were injected with *control* or *tnnt2a* morpholino (MO) (see method 2.2.1.20). *tnnt2a*/*silent-heart* MO binds to the cardiac troponin T2a translation start site and therefore inhibits translation of *tnnt2a* that is required for sarcomere assembly and cardiac contractility (Sehnert *et al.*, 2002). The injected embryos therefore displayed absence of heartbeat and blood flow throughout development.

As reported previously, the position and shape of the SIVP are similar but not precisely the same among embryos (Goi and Childs, 2016), which could hinder the comparison between the two morphants. In order to compare the difference quantitatively, I developed a method to measure SIVP morphology (see section 2.2.1.32), including plexus area, length, vascular loops, leading sprouts and cell number.

Compared to controls, *tnnt2a* morphants did not differ significantly in SIVP area (*control* 56880±9371 μm^2 vs. *tnnt2a* 52302 ±11413 μm^2) (Figure 3.2C, &A'/A'', green circle). However, in the absence of flow the number of vascular loops was reduced (*control* 16±3 vs. *tnnt2a* 13±2) (Figure 3.2D &A', asterisks), which exhibited collapsed vertical branches and defects in formation of secondary branches deep in the tissue. Although the total length of the SIVP was unchanged (*control* 203±27μm vs. *tnnt2a* 206 ±32μm) (Figure 3.2E &B', green line), the length of the main plexus was reduced (*control* 189±27μm vs. *tnnt2a* 145 ±34μm) (Figure 3.2E &B', blue line) and the length of leading sprouts was increased (*control* 22±22μm vs. *tnnt2a* 56±16μm) (Figure 3.2E

&B', magenta line). This indicated that in the absence of flow, ECs within the leading sprouts were able to migrate a similar distance as control ECs, while the ECs within the main plexus may fail to catch up with the leading cells, resulting in a shortened main plexus and elongated leading sprouts. The number of the leading sprouts was also significantly increased in the absence of flow (*control* 0.7±0.7 vs. *tnnt2a* 3.1±1.5) (Figure 3.2F &B', arrows). Taken together, this indicates that blood flow is required to control the morphology of the SIVP, including the development of the vertical branches, expansion of the main plexus, and the remodelling of the leading sprouts.

While the total number of ECs within the SIVP was not significantly different between *control* (101±16) and *tnnt2a* morphants (110±18) (Figure 3.2G & A''/B'', EC nuclei dots in RFP channel), there was a significant increase of EC number within the leading sprouts (*control* 1.4±1.3 vs. *tnnt2a* 7.3±2.4) (Figure 3.2H). Moreover, by grouping ECs into three subsets based on their location at 72hpf (branch, orange; SIV, blue; leading sprout, magenta , as indicated in Figure 3.2B''), I found that there were differences in the EC distribution within the SIVP (Figure 3.2I). In the absence of flow, the number of ECs in SIVP branches were reduced (*control* 50% vs. *tnnt2a* 26%) whereas the number of ECs present within leading sprouts were increased (*control* 2% vs. *tnnt2a* 23%) (Figure 3.2J). Collectively, these data indicate that although the total number of ECs in the SIVP were unaltered in the absence of flow, the distribution of ECs was altered by blood flow. This suggests that blood flow may control EC proliferation or migration among different subsets within the SIVP.

Morpholinos have been reported to cause numerous off-target effects (Stainier *et al.*, 2017), therefore to evaluate the phenotypes observed within the SIVP of *tnnt2a* morphants, I inhibited the blood flow using two additional methods: high dose tricaine treatment and injection of CRISPR/Cas9 targeting *tnnt2a*.

Tricaine is an anaesthetic commonly used in zebrafish (Matthews and Varga, 2012), and high concentration of tricaine has been employed to manipulate blood flow velocity (Kochhan *et al.*, 2013). To inhibit flow in the SIVP, a concentration of 4X tricaine (16.8%) was used and embryos were treated from 48hpf to 72hpf. Embryos were imaged at 72hpf and morphological quantification was performed as in Figure 3.2. I observed similar morphological changes in the SIVP as in *tnnt2a* morphants, including increased number of leading sprouts; however, the total EC number was decreased in tricaine-treated embryos (Appendix Figure 7.1E). Tricaine-treated *tnnt2a* morphants displayed significantly reduced numbers of ECs within the SIVP compared to untreated *tnnt2a* morphants (Figure 7.1F), suggesting that the high concentration of tricaine employed during the treatment was responsible for this reduction.

In parallel studies, I employed CRISPR/Cas9 to generate F0 *tnnt2a* mutants (Wu *et al.*, 2018). Embryos were injected with four *tnnt2a* guides along with Cas9 protein, assayed for inhibition of cardiac contraction and were imaged at 72hpf. Morphological quantification was again performed as in Figure 3.2. I observed similar phenotypes as in *tnnt2a* morphants (Figure 3.3), and the total number of ECs was also not significantly different as in *tnnt2a* morphants (Figure 3.3H), suggesting that the phenotype observed in *tnnt2a* morphants was specific to *tnnt2a* loss of function. Thus flow regulates SIVP morphology during development associated with differences in EC distribution.

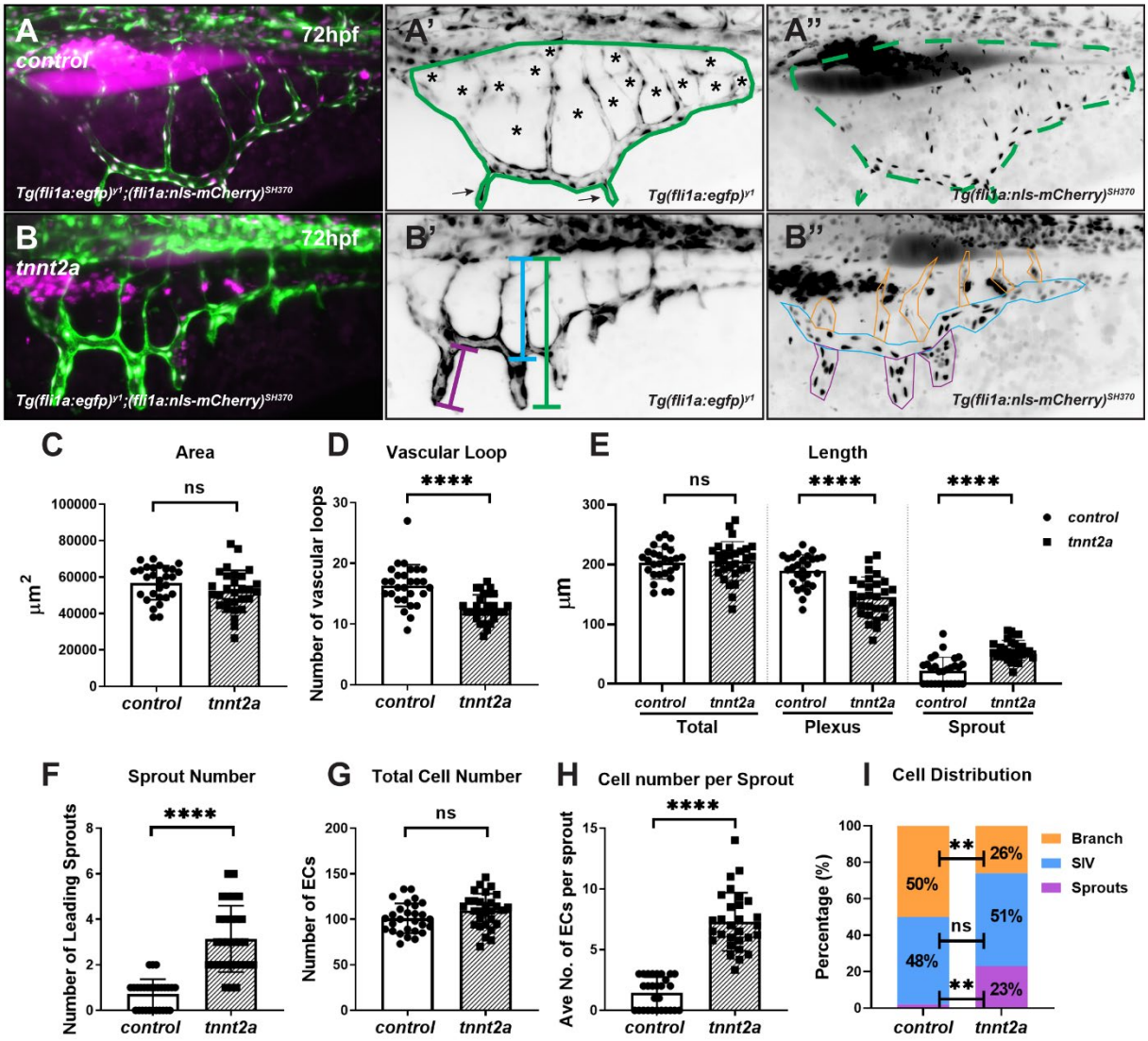

Figure 3.2. Blood flow is required for morphogenesis and cell distribution of the SIVP.

Comparison of SIVP morphology at 72hpf in the presence (**A**) or absence of blood flow (*tnnt2a* morphants) (**B**). (**C**) Measurement of area (circled area in green in **A'**& **A''**) does not show significant difference. (**D**) Embryos without flow exhibit reduced vascular loops (**A'**, asterisks). (**E**) The total length of the SIVP does not differ (**B'**, green line) but *tnnt2a* embryos exhibit decreased length of the main plexus (**B'**, blue line) and increased sprout length (**B'**, magenta line). (**F**) The number of leading sprouts (**A'**, arrows) are increased in *tnnt2a* morphants. Although the total number of ECs in the SIV is not altered in the presence and absence of flow (**G**), there is an increase in cell number within the leading sprouts (**H**). (**I**) Lack of flow reduces the percentage of cells in the branch (orange bar) but increases that of the leading sprouts (magenta bar). Embryos of *Control*, n=28; *tnnt2a*, n=29; from three independent replicates. Unpaired t-test, ****p<=0.0001, ns, no significance.

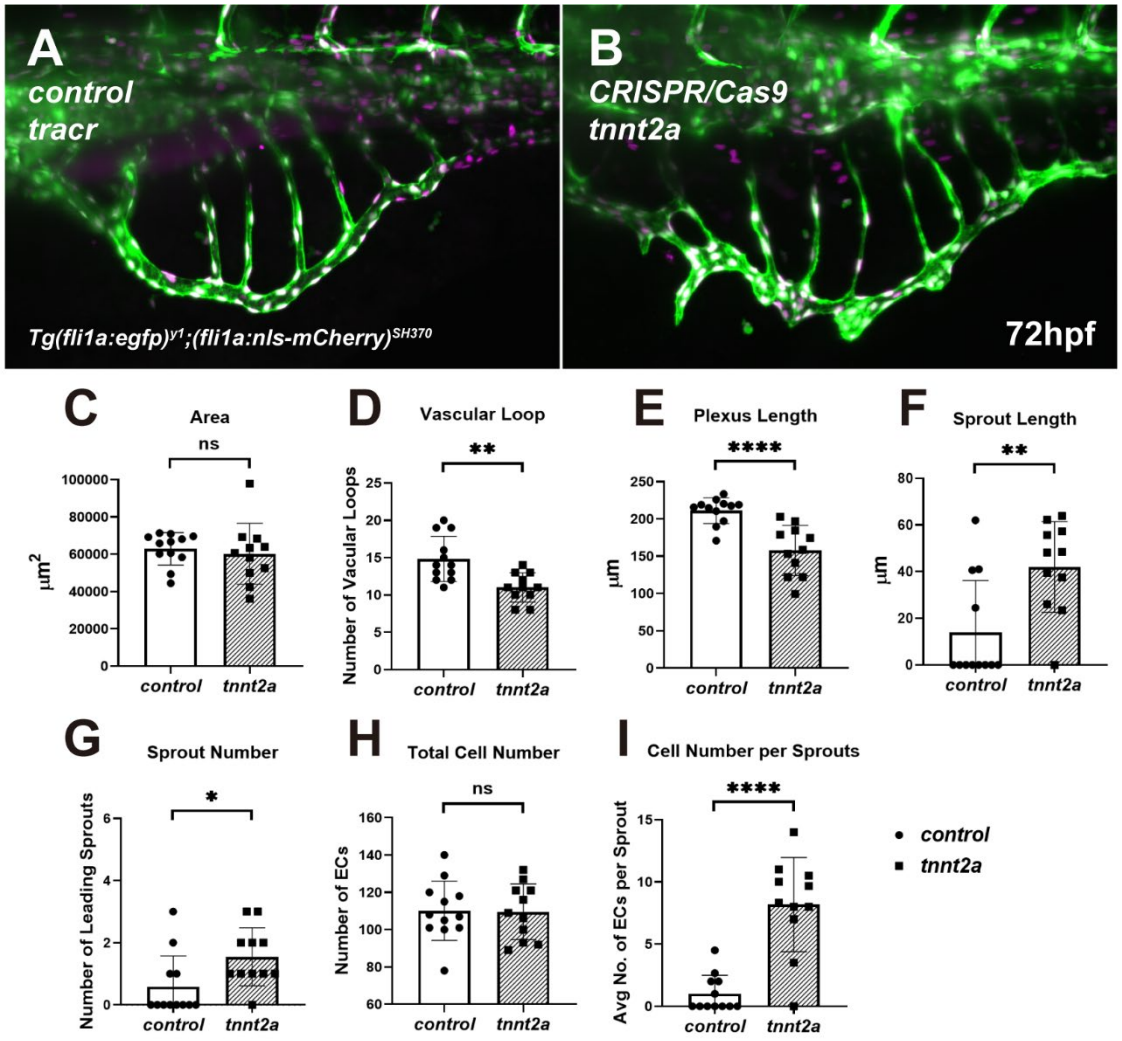

Figure 3.3 *tnnt2a* crispants exhibit similar morphological phenotypes that are comparable to *tnnt2a* morphants

Embryos are injected with tracr (**A**) or *tnn2a* guides (**B**) along with Cas9 protein and imaged at 72hpf. Similar to the morphological differences observed between *control* and *tnnt2a* morphants, measurement of area is not altered (**C**) while the number of vascular loops is reduced in the absence of flow (**D**). *tnnt2a* cripspants also exhibit decreased plexus length (**E**) and increased sprout length (**F**). The number of leading sprouts (**G**) are increased in *tnnt2a* crispants. Moreover, the total number of ECs in the SIV is not altered in the presence and absence of flow (**H**), which is comparable to *control* or *tnnt2a* morphants. Similarly, there is also an increase in cell number within the leading sprouts (**I**). Embryos of *Control*, n=12; *tnnt2a*, n=11; Unpaired t-test, ****p<=0.0001, ns, no significance.

3.4 Blood flow regulates leading sprout remodelling by promoting sprout regression.

Although previous data have shown that the absence of flow leads to ectopic leading sprouts in the SIVP, it is unclear whether the phenotype resulted from hyper-sprouting or remodelling defects in the sprouts in the absence of flow. To investigate this, embryos injected with *control* or *tnnt2a* morpholino were imaged using light-sheet microscopy over a 22-hour period (50-72hpf).

Still images of the sprout development in the SIVP were obtained from time-lapse video which was presented in Appendix Movie 3. Before the onset of flow, angiogenic sprouts protruded from the primary SIV, which either anastomosed to form vascular loops (Figure 3.4A, asterisks) or led at the migration front (Figure 3.4A, arrows). Upon the onset of blood flow at 56hpf, some of the sprouts regressed and incorporated into the main SIV (Figure 3.4B, arrows), resulting in a decrease in number of leading sprouts. At approximately 72hpf, most of the leading sprouts had regressed, leading to a basket-like plexus with a smooth ventral edge (Figure 3.4C).

Similarly, in the absence of flow, sprouts were formed from the primary SIV, and the plexus migrated ventrally (Figure 3.4D, arrows), suggesting that blood flow is not required for sprouting from the SIVP and its subsequent expansion. However, in *tnnt2a* morphants, the leading sprouts at the migration front failed to regress in comparison to controls, resulting in formation of a basket-like plexus lacking a smooth ventral edge (Figure 3.4E-F, arrows).

To determine whether the increased number of leading sprouts was due to increased sprout formation, the number of leading sprouts was quantified from 50hpf to 72hpf. Compared to controls, *tnnt2a* morphants did not differ significantly in the

mean number of sprouts produced (5.5 ±1.2 per SIVP, Figure 3.4G, 'Total'), suggesting that sprout formation in the SIVP is not flow-dependent. Only a few leading sprouts underwent anastomosis (0.4 ±0.7 per SIVP) and did not significantly differ in frequency in the absence of flow (0.9 ±0.8 per SIVP, Figure 3.4G, 'anastomosis'). However, sprout regression was significantly reduced in the absence of flow, with only 0.5 ±0.7 per SIVP (9.1%) sprouts having regressed compared to controls (3.4 ±0.7 per SIVP, 68.6%, Figure 3.4G &H, 'regression'). The majority of the sprouts failed to regress by the end of the imaging period in *tnnt2a* morphants, with 4.1 ±1.8 per SIVP (75.0%) whereas 1.1 ±0.8 per SIVP (22.9%) were present in *control* embryos (Figure 3.4G &H, 'non-remodel'). These data indicate that lack of flow does not affect the production of leading sprouts but impairs sprout remodelling, by inhibiting sprout regression, which is the primary mechanism of sprout remodelling in the SIVP (Figure 3.4H).

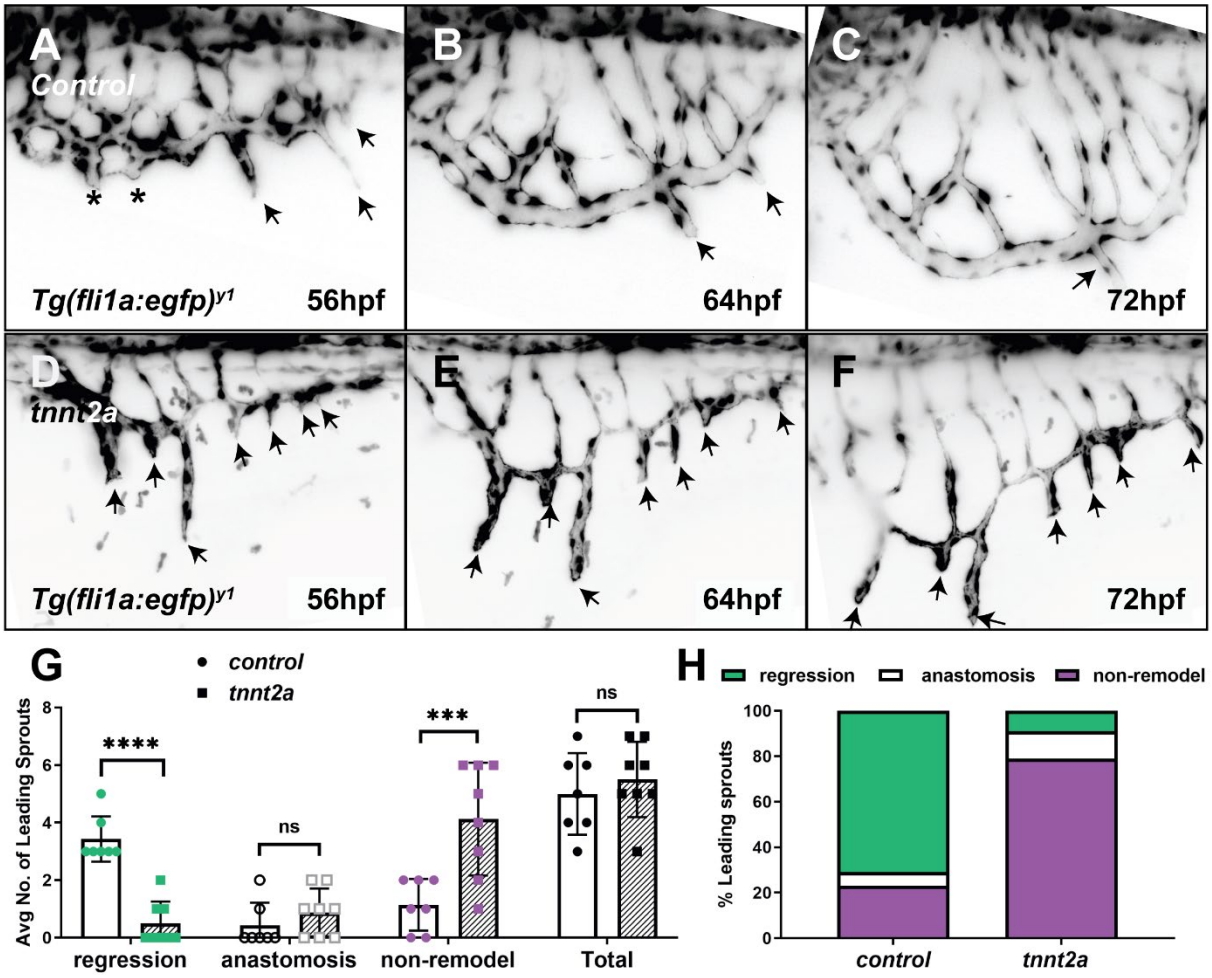

Figure 3.4. Blood flow regulates leading sprout remodelling via regression.

(**A-F**) SIVP development in the presence and absence of flow. *Tg(fli1a:egfp)*^{y1} are used to label endothelial cells and images were coloured coded in grey. Still images are from Movie 3. (**A**) Before blood flow enters the plexus, angiogenic sprouts from the primary SIV fuse together (asterisks) to form vascular loops or lead at the migration front (arrows). Upon the onset of blood flow, the leading sprouts regress, and their ECs incorporate into the main ventral SIV (**B-C,** arrows). In the absence of flow, the leading sprouts failed to regress (**D-F**, arrows). (**G**) The mean number of leading sprouts regressed during remodelling, and the number of sprouts pruned via anastomosis, the number of non-remodelled sprouts and the sum of all sprouts during development from 53hpf to 72hpf are quantified (embryos of *control*, n=8; *tnnt2a*, n=7). The total number of sprouts produced per SIVP does not significantly differ in the presence or absence of flow. While the majority of sprouts are remodelled via regression in controls, the sprouts fail to regress in the absence of flow. Unpaired t-test, ****p<=0.0001, ns, no significance. (**H**) The events observed in (**G**) are presented as percentages comparing *control* versus *tnnt2a* morphants. The percentage of regressed sprouts is reduced in the absence of flow.

3.5 Blood flow controls EC rearrangement but not proliferation within the developing SIVP

As previously described (Figure 3.2I), the disrupted EC distribution in the SIVP could be due to increased proliferation of tip cells and/or apoptosis of branch cells, or impaired EC rearrangement in the absence of flow. To investigate this, I employed the transgenic lines *Tg(fli1a:egfp)^{y1};(fli1a:nls-mCherry)^{SH370}* for time-lapse imaging, and tracked the movements of the ECs within the SIVP from 56hpf to 72hpf (see examples in Movie 4 & Movie 5). Similar numbers of ECs were tracked at the beginning of each video (Table 3.1, average 48±9 cells per *control* embryo, 41±8 cells per *tnnt2a* embryo). There was a significant increase of total cell number in both groups at the end of the observation period, with an average of 68±13 cells per *control* embryo and 59±14 cells per *tnnt2a* embryo (Table 3.1, 'end'). No ECs were observed to undergo apoptosis, and proliferation accounted for the increase in total EC number, with an average of 19±9 cell division events per embryo in each group (Table 3.1, 'proliferation events'). These data are in line with previous finding that the total number of ECs in the SIVP were not changed in the absence of flow (Figure 3.2G).

Interestingly, whilst tracking the movements of the ECs within the SIVP, I observed that ECs were not only actively proliferating, but also exchanged position between different EC subsets. For example, an EC originally located within the SIV would migrate into the vertical branches and ECs within the sprouts would enter the SIV during sprout regression. To simplify the definition of each subset, ECs were grouped based on their *initial* position at 56hpf, namely the branch (orange), SIV (blue) and tip cells (pink) (Figure 3.5A).

In the presence of flow, the proliferation events were observed in all EC subsets

(Table 3.1, 'proliferation events') and these ECs proliferated at similar rates (approximately 40%-50%, Figure 3.5B). There were no significant differences in proliferation rates in total or subsets of ECs between *control* and *tnnt2a* morphants, suggesting that the ability of ECs to proliferate did not alter in the absence of flow (Figure 3.5B). During proliferation, the division direction is mostly parallel to (or the division plane is perpendicular to) the long axis of the vessel tube in either presence or absence of flow (examples shown in Figure 3.5A & Movie 6). In addition, although the division direction of SIV cells was horizontal, it switched to vertical once ECs entered and proliferated within the branches (Figure 3.5A, upper panel, blue circles). And such behaviour was also observed in *tnnt2a* morphants, suggesting that the division direction is dependent on relative position of ECs in the plexus but is independent of blood flow. Collectively, these data suggest that not only the frequency of cell division but also the orientation of cell division is independent of blood flow.

control	Onset (56hpf)	Proliferation Events	Onset+ proliferation	Moving Away	Receiving	End (72hpf)
Tip	9 ±3	4 ±3	13 ±3	10 ±2	0 ±0	3 ±3
vSIV	21 ±3	8 ±5	29 ±4	10 ±4	10 ±2	29 ±3
Branch	17 ±7	8 ±4	25 ±6	0 ±1	10 ±4	35 ±11
Total	48 ±9	19 ±9	68 ±9			68 ±13
tnnt2a	**Onset (56hpf)**	**Proliferation Events**	**Onset+ proliferation**	**Moving Away**	**Receiving**	**End (72hpf)**
Tip	13 ±5	7 ±0	20 ±2	5 ±2	4 ±3	19 ±5
vSIV	19 ±3	7 ±1	26 ±2	10 ±5	6 ±3	22 ±8
Branch	9 ±5	5 ±0	14 ±2	2 ±1	6 ±4	18 ±9
Total	41 ±8	19 ±1	59 ±5			59 ±14

Table 3.1 The average number of ECs within the SIVP in the presence and absence of flow.

ECs within the SIVP are grouped into three subsets according to their *initial* position in the SIVP at the beginning of cell tracking at 56hpf. The average number of ECs per embryo at 56hpf is shown in 'onset' and the average proliferation events per embryo is shown in 'Proliferation Events'. The sum of 'onset' and 'proliferation' indicates the total number of ECs in each subset. ECs migrated from one subset to another are shown in 'Moving Away' and ECs migrated from another subset are shown in 'Receiving'. The average number of ECs at their final position at 72hpf is shown in 'End'. *Control*, n=7; *tnnt2a,* n=6. Values are mean ±SD.

Given that EC apoptosis and proliferation were not altered by blood flow, I reasoned that cell rearrangement might account for the disrupted cell distribution of the SIVP in the absence of flow. Therefore, the positions of the endothelial nuclei were traced from 56hpf to 72hpf in *control* and *tnnt2a* morphants.

In the presence of flow, over 70% of the leading sprouts (11/15 sprouts observed) consisted of a pair of tip cells positioned in parallel to each other, consistent with previous reports (Hen *et al.*, 2015). Interestingly, the newly proliferated daughter cells of the tip cells often migrated into the SIV rapidly, leaving only the paired ECs within the sprout (Figure 3.5A, bottom panel, pink circles, & Movie 6). The majority of tip cells (average 10±2 out of 13±3 cells) migrated away from the leading sprouts to contribute to the SIV in the presence of flow (Table 3.1). In rare cases (<2%), tip cells contributed to the branches by 72hpf. No ECs were observed to migrate into the sprouts, although the bridging SIV cells adjacent to a sprout might transiently appear in the sprout. On the other hand, in the absence of flow, tip cells exhibited a significant reduction in cell rearrangement, with only 23% cells (Table 3.1, average 5±2 cells) contributing to the SIV, while the majority of the tip cells remained within the leading sprout by 72hpf (Figure 3.5C, 'tip→SIV'). In addition, there were on average 4±3 cells which migrated ventrally from the SIV to contribute to the leading sprouts in the absence of flow (Table 3.1 & Figure 3.5C, 'SIV→tip'). Collectively, approximately 80% of the ECs which accumulated within the leading sprouts resulted from failure of dorsal rearrangement of tip cells while ventral migration of the SIV cells also contributed to the population.

Cell rearrangement also occurred in ECs located in bifurcations between branches and the SIV. While less than 1% of branch cells migrated to the SIV in the presence of flow, most of the cell rearrangement events occurred from SIV to branch. One third of the SIV cells (average 10±4 out of 29±4 cells) were rearranged dorsally

and incorporated into recipient branches (Table 3.1 & Figure 3.5C, 'SIV→branch'). However, the dorsal rearrangement was disrupted in the absence of flow. Apart from a significant increase of ventral SIV-to-tip rearrangement as mentioned above (Figure 3.5C), there was also a significant increase of branch cells (average 2 ±1 cells) that migrated ventrally to join the SIV (Table 3.1 & Figure 3.5C, 'branch→SIV').

Collectively, these data showed that although the total number of cell rearrangement events did not differ between *control* and *tnnt2a* morphants (Figure 3.5C), ECs exhibited distinct directional migratory behaviours depending upon their position in response to flow. In the presence of flow, the ventral expansion of the SIVP is supported by proliferation and dorsal rearrangement of ECs. In contrast, in the absence of flow, ECs displayed persistent ventral cell movement, resulting in stretched branches (with fewer cells) and elongated leading sprouts (with accumulation of tip and SIV cells). Taken together, these results suggested that blood flow is required for directed rearrangement of ECs, rather than cell proliferation, during SIVP development.

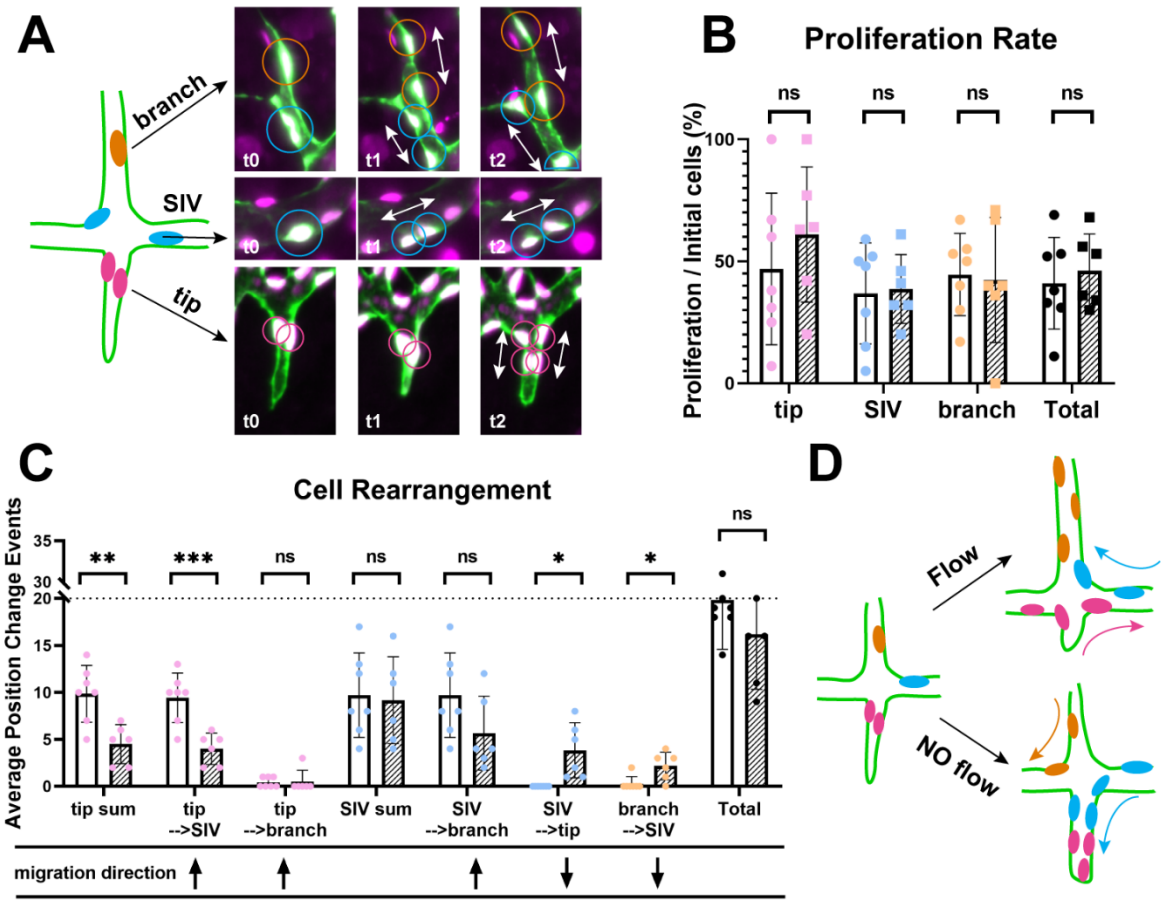

Figure 3.5. Aberrant cell rearrangement but not proliferation results in accumulated ECs in SIVP leading sprouts in the absence of flow.

(**A**) The ECs within the SIVP are grouped into three subsets base on their *initial* position at 56hpf: branch cells (orange) in the branch, SIV cells (blue) in the SIV and tip cells (pink) within the sprouts. See Movie 4 & Movie 5. Examples of cell proliferation in each subset are shown branch cells, upper panel; SIV cells, middle; and tip cells, bottom. The direction of cell division is parallel to the long axis of the vessel tube and is independent on blood flow. See Movie 6. (**B**) The proliferation rate (cell division/initial number of ECs) does not differ in total or subsets of ECs in the presence or absence of flow. (**C**) There is a significant reduction in tip cell rearrangement towards SIV in *tnnt2a* morphants, indicating that flow is required for tip cell dorsal rearrangement. However, there is an increase in SIV cell migrating to leading sprouts, displaying ventral cell movement in the absence of flow. Branch cells mostly remain within the branches under flow, but these migrate ventrally to join SIV at the lack of flow. White bars, *control* morphants (n=7); Shaded bars, *tnnt2a* morphants (n=6). Values see Table 3.1. Unpaired t-test, *p<=0.05, ns, no significance. (**D**) Schematics show the cell rearrangement within the SIVP in the presence and absence of flow. With flow, ECs display dorsal rearrangement from the sprout to the SIV, and from the SIV to the branch. However, in the absence of flow, this dorsally directed rearrangement is reversed to ventral, with branch cells ended up in SIV and the SIV cells in the leading sprouts.

3.6 Blood flow promotes direction preference for dorsal-lateral migration in ECs during sprout regression

Previous data showed that ECs within the SIVP display dorsal rearrangement, indicating directed EC migratory behaviour (ventral to dorsal) against flow (SIA to SIV, dorsal to ventral). To better understand how ECs coordinate their migratory behaviours, I investigated in detail every migration step the tip and SIV cells took in their migratory trajectories (examples in Figure 3.6A, Movie 4 & Movie 5). ECs close to the most ventral sprout of each embryo were selected and grouped into tip cells (pink) and SIV cells (blue) based on their *initial* position at 56hpf. The movement of a cell migrating in two consecutive time points (30min-interval) which are hereafter referred as a 'step', were indicated by step Δx and Δy (Figure 3.6a', black arrows). The Δx and Δy coordinates were plotted in a scatter chart to show the distance and orientation of the migration steps (Figure 3.6B &E). The movements of branch cells were also traced and analysed but to focus on sprout regression, which was the main aim of the thesis, these results were presented in appendix Figure 7.2 & Figure 7.3.

In the presence of flow, the coordinates of SIV cell steps mostly fell within the blue circle (radius = 5μm) and display an anisotropy towards the right semi-circle (Figure 3.6B), indicating that the SIV cells were able to migrate in every direction yet displayed a preference in posterior direction. Whereas steps of SIV cells favoured anterior-ventral direction in *tnnt2a* morphants (Figure 3.6B, the third quadrant of the blue circle). In addition, I did not observe SIV cells overtaking the position of tip cells during migration in the presence of flow while these cells were often mingled with tip cells

within the leading sprouts without flow (Movie 4 & Movie 5).

To determine whether blood flow regulates the migratory direction preference of SIV cells, the relative distributions of migration angles were plotted in a rose chart (Figure 3.6C) and the percentage of each direction were compared in the presence and absence of flow (Figure 3.6D). Approximately half of migration steps displayed ventral direction (225-315°) in both *control* and *tnnt2a* morphants (Figure 3.6C &D), which was consistent with the ventral expansion of the SIVP. However, there was a significant bias towards anterior direction (Figure 3.6C, 135-225°, green arrow) in the absence of flow (10% of migration angles) compared to controls (17%) (Figure 3.6D), suggesting that blood flow influences the SIV cells to migrate posteriorly.

Similarly, in the presence of flow, the coordinates of tip cell steps were anisotropic and displayed similar patterns as in SIV cells (Figure 3.6E), reflecting that the tip and SIV cells were in close contact and migrated collectively during SIVP development. In addition, the tip cells sometimes took long migration steps (>5μm) which were often observed when they coordinated with other cells and exhibited a drastic directional change (see examples in Figure 3.6a', green arrows). Although the tip cell coordinates were also anisotropic within the magenta circle in the absence of flow, the steps were more confined along y-axis (Figure 3.6E) compared to controls, reflecting that the ECs were more crowded within the leading sprouts.

Analysis of the relative distributions in migration angles showed a significantly increased preference for ventral migration in the absence of flow (56%) compare to controls (45%) (Figure 3.6F &G). Migration steps of tip cells without flow also displayed a reduced preference for dorsal migratory directions (45-135°, 17% vs. 25% in controls) (Figure 3.6F &G). This suggested that blood flow regulates sprout regression by increasing the fraction of steps in tip cells to undergo dorsal migration.

Taken together, these data suggest that blood flow regulates the preference of EC migration direction (Figure 3.6H). During SIVP development, while all ECs migrate collectively towards ventral direction for plexus expansion, upon the onset of flow, the SIV cells favoured posterior migration against flow (Figure 3.6D) and the tip cells favoured dorsal migration (Figure 3.6G), resulting in regression of the leading sprouts. It was noted that the tip cells display transient/stochastic dorsal migration to trigger sprout regression while collectively migrating ventrally with the plexus, rather than simply migrating ventrally first and then migrating in reverse later. In contrast, the EC migratory direction was disrupted by the absence of flow, with the SIV and tip cells displaying migratory preferences in opposite directions (Figure 3.6D &G).

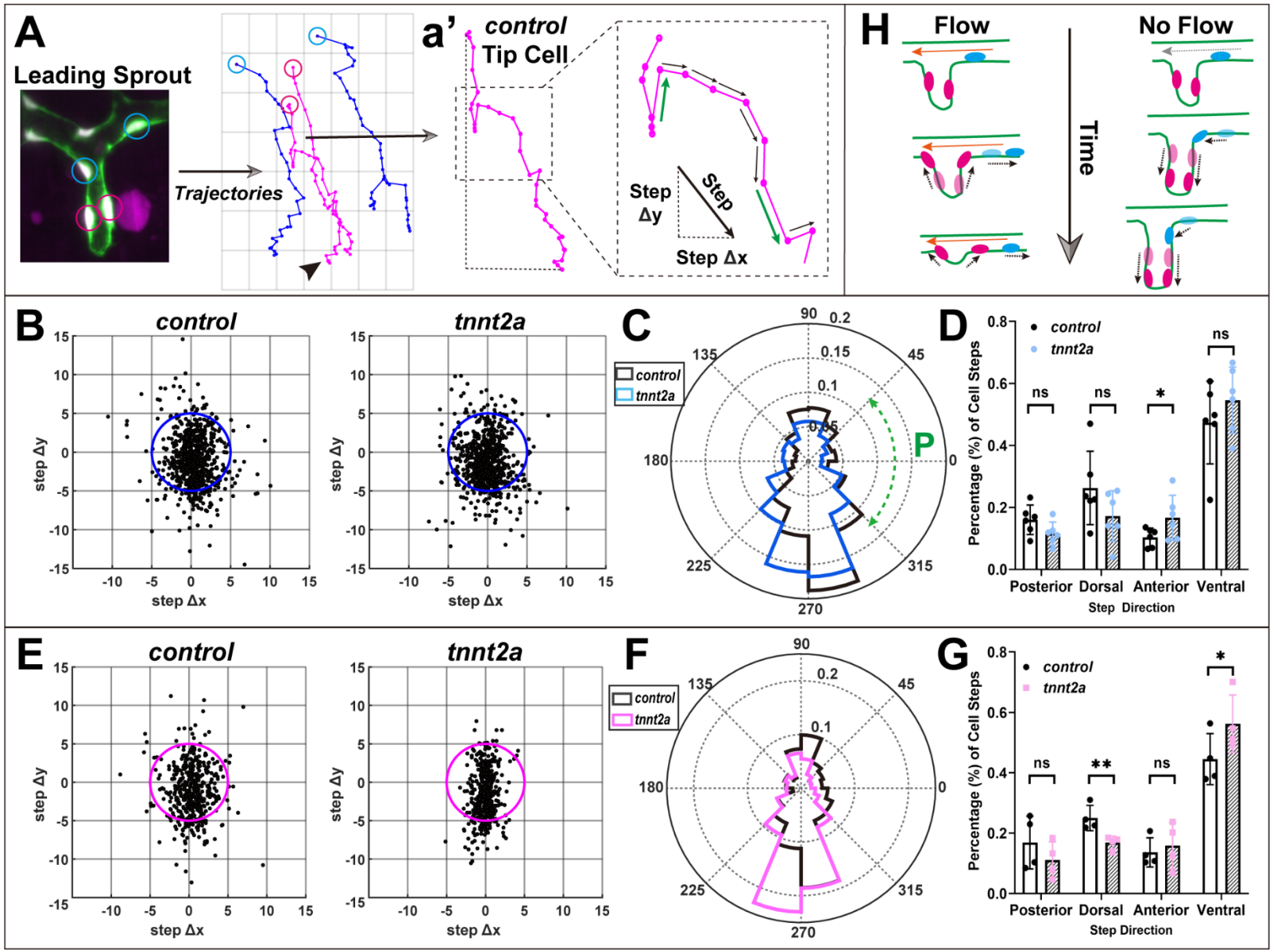
A
Leading Sprout
Trajectories
a'
control
Tip Cell
Step Δy
Step
Step Δx
H
Flow
No Flow
Time
B
control
tnnt2a
step Δy
step Δx
C
control
tnnt2a
P
D
control
tnnt2a
Percentage (%) of Cell Steps
ns
ns
*
ns
Posterior
Dorsal
Anterior
Ventral
Step Direction
E
control
tnnt2a
step Δy
step Δx
F
control
tnnt2a
G
control
tnnt2a
Percentage (%) of Cell Steps
ns
**
ns
*
Posterior
Dorsal
Anterior
Ventral
Step Direction

Figure 3.6 Blood flow regulates direction preference of EC migration during sprout regression.

(**A**) Example of ECs within the sprout that are analysed. The trajectories of the ECs are traced and grouped into subsets based on their *initial* position at 56hpf. Tip cells are in pink and SIV cells in blue. The migration 'step' is defined as the movement of ECs between two consecutive time points (green and black arrows). (**B**) The coordinates of SIV cell migration steps in the *control* or *tnnt2a* morphants are shown in scatter plot. The blue circle (radius = 5μm) in each plot is outlined as a reference for coordinate distribution. The steps are anisotropic yet favour in bottom-left of the circle in the absence of flow. (**C**) The angles of SIV cell migration steps are plotted in rose chart (polar histogram). The length of each bar indicates the relative number of migration steps towards that direction (normalised to the total number of migration steps). The values in rose chart are grouped in bar chart for comparison in D. (**D**) There is a significant increase in anterior migration in the absence of flow. *control*, n=1313 steps from 6 embryos; *tnnt2a*, n=744 steps from 6 embryos. Green arrow indicates anterior direction. (**E**) The coordinates of tip cell migration steps in the *control* or *tnnt2a* morphants are shown in scatter plot. The magenta circle (radius = 5μm) in each plot is outlined as a reference for coordinate distribution. The steps are more confined along y-axis in the absence of flow compared to controls. (**F**) Each angle of the migration steps taken by the tip cell are plotted in rose chart and is normalised to the total number of angles. The values are grouped in bar chart for comparison in G. (**G**) There is a significant increase in ventral migration in expense of dorsal migration in the absence of flow. *control*, n=383 steps from 4 embryos; *tnnt2a*, n=860 steps from 4 embryos. (**H**) Schematics show the migratory behaviour of EC migration during sprout regression. In the presence of flow, the SIV cells migrate laterally to 'make room' for tip cells which migrate dorsally to undergo sprout regression. However, in the absence of flow, tip cells migrate more ventrally while SIV cells more anteriorly, resulting in an elongated leading sprout. Unpaired t-test, *p<=0.05; ns, no significance.

3.7 Lateral migration of ECs is dependent of blood flow during vascular remodelling.

Previous data showed that although the migration steps of ECs are variable, blood flow influences the preference of direction, which leads to significant differences in final trajectory paths (examples in Figure 3.7F). To quantify such differences, I measured several parameters of the tracks, including total migration distance, velocity, tortuosity ratio (distance/displacement ratio), and track ΔX and ΔY of displacement (Figure 3.7A).

No significant differences in the total migration length between *control* and *tnnt2a* morphants were observed (Figure 3.7B), indicating that the ability of ECs to migrate was not diminished by the absence of blood flow. However, I observed that migration trajectories in the presence of flow displayed longer steps at the beginning and shorter near the end of the migration path, whereas in the absence of flow the migration steps displayed similar length, suggesting that the migration velocity was different.

The migration velocity in *control* or *tnnt2a* morphants displayed distinct patterns. In the presence of flow, tip cells migrated at a velocity of 9.2 μm/hour at the beginning, and significantly decreased to 7.0 μm/hour and then 5.4 μm/hour (Figure 3.7B, black line). The gradual reduction of migration velocity of tip cells in response to flow was disrupted in *tnnt2a* morphants which displayed a moderate migration speed ranging between 6.2-7.6 μm/hour during the entire observation period and exhibited a significant increase in velocity during the completion period (66-72hpf) compared to controls (Figure 3.7B, magenta line). Similarly, in the presence of flow, SIV cells started off with a velocity of 8.1 μm/hour and significantly slowed down by 72hpf with a velocity

of 5.4 μm/hour (Figure 3.7B, black line). In contrast, this decreasing trend of velocity was disrupted in SIV cells in the absence of flow, which displayed a moderate velocity ranging between 6.2-7.6 μm/hour. These data suggested that blood flow may progressively limit the migration velocity of the ECs during SIV development.

Although the total migration distance of tip and SIV cells did not differ between *control* and *tnnt2a* morphants (Figure 3.7B), the distance/displacement ratio, termed tortuosity ratio, was decreased in tip cells in the absence of flow (Figure 3.7C). The tortuosity ratio was close to 1 which indicated the cells migrate close to a straight line while the larger the ratio, the more complicated a cell migrated. The reduction of tortuosity ratio in tip cells without flow could result from a reduction of lateral (ΔX) or vertical (ΔY) migration distance of tip cells, therefore I compared the track ΔX and ΔY between *control* and *tnnt2a* morphants. While in the presence of flow over 75% of tip cells migrated posteriorly (ΔX>0, posterior, median ΔX of +10.8 μm), less than 50% of tip cells exhibited posterior migration in the absence of flow (Figure 3.7C). Moreover, tip cells in *tnnt2a* morphants almost remained at the same position on the X-axis, showing a significant reduction of ΔX compared to controls (ΔX<0, anterior, ΔX median of -2.3 μm) (Figure 3.7C). Track ΔY of tip cells in *control* or *tnnt2a* morphants was negative (Figure 3.7C), suggesting that all tip cells migrated more ventrally than their initial position. Although track ΔY of tip cells was not affected by the lack of flow, the distribution of the data was very different. The shapes of *control* and *tnnt2a* violin plots were similar but inverted, showing a quarter of *control* tip cells with track ΔY higher than -50 μm while a quarter of *tnnt2a* tip cells with track ΔY lower than -100 μm (Figure 3.7C). This was in line with previous findings that tip cells rearranged to become SIV cells in the presence of flow whereas these continued migrating ventrally in the absence of flow.

Similarly, the distribution of SIV cells migrated along X- and Y- axis were different with or without flow (Figure 3.7D). In the presence of flow, track ΔX of SIV cells exhibited a wider range than those in *tnnt2a* morphants and approximately 75% of the control cells migrated posteriorly (median ΔX of +11.3 μm) (Figure 3.7D), suggesting that ECs in the SIV migrated posteriorly in longer distance. This was in line with previous data that SIV cells preferred posterior migration in the presence of flow (Figure 3.6D), leading to a cumulative migration at posterior direction which resulted in posterior tracks. Whereas in the absence of flow the SIV cells remained at similar location at X-axis (median ΔX of -1.4 μm). This suggested that the migration path of ECs without flow were more confined, resulting in accumulation of cells within the leading sprouts. Although the majority of the SIV cells migrated ventrally (for SIVP expansion) with or without flow, there were ECs which migrated dorsally with positive track ΔY, indicating that these reached at a position that was higher than their initial position to join the branches in the presence of flow. This active migratory behaviour was almost lost in the absence of flow (Figure 3.7D), reflected as a decrease of cell rearrangement from SIV to branches (Figure 3.5C).

In the presence of flow, as a consequence of ECs migrating laterally in various distances (large variation of ΔX), the ECs were distanced two-folds higher (mean 21μm, example in Figure 3.7F) than their nucleus diameter (mean 10μm) (Figure 3.7E). However, in the absence of flow, the nuclear spacing was significantly decreased (14μm) (Figure 3.7E), as the ECs were crowded within the leading sprouts (Figure 3.7F, *tnnt2a* trajectories). This suggested that blood flow regulates proper EC spacing within the SIVP.

Collectively, these data combined with the migration step analysis maps out the migratory behaviour of ECs which comprise the leading sprouts (Figure 3.5H & Figure

3.7F). At the onset of blood flow, ECs migrate ventrally at relatively high velocity as the SIVP expands rapidly (Figure 3.7B). While blood flow increases, migration of these cells progressively slows down, and ECs display complex migration-driven rearrangement. The SIV cells that experience blood flow from the posterior to anterior migrate against the direction of flow (Figure 3.5D) and drive lateral expansion of the SIVP (Figure 3.7D). The adjacent tip cells that are membrane-bound to the SIV cells also migrate posteriorly (Figure 3.7C), while they also display dorsal migration which leads to sprout regression (Figure 3.5G). When the sprout regression completes, the ECs within the SIV are aligned and more evenly spaced (Figure 3.7E). However, in the absence of flow, ECs display a moderate velocity throughout remodelling (Figure 3.7B) and exhibit decreased preference for dorsal-lateral migration (Figure 3.5D &G), resulting in crowding of ECs with decreased intercellular spacing within the leading sprouts (Figure 3.7E). The track ΔY of the tip and SIV cells did not differ in the presence and absence of flow, suggesting that ventral migration of the ECs is instructed by flow-independent signals. However, blood flow may provide a force for ECs to migrate laterally, which is impaired in the absence of flow (Figure 3.7F).

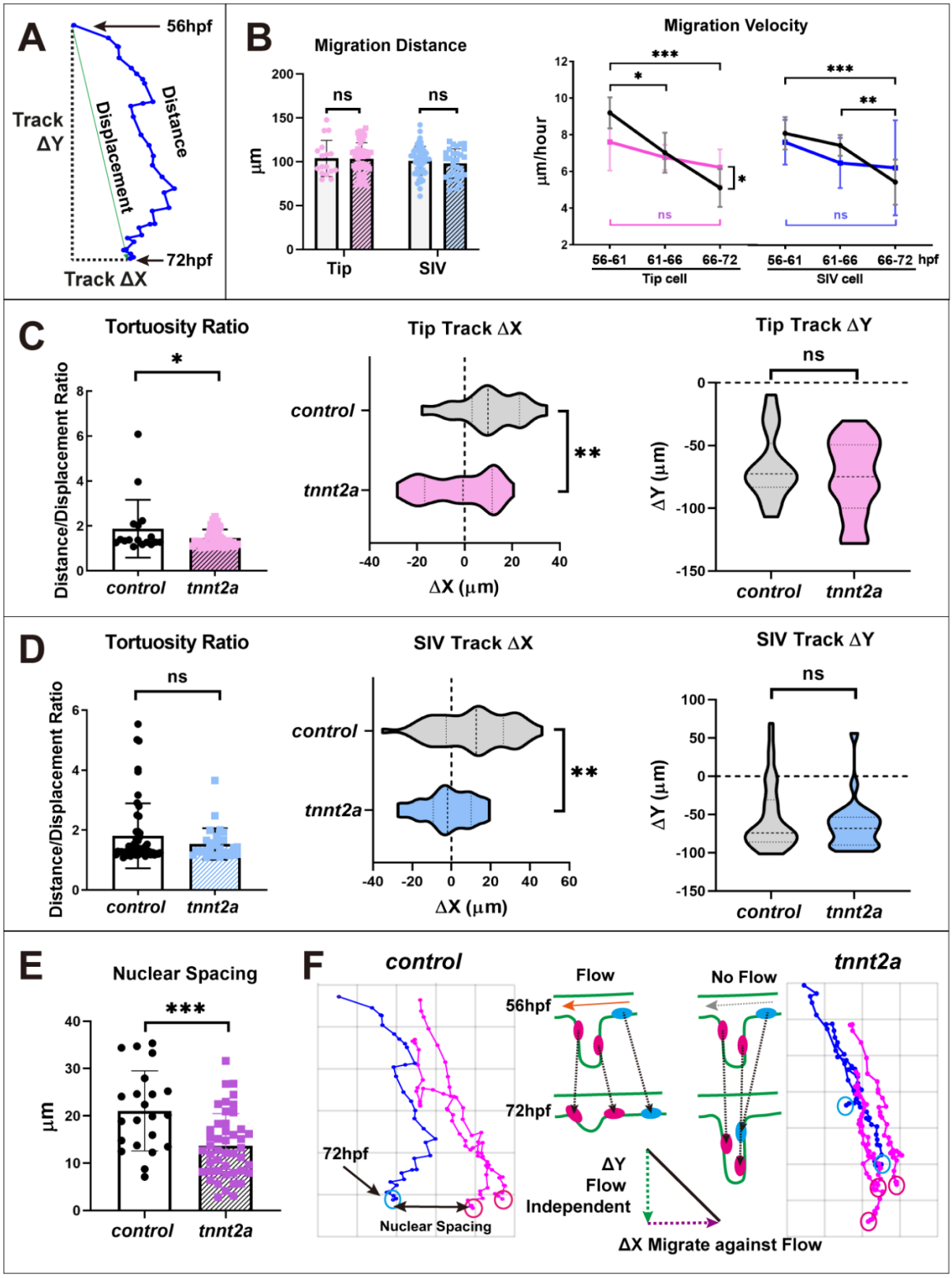
A
56hpf
Distance
Displacement
Track ΔY
72hpf
Track ΔX
B
Migration Distance
ns
ns
μm
Tip
SIV
Migration Velocity
***
*
*
ns
***
**
ns
μm/hour
56-61
61-66
66-72
Tip cell
56-61
61-66
66-72 hpf
SIV cell
C
Tortuosity Ratio
*
Distance/Displacement Ratio
control
tnnt2a
Tip Track ΔX
control
tnnt2a
**
ΔX (μm)
Tip Track ΔY
ns
ΔY (μm)
control
tnnt2a
D
Tortuosity Ratio
ns
Distance/Displacement Ratio
control
tnnt2a
SIV Track ΔX
control
tnnt2a
**
ΔX (μm)
SIV Track ΔY
ns
ΔY (μm)
control
tnnt2a
E
Nuclear Spacing
***
μm
control
tnnt2a
F
control
Flow
No Flow
tnnt2a
56hpf
72hpf
72hpf
Nuclear Spacing
ΔY
Flow
Independent
ΔX Migrate against Flow

Figure 3.7. Blood flow regulates EC migration velocity and lateral migration during vascular remodelling.

(**A**) Examples of the parameters that are quantified: track displacement (green line), distance (blue trajectory), track ΔX and ΔY as indicated in dashed lines and time points (blue dots, interval 30mins). (**B**) The total distance does not significantly differ in tip or SIV cells of *control* (white bars) and *tnnt2a* (shaded bars) morphants. The migration velocity of the tip or SIV cells is significantly decreased in the presence of flow overtime (black lines), whereas this trend is absent in *tnnt2a* morphants (coloured lines). (**C**) The tortuosity ratio of tip cells is significantly decreased in the absence of flow compared to controls. The track ΔX and ΔY of each track are quantified and compared between *control* (grey) and *tnnt2a* (pink) morphants. There is a significant difference in track ΔX in tip cells in the presence or absence of flow, showing positive track ΔX in controls while those without flow are negative. The track ΔY does not differ with/without flow, but the distributions of the track ΔY are different. (**D**) The track tortuosity ratio of SIV cells is not altered with or without flow. However, there is a significant difference in track ΔX between *control* and *tnnt2a* morphants. The track ΔY of SIV cells does not differ with or without flow, but the distributions of the track ΔY are different. (**E**) At 72hpf, ECs display decreased distance between nuclei in *tnnt2a* morphants compared to controls. (**F**) Schematics showing the difference of track displacement in the presence and absence of flow during SIVP development. ECs migrate ventrally and support the expansion of the SVIP in the presence and absence of flow, indicating a directed ventral migration driven by flow-independent signals (green arrow). However, since blood flow circulates from posteriorly to anteriorly in the SIV (orange arrow), it provides a horizontal force against which ECs migrate (magenta arrow). Migration along these two directions results in track displacement pointing ventral-posterior direction. Each dot represents a migration track of a single EC. *control*, n=70 tracks from 5 embryos; *tnnt2a*, n=73 tracks from 5 embryos. Unpaired t-test, *p<=0.05, ns, no significance. Orientation: down, ventral; right, posterior.

3.8 Blood flow regulates EC axial polarity during sprout regression

ECs display polarisation during migration and in response to blood flow (Franco *et al.*, 2016, 2015; Kwon *et al.*, 2016). The relative position of the Golgi and nucleus is used as an indicator for EC polarity, for example by assaying whether the Golgi is localised at the migration front or upstream of the nucleus with respect to the direction of flow; Golgi which are localised medially relative to the nucleus indicates non-polarisation of the ECs (Kwon *et al.*, 2016). To investigate whether blood flow regulates EC polarisation during migration-driven sprout regression, I generated the transgenic lines, *Tg(fli1a:golgi-tagRFP);(cry:CFP)*^{SH529}; *(fli1a:nls-GFP)*^{SH549} (method 2.2.1.19.1) to analyse the Golgi-nucleus polarisation in the leading sprouts. Golgi labelled with RFP were colour-coded in magenta and schematics were shown based on original still images (Movie 7, Movie 8 & Figure 3.8).

At the beginning of the time-lapse, in the presence of flow, the sprout consisted of two tip cells (Figure 3.8A & A'). When one of the tip cells (dark blue) underwent mitosis, the two Golgi apparatuses polarised in opposite directions and the two daughter cells divided (Figure 3.8B & B'). One of the daughter cells (dark blue) displayed a ventrally positioned Golgi and joined the existing tip cell (pink) to comprise the leading sprout (Figure 3.8C & C') The Golgi of the other daughter cell (light blue) located towards the posterior side of the SIV and migrated rapidly against flow (Figure 3.8D & D'). Subsequently, the Golgi of the EC labelled in dark blue promptly polarised upstream of the nucleus and the cell migrated against flow (Figure 3.8E & E'). Eventually, the sprout regressed and the Golgi of the last cell (pink) remained close to the nucleus and localised to the luminal side of the EC (Figure 3.8F & F'), suggesting

establishment of apical polarity (Kwon *et al.*, 2016). Interestingly, it was noted that although ECs displayed sustained dorsal-posterior polarisation, their net displacement was ventral. This was in line with previous cell tracking data that tip cells displayed transient dorsal migration during collective ventral expansion.

In the absence of flow, ECs within the leading sprout did not polarise (Figure 3.8a & a'). The Golgi apparatus in proliferating cells positioned at the opposite ends of the two daughter cells (blue pairs and green pairs), which was parallel to the division direction (Figure 3.8b & b'). The Golgi of the daughter cells (light blue and light green) that were divided at the rear end of the sprout moved up and down near the nucleus and the net displacements were roughly unchanged (Figure 3.8b'-f'). The other daughter cells (dark blue and dark green) however, displayed persistently ventral Golgi-nucleus position, and continued migrating ventrally, resulting in the elongation of the leading sprout (Figure 3.8e' & f'). The cell at the front of the leading sprouts (pink) remained non-polarised until the two dark-coloured cells arrived (Figure 3.8c'- e'), indicated that this cell (pink) may have been restricted from moving, probably due to membrane tension. The Golgi of the cell (pink) then polarised at the migration front as it started moving ventrally (Figure 3.8f').

Taken together, these observations revealed the dynamics of cell polarity during sprout regression, and that the Golgi rearrangements was flow dependent (Figure 3.8G). In the presence of flow, ECs polarise before migration, with their Golgi localised at the migration front. Since blood flow within the SIV circulates from posterior to anterior (Figure 3.8G), SIV cells polarise posteriorly with subsequent posterior migration against flow. Following this, either being pulled by the SIV cells or sensed the circulating flow, the tip cells that were migrating ventrally reverse their Golgi position from ventral to dorsal. Later sustained dorsal polarisation suggested the tip

cells might sense the flow and actively migrate away from the sprout and dorsally towards the SIV. However, in the absence of flow, tip cells fail to polarise dorsally and their Golgi apparatus ‘shuffles’ between non-polarised and ventral localisation, resulting in elongated sprouts. These data are consistent with previous EC trajectory migration results, supporting the close link of EC polarisation and migration during vascular remodelling within the SIVP.

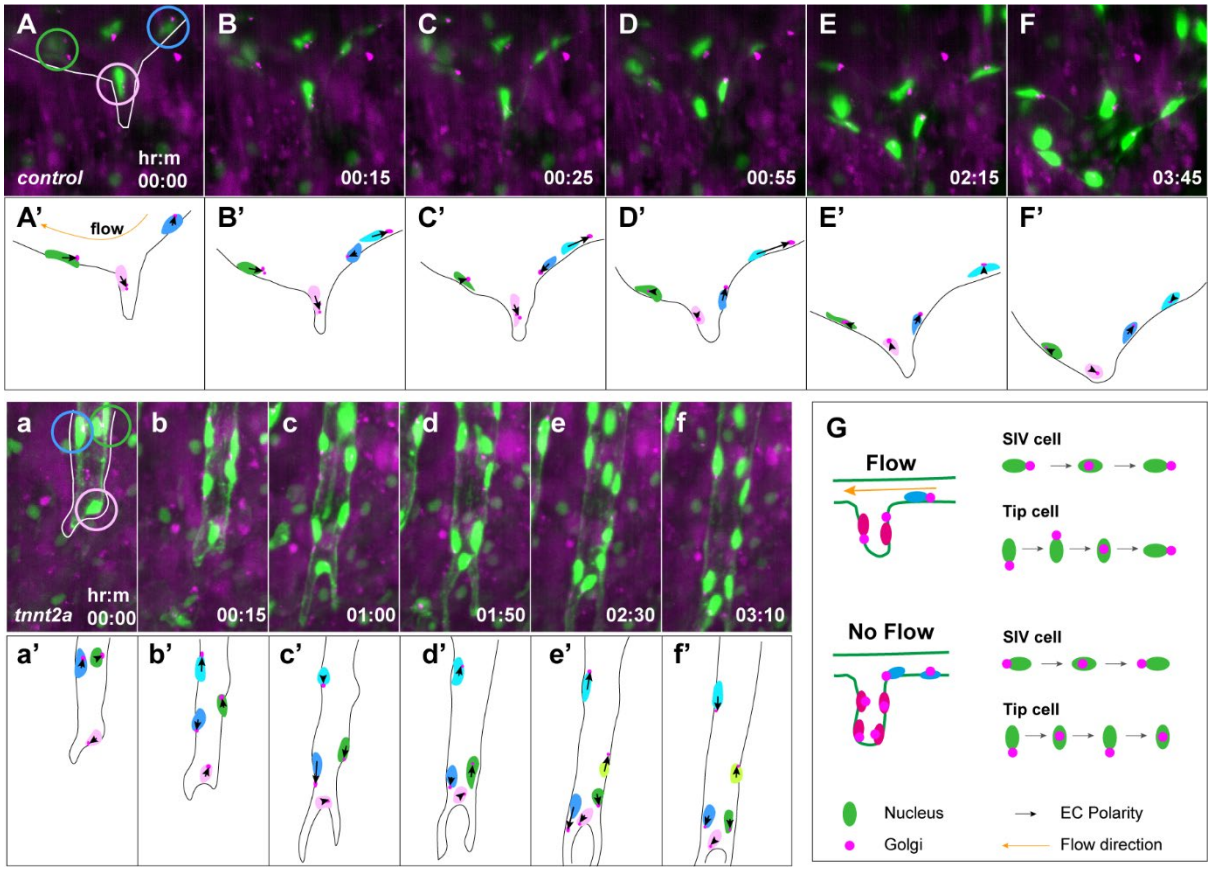

Figure 3.8 ECs migrate against blood flow during sprout regression.

(**A-F**) Still images are obtained from time-lapse Movie 7. The location of Golgi apparatus within a regressing sprout is shown in the presence of flow. *Tg(fli1a:golgi-tagRFP);(cry:CFP)*^{SH529}; *(fli1a:nls-GFP)*^{SH549} line is used to label endothelial nucleus (green) and Golgi (magenta). (**A'-F'**) Schematics show the EC polarity indicated by nucleus-Golgi position, based on still images in **A-F**. One of the cells within the sprout (dark blue) proliferates (**A'** & **B'**): the daughter cell (dark blue) migrates ventrally to comprise the leading sprout (**C'**); the other one migrates dorsal-laterally with its Golgi in front of nucleus (**D'**). Subsequently, the Golgi of the cell in dark blue locates against flow, and the cell migrates towards the SIV, leading to sprout regression (**E'-F'**); the last cell (pink) is non-polarised with its Golgi facing to the lumen. (**a-f**) Still images are obtained from time-lapse Movie 8. The Golgi position of the ECs in a leading sprout that fails to regress in the absence of flow. (**a'-f'**) Schematics show the EC polarity indicated by nucleus-Golgi position, based on still images in **a-f**. Two cells proliferate during imaging: the Golgi apparatus of the two daughter cells (light blue and light green) are shuffling up and down (**b'-f)**; while the other two cells (dark blue and dark green) and the most front cell (pink) migrate ventrally, resulting in an elongated sprout (**c'-f'**). (**G**) A schematic model showing the pattern of cell polarisation in the presence or absence of flow. During sprout regression, SIV cells receiving a horizontal force polarise and migrate laterally. Tip cells that polarised ventrally during sprouting, and display reversed Golgi arrangement towards dorsal direction, leading to ECs migrating away from the sprout and towards the SIV. In the absence of flow, SIV cells and tip cells fail to polarise posteriorly or dorsally, and their Golgi apparatus 'shuffles' between non-polarised and ventral direction, resulting in elongated sprouts.

To understand when ECs become polarised in response to flow during SIV remodelling, I imaged the embryos at different time points: 56hpf (onset of flow), 64hpf (remodelling), and 72hpf (completion of sprout regression). ECs located in the SIV (termed ventral cells) and the sprouts (termed sprout cells) were quantified. Notably, 'sprout cells' might contain a combination of tip and SIV cells in the absence of flow (based on previous conclusions, Figure 3.5D) while there were only tip cells in the presence of flow (Figure 3.9C). Similarly, tip cells became SIV cells during sprout regression therefore the 'SIV cells' might contain tip and SIV cells in the presence of flow (Figure 3.9B). The position of Golgi at either side of the elongated nucleus was considered as 'polarised': dorsal (45-135°) and ventral (225-315°) in sprout cells; upstream (0-45°) or downstream (135-180°) in ventral cells.

Before the onset of blood flow, and since tip/sprout cells in controls do not experience blood flow and undergo rapid ventral migration (Figure 3.6), 45% of sprout cells had their Golgi positioned ventrally at the migration front (Figure 3.9B, green bar) while 21% of sprout cells displayed dorsal polarisation of Golgi (Figure 3.9B, magenta bar). The percentage of dorsal polarisation did not significantly alter in *tnnt2a* morphants (Figure 3.9B, shaded magenta bar). However, the percentage of dorsally positioned Golgi was significantly increased by 62hpf in response to flow (40%, '64hpf' in Figure 3.9B), suggesting that sprout cells were actively polarising dorsally during regression. This increase of polarisation was disrupted in the absence of flow, with only 16% of sprout cells displaying dorsal polarisation by 64hpf in *tnnt2a* morphants (Figure 3.9B, shaded magenta bar). The leading sprouts were eventually incorporated into the SIV, therefore no sprout cells were observed at 72hpf (Figure 3.9B). In the absence of flow, less than 20% of sprout cells polarised dorsally at all time points. Instead, more sprout cells polarised ventrally during remodelling (54% at 64hpf) or

were non-polarised at the end of imaging (58% at 72hpf) (Figure 3.9B), suggesting that blood flow is required for cell polarisation during sprout regression.

At the onset of flow at 56hpf, approximately 80% of SIV cells were non-polarised in either *control* or *tnnt2a* morphants (Figure 3.9C, white bars) and there was no significant change in EC Golgi localised upstream of the nucleus between these morphants (Figure 3.9C, blue bars). ECs became polarised upstream of flow between 56hpf and 64hpf in controls as blood flow became more vigorous, showing a significant increase from 13% of ventral cells to 36% (Figure 3.9C, blue bars). Conversely, in the absence of flow, ventral cells displayed reduced upstream Golgi polarisation compared to controls at 64hpf (Figure 3.9C, shaded blue bar). At 72hpf, 33% of ventral cells exhibited upstream Golgi localisation, yet the majority of ventral cells (>60%) remained non-polarised during the observation period (Figure 3.9C), which was in line with previous reports that venous ECs were usually less polarised than arterial ECs (Kwon *et al.*, 2016). In the absence of flow, more than 65% of ventral cells were non-polarised and fewer ventral cells (less than 20%) polarised towards the posterior (upstream, as if there had been blood flow) (Figure 3.9C, shaded green bar).

Collectively, these results suggest that blood flow confers directionality for ECs to migrate. As blood flows to the horizontal SIV, the SIV cells receive a lateral force which directs them to polarise and migrate laterally. This was in line with previous observation that the SIV cell exhibited preference for posterior direction (Figure 3.6D). In the case of tip cells located within the leading sprouts that were free of flow (Figure 3.1F), the perfused SIV might be more ‘attractive’ for them to polarise and led to subsequent dorsal migration (Figure 3.6D). In contrast, most of the SIV cells were non-polarised and more tip cells polarised ventrally when the horizontal force was withdrawn in the absence of flow (Figure 3.9C), resulting in elongation of the leading sprouts.

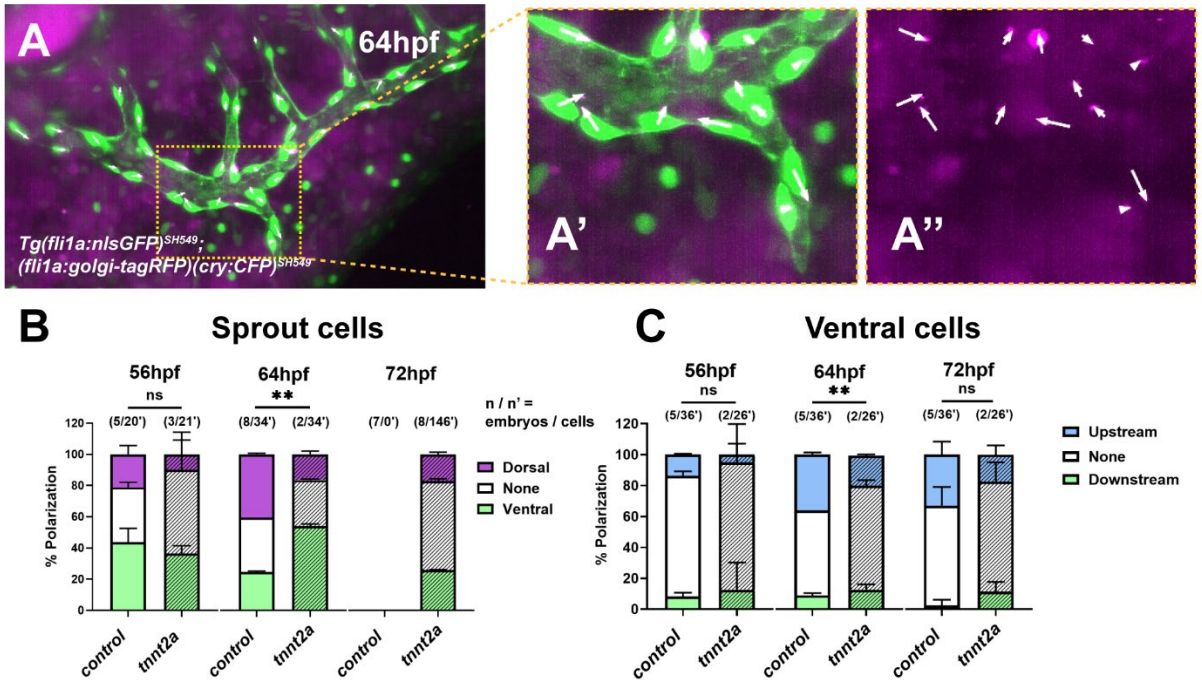

Figure 3.9 Blood flow confers directionality for ECs in the SIVP.

(**A**) Examples of the endothelial polarity based on nucleus-Golgi position. Area in yellow square is enlarged in A' & A (RFP channel). The Golgi polarity was quantified at 56hpf (onset of flow), 64hpf (sprout regressing) and 72hpf (completion of regression) in ECs within the sprout and the SIV (**B** & **C**). (**B**) Comparison of the percentage of polarised sprout cells in the presence and absence of flow at different time points. There is a significant decrease in the percentage of dorsally polarised sprout cells in the absence of flow at 64hpf. (**C**) Comparison of the percentage of polarised sprout cells in the presence and absence of flow at different time points. There is a significant decrease in the percentage of dorsally polarised sprout cells in the absence of flow at 64hpf. Number on bars: (n/n') = embryos/cells. Unpaired t-test, *p<=0.05, ns, no significance.

3.9 Dynamic nuclear and membrane arrangement ensures regression of leading sprouts without compromising vessel integrity

Tip cells display sustained dorsal-lateral polarisation during transition from sprout to the SIV (Figure 3.8), which could be triggered by the horizontal blood flow. Yet how the ECs sense the local difference in flow during sprout regression is unknown. In addition, ECs maintain the connection between the perfused SIV and the non-perfused sprout without compromising vascular integrity, suggesting well-orchestrated cell-cell contacts. To investigate how ECs sense flow and maintain vessel integrity during sprout regression, I employed embryos from *Tg(fli1a:egfp)^{y1};(fli1a:AC-tagRFP)^{SH511}* which labels endothelial cytosol in GFP and actin in RFP. The GFP labelled cytosol is brighter near nucleus. The fusion of RFP to an actin chromobody (AC), actin-targeting nanobodies, visualises actin structures, such as cortical F-actin and junctional boundaries (Panza *et al.*, 2015; Savage *et al.*, 2019). The identification of individual cells and their relative position in the regressing sprout was achieved via analysis of z-stacks of the images (see Movie 9).

Live imaging of the regressing sprout revealed a dynamic process of cell arrangement and junctional actin polymerisation (Movie 9 & Figure 3.10). A pair of ECs consisted of the leading sprout which was non-perfused, and the rear end of membrane of the two cells shared limited surface connected to the SIV cells (Figure 3.10A). The sprout displayed a longitudinal cell-cell border with F-actin polymerisation (Figure 3.10A), which could be a site of apical polarisation for later lumen formation (Pelton *et al.*, 2014). When the leading sprout underwent regression, both of the tip

cells crawled over each other reaching the edge of the SIV (Figure 3.10A). One of the cells (green, at front) re-orientated its nucleus from vertical to horizontal axis, with most of its membrane incorporated into the main vessel. The other tip cell (pink, at the back of the sprout) had its cell body and nucleus located within the main vessel which contained blood flow, while its distal membrane remained in contact with the adjacent tip cell (green) (Figure 3.10B). Subsequently, the formation of actin filaments at the boundary of the two tip cells was clearly seen; the nucleus of the green cell now aligned horizontally to maintain integrity and its membrane completely retracted in the SIV, while the adjacent tip cell (pink) retracted its distal membrane at which an actin ring formed (Figure 3.10C). The adjacent tip cell (green) retained its position and nuclear alignment until the membrane of the neighbouring tip cell (pink) had completely retracted (Figure 3.10D &E). The actin ring at the distal end of the pink cell began as a single focus of actin (Figure 3.10B) and progressed to a ring structure (Figure 3.10C) which became larger (Figure 3.10D), and eventually closed again as the membrane converged into the main vessel (Figure 3.10E).

Collectively, these results suggested that during regression, the proximal end of the tip cell membrane was in close contact with blood flow which might promote reverse cell migration towards the SIV. I also observed delicate cellular collaboration between the two regressing tip cells: one cell retracted its membrane first and re-oriented the nucleus to prevent leakage, and the other cell subsequently retracted its remaining membrane likely via dynamic actin organisation.

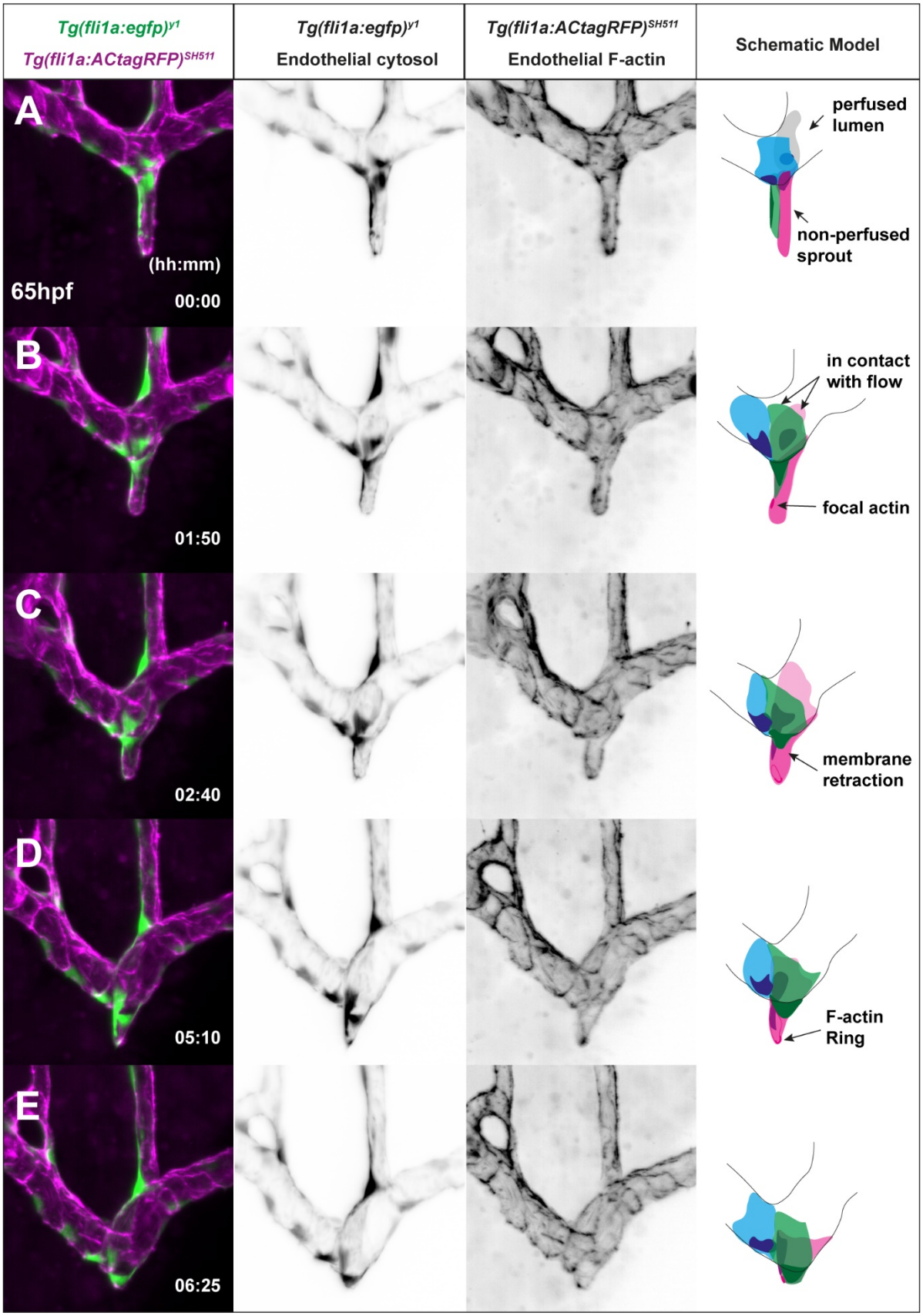
Tg(fli1a:egfp)y1
Tg(fli1a:ACtagRFP)SH511
Tg(fli1a:egfp)y1
Endothelial cytosol
Tg(fli1a:ACtagRFP)SH511
Endothelial F-actin
Schematic Model
A
(hh:mm)
65hpf
00:00
perfused lumen
non-perfused sprout
B
01:50
in contact with flow
focal actin
C
02:40
membrane retraction
D
05:10
F-actin Ring
E
06:25

Figure 3.10 The cellular mechanics of sprout regression

(**A-E**) Representative of live-imaging of a regressing leading sprout starting from 65hpf in *Tg(fli1a:egfp)^{y1};(fli1a:AC-tagRFP)^{SH511}* embryo (Movie 9). GFP (endothelial membrane) and RFP (endothelial actin) channels were shown separately. The schematic model is drawn to illustrate the dynamic process of cell arrangement. (**A**) A pair of tip cells consists of a non-perfused leading sprout. The rear end of the cells displays limited contact with blood flow. (**B**) During regression, one of the tip cell (green) retracts most of its cell body within the SIV and positions its nucleus at the edge of the main vessel. The other tip cell (pink) retracts most of the rear membrane into the SIV which contains blood flow while the distal end consists of the sprout. (**C**) One of the tip cell (pink) continues to retract its distal membrane while the other tip cell (green) holds its position to maintain vessel integrity. (**D**) A focal F-actin dot progressively grows into a ring which closes again when the tip cell completed sprout regression. (**E**) Both tip cells regress and become a part of the multicellular SIV.

3.10 Leading sprouts display impaired formation of filopodia and lamellipodia in the absence of flow

A hallmark of tip cells is the formation of actin-rich filopodia or lamellipodia (Siekmann *et al.*, 2013). Although recent studies suggested a dispensable role of filopodia for tip cell guidance, the absence of which reduces migration velocity and impaired endothelial anastomosis (Phng *et al.*, 2013; Wakayama *et al.*, 2015). Given that the linear reduction of EC migration velocity is disrupted in the absence of flow (Figure 3.7), it is formally possible that the filopodia or lamellipodia formation could be altered by the lack of flow. To investigate this, embryos from *Tg(fli1a:lifeact-mClover)*^{SH467}*;Tg(fli1a:ACtagRFP)*^{SH511} were used to label endothelial filopodia/lamellipodia in GFP and junctional F-actin in RFP (Figure 3.11A-B). Filopodia that were longer than 2 μm were quantified. The RFP junctional edges were used as the baseline and the length of filopodia was quantified from the baseline to the distal tip of the filopodia.

In the absence of flow, I observed a significant increase in the number of filopodia in the leading sprouts compared to controls (Figure 3.11C). However, the length of the filopodia was significantly reduced without flow (Figure 3.11D). Interestingly, unlike in the CVP which only forms filopodia (Wakayama *et al.*, 2015), I observed clear lamellipodia at the front of the leading sprouts. The number of lamellipodia was significantly reduced in *tnnt2a* morphants (Figure

3.11E). Collectively, these results showed that leading sprouts exhibited impaired formation of filopodia and lamellipodia in the absence of flow, which might lead to reduced migration velocity (Figure 3.7B).

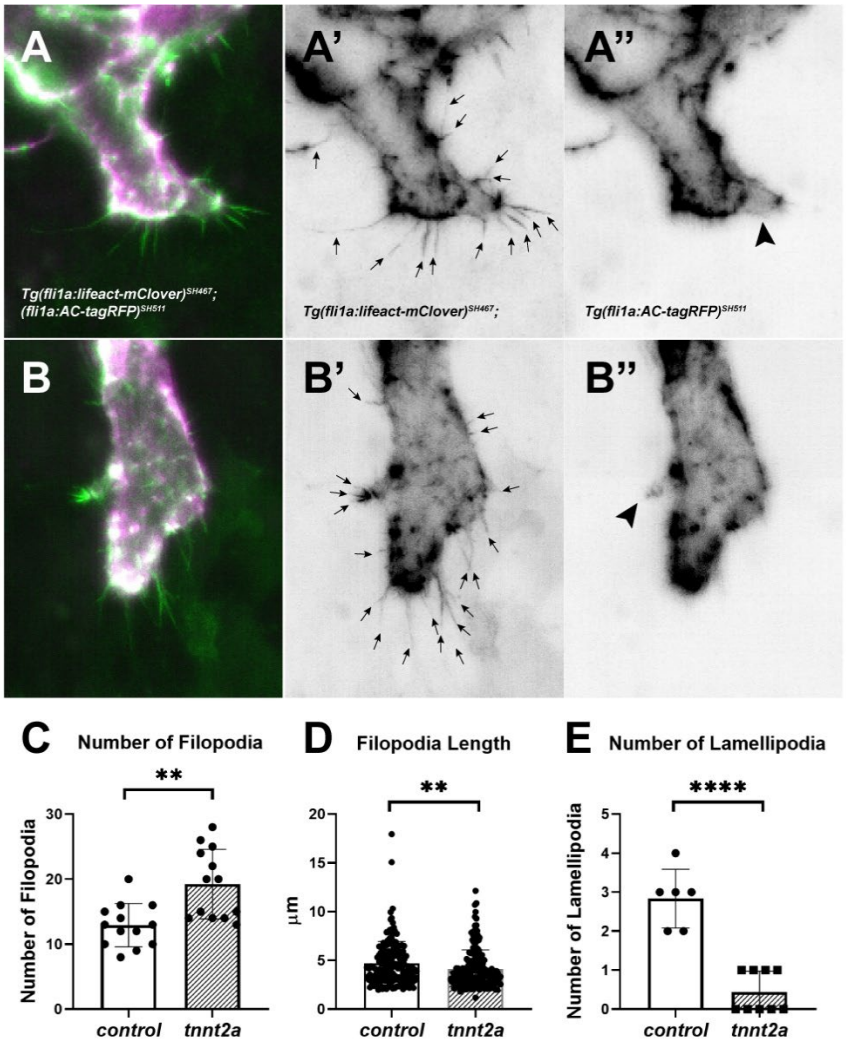

Figure 3.11 Leading sprouts exhibited decreased length of filopodia and reduced number of lamellipodia in the absence of blood flow.

(**A**-**B**) Examples of leading sprouts in *control* or *tnnt2a* morphants at 64hpf from *Tg(fli1a:lifeact-mClover)*^{SH467}*;(fli1a:ACtagRFP)*^{SH511}, showing endothelial filopodia (**A'** & **B'**, arrows) and lamellipodia (**A''** & **B''**, arrow head). The number of filopodia was increased in *tnnt2a* morphants (**C**) but the length of filopodia was decreased (**D**). (**E**) The number of lamellipodia was decreased in *tnnt2a* morphants. *control*, n=13; *tnnt2a*, n=13. Unpaired t-test, ****p<=0.0001.

3.11 Leading sprouts are able to regress under low shear stress condition

It has been demonstrated that flow is required for the pruning of the cross-branches of the SIVP (Lenard *et al.*, 2015) and that the differential high/low flow pattern in juxtaposed branches drives the pruning (Franco *et al.*, 2015). Shear stress relates directly to flow and blood viscosity (Heil & Schaper, 2004) and RBC depletion reduces shear stress exerted by flow (Zhou *et al.*, 2020). Given that tip cells in regressing sprouts are attracted from non-perfused sprouts towards the perfused SIV, the reduced shear stress might generate ectopic sprouts as the low flow is not sufficient to sustain EC polarisation and migration. To test this, I injected embryos with *gata1a* MO, which inhibits red blood cell formation and therefore reduces blood viscosity, and compared the morphology of the *control* and *gata1a* morphants.

To evaluate the effects of *gata1a* knockdown, I quantified the number of RBC passing through the SIV within 30 seconds using time-lapse imaging (representatives in Figure 3.12, magenta, indicated by yellow arrows). There was a significant reduction in the number of circulating RBCs in *gata1a* morphants compared to control (Figure 3.12C), suggesting that the morpholino was functional. The ICVs remained in connection with the SIA and the number of vascular loops was not changed (data not shown), although most vascular loops were collapsed due to fewer circulating RBCs. Surprisingly, I did not observe a significant difference in the number of leading sprouts between

control and *gata1a* morphants (Figure 3.12D). Rather, the diameter of the SIV was increased (Figure 3.12E) and the plexus length was decreased under low-shear conditions (Figure 3.12F). Low shear stress generally induces inward remodelling, causing vessel constriction in the arteries (Silver & Vita, 2006). The enlargement of SIV diameter suggested that flow might act differently during venous vessel remodelling. Collectively, these results suggested that low blood flow conditions are sufficient to induce sprout regression.

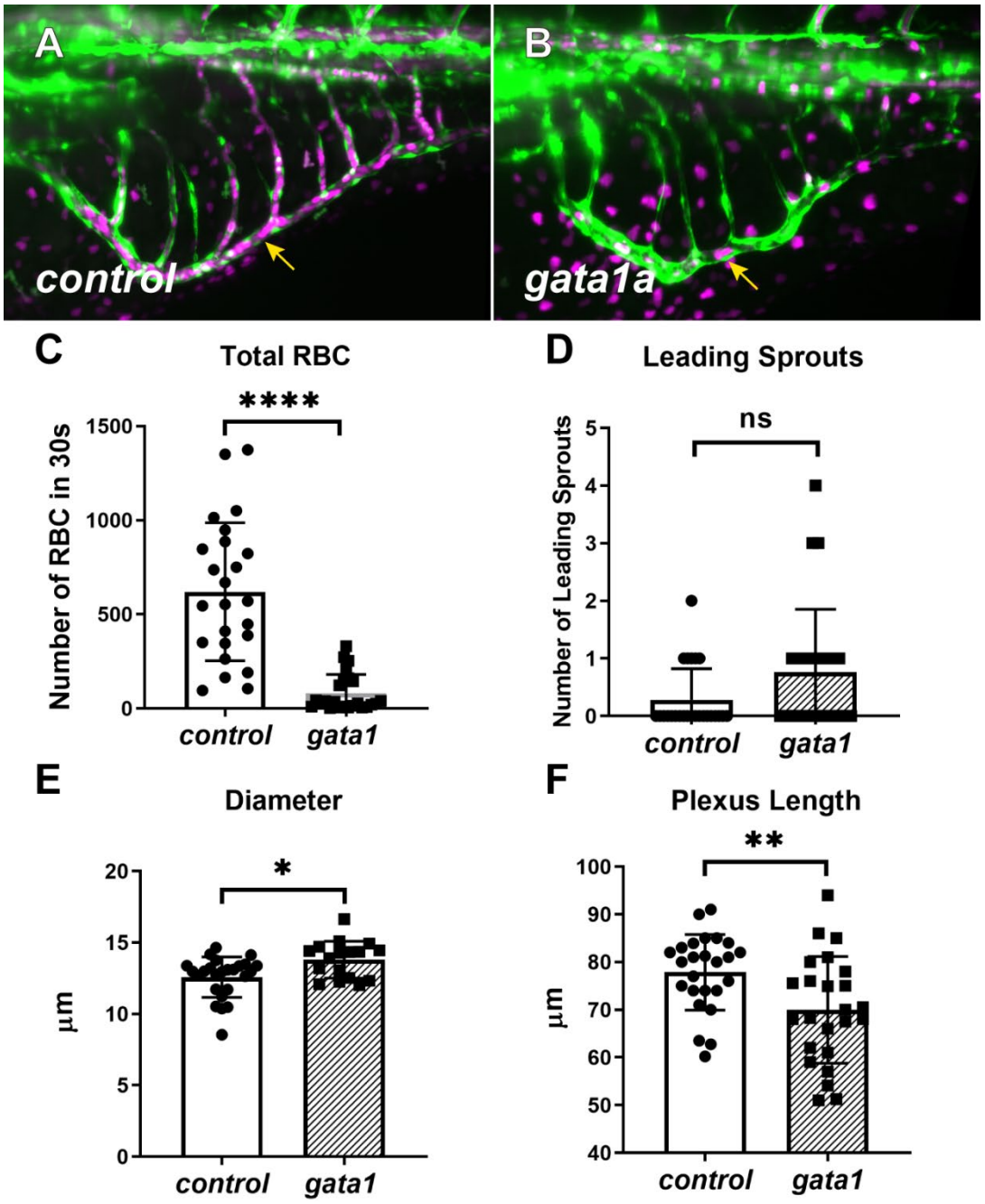

Figure 3.12 Low shear stress does not cause defects in sprout regression

Embryos from *Tg(fli1a:egfp)^{y1};(gata1a:dsRED)^{sD2}* are injected with *control* (**A**) or *gata1a* morpholino (**B**), and are imaged at 72hpf. (**C**) The number of RBC passing through the SIV within 30 seconds are quantified. It is significantly decreased in *gata1a* morphants compared to controls. (**E**) The number of leading sprouts is unchanged between the two morphants, whereas the diameter of the SIV is increased (**D**) and the plexus length is decreased in *gata1a* morphants (**F**). Unpaired t-test, *p<=0.05. *control*, n=24; *gata1a*, n=24 from three replicates.

3.12 Discussion

A major focus of this thesis is to understand how blood flow regulates EC behaviour during vessel remodelling. A key finding is that blood flow controls sprout regression by regulating EC polarisation and co-ordinating migration.

I have investigated the role of blood flow during vessel remodelling, by directly comparing the morphogenesis of the SIVP and EC proliferation and migratory behaviour in the presence and absence of flow. My results demonstrated that blood flow regulates EC Golgi polarisation and subsequent cell migration and membrane retraction during sprout regression.

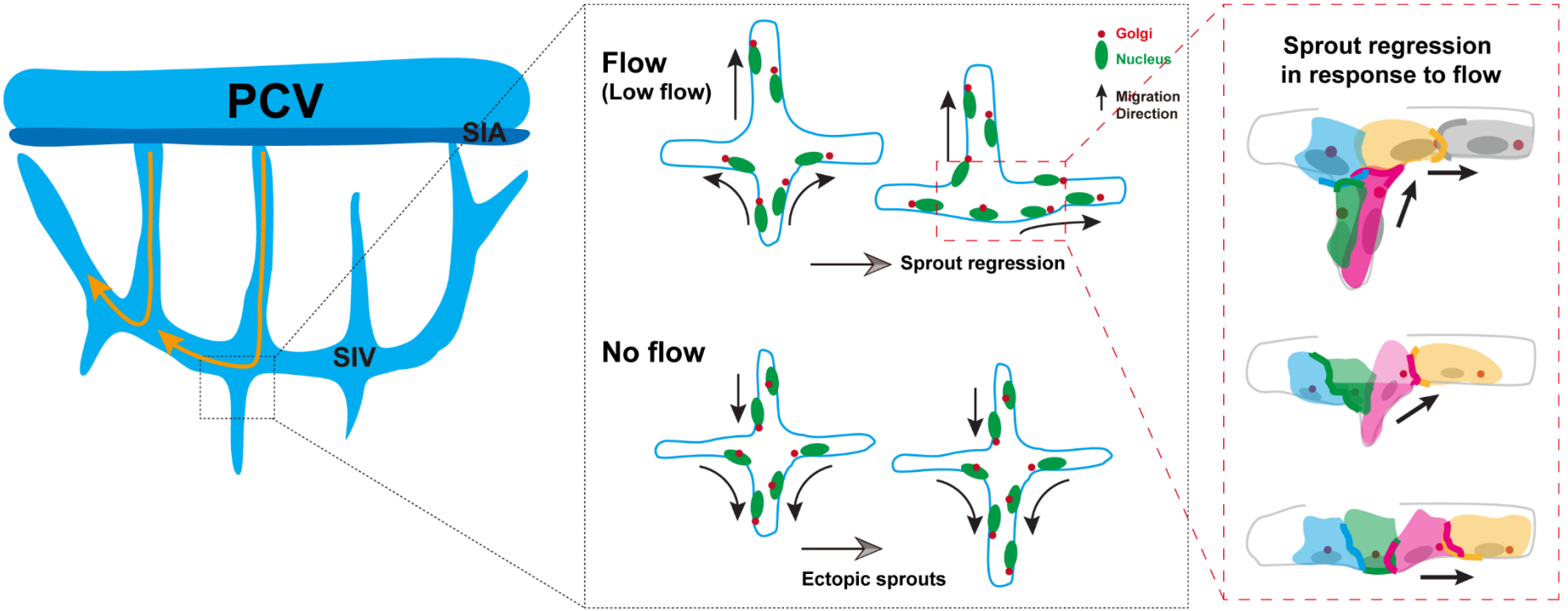

Figure 3.13 Cellular mechanisms underlying SIVP sprout regression

Schematic illustrations depicting the cellular behaviours during SIVP sprout regression in the presence and absence of flow. Blood flow regulates EC polarisation and migration towards dorsal-lateral direction and leads to sprout regression. Schematic illustrations in red box depicting the cell coordination during sprout regression in response to flow. ECs (in grey and yellow) at the luminal surface migrate against flow and ECs (in green and pink) in the regressing sprout are pulled or use their neighbouring cells as migratory substrate via cell-cell junctions (thickened lines), followed by cell rearrangements that lead to sprout regression. In the absence of flow, ECs display reverse directions of polarisation and migration, resulting in ectopic sprouts

3.12.1.1 EC migration drives sprout regression

Developmental remodelling of vascular networks have been described in various models, mostly in vascular cross-branches (Chen *et al.*, 2012; Franco *et al.*, 2015; Kochhan *et al.*, 2013; Lobov *et al.*, 2011; Phng *et al.*, 2009). In this context, pruning occurs in 'O-type' (loop-forming) or 'H-type' (cross-branch) segments (Chen *et al.*, 2012), which ultimately leads to the regression of the cross-branch and leaves behind the two parallel vessels. This is mainly achieved by EC migration although apoptosis also contributes to this process (Zhang, Y. *et al.*, 2018). Dynamic EC migration and rearrangement have also been described in sprouts, however studies mostly focus on angiogenic sprouting and anastomosis (Arima *et al.*, 2011; Bentley *et al.*, 2014; Jakobsson *et al.*, 2010). Whether the sprouts all face the fate of anastomosing with each other, or if not how they are remodelled at later stages was unknown. The zebrafish SIVP provides an *in vivo* model to study this, with the advantages of rapid development and live imaging. By employing this model, I presented here that the majority of the leading sprouts in the SIVP do not anastomose at later stages and are remodelled via EC migration-driven regression (Figure 3.4H).

There are certain similarities and differences between branch pruning and sprout regression. Given that the leading sprouts are non-perfused (Figure 3.1F), sprout regression resembles type II pruning in which branches are

collapsed before remodelling (Betz *et al.*, 2016). In vessel pruning, ECs bridging the recipient and pruning branches display Golgi polarisation and directed migration towards the recipient vessels (Franco *et al.*, 2015). Similarly, the tip cells in the leading sprout exhibit dorsal polarisation and migration towards the SIV (Figure 3.5G & Figure 3.8G). However, the detachment of the pruning branch occurs via a single lasting EC which resolves the connection and retracts its long membrane tail (Chen *et al.*, 2012; Lenard *et al.*, 2015). Whereas in the SIVP, the leading sprout consists of a pair of ECs migrating collectively without dominancy over each other (Figure 3.8G & Hen *et al.*, 2015). Interestingly, EC in the pruning branch breaks the connection immediately adjacent to the nucleus to facilitate the separation of luminal compartments (Lenard *et al.*, 2015). I also observed one of the tip cells positioned its nucleus at the site where the other tip cell retracts its membrane (Figure 3.10). This appears to be a common mechanism of ECs to maintain vascular integrity of the perfused vessel without haemorrhage (Chen *et al.*, 2012; Herwig *et al.*, 2011; Kochhan *et al.*, 2013; Lenard *et al.*, 2015).

While apoptosis occurs in certain mouse retinal vessels where circulation is compromised (Franco *et al.*, 2016, 2015; Hughes and Chan-Ling, 2000) and in zebrafish cranial arteries (Kochhan *et al.*, 2013; Zhang, Y. *et al.*, 2018), no apoptotic cells are observed in the pruning branches of the SIVP (Lenard *et al.*, 2015). In line with this, by tracking the majority of the individual ECs, I did not

observe any cell death during SIVP development, either in the presence or absence of flow. Considering that approximately 70% of total SIVP ECs were traced in each embryo, I cannot exclude the possibility that the apoptosis of ECs occurs in the most anterior or posterior part of the SIVP or in the SIA. However, no apoptotic events occurred in over a hundred leading sprouts observed using live imaging. Therefore, I conclude that EC migration is the primary mechanism of sprout regression within the SIVP.

3.12.1.2 **Regression as sprouting in reverse**

In reticular vasculatures including the SIVP, the mouse retinal and yolk sac vessels (Franco *et al.*, 2015; Lenard *et al.*, 2015; Udan *et al.*, 2013), blood vessels usually form a primitive structure and then remodel to a more mature network once flow enters. This allows temporal separation of sprouting at the migration front and pruning of branches during angiogenesis (Lenard *et al.*, 2015). In the SIVP, new sprouts are rarely produced after the onset of flow and most of the existing ones remodel via regression (Figure 3.4), therefore in this thesis I considered the time after the onset of flow as the period of sprout regression (or remodelling of the plexus). However, as the whole plexus still expands ventrally during this period, the tip cells do not simply migrate ventrally first and then dorsally during regression, but instead display transient/stochastic dorsal migration steps while collectively migrating ventrally (Figure 3.6). This

suggests that sprouting and regression are interlinked during sprout development. An interesting question is at what point such steps leads to irreversible sprout regression?

One possibility is when the tip cells are in direct contact with blood flow. At the onset of flow, the posterior membrane of the tip cells are connected with adjacent SIV ECs and has limited surface experiencing flow. When flow creates sufficiently high shear forces on the SIV cells and drives their migration against flow, this might exert a pulling force on tip cells. Subsequently, the tip cells migrate dorsally with the posterior membrane in contact with flow which triggers dorsal-lateral migration of the tip cells and therefore sprout regression (Figure 3.10). The SIV cells and the tip cells in contact with flow might act as the bridging ECs in branch pruning to sense differences in local flow environment (Franco *et al.*, 2015). In addition, it has been demonstrated that sprouts with multiple ECs display a longitudinal cell-cell border which appears to be a site of apical polarisation for later lumen formation between the tip cells (Pelton *et al.*, 2014). In the SIVP sprouts, dynamic junctional actin polymerisation was observed between the two tip cells (Figure 3.10). Taken together, sprouting and regression share similar cellular behaviours but in a reverse mode. While in sprouting tip cells extend their membrane with filopodia at the migration front, and display ventral polarisation and migration, during regression they polarise and migrate reversely and retract their membrane (Figure 3.8 & Figure 3.10).

3.12.1.3 Blood flow instructs directed EC migration

A primary question in vessel pruning and regression is how the vessels are selected and what triggers the remodelling of a particular vessel. Haemodynamic force exerted by blood flow has been proposed to be one such factor (Chen *et al.*, 2012; Franco *et al.*, 2015; Kochhan *et al.*, 2013; Lenard *et al.*, 2015; Lucitti *et al.*, 2007). Pruning mostly occurs in small and bifurcated branches which contain relatively instable or low flow compared to adjacent large vessels. Artificially halted flow or an absence of flow in these vessels inhibits pruning, suggesting that the local difference in flow patterns between branches triggers pruning (Chen *et al.*, 2012; Lenard *et al.*, 2015). The difference of flow induces polarisation which directs migration of cells against flow, from low-flow segments to high flow ones (Franco *et al.*, 2015). Based on my observations, this idea is consistent with sprout regression.

Upon initiation of sprout regression, ECs within the non-perfused leading sprouts are ‘attracted’ by the relatively high flow in the main vessel, and they polarise and migrate out of the regressing sprouts, towards the recipient vessel. My cell tracking and Golgi polarisation analysis support this view and show that the dorsal-lateral polarisation and migration induced cell rearrangement are highly dynamic processes and are strongly influenced by the presence of flow (Figure 3.6 &Figure 3.7). Such directed behaviour is impeded by the absence of flow, showing reversed cell rearrangement and disrupted EC distribution

within the ectopic sprouts (Figure 3.2 &Figure 3.5). My analysis of cell migration trajectories also reveals that ventral EC migration is independent of flow, indicating a flow-independent signal likely controls this aspect of migration.

Erythroblast circulation is required for mouse yolk sac vascular remodelling (Lucitti *et al.*, 2007). Uneven RBC distribution in bifurcations enhances local shear stress differences between pruning and remaining vessels, therefore is strongly associated with vessel regression (Zhou *et al.*, 2020). Our results show that although the plexus length is decreased in *gata1a* morphants, the number of leading sprouts does not differ from the controls, pointing at a role of blood viscosity in general remodelling but a dispensable role in sprout regression. Given that the tip cells experience no flow within the sprouts, a low level of flow with skimmed plasma might still attracts dorsal migration of the cells. I observed some extreme cases which *gata1a* morphants had zero RBC passing through, the SIVP remained lumenised but still did not exhibited ectopic sprouts (data not shown), indicating a high tolerance of low shear stress for SIVP remodelling. How ECs sense a low level of flow is still unclear and several possible molecular mechanisms have been proposed. The level of VEGFR3 has been suggested to maintain a threshold of shear stress sensed by ECs (Baeyens *et al.*, 2015). The interaction of BMP receptors ALK1 and ENG has been reported to enhance EC sensitivity of flow sensing (Baeyens *et al.*, 2016b). Non-canonical Wnt signalling may control vessel regression by modulating the threshold for flow-

induced EC polarisation (Franco *et al.*, 2016). An alternative explanation of sprout regression under low flow is that ECs are regulated by the molecules carried by blood flow instead of the force itself. Inhibition of Notch signalling or VEGF receptor Flt1 has been shown to induce ectopic sprouts (Hen *et al.*, 2015). The functions of some of these pathways and their interactions with blood flow will be investigated in following chapters.

Chapter 4 The role of VEGF signalling in flow-mediated vascular remodelling

4.1 Introduction

Analysis of EC migration trajectory suggests that SIVP formation is instructed by two different signals: a flow-independent signal which guides ventral migration and formation of a basket-like vasculature, and a flow-mediated signal that refines the structure by regulating branch pruning (Lenard *et al.*, 2015) and sprout regression (Figure 3.7). Little was known about the molecular mechanisms underlying SIVP development, until several studies in recent years began to investigate its origin and the signalling pathways involved (Goi and Childs, 2016; Hen *et al.*, 2015; Koenig *et al.*, 2016; Nicenboim *et al.*, 2015). Surprisingly, small molecule screening revealed that few signalling pathways are required for SIVP development (Goi and Childs, 2016). Pathways known to regulate angiogenesis in other vascular beds including Sonic Hedgehog (Shh), Platelet-derived growth factor (PDGF) and Notch signalling, were shown to have no effect on SIVP formation (Goi and Childs, 2016), although Notch has also been shown to be required for sprout retraction in another study (Hen *et al.*, 2015). SIVP formation is sensitive to VEGF and BMP signalling (Goi and Childs, 2016; Hen *et al.*, 2015; Koenig *et al.*, 2016). In this chapter, I will focus on VEGF signalling and the role of BMP signalling is investigated in the following chapter.

vegfaa mutants display strong inhibition or complete absence of SIV

development (Koenig *et al.*, 2016). *Kdrl* mutants exhibit loss of branches but the SIV remains, whereas morpholino knockdown of *kdr* leads to a mis-patterned SIV with retained connection to the SIA. Combined loss of both *kdrl* and *kdr* abolishes the formation of SIVP, resembling *vegfaa* mutants (Koenig *et al.*, 2016). These results suggest that Vegfaa-Vegfr2/4 signalling is required for SIVP sprouting and formation. Inhibition of VEGF signalling at different developmental stages causes distinct phenotypes; blocking Vegfr2 activity using DMH4 prior to PCV formation at 4hpf results in complete absence of SIVP, whereas inhibition starting at 24hpf (when sprouts are present from the PCV) allows partial formation of the SIV without branch connections (Goi and Childs, 2016). This suggests that Vegfr2 is not required for SIV ventral migration but is essential for dorsal migration and/or formation of SIVP branches. Flow-dependent EC dorsal migration drives sprout regression (Figure 3.6G). It is possible that VEGF might also regulate dorsal migration of ECs within the sprouts.

By contrast, *vegfc* or *flt4* mutants have no apparent vascular defects in venous sprouting or SIVP morphology, although overexpression of *vegfc* induces ectopic sprouts, suggesting that Vegfc is sufficient to induce sprouting (Hen *et al.*, 2015; Koenig *et al.*, 2016). Taken together, these findings suggest that Vegfaa-Kdrl signalling is the primary pathway that regulates SIVP development. Furthermore, inhibition of Notch signalling or

VEGF decoy receptor Flt1 resulted in ectopic leading sprouts, suggesting that sprout regression might be Notch and Flt1 dependent (Hen *et al.*, 2015). Overall, these studies provide evidence for the involvement of VEGF signalling during SIVP development. However, the studies focused on the initial stages of SIVP formation and omitted the effects of blood flow which profoundly regulates endothelial cell behaviour as demonstrated in the previous chapter.

Hypothesis

VEGF signalling is required for sprout regression and blood flow refines VEGF signalling during this process.

Aims

1. To determine the role of VEGF signalling at later stages of SIVP development (i.e. after onset of blood flow);

2. To investigate potential interactions between flow and VEGF signalling during vascular remodelling.

Here I present that expression of particular VEGF receptors are increased in the absence of flow, suggesting that blood flow suppresses VEGFR expression. Overexpression of *vegfaa*$_{165}$ or *vegfc* in the presence of

flow results in ectopic leading sprouts due to remodelling defects but not over-sprouting, suggesting that VEGF ligands are sufficient to override flow-induced sprout regression. However, enforced expression of these ligands in the absence of flow does not induce more ectopic sprouts. Knockdown of *flt4* reduces ectopic leading sprouts in the absence of flow, suggesting that blood flow inhibits *flt4* expression during sprout regression. However, knockdown of *flt4* under low flow conditions results in increased number of sprouts, suggesting a different function of *flt4* that is required for sprout regression under low flow.

4.2 Blood flow does not alter the expression of VEGF ligands during SIVP development

The requirement of Vegfa and Vegfc during SIV development have been reported at early stages (before 48hpf) (Goi and Childs, 2016; Koenig *et al.*, 2016), however, their roles during remodelling in response to flow are unknown. To determine whether the expression of *vegfa* and *vegfc* are present at later stages and whether flow affects their expression, I examined their mRNA expression in *control* and *tnnt2a* morphants at 72hpf, when the sprout regression had completed.

The expression of *vegfaa* was detected in the glomerulus of the developing kidney (Figure 4.1A &B, green arrows), and also in the region between the embryo and yolk extension, where angioblasts sprout and form the primitive SIV and SIA (dotted rectangle). More importantly, there was no apparent difference in the expression of *vegfaa* between *control* and *tnnt2a* morphants (Figure 4.1A &B), suggesting that *vegfaa* expression is not altered in the absence of flow. The expression of *vegfc* was not detectable in regions near the SIVP using *in situ* hybridisation and did not differ between *control* and *tnnt2a* morphants (Figure 4.1C &D).

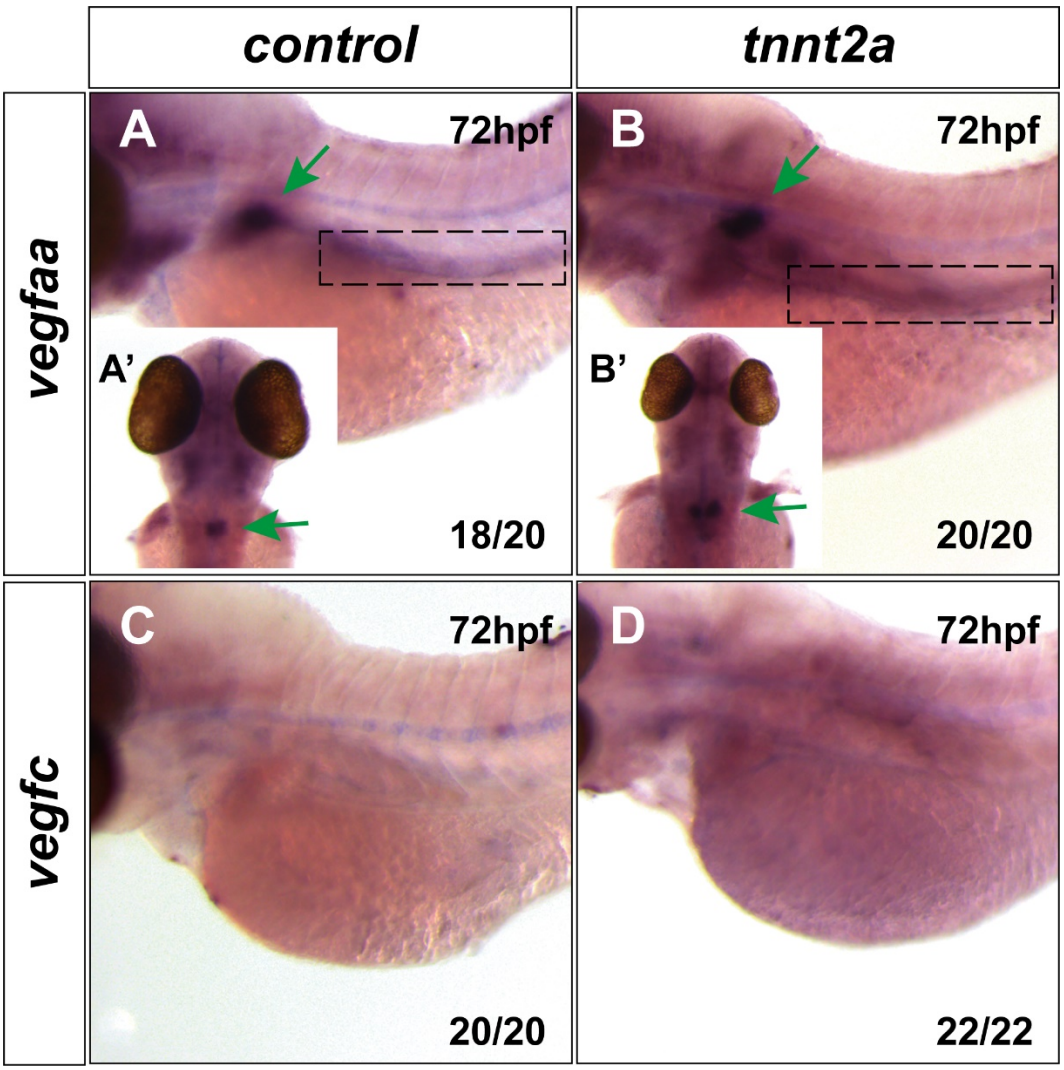

Figure 4.1 Expression of *vegfaa* or *vegfc* are not altered by the absence of flow

(**A**-**B**) Expression of *vegfaa* is detected in the glomerulus of the developing kidney (green arrows) and regions near the SIA (dotted rectangles) and does not differ between *control* and *tnnt2a* morphants. The dorsal view of the embryos is shown at the bottom left (A'-B'). (**C**-**D**) Expression of *vegfc* is not detectable near the SIVP region in either groups. Image orientation: anterior-left, dorsal-top. Numbers indicate embryos in each group.

4.3 Expression of VEGF receptors, *kdrl* and *flt4*, are increased within the sprouts in the absence of flow

To investigate whether flow alters VEGF receptor expression during SIVP development and thus, to investigate whether the response of ECs to VEGF may have been altered by the absence of blood flow, I analysed expression of *kdrl* and *flt4* using *in situ* hybridisation in both *control* and *tnnt2a* morphants at 53hpf (before onset of flow), 60hpf (during remodelling), and 72hpf (completion of sprout regression).

The VEGF receptor *kdrl* was restricted to ECs during all stages of SIVP development (Figure 4.2, yellow arrows). Notably, *kdrl* mRNA was highly expressed in the leading sprouts but was much lower in the branches (white arrowheads) in *tnnt2a* morphants at 72hpf (Figure 4.2E &F). This suggests that in the absence of flow, the branch cells exhibited decreased expression of *kdrl* which is required for dorsal migration (Goi and Childs, 2016). *flt4* was mostly expressed in the SIV (yellow arrows) but not in the branches (white arrowheads) (Figure 4.2G-L). The level of *flt4* expression was comparable between *control* and *tnnt2a* morphants before 60hpf when flow shear stress is low (Figure 4.2G-J). Interestingly, *flt4* expression was elevated at 72hpf in the absence of flow, especially in the leading sprouts (Figure 4.2L, yellow arrow), while the staining was barely detectable in the presence of flow at this stage (Figure 4.2K). These

results suggested that while *flt4* is expressed under conditions of no flow or low flow, it is downregulated under higher flow conditions. More importantly, both *kdrl* and *flt4* were upregulated in the leading sprouts in the absence of flow at later stages.

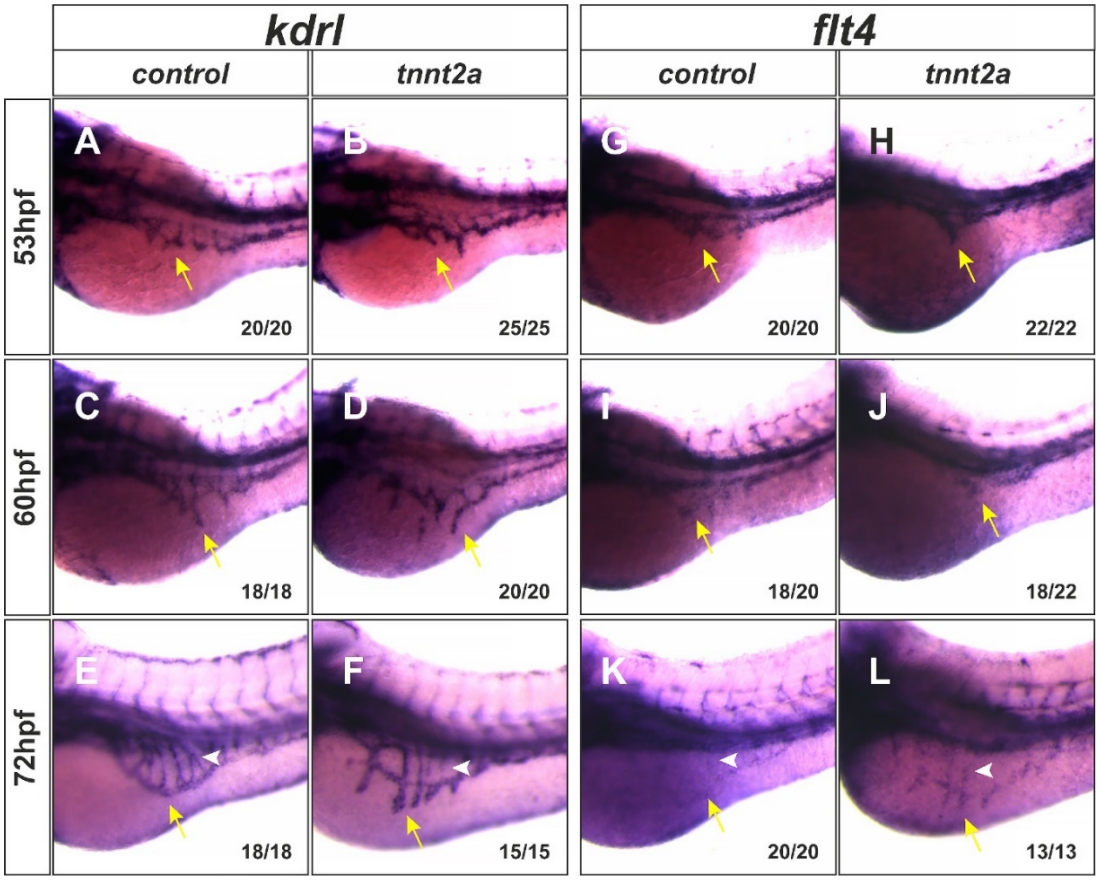

Figure 4.2 Expression of *kdrl* and *flt4* are increased in leading sprouts in the absence of flow

(**A-L**) Expression of VEGF receptors, *kdrl* and *flt4*, is detected using *in situ* hybridisation during SIVP development and compared between *control* and *tnnt2a* morphants. (**A-F**) *kdrl* is expressed in the ECs of the SIVP at 53hpf, 60hpf, and 72hpf with or without flow (yellow arrows). (**F**) The expression of *kdrl* is increased in the leading sprouts in the absence of flow at 72hpf. (**G-L**) *flt4* is expressed in the ECs of the SIVP at 53hpf (**G&H**), 60hpf (**I&J**) with or without flow; the expression is decreased in the presence of flow (**K**) but is maintained in the absence of flow at 72hpf (**L**) (yellow arrows). Image orientation: anterior-left, dorsal-top. Numbers indicate embryos in each group. Experimental repeats N=3.

4.4 Inhibition of VEGF signalling does not alter SIVP sprout regression

Since the expression of VEGF ligands was not altered by the lack of flow (Figure4.3B), but VEGF receptor expression was increased in the leading sprouts in the absence of flow (Figure4.3F &L), this suggested that the potential of SIVP ECs to respond to VEGF signalling was altered by the absence of flow. Inhibition of VEGF signalling at different developmental stages induces distinct phenotypes. Zebrafish *vegfaa* or *kdrl* mutants exhibit a completely loss of SIVP (Koenig *et al.*, 2016) while inhibition of VEGF signalling with DMH4 at 24hpf (sprouting stage) allows the formation of a primitive SIV (Goi and Childs, 2016). Therefore, I asked whether VEGF signalling was required for SIVP remodelling when blood flow was present. I treated *control* or *tnnt2a* morphants with AV951 (also known as Tivozanib, dissolved in DMSO), which is a potent and selective inhibitor of VEGF receptors (VEGFR2/R3/R1) (Chimote *et al.*, 2014). Considering it might take some time for the drug to diffuse into the SIVP region, embryos were treated from 48hpf (before onset of flow) and imaged at 72hpf. Embryos from the transgenic line *Tg(fli1a:egfp)^{y1}; (gata1a:DsRED)^{sD2}* were used to label endothelial cells with GFP and circulating red blood cells with RFP, which indicated the presence of blood flow through the SIVP.

To test the dosage range, embryos were treated at concentrations ranging from 25nM to 250nM. Concentrations over 100nM resulted in complete

abolishment of vertical branches while the primitive SIV remained (data not shown). This was in line with previous report that VEGF signalling is required for the dorsal migration and survival of the branch cells (Goi and Childs, 2016; Koenig *et al.*, 2016). However, blood flow was absent in these embryos due to aberrant connection between the SIA and SIV.

To uncouple the effects of blood flow and VEGF signalling on sprout regression, I reduced the concentration to 25nM at which blood flow was able to develop in the SIVP (Figure4.3C, RFP). As shown in the representative figures, the formation of branches was severely impaired by the AV951 treatment, in both *control* and *tnnt2a* morphants (Figure4.3C &D, asterisks). Quantification of vascular loops in both groups showed a significant reduction following AV951 treatment in comparison to controls (Figure4.3E). However, inhibition of VEGF signaling did not impair plexus length in either group, suggesting that VEGF is not required for ventral expansion of the SIVP (Figure4.3F). This was in line with previous reports (Goi and Childs, 2016; Hen *et al.*, 2015; Koenig *et al.*, 2016). More importantly, AV951 treatment did not adversely affect sprout regression in either the presence or absence of flow (Figure4.3C &D, arrows, &G). Two-way ANOVA analysis indicated there was no interaction between flow and VEGFR inhibition on the vascular loops, plexus length or the number of leading sprouts (Figure4.3E, F &G). Collectively, these results suggested that although VEGF signalling was required for the formation

of branch cells, it did not seem to regulate sprout regression. However, given the low concentration of inhibitor used (to maintain blood flow in the SIVP), it is possible that residual VEGF receptor activity remained, including potential VEGF-independent activation of protein kinase (Jin *et al.*, 2003).

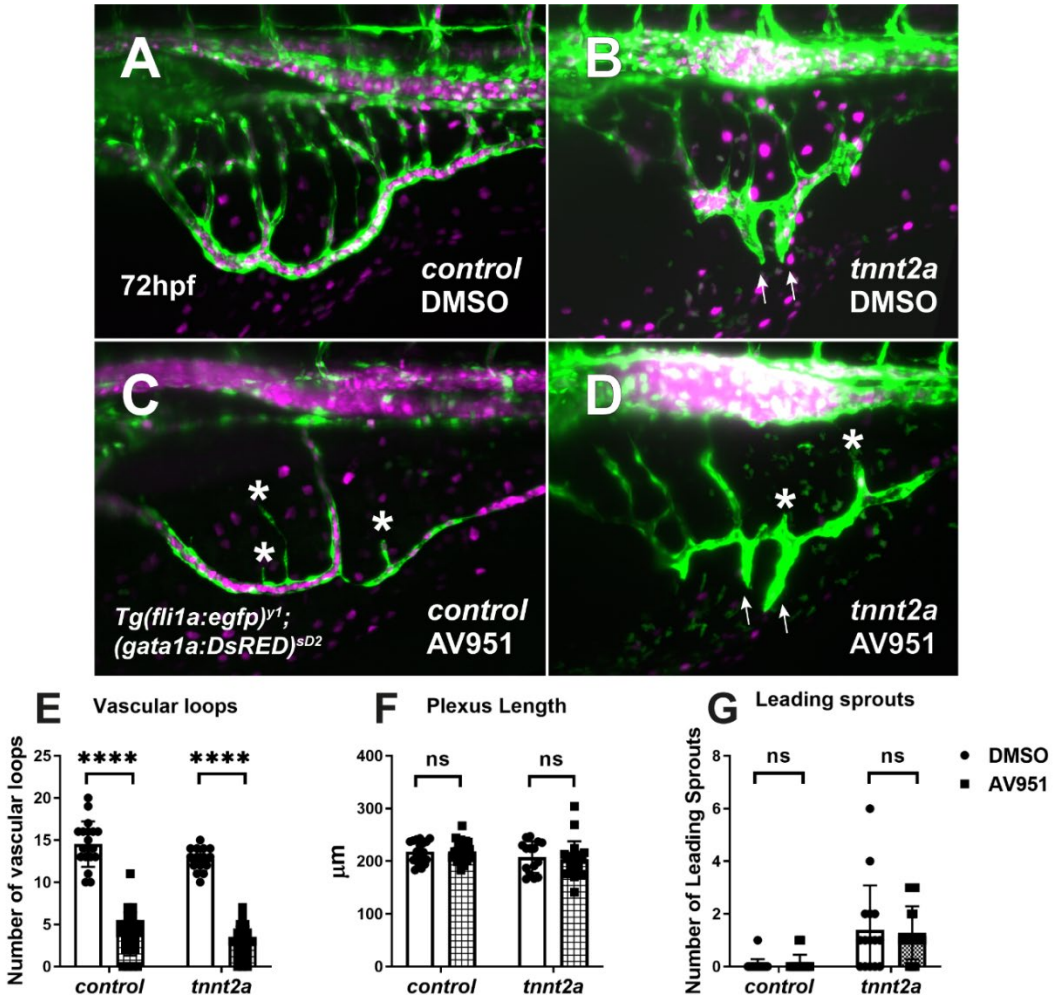

Figure4.3 Inhibition of VEGF receptors impairs formation of branches but does not affect sprout regression at low concentration of AV951

(**A**-**D**) The *control* and *tnnt2a* morphants are treated with 25nM AV951 or 0.2% DMSO at 48hpf and imaged at 72hpf. (**C**&**D)** Inhibition of Vegf receptors leads to impaired branch formation (asterisks) and decreased number of vascular loops (**E**). (**F**) AV951 treatment does not affect plexus length of the SIVP in the presence or absence of flow. (**G**) AV951 treatment does not alter the number of leading sprouts in presence or absence of flow. Two-way ANOVA test suggests no interaction. n=15-25 from 2 replicates; ****<=0.0001; ns, no significance.

4.5 Overexpression of *Vegfaa$_{165}$* results in ectopic sprouts due to remodelling defects but not hyper-sprouting

Although VEGF receptor expression is increased in the leading sprouts in the absence of flow (Figure4.4F &L), inhibition of VEGF receptors does not rescue this phenotype (Figure4.3D &G), pointing to a dispensable role of VEGF in sprout regression. I next examined whether increased VEGF signalling could contribute to ectopic sprouts observed in the absence of flow. To enforce Vegfa expression in the presence or absence of flow, I injected *vegfaa$_{165}$* mRNA or control mRNA (encoding mTurquoise2 fluorescent protein, *mTQ2*) along with *control* or *tnnt2a* morpholino into embryos. Given that Vegfaa, as a pro-angiogenic signal, induces vessel sprouting when activated, I imaged the injected embryos at 48hpf (sprouting stage, before the onset of flow) and 72hpf (completion of sprout regression).

Overexpression of *vegfaa$_{165}$* in the presence of flow did not increase production of leading sprouts (Figure4.4A-C, quantified in D). In contrast, half of the injected embryos (n=11/24) displayed an enlarged primitive SIV carrying blood flow at 48hpf (Figure4.4C). These embryos exhibited decreased number of leading sprouts (Figure4.4D), probably due to early onset of remodelling mediated by blood flow. Notably, the branches were thickened (asterisks), reminding one of arteriovenous malformations in which arteries and veins

connect directly without efficient capillaries (Rochon *et al.*, 2016). The same batch of embryos were then imaged again at 72hpf. While the leading sprouts of the controls had regressed by 72hpf (Figure4.4I, *control*), those exposed to increased *vegfaa*$_{165}$ were only partially regressed (Figure4.4E, green) or remained non-remodelled (Figure4.4E, magenta), indicating failure of vessel remodelling rather than increased sprout formation. These data also indicated that VEGF signalling can override the effect of blood flow on sprout regression, and thus may act downstream or in parallel to flow-mediated cell behaviours.

To understand whether there was a synergistic effect of inhibition of flow and exogenous upregulation of VEGF, I compared *vegfaa*$_{165}$ injected embryos with or without flow at 48hpf and 72hpf. Similar to the controls (Figure4.4A &B), overexpression of *vegfaa*$_{165}$ in *tnnt2a* morphants (Figure4.4F &G) did not increase the number of leading sprouts produced at 48hpf (Figure4.4H, only the embryos without flow at 48hpf were quantified in *control* morphants). At 72hpf, while there was a significant increase of leading sprouts in *vegfaa*$_{165}$-injected embryos in the presence of flow, the number was not changed in *tnnt2a* morphants with overexpression of *vegfaa*$_{165}$ (Figure4.4I). These data showed that upregulation of *vegfaa* induces remodelling failure in the presence of flow but not in the absence of flow, indicating a strong correlation of presence of blood flow and overexpression of *vegfaa*$_{165}$ (two-way ANOVA, interaction P=0.0053). It also indicated no synergistic effects of exogenous VEGF

signalling and that induced via the lack of flow.

Collectively, these results suggested that VEGF overexpression is sufficient to inhibit sprout regression in the presence of flow, but that there is no additive effect of inhibiting blood flow and overexpressing VEGF, indicating that VEGF acts in parallel to or downstream of the effects of blood flow during sprout regression.

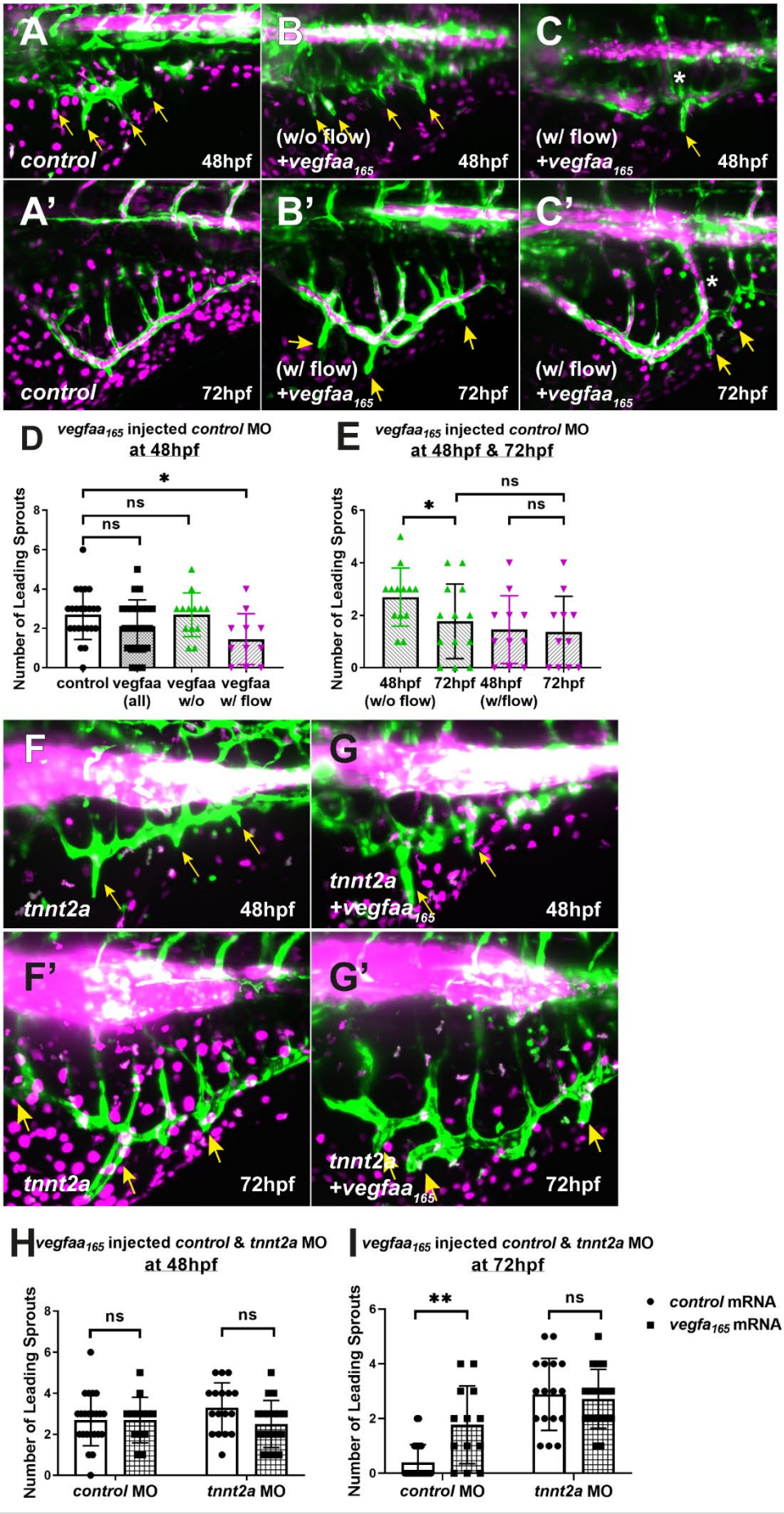
A
control
48hpf
B
(w/o flow)
+vegfaa165
48hpf
C
(w/ flow)
+vegfaa165
48hpf
A'
control
72hpf
B'
(w/ flow)
+vegfaa165
72hpf
C'
(w/ flow)
+vegfaa165
72hpf
D
vegfaa165 injected control MO
at 48hpf
Number of Leading Sprouts
control
vegfaa (all)
vegfaa w/o
vegfaa w/ flow
E
vegfaa165 injected control MO
at 48hpf & 72hpf
Number of Leading Sprouts
48hpf (w/o flow)
72hpf
48hpf (w/flow)
72hpf
F
tnnt2a
48hpf
G
tnnt2a
+vegfaa165
48hpf
F'
tnnt2a
72hpf
G'
tnnt2a
+vegfaa165
72hpf
H
vegfaa165 injected control & tnnt2a MO
at 48hpf
Number of Leading Sprouts
control MO
tnnt2a MO
I
vegfaa165 injected control & tnnt2a MO
at 72hpf
Number of Leading Sprouts
control MO
tnnt2a MO
control mRNA
vegfa165 mRNA

Figure4.4 Overexpression of *vegfaa*$_{165}$ induces failure of sprout regression

Embryos from *Tg(fli1a:egfp)*^{y1}*;(gata1a:DsRED)*^{sD2} are injected with *vegfaa*$_{165}$ plus *control* or *tnnt2a* morpholino and the same embryos are imaged at 48hpf and 72hpf. The leading sprouts (yellow arrows) of *control* morphants (**A**) and of those with *vegfaa*$_{165}$ overexpression (**B** & **C**) do not differ at 48hpf. However, half of the *vegfaa*$_{165}$ injected SIVP display enlarged SIV carrying flow (**C**), and exhibit fewer leading sprouts (**D**, One-way ANOVA). The same embryos are imaged at 72hpf (**A'**, **B'** & **C'**), and the number of leading sprouts is quantified (paired t-test). (**E**) Enforcing *vegfaa*$_{165}$ in the presence of flow leads to failure of sprout regression in all injected embryos in the presence of flow. *<=0.05, n=13-23 from 3 replicates; ns, no significance.

The *tnnt2a* morphants with or without *vegfaa*$_{165}$ overexpression are shown at 48hpf (**F** & **G**) and 72hpf (**F'** & **G'**). The numbers of leading sprouts are quantified and compared between *control* and *tnnt2a* morphants at 48hpf (**H**) and 72hpf (**I**), showing an increase of leading sprout number in *vegfa*$_{165}$-injected *control* morphants but not in *tnnt2a* morphants. Two-way ANOVA test, Interaction, p=0.0053**, at 72hpf; n=13-23 from 3 replicates; ns, no significance.

4.6 Notch signalling is dispensable for SIVP remodelling

Notch signalling is a well-established negative regulator of VEGF signalling via lateral inhibition during angiogenic sprouting and remodelling (Phng *et al.*, 2009; Ubezio *et al.*, 2016; Weijts *et al.*, 2016). The function of Notch signalling has also been investigated during SIVP development, however, while one study suggested that Notch was required for leading sprout retraction (Hen *et al.*, 2015), another group argued that it was dispensable for SIVP development (Goi and Childs, 2016). I suspected that the discrepancy between these studies resulted from the status of blood flow which was not demonstrated in either study. Embryos from *Tg(fli1a:egfp)^{y1};(gata1a:DsRED)^{sD2}* which labels ECs (GFP) and RBCs (RFP) were used to monitor blood flow in the SIVP.

To inhibit Notch signalling, I treated embryos with 0.2% DMSO or DAPT, a γ-Secretase inhibitor, at concentration of 100μM which was the concentration used in both published studies (Goi and Childs, 2016; Hen *et al.*, 2015). Embryos were treated at the same time range (Hen *et al.*, 2015) from 24hpf, before angioblasts sprouted from the PCV, until 72hpf when sprouts had normally regressed. DAPT treated embryos exhibited an upwardly curled body axis which is a phenotype associated with inhibition of Notch signalling (Goi and Childs, 2016), suggesting that the DAPT was effective at inhibiting Notch signalling.

Most DAPT-treated embryos (n=18/20) contained blood flow in the SIVP and these did not display ectopic leading sprouts (Figure4.5C). Interestingly, the development of the SIA was not affected by DAPT treatment (Figure4.5A &C, white arrows), while Hen *et al.* observed malformed SIA in DAPT-treated embryos (Hen *et al.*, 2015) and therefore those embryos were unlikely to carry blood flow in the SIVP. DAPT treatment in *tnnt2a* morphants did not alter the number of leading sprouts (Figure4.5B & D). Treating embryos with DAPT concentrations over 200μM led to flow stasis in *control* morphants, which exhibited ectopic leading sprouts that resembled *tnnt2a* morphants (data not shown).

These data suggested that Notch signalling is dispensable for initiation of SIVP formation or leading sprout retraction and that the observations from Hen *et al.*, were likely due to inhibition of blood flow in those studies.

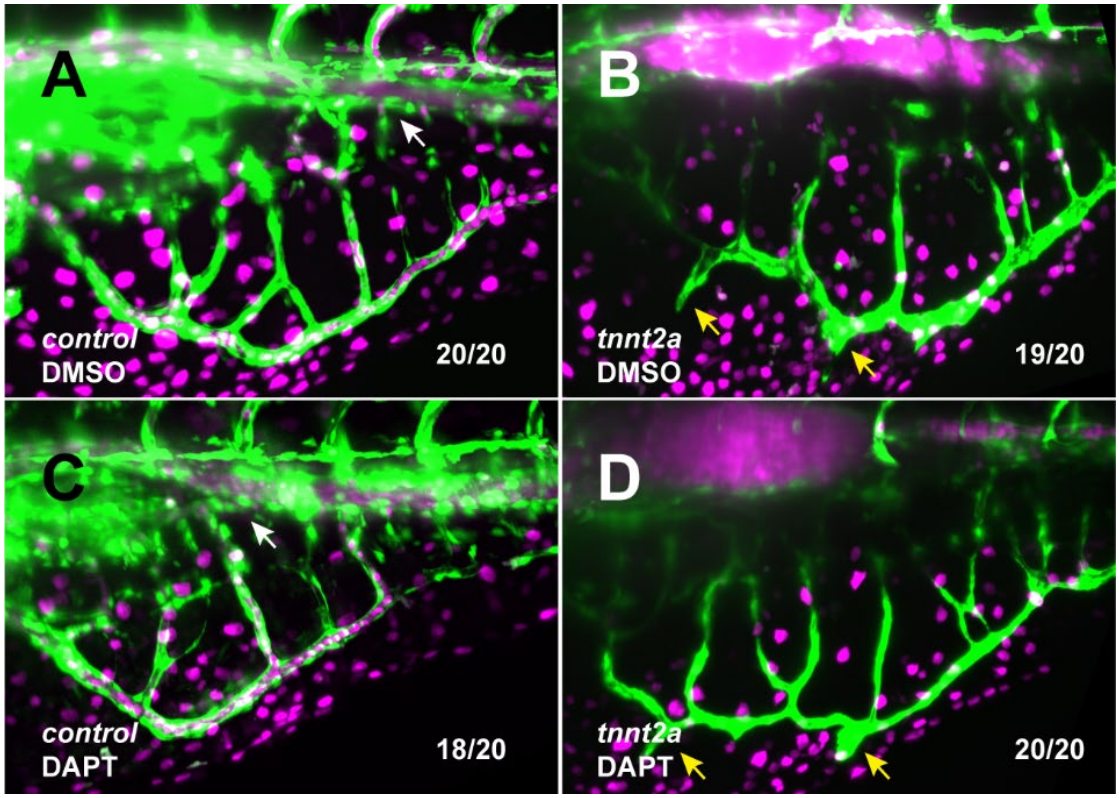

Figure4.5 Notch signalling is dispensable for SIVP remodelling

The *control* and *tnnt2a* morphants are treated with 100μM DAPT (**C** & **D**) or 0.2% DMSO (**A** & **B**) at 48hpf and imaged at 72hpf. Inhibition of Notch does not affect formation of SIA (white arrows) or sprout regression in either presence (**C**) or absence of flow (**D**).

4.7 Expression of a VEGF decoy receptor, *flt1,* is increased in the SIVP in the absence of flow

VEGFR1 (FLT1) functions as a decoy receptor, or molecular sink, for VEGFA to inhibit VEGF signalling (Park *et al.*, 1994). There are two isoforms of Flt1, including soluble *flt1* (*sflt1*) and membrane *flt1* (*mflt1*) (Krueger *et al.*, 2011). Knockdown of *flt1* with morpholino induced ectopic leading sprouts in the SIVP, suggesting that *flt1* may be required for sprout regression (Hen *et al.*, 2015). Since the flow status of the SIVP had not been considered in those studies (Hen *et al.*, 2015), I examined the expression level of *flt1* using *in situ* hybridisation during SIVP development in the presence and absence of flow. Given that embryos displayed ectopic leading sprouts in the absence of flow, I hypothesised we may expect to see reduced *flt1* expression in those embryos.

The expression of *sflt1* in the SIVP was undetected in the presence of flow (Figure4.6A, C &E), suggesting that *sflt1* was not normally expressed (or expressed at a very low level that was not detected by *in situ*) in this vascular bed. However, surprisingly, the expression of *sflt1* was upregulated in the absence of flow at 72hpf (Figure4.6F, yellow arrow, 10/25 embryos). The absence of *sflt1* expression in control SIVP was not due to technical issues, since in the same embryos, its expression was detected in cranial vessels (Figure4.6A'-F'). *sflt1* expression was maintained in the brain vessels at 48hpf

and 56hpf in the presence or absence of flow and was indistinguishable between control and experimental groups (Figure4.6A'-D'). However, by 72hpf, *sflt1* expression was absent from central arteries in the presence of flow (Figure4.6E' &E'') but was retained in these vessels in the absence of flow (Figure4.6F' &F''), suggesting that blood flow inhibits *sflt1* expression in the brain arteries at 72hpf.

The expression of *mlft1*, on the other hand, was not detected in the presence or absence of flow at all time points detected (Figure4.6G-L). Collectively, our results suggested that *sflt1* may be negatively regulated by blood flow within the central arteries and the SIVP, and that ectopic sprouts observed in *sflt1* morphants in the studies by Hen *et al.*, were likely due to the inhibition of blood flow in those embryos.

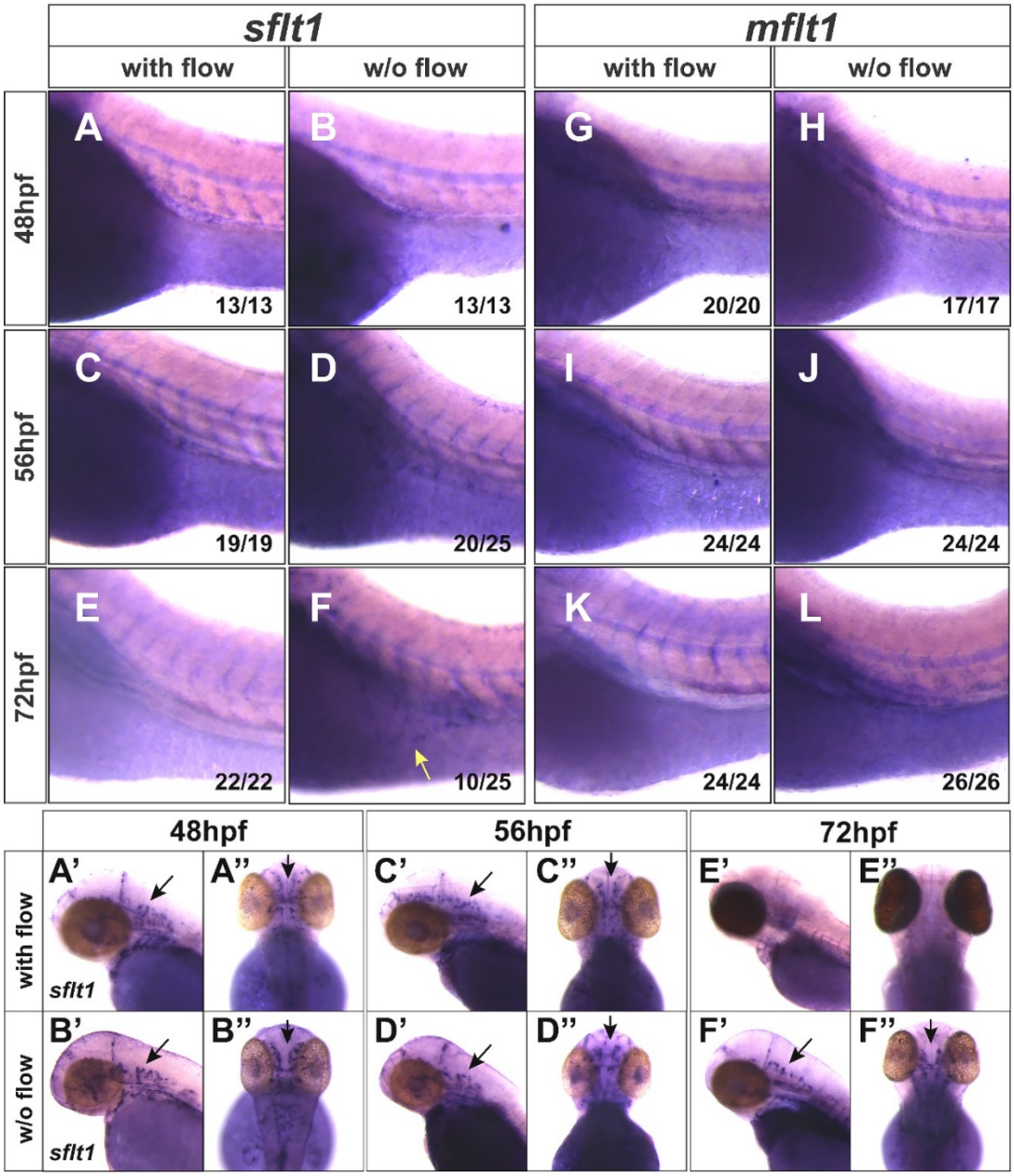

Figure4.6 Expression of VEGF decoy receptor *sflt1* is upregulated in the SIVP in the absence of flow

Expression of *sflt1* and *mflt1* is detected using *in situ* hybridisation in the presence or absence of flow. (**A, C & E**) The expression of *sflt1* is not detected in the SIVP under flow, whereas its expression is upregulated in the absence of flow at 72hpf (**F**, yellow arrow). (**G-L**) The expression of *mflt1* was not detected in control and experimental groups during SIVP remodelling. (**A' & C'**)) *sflt1* expressed at 48hpf and 56hpf in the central arteries and decreased at 72hpf (**E'**) in the presence of flow; whereas its expression remained from 48hpf to 72hpf without flow (**B'**, **D'** &**F'**). Anterior-left, dorsal-top. (**A''-F''**) are dorsal views of (A'-F'). Numbers indicate embryos in each group.

4.8 Overexpression of *Vegfc* results in ectopic sprouts due to remodelling defects but not hyper-sprouting

Although the expression of *vegfc* has not been observed in regions near the SIVP using *in situ* hybridisation, it has been shown to induce ectopic leading sprouts when overexpressed (Koenig *et al.*, 2016), suggesting that Vegfc is sufficient to induce ectopic sprouts or override sprout regression. In previous studies, *vegfc* was induced using *Tg(hsp70:Vegfc)*^{ci25} (Koenig *et al.*, 2016), however, the flow status was not considered after heat-shock. Thus, whether the ectopic sprouts observed were due to overexpression of *vegfc* or the absence of flow is unknown. Furthermore, whether these ectopic sprouts were caused by hyper-sprouting or failure of remodelling is unclear. Therefore, I employed *Tg(fli1a:egfp)*^{y1}*; (gata1a:DsRED)*^{sD2} to monitor blood flow in the SIVP. Similar to the *vegfaa*$_{165}$ overexpression experiment (Figure4.4), I injected *vegfc* or *mTQ2* mRNA along with *control* or *tnnt2a* morpholino into embryos which were imaged at both 48hpf and 72hpf.

Compared to *mTQ2*-injected embryos, overexpression of *vegfc* did not increase production of leading sprouts at 48hpf in the presence or absence of flow (Figure4.7A-D, quantified in E). Unlike overexpression of *vegfaa*$_{165}$, I did not observe enlarged SIV carrying blood flow or AVMs (Figure4.4C) in *vegfc*-injected controls. However, *vegfc* overexpression inhibited sprout regression in

the presence of flow but not in the absence of flow at 72hpf (Figure4.7A'-D', quantified in F), which resembled the phenotypes observed following *vegfaa*$_{165}$ overexpression (Figure4.4I). Two-way ANOVA analysis indicated a significant interaction between flow and overexpression of *vegfc* (Figure4.7F). These results suggested a redundant role of Vegfa and Vegfc during SIVP remodelling and that Vegfc when overexpressed is sufficient to induce ectopic leading sprouts due to failure in sprout regression.

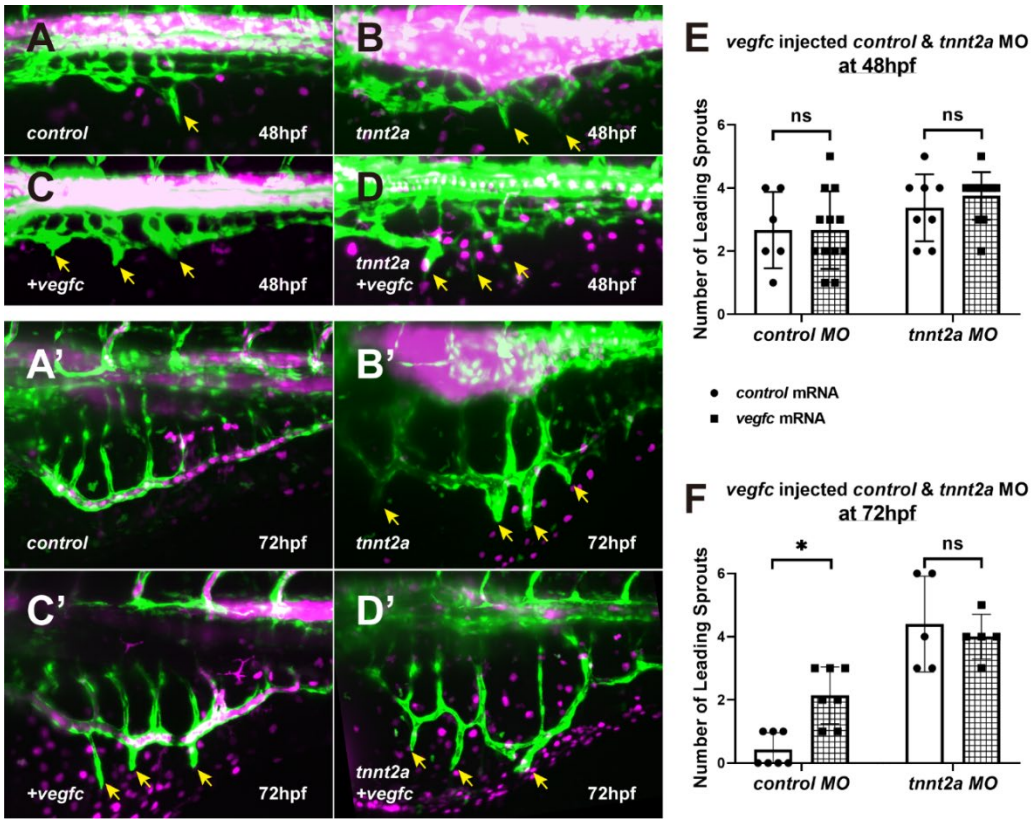

Figure4.7 Overexpression of *vegfc* results in ectopic leading sprouts due to sprout regression failure.

Embryos that are injected with *vegfc* plus *control* or *tnnt2a* morpholino are imaged at 48hpf and 72hpf (the same embryos). The leading sprouts (yellow arrows) of *control* or *tnnt2a* morphants (**A** & **B**) and of those with *vegfc* overexpression (**C** & **D**) do not differ at 48hpf (quantified in **E**). The same embryos were imaged at 72hpf (**A'- D'**), and the number of leading sprouts is quantified in (**F**). Results show a failure of sprout regression under upregulation of *vegfc* in the presence of flow at 72hpf (**F**). The number of leading sprouts in *tnnt2a* morphants with (**D'**) or without *vegfc* (**B'**) overexpression is not significantly altered at 72hpf (**F**). Two-way ANOVA test, Interaction, p=0.0135*, at 72hpf; n=5-7; ns, no significance.

4.9 Knockdown of *flt4* reduces ectopic sprouts in *tnnt2a* morphants

Previous data showed that *flt4* expression was increased in the ectopic leading sprouts in *tnnt2a* morphants (Figure4.8L) and that overexpression of *vegfc* increased the number of leading sprouts in the presence of flow due to defects in sprout regression (Figure4.7F). This suggests that blood flow may negatively regulate VEGFC signalling during sprout regression. To examine whether inhibition of *flt4* could rescue ectopic sprouts in the absence of flow, I injected *Tg(fli1a:egfp)^{y1}; (gata1a:DsRED)^{sD2}* embryos with *control*, *flt4*, *tnnt2a* or *flt4* plus *tnnt2a* morpholinos. The four groups of morphants were then imaged at 72hpf to compare any morphological differences.

In comparison to controls, *flt4* knockdown in the presence of flow did not alter the number of leading sprouts (Figure4.8A &C, quantified in E), which was in line with previous observations that *flt4* mutants do not exhibit apparent defects in SIVP development (Hen *et al.*, 2015; Koenig *et al.*, 2016). However, inhibition of *flt4* in *tnnt2a* morphants significantly reduced the number of leading sprouts (Figure4.8B &D, quantified in E). To determine whether the reduction of sprouts was due to increased cell death, I employed embryos from *Tg(fli1a:egfp)^{y1}; (fli1a:nls-mCherry)^{SH370}* to quantify EC nuclei. The total number of ECs in all groups was not significantly changed (Figure4.8F), therefore, the reduction of leading sprouts in *flt4/tnnt2a* double morphants was not because

of reduced ECs in the SIVP. Taken together with my previous observations, these results suggested that blood flow normally inhibits *flt4* expression during sprout regression and that increased *flt4* expression in the absence of flow may account for the accumulation of ECs in the leading sprouts (Figure 3.2H & Figure 4.2).

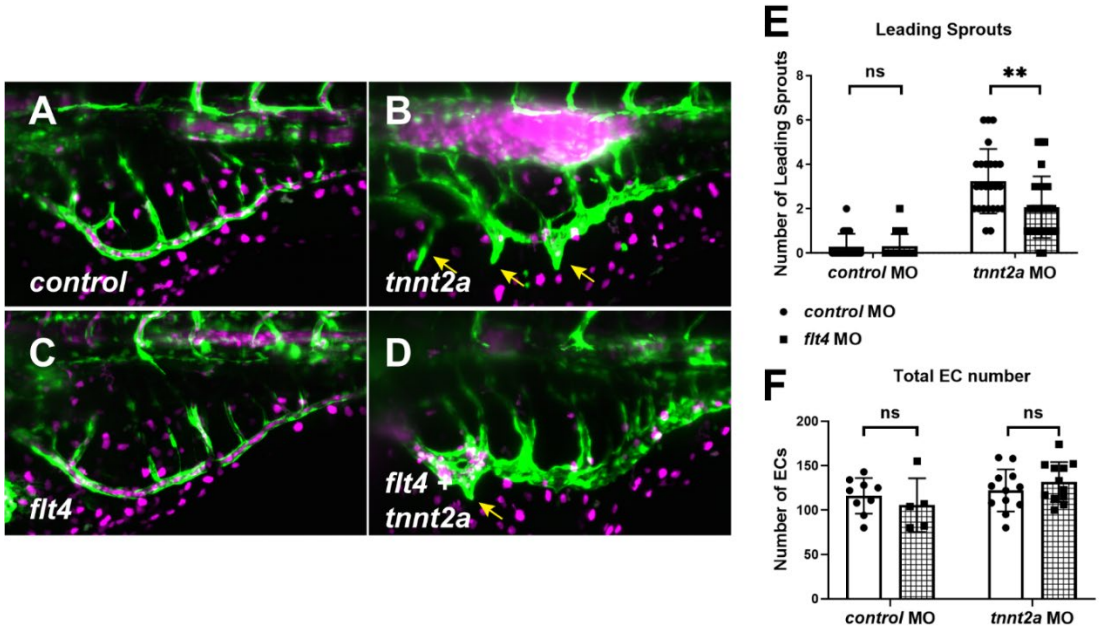

Figure4.8 Knockdown of *flt4* reduces ectopic sprouts in *tnnt2a* morphants

Embryos from *Tg(fli1a:egfp)^{y1};(gata1a:DsRED)^{sD2}* are injected with *control* (**A**), *tnnt2a* (**B**), *flt4* (**C**) or *flt4* plus *tnnt2a* (**D**) morpholino, and are imaged at 72hpf. (**E**) The number of leading sprouts is significantly decreased in *flt4/tnnt2a* double morphants compared to *tnnt2a* morphants. Two-way ANOVA, significant interaction (**p=0.0099); n=20-26. (**F**) Embryos from *Tg(fli1a:egfp)^{y1};(fli1:nls-mCherry)^{SH370}* are injected with *control*, *tnnt2a*, *flt4*, or *flt4/tnnt2a* MO. The number of ECs in the SIVP are quantified in RFP channel. The total number of ECs in the four groups is not significantly altered. Two-way ANOVA, no interaction, n=5-12 from two replicates, *p<=0.05; ns, no significance.

4.10 *flt4* is required for sprout regression under low flow shear stress

The mechanosensory complex including VEGFR2/R3, PECAM1 and VE-cadherin has been previously reported to regulate flow-mediated vascular remodelling that is independent of VEGF ligands (Coon *et al.*, 2015). It has been suggested that VEGFR3 maintains a low set point of flow shear stress for EC sensing and vessel remodelling (Baeyens *et al.*, 2015). Inducible knock out of VEGFR3 in mice leads to decreased diameter of aorta (Baeyens *et al.*, 2015). The mechanism underlying this is proposed as that loss of VEGFR3 increases shear set point and the vessel lumen narrows to create a higher shear stress to compensate (Baeyens *et al.*, 2015), suggesting that vessel lumen diameter is controlled by a VEGFR3-dependent shear stress set point. Given that low-shear flow is sufficient to induce sprout regression (Figure 3.12D), I hypothesised that *flt4* within the SIVP supports a low set point for EC sensing during sprout regression.

To test this, the transgenic line *Tg(fli1a:egfp)^{y1};(gata1a:DsRED)^{sD2}* was employed and embryos were injected with *control*, *gata1a*, *flt4*, and both *flt4* and *gata1a* morpholinos. The number of RBC was drastically reduced via *gata1a* knockdown as previously demonstrated (Figure 3.12C & Figure4.9B & D, magenta). The number of leading sprouts in *flt4* or *gata1a* morphants did not change significantly whereas the combined loss of both *flt4* and *gata1a* resulted

in ectopic leading sprouts (Figure4.9D &E). These results indicated a very low set point of EC sensing during SIVP remodelling, which requires, at least partially, the VEGF receptor Flt4 during sprout regression.

Interestingly, while consistent with previous data that *gata1a* morphants displayed enlarged lumen diameter of the SIV (Figure 3.12E), *gata1a/flt4* double morphants displayed decreased lumen diameter which was comparable to the controls (Figure4.9F). This was in line with previous studies that loss of VEGF3 reduces vessel diameter of aorta (Baeyens *et al.*, 2015). However, it was noted that the SIVP as a venous plexus displays increased diameter under low flow (Figure 3.12E & Figure4.9F), which is different from arterial aorta of which diameter decreases (Baeyens *et al.*, 2015). Therefore, the mechanisms of flt4/VEGFR3-medated diameter regulation in different vascular beds may differ.

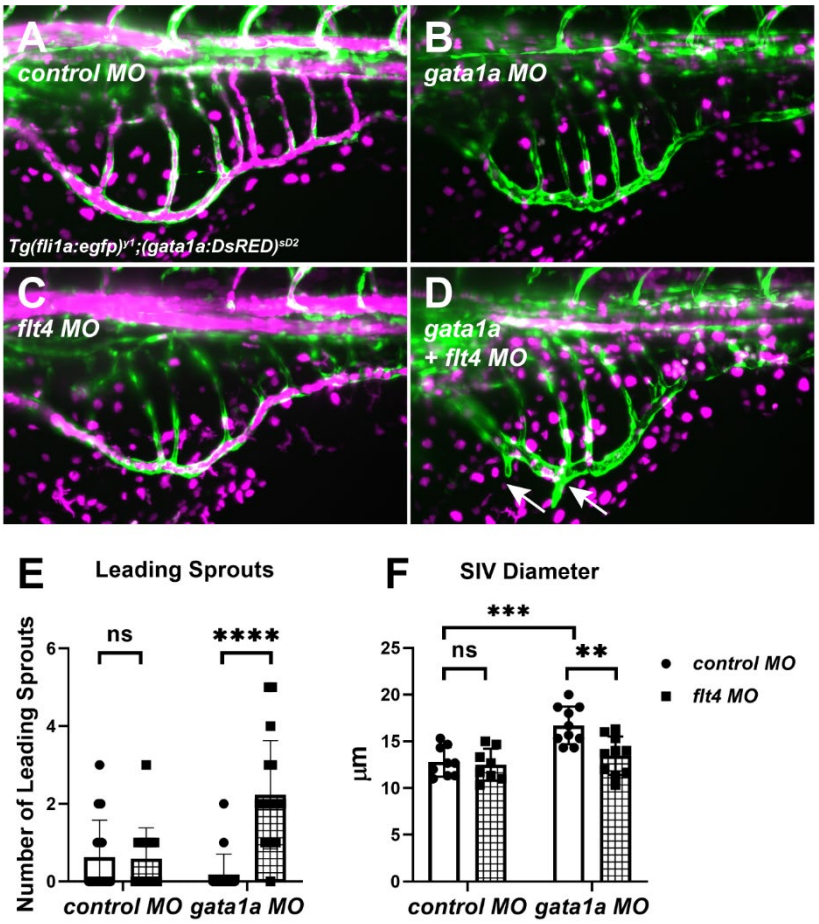

Figure4.9 *flt4* is required for sprout regression under low flow

Embryos from *Tg(fli1a:egfp)^{y1};(gata1a:DsRED)^{sD2}* are injected with *control* (**A**), *gata1a* (**B**), *flt4* (**C**) or *flt4* plus *gata1a* (**D**) morpholinos, and are imaged at 72hpf. (**E**) The number of leading sprouts is significantly increased in *flt4/gata1a* double morphants compared to *flt4* or *gata1a* morphants. (**F**) The SIV diameter is enlarged under low flow in *gata1a* morphants but is constricted in the absence of *flt4* under low flow. Two-way ANOVA, n=10-17 from 3 replicates, *p<=0.05; ns, no significance.

4.11 Discussion

In this chapter, I investigated the role of VEGF in the SIVP after onset of flow and its potential interaction with blood flow in regulation of sprout regression. Our data indicate a complex role of VEGF during SIVP remodelling, including differential functions in branch cells and sprout cells, and under normal and low flow conditions. Here I summarise the key findings below:

1. VEGF signalling is required for the formation of branches during remodelling.

2. Vegfa and Vegfc are sufficient to induce ectopic sprouts due to failure of sprout regression but not overproduction of sprouts.

3. Blood flow inhibits *flt4* expression which induces ectopic sprouts in the absence of flow.

4. *flt4* promotes sprout regression under low flow condition.

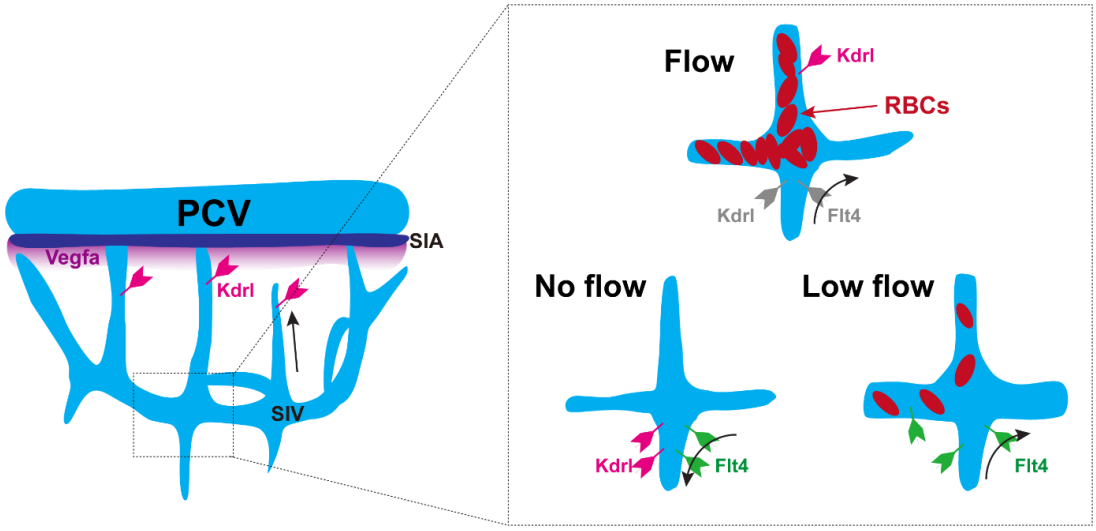

Figure 4.10 The role of VEGF signalling during SIVP development under different blood flow conditions

Branch cells expressing Kdrl are activated by Vegfaa and migrate dorsally towards the SIA. During late stages of sprout regression, Kdrl and Flt4 are suppressed by blood flow within the sprouts whereas in the absence of flow, they are activated and promote angiogenic sprouting. Under low flow, Flt4 is activated in the sprouts and induces sprout regression.

4.11.1.1 The differential roles of VEGF signalling in branches and sprouts

kdrl and *plcg1* mutants displayed reduced branches that failed to connect with the SIA (Hen *et al.*, 2015). Chemical treatment with Vegfr inhibitors (SU5416 or DMH4) before sprouting (<30hpf) completely prevents SIVP formation or only allows formation of a mis-patterned SIV (Goi and Childs, 2016; Koenig *et al.*, 2016), indicating that VEGF is required for EC sprouting from the PCV to form SIVP and from the SIV to form branches. Our treatment with AV951 at later stages (48-72hpf) showed a more specific effect on the branches without affecting the formation and ventral expansion of the SIV (Figure4.3C

&D). These observations suggest that VEGF is constantly required for proper SIVP development in a 24-72hpf time window, including EC sprouting and dorsal migration. Analysis of EC migration trajectory indicates that ECs follow a flow-independent signal for ventral migration (Figure 3.7F), however, AV951-treated embryos did not display apparent defects in ventral expansion (Figure4.3F), suggesting that this signal is unlikely to be VEGF. Given that *vegfaa* is highly expressed in the glomerulus and regions near the SIA (Figure 4.1A), it is possible that these tissues serve as a source of VEGF ligand to promote dorsal migration of the branches.

Although VEGF regulates the dorsal migration of the branch cells, it does not appear to be required for sprout regression. Expression of *kdrl* and *flt4* were increased within the sprouts in the absence of flow (Figure 4.2F &L) and inhibition of Vegfr did not alter the number of leading sprouts with or without flow (Figure4.3F). Moreover, knockdown of *flt4* reduced sprout number in the absence of flow (Figure4.8E). These data together suggested that blood flow inhibits Vegfr during sprout regression. In addition, overexpression of *vegfaa* or *vegfc* was sufficient to induce ectopic sprouts in the presence of flow (Figure4.4I & Figure4.7F), indicating that VEGF might act as a permissive cue and is negatively regulated by blood flow during sprout regression. Given that sprout regression is an interlinked process of EC sprouting forward and regressing reversely (Figure 3.6), enhanced VEGF might promote the sprouting property

of the ECs. This was in line with its pro-angiogenic functions (Karaman *et al.*, 2018), and in the expense of regression, elevated VEGF signalling results in defects in sprout remodelling. VEGFA and VEGFC mediated formation of VEGFR2/R3 heterodimers has been shown to frequently localise to tip cell filopodia and promote angiogenic sprouting (Nilsson *et al.*, 2010). Enhanced VEGFA/C signals may also promote R2/R3 heterodimers and subsequent sprouting. However, *kdrl* mutants or inhibition of Vegfr at late stages impairs branch formation and therefore blocks blood circulation in the SIV (Hen *et al.*, 2015; Koenig *et al.*, 2016 & Figure4.3C). This makes it difficult to uncouple the flow-dependent and ligand-dependent roles of VEGFR2 during sprout regression. Therefore it is possible that VEGF might contribute to EC dorsal migration during sprout regression. Inhibition of VEGFR2 specifically in sprout cells would be needed to address this issue. Also, it is not possible to exclude that multiple Vegf ligand-receptor interactions in some cases, including Vegfd-Kdr/Flt4 (Vogrin *et al.*, 2019) and VEGFC-VEGFR2 (Eichmann *et al.*, 1998) function to regulate sprout regression.

It has been proposed that Notch signalling and *flt1* are required for sprout regression (Hen *et al.*, 2015). Loss of Notch and loss of *flt1* (similar to gain of function VEGF) induce defects in sprout regression, suggesting a feedback interaction between Notch and Vegf that resembles ISV sprouting (Figure 1.2A). Albeit plausible, these studies did not consider the effects of blood flow, which

has been shown to be a key regulator in sprout regression (Figure 3.2F). Our results go against this proposal by carefully looking into the flow status when inhibiting Notch and observed no ectopic sprouts (Figure4.5C). Given that Notch signalling is suppressed in veins (You *et al.*, 2005), it is reasonable that it is not required for sprout regression in the SIVP. Similarly, I did not observe *flt1* expression within the sprouts in the presence of flow during regression, but contradictorily observed increased *sflt1* expression in the absence of flow (Figure4.6F). I also did not observe RFP positive cells within the SIVP using *Tg(-0.8flt1:enhRFP)*^{hu5333} line (data not shown). Taken together, these results indicate that it is unlikely that Notch or Flt1 regulates sprout regression.

4.11.1.2 The function of *flt4* under normal flow and low flow

Reduction of blood viscosity or knockdown of *flt4* alone did not impair sprout regression, however, loss of *flt4* under low flow resulted in ectopic sprouts (Figure4.9E), suggesting that *flt4* is required for sprout regression under low flow. In addition, *flt4* expressed in the sprouts before 60hpf and decreased at 72hpf when blood flow is stronger (Figure 4.2K). It has been suggested that ECs have a defined threshold to respond to flow and that high level of VEGFR3 (FLT4) increases EC sensitivity to shear and therefore maintains a low shear set point (Baeyens *et al.*, 2015). This may potentially explain the phenotypes

observed in different morphants: *flt4* is suppressed under normal flow and sprouts regress via additional signals, therefore *flt4* morphants do not display apparent defects; *gata1a* morphants that carries low flow activates *flt4* which decreases the set point for EC migration during regression; and *gata1a*/*flt4* double morphants fail to activate *flt4* under low flow therefore display ectopic sprouts. The redundant function of Flt4 helps to maintain proper vessel remodelling under dysregulated condition such as low flow, whereas loss of *flt4* under low flow disrupts sprout regression. However, while knockdown of *flt4* under low flow leads to ectopic sprouts (Figure4.9E), it seems to contradict my observation that knockdown of *flt4* in the absence of flow leads to reduction of sprouts (Figure4.8E). The discrepancy might result from different aspects of Flt4 functions under different flow conditions. Activation of *flt4* in the absence of flow promotes sprouting whereas *flt4* in response to flow lowers shear set point. Alternatively, additional signalling pathways may be involved to modulate Flt4 functions, such as Wnt and BMP signalling.

A key step during sprout regression is that the rear membrane of tip cells comes into contact with blood flow (Figure 3.10), triggering directed polarisation and migration of SIV cells and tip cells (Figure 3.6). Non-canonical Wnt signalling has been found to stabilise existing vessel branches under low-shear conditions in the mouse (Franco *et al.*, 2016). *Wnt*-deficient ECs are able to reorient and polarise against low-shear flow, leading to an increase of

regression profiles. This suggests that enhanced flow could overcome the threshold set by non-canonical Wnt signalling and leads to vessel pruning. However, *Wnt5a/Wnt11*-depleted ECs did not alter expression of flow-sensing genes, suggesting that these molecules regulates cell polarisation-mediated regression rather than flow sensing *per se* (Franco *et al.*, 2016). Rspo1/Wnt signalling has been shown to promote angiogenesis via Vegfc-Vegfr3 signalling (Gore *et al.*, 2011). It is possible that at early stages when primitive SIV start sprouting, Flt4 senses flow to hold a low set point and interacts with Wnt signalling to support lumen opening of the vessels; at later stages when ECs are exposed to flow levels above the threshold, Flt4 is suppressed and Wnt signalling is overcome, therefore the cells polarise and migrate against flow during remodelling. In the case of *gata1a* morphants in which blood flow remains low at later stages, Flt4 is constantly activated to lower the threshold for EC migration and this back-up machinery is impaired in *gata1a/flt4* double morphants and therefore leads to ectopic sprouts.

It has been suggested that high shear induces outward remodelling while low shear induces inward remodelling. Conditional deletion of *Vegfr3* in mice induces inward remodelling of the aortic arch and descending aorta with decreased vessel diameter (Baeyens *et al.*, 2015). The mechanism underlying this is that deletion of *Vegfr3* elevates the set point and causes the endothelium to signal low shear, leading to inward remodelling. However, I observed

increased vessel diameter of the SIV in *gata1a* morphants which potentially have lower shear stress (Figure4.9F). It is unknown whether this is a differential response to flow between arterial and venous vessels, but given their molecular and signalling differences, this seems likely. Interestingly, knockdown of *flt4* in *gata1a* morphants decreases vessel diameter. This suggests that in addition to setting a threshold, *flt4* itself may function to increase vessel diameter. Another important factor in controlling vessel diameter is BMP signalling. *endoglin*-deficient ECs fail to respond to increases in haemodynamic forces so that vessels are enlarged, leading to formation of AVM (Sugden *et al.*, 2017). In addition, the BMP receptor Alk1 has been shown to regulate directed EC migration against flow (Rochon *et al.*, 2016). VEGFR3 and VEGFR1 can interact with ALK1, ENG, and BMPR2 and regulate their functions in angiogenic sprouting and AVM development (Hwangbo *et al.*, 2017; Jin *et al.*, 2017; Thalgott *et al.*, 2018). Therefore, BMP signalling may also regulate EC migration mediated SIV diameter and sprout regression.

Chapter 5 The role of BMP signalling in flow-mediated vascular remodelling

5.1 Introduction

BMP signalling has recently emerged as a fundamental pathway in endothelial regulation. Impaired endothelial BMP signalling is directly associated with two vascular disorders, hereditary haemorrhagic telangiectasia (HHT) and pulmonary hypertension (PAH) (Dyer *et al.*, 2014). BMP signalling also plays important roles in endothelial venous differentiation and flow sensing during embryonic development (de Vinuesa *et al.*, 2016; Dyer *et al.*, 2014; Franco and Gerhardt, 2016). In zebrafish, *alk1* mutants display enlarged brain vessels and severe AVMs and *bmp10/bmp10-like* double morphants show similar but milder phenotypes (Corti *et al.*, 2011; Laux *et al.*, 2013; Rochon *et al.*, 2016), suggesting that BMP signalling regulates vessel diameter.

BMP signalling has also been implicated in the development of the SIVP. Zebrafish embryos treated with the BMP inhibitor, DMH1, or in which *bmp4* was knocked down using morpholino displayed defects in SIVP outgrowth (Goi and Childs, 2016). Overexpression of the BMP antagonist *noggin3* also reduced SIVP expansion (Hen *et al.*, 2015). These results suggest a role for BMP signalling in ventral expansion of the SIVP. However, these studies inhibited BMP signalling at early stages before the onset of flow and also overlooked any potential effects of flow on plexus development (Goi and Childs, 2016; Hen *et al.*, 2015). Whether BMP signalling is required continually during SIVP development or during the remodelling phases after the onset of flow remains

unknown. The ectopic sprouts present in the flow-deprived SIVP may result from elevated pro-angiogenic (BMP2/4) or disrupted anti-angiogenic (BMP9/10) signals. In addition, which components of the BMP signalling pathway, including ligands, receptors and downstream effectors are involved in SIVP remodelling have not been demonstrated.

Hypothesis

BMP signalling is continually required for development of the SIVP including ventral expansion and vessel remodelling and blood flow refines BMP signalling during sprout regression.

Aims

1. To determine the role of BMP signalling at later stages of SIVP development (i.e. after onset of blood flow), with respect to sprout regression and regulation of vessel diameter and ventral expansion.

2. To investigate potential interactions between flow and BMP signalling during vascular remodelling.

Here I present that BMP ligands including *bmp2b* and *bmp4* are present in the developing gut and may serve as the source of BMP for SIVP development. BMP type I receptor *alk1* and type II receptor *bmpr2b* are expressed in the SIVP

and are elevated within leading sprouts in the absence of flow. Inhibition of BMP signalling at different time points either leads to abolishment or partial ventral expansion of the SIVP, suggesting that BMP is constantly required for EC migration during SIVP development. Although loss of BMP does not affect early angiogenic sprouting in the SIVP, inhibition at later stages increases ectopic sprouts in either presence or absence of flow, suggesting synergistic effect of lack-of-flow and loss-of-BMP signalling. Overexpression of *bmpr2b* shortens the plexus length and overexpression of *bmp4* restricts SIV diameter. BMP signalling is transduced via a Smad1/5-independent mechanism during SIVP development.

5.2 BMP type I receptor *alk1* and type II receptor *bmpr2b* are expressed in the developing SIVP

To understand which BMP receptors are involved in SIVP development, the expression pattern of the receptors was detected using *in situ* hybridisation. This included the BMP type I receptors *alk1*, *alk8/2*, *alk3a*, *alk3b*, *alk6a*, as well as the type II receptors *bmpr2a* and *bmpr2b*. Expression of *cdh5* was employed as a positive control to show the presence of the SIVP (Figure 5.1V-X, yellow arrowheads). Embryos were fixed for *in situ* at 52hpf (before the onset of blood flow), 57hpf (SIVP remodelling in the presence of flow) and 72hpf (completion of sprout regression under flow).

Expression of *alk1* was not detectable in the SIVP before 57hpf but was clearly observed at 72hpf (Figure 5.1C, arrowhead). In the literature, *alk1* is expressed mostly in arteries such as basal communicating artery (BCA), AA1, DA but also in PCV (Corti *et al.*, 2011; Laux *et al.*, 2013; Rochon *et al.*, 2016). These results indicate that *alk1* is also expressed in veins. *bmpr2b* was expressed in the SIVP at all time points tested (Figure 5.1S-U, yellow arrowheads). Expression of other BMP receptors, including *alk2*, *alk3a*, *alk3b*, *alk6a*, and *bmpr2a*, was observed in regions underneath the PCV, where the primitive intestine forms (Figure 5.1D-R, white arrows); however, their expression was not detected in the SIVP. Collectively, these results suggest

that *alk1* and *bmpr2b* are the main type I and type II receptors which transduce BMP signalling in the developing SIVP.

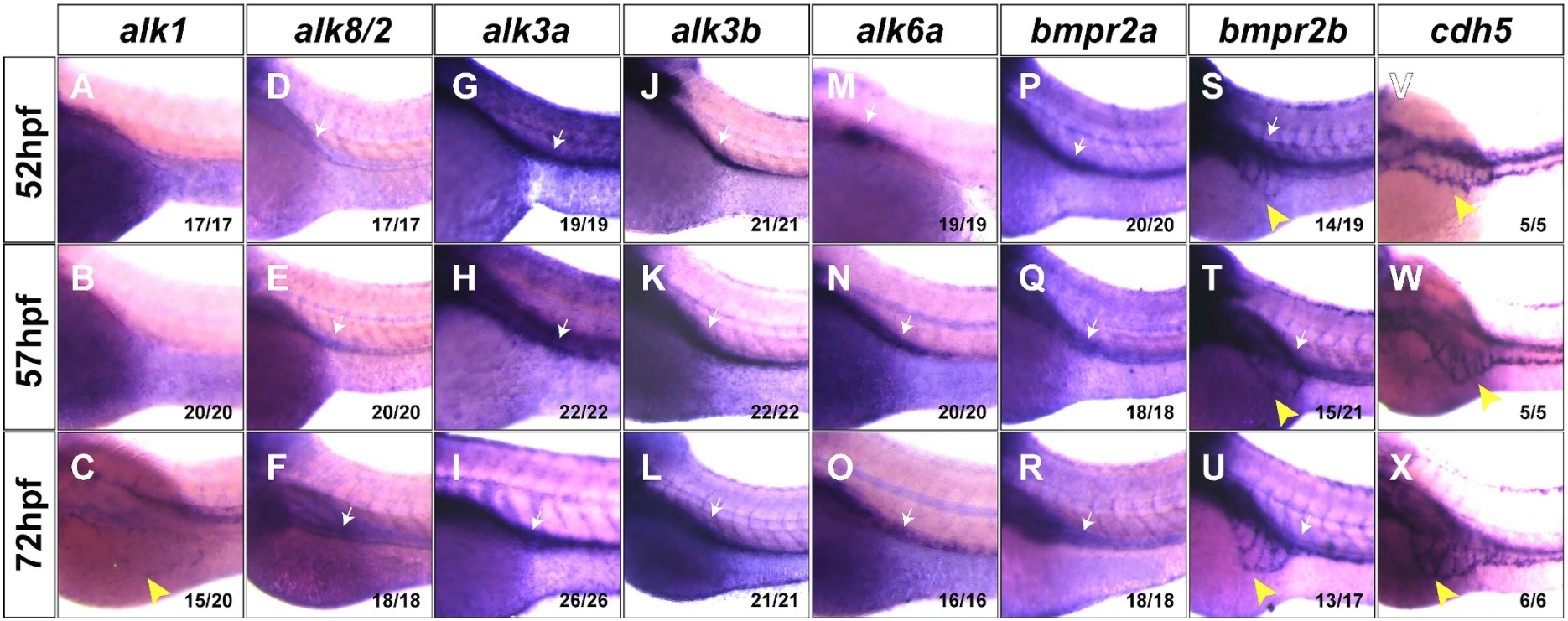

Figure 5.1 *alk1* and *bmpr2b* are expressed in the SIVP

Zebrafish embryos are fixed at 52hpf, 57hpf, and 72hpf, and are examined using *in situ* hybridisation for BMP type I and type II receptors. (**A-C**) Expression of *alk1* is not detectable until 72hpf in the SIVP (yellow arrowhead). (**D-U**) Expression of *alk2, alk3a*, *alk3b*, *alk6a*, *bmpr2a*, and *bmpr2b* is detected in the region underneath the PCV (white arrows), where the primitive intestine forms. (**S-U**) Expression of *bmpr2b* is detected in the SIVP at all time points tested (yellow arrowheads). (**V-X**) *cdh5* is expressed in the endothelial cells of the SIVP. Cranial, left; dorsal, up. Numbers indicate embryos in each group. Experimental repeats N=2.

5.3 Expression of *alk1* and *bmpr2b* are increased in the leading sprouts in the absence of flow

To investigate whether expression of BMP receptors (*alk1* and *bmpr2b*) as well as ligands (*bmp2b*, *bmp4*, and *bmp7*) were altered in the presence or absence of flow, we tested their expression using *in situ* hybridization on *control* and *tnnt2a* morphants at 72hpf.

alk1 was expressed in the SIVP in both *control* and *tnnt2a* morphants and was slightly increased in the absence of flow, especially within the leading sprouts (Figure5.2A &B, yellow arrowheads). Previous studies have shown that *alk1* is downregulated in cranial arteries in the absence of flow in *tnnt2a* morphants or following tricaine treatment (Corti *et al.*, 2011). Our results indicated that *alk1* might function differently between arteries and veins in response to flow. Similarly, expression of *bmpr2b* was increased in the leading sprouts in the absence of flow (Figure5.2C &D, yellow arrowheads).

Expression of ligands *bmp2b* and *bmp4* were clearly detected in the zebrafish gut (Figure5.2E-H, white arrows), while their expression was more diffuse in the same region, suggesting that the formation of the intestine might be defective in *tnnt2a* morphants. However, the expression level of *bmp2b* or *bmp4* did not alter with or without flow (Figure5.2 E-H). *bmp7* was also expressed in areas between the embryo and the yolk ball and was slightly

increased in the absence of flow (Figure5.2I & J, white arrows).

Collectively these results suggested that *bmp2b* and *bmp4* which are expressed in the intestine could serve as a source for BMP signalling and could be transduced by *alk1* and *bmpr2b* receptors. The expression of *alk1* and *bmpr2b* were increased in the absence of flow, indicating that blood flow downregulates *alk1* and *bmpr2b* during SIVP remodelling.

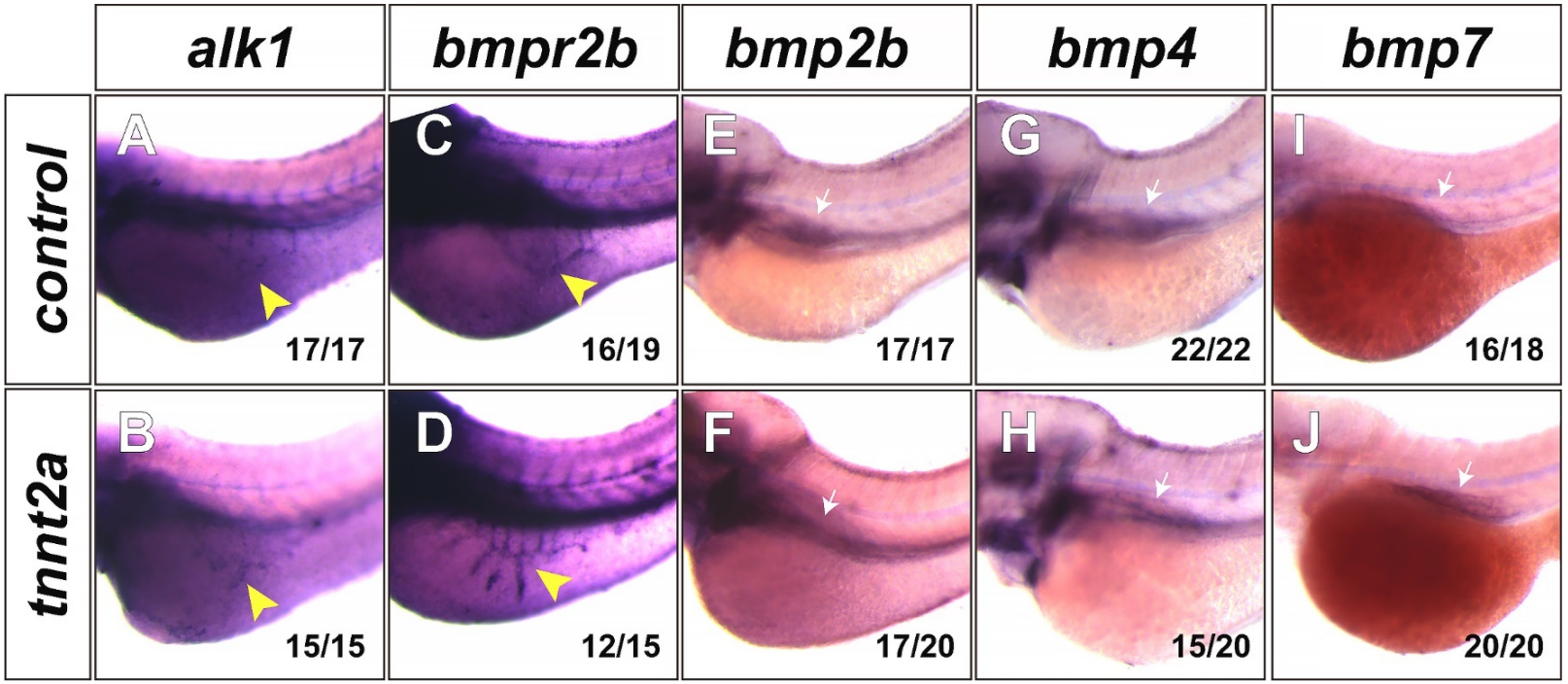

Figure5.2 Comparison of the expression of BMP receptors and ligands in the presence and absence of flow

Expression of BMP receptors, *alk1* and *bmpr2b*, and ligands including *bmp2b*, *bmp4*, and *bmp7* are tested using *in situ* hybridisation in both *control* and *tnnt2a* morphants at 72hpf. (**A-D**) The expression of *alk1* and *bmpr2b* are increased in the absence of flow, especially within the leading sprouts (yellow arrowheads). (**E-H**) *bmp2b* and *bmp4* ligands are present in the zebrafish gut (white arrows), and do not alter in the presence or absence of flow. (**I&J**) *bmp7* is detected in the areas between the embryo and the yolk ball, and the expression is slightly increased in the absence of flow. Cranial, left; dorsal, up. Numbers indicate embryos in each group. Experimental repeats N=2.

5.4 BMP signalling is required for plexus expansion, leading sprout regression and vasoconstriction

Dorsomorphin homolog 1 (DMH1) is an inhibitor of BMP type I receptors, which is selective to Alk2 but can also inhibit Alk1, Alk3 and Alk6 (Hao *et al.*, 2010; Kirmizitas *et al.*, 2017). It has been used to block BMP signalling in the SIVP from 24hpf to 48hpf, at a concentration of 50μM, and reduced plexus length in treated embryos (Goi and Childs, 2016). However, in these studies embryos were imaged at 48hpf, before the onset of flow and the active ventral migration of the plexus, therefore, whether BMP is still required for remodelling at later stages was unknown. Furthermore, since blood flow begins at approximately 55hpf (Figure 3.1B), the effects of blood flow on BMP signalling were unclear. My pilot experiments using 50μM DMH1 caused heart defects (enlarged heart and peri-cardiac oedema) in controls and led to mortality of *tnnt2a* morphants. I then lowered the concentration to 25μM which did not cause obvious defects in the heart, while the drug was still functional, as confirmed by dorsalisation of body axis when treated at 4hpf (data not shown). I treated the *control* or *tnnt2a* morphants with DMH1 between different time ranges: 24hpf-72hpf (window of SIVP development), 24-48hpf (before onset of flow), and 48-72hpf (after onset of flow).

Compared to DMSO treated morphants (Figure5.3A &B), embryos treated

with DMH1 from 24hpf to 72hpf showed a drastic reduction in the plexus length with or without flow (Figure5.3C &D, white lines), although the primitive SIV with sprouts was still present, indicating that sprouting of the SIVP does not require BMP signalling. This was in line with previous findings in which embryos were treated with DMH1 (Goi and Childs, 2016) or with BMP antagonist *noggin3* (Hen *et al.*, 2015).

I also treated the embryos with DMH1 from 24hpf to 48hpf and washed off after 48hpf (Figure5.3E &F). The DMH1 treatment led to a shortened SIVP but allowed partial ventral expansion compared to DMSO-treated ones. The SIVP was mis-patterned in both *control* and *tnnt2a* morphants, showing numerous branches that did not support proper blood flow (Figure5.3E &F). This suggests that BMP signalling is critical for proper formation of primitive SIV to ensure correct blood flow perfusion.

DMH1 treatment from 48hpf to 72hpf did not shorten the plexus length of the SIVP (Figure5.3G &H, white lines); however, DMH1-treated SIVPs displayed ectopic leading sprouts (yellow arrows), suggesting that BMP signalling is required for sprout regression in the presence of flow. The number of the leading sprouts was also increased in the absence of flow with DMH1 treatment (Figure5.3H, yellow arrows) suggesting that there might be synergistic effects of loss of- flow and -BMP signalling during vascular remodelling (quantification in following section). DMH1 treatment did not impair SIA development in either group (Figure5.3G &H, arrowheads). Collectively,

these results suggested that BMP signalling is continuously required for SIVP ventral expansion and proper remodelling.

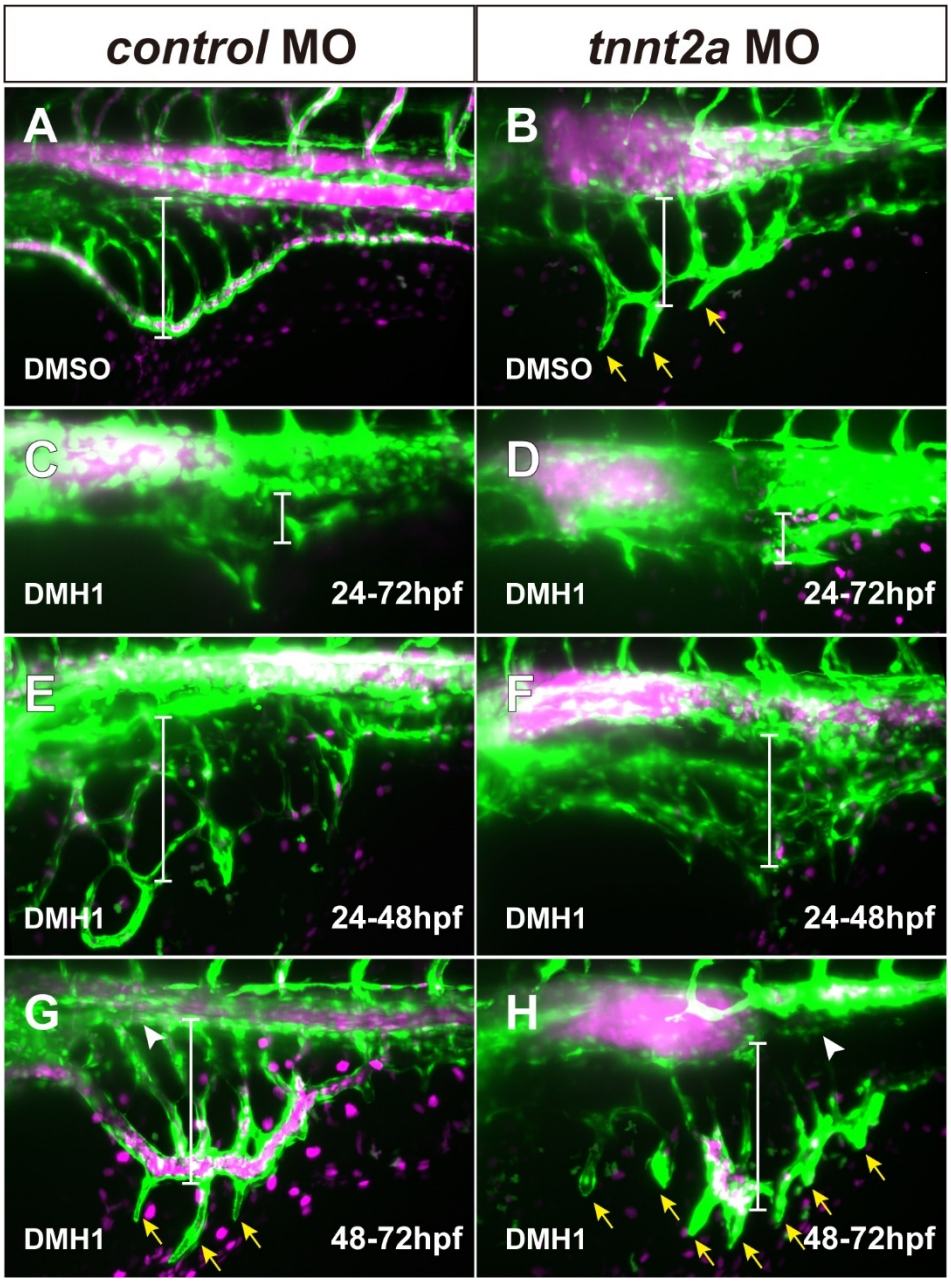

Figure5.3 BMP signalling is required for SIVP expansion and remodelling at different developmental stages

The *control* and *tnnt2a* morphants are treated with 0.2% DMSO (**A** & **B**) or 25μM DMH1 at different time points: 24-72hpf (**C** & **D**), 24-48hpf (**E** & **F**), 48-72hpf (**G** & **H**). All embryos are imaged at 72hpf. (**C** & **D**) Inhibition of BMP signalling throughout the SIVP formation (24-27hpf) results in failure of ventral expansion. (**E** & **F**) Treatment from 24hpf to 48hpf and wash-off after 48hpf lead to shortened plexus length but allow partial expansion in both *control* and *tnnt2a* morphants. (**G** & **H**) Treating with DMH1 from 48hpf to 72hpf results in increased ectopic leading sprouts in the presence of flow, and even more sprouts in the absence of flow. The SIA (arrowhead) is intact following DMH1 treatment. White line, plexus length; Yellow arrow, leading sprout.

To investigate the potential interaction of blood flow and BMP signalling, I analysed the general morphology of the SIVP in embryos treated with DMH1 at 48-72hpf (Figure5.4A-D). The vascular area or loops were not altered in *control* or *tnnt2a* morphants with or without DMH1 treatment (data not shown). Previously I have shown that the primitive SIV actively migrates in a ventral direction from 48hpf (Figure 3.2 & Figure 3.7), however, DMH1-treatment during the vascular expansion period (48-72hpf) surprisingly did not affect the plexus length in both *control* and *tnnt2a* morphants (Figure5.4E). In contrast, the number of leading sprouts was significantly increased in DMH1-treated embryos in the presence of flow (Figure5.4C &F) consistent with previous results (Figure5.3G &H, arrowheads). Moreover, the presence of ectopic sprouts in *tnnt2a* morphants was exaggerated following DMH1 treatment (Figure5.4D &F), suggesting that BMP signalling functions to promote sprout regression in the presence and absence of flow in the SIVP but that there is a synergistic effect of the lack of flow and inhibition of BMP signalling on sprout regression.

In addition to the increased number of leading sprouts, I also observed that the diameter of the ventral SIV was enlarged. To compare the vessel diameter and cell number, the transgenic line *Tg(fli1a:AC-tagRFP)^{SH511};(fli1a:nls-GFP)^{SH549}* was employed, which labels endothelial junctional F-actin with RFP and endothelial nucleus with GFP. Upon DMH1 treatment, the diameter of the SIV was significantly enlarged (Figure5.4H', blue lines & I) compared to DMSO

treated embryos. The total number of ECs in the SIVP was not changed (Figure5.4G'', H'', & J), suggesting that increased vessel diameter was not due to increased numbers of ECs. Rather, it may result from an enlarged cell size because the cell density was decreased within the same area when treated with DMH1 (Figure5.4K).

In summary, combined with the results in which embryos were treated with DMH1 at different time ranges, I found that BMP signalling is required continuously throughout SIVP development, for different functions. Firstly, BMP signalling is important for plexus ventral expansion, especially in the initial phases, as previously reported (Goi and Childs, 2016; Hen *et al.*, 2015). Loss of BMP signalling at early stage (24hpf) has a more negative impact on plexus expansion than at later stages (after 48hpf) when SIVP ECs show more active ventral migration. It is possible that the ventral expansion of the SIVP is pre-determined by BMP signalling while the exact distance ECs migrate during expansion is refined by other factors, such as blood flow. Secondly, although the BMP signalling is not required for plexus expansion at later stages, it is important for sprout regression and regulation of cell size, since the number of leading sprouts and the vessel diameter were increased following BMP inhibition. Overall, these results suggest important roles for BMP signalling during vascular remodelling, including regulation of cell migration and cell size.

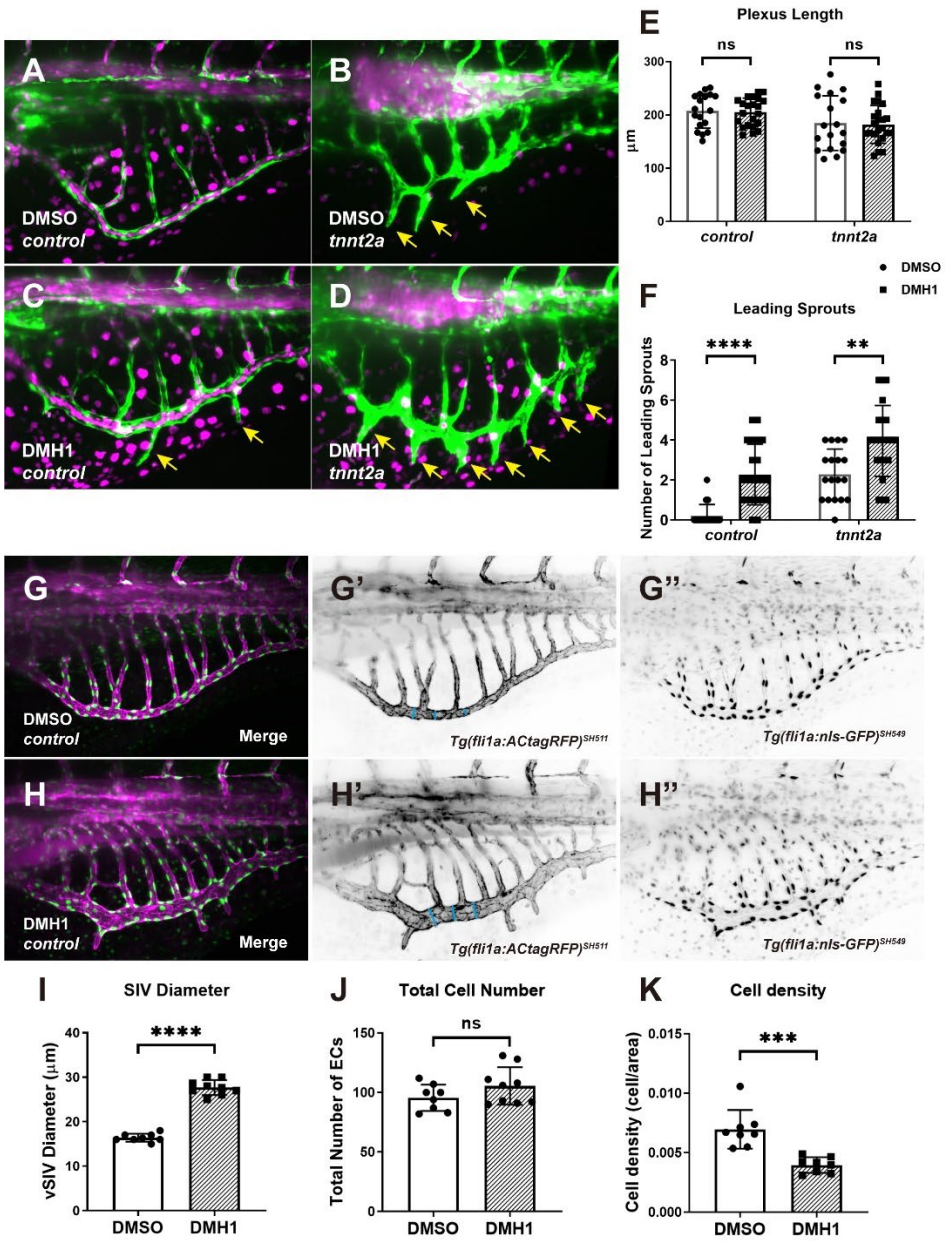

Figure5.4 BMP signalling is required for sprout regression and vessel diameter restriction

(**A-D**) Embryos from *Tg(fli1a:egfp)^{y1};(gata1:DsRED)^{sD2}* are injected with *control* or *tnnt2a* morpholino, and are treated with 0.2% DMSO or 25µM DMH1 from 48hpf to 72hpf. (**E-F**) The plexus length is not altered with DMH1 treatment, but the number of leading sprouts is increased in both *control* and *tnnt2a* morphants. n=18-23 each from 2 replicates. Two-way ANOVA, ****p<=0.0001. (**G-H**) *Tg(fli1a:AC-tagRFP)^{SH511};(fli1a:nls-GFP)^{SH549}* embryos are treated with 0.2% DMSO or 25µM DMH1 at 48-72hpf. (**I**) The diameter of ventral SIV is increased with DMH1 treatment. (**J**) The total number of ECs in the SIVP plexus is not altered. (**K**) The cell density of the SIV is reduced with DMH1 treatment, suggesting an increased cell size. DMSO, n=8; DMH1, n=9. Unpaired t-test, ****p<=0.0001.

5.5 *alk1* may be dispensable for leading sprout regression

Since DMH1 treatment induced ectopic leading sprouts (Figure5.4F), and DMH1 is known to inhibit BMP type I receptor function (Hao *et al.*, 2010; Kirmizitas *et al.*, 2017), and since Alk1 is likely to be the type I receptor transducing the signals within the SIVP (Figure 5.1A-C & Figure5.2A-B), I investigated the roles of Alk1 in vascular remodelling by knockdown of *alk1* using morpholinos. A previously published *alk1* morpholino (splice blocking) was used (Rochon *et al.*, 2016).

Injection of 2.5ng *alk1* (the same concentration as previously used by Rochon *et al.*,) resulted in high mortality (187/244, death/total embryos) in my hands. The remaining embryos that survived were imaged at 48hpf and 72hpf to compare the phenotype in cranial vessels showed by Rochon *et al.* The *alk1* morphants (2.5ng) exhibited apparent enlargement of the BCA (Figure5.5B, white arrowheads) and posterior communicating segments (PCS), as well as development of AVMs (Figure5.5B, asterisks) between the BCA and primordial midbrain channel (PMBC). This cerebral vascular phenotype was observed in all surviving *alk1* morphants. However, because of the drastic dilation of the brain vessels which carried the majority of the blood flow and prevented blood circulation in the trunk and the SIV (Figure5.5A'), it was difficult to assess the interaction of Alk1 and blood flow in the SIVP.

To address this confounding factor, I then lowered the concentration of the

alk1 morpholino to ensure the presence of blood flow in the SIV. The original dose (2.5ng) of *alk1* morpholino was diluted into1.25ng, 0.625ng, and 0.25ng, and injected into embryos. Embryos injected at 1.25ng and 0.625ng doses showed similar cranial AVM-phenotype to those injected with 2.5ng and no blood flow was present in the SIV. Approximately 50% of *alk1* morphants that were injected with 0.25ng exhibited an enlarged BCA (Figure5.5C &D). However, among these phenotypical morphants, only a few had blood circulation as indicated by circulating RBCs within the SIVP (Figure5.5D') whereas 8/10 morphants imaged displayed a lumenised SIV without RBCs (Figure5.5C'). Moreover, these *alk1* morphants did not show a significant reduction of plexus length or an increase in leading sprout number.

In summary, these results showed that loss of *alk1* led to arterial vasodilation, contributing to vessel enlargement and AVM development, suggesting that *alk1* is critical for the proper vascular remodelling of the cranial arteries. However, cranial vessel dilation also prevented blood circulation in other vascular beds such as the SIVP. The attempts to uncouple *alk1* function and blood flow in the SIVP failed due to the comprised perfusion of the vessels. Interestingly, inhibition of *alk1* did not phenocopy the DMH1-treated embryos which showed reduction of plexus length (Figure5.3C) or increased number of leading sprouts (Figure5.4F), although DMH1 inhibits Alk1/2/3 and *alk1* was the only type I receptor detected in the SIVP (Figure 5.1C). This suggested that inhibition of type I receptors by DMH1 in the SIVP might activate or

downregulate secondary signals which were responsible for the shortened plexus and ectopic sprouts. Moreover, *alk1* morphants with 0.25ng pointed to a dispensable role of *alk1* in SIVP formation and sprout regression, given that these showed a relatively normal SIVP, although flow circulation is partially compromised. However, we cannot exclude the possibility that sub-optimal inhibition of *alk1* was not sufficient to cause apparent defects in the SIVP.

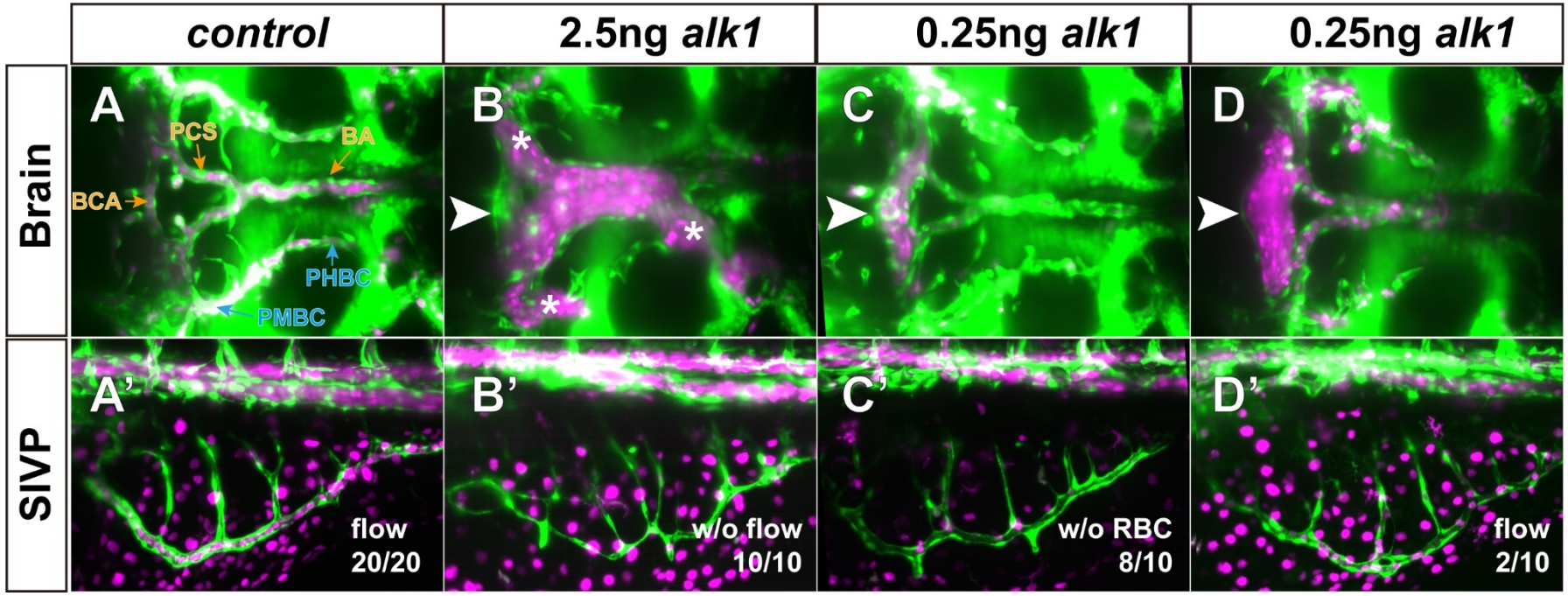

Figure5.5 *alk1* morphants do not show apparent defects in SIVP remodelling

Embryos from *Tg(fli1a:egfp)^{y1};(gata1a:DsRED)^{sD2}* are injected with *control* or *alk1* morpholino at 2.5ng or 0.25ng concentration. (**A-D**) Compared to *control* morphants, *alk1* morphants exhibit AVM (asterisks) and vasodilation of cranial vessels including BCA (white arrowhead) and PCS. (**B'**) Blood circulation is absent in the SIVP of the 2.5ng *alk1* morphants. (**C'**) Eight out of ten 0.25ng *alk1* morphants imaged do not contain circulating red blood cells (RBCs) in the SIVP and n=2/10 had blood circulation (**D'**). The 0.25ng *alk1* morphants do not show apparent defects in plexus length or the number of leading sprouts compared to controls. 0.25ng *alk1* MO, n=10 each from two replicates. BCA, basal communicating artery; PCS, posterior communicating segments; PMBC, primordial midbrain channel.

5.6 Inhibition of *bmp10* and *bmp10-like* results in decreased vascular loops in the SIVP

BMP9 and BMP10 are the BMP ligands that bind to ALK1 in endothelial cells (Ricard *et al.*, 2012). It has been shown that loss of *bmp10* and *bmp10-like*, a paralog of *bmp10* due to teleost genome duplication, resulted in AVM development in cranial vessels which was similar to but milder than that of *alk1* morphants (Laux *et al.*, 2013). I suspected that a less severe AVM-phenotype in the head would probably allow blood circulation in other vascular beds. Therefore, I injected *Tg(fli1a:egfp)^{y1};(gata1a:DsRED)^{sD2}* embryos with large doses of morpholino targeting *bmp10* (15ng) + *bmp10-like* (3ng) as suggested by (Laux *et al.*, 2013). Co-injection of the two morpholino resulted in high mortality of 43-66% (n=127/224 embryos died) and only half of the surviving embryos exhibited AVMs and vasodilation in the cranial vessels (Figure5.6B). Lower concentrations (0.5X and 0.1X) of *bmp10* + *bmp10-like* morpholinos were phenotypically normal.

Inhibition of *bmp10* + *bmp10-like* led to moderate enlargement of the BCA (Figure5.6B, white arrowhead) and PCS, in addition to development of AVMs (white asterisks) in the brain vessels. Within the same embryos, the blood flow was present in the SIVP (Figure5.6B'). Interestingly, there were fewer vascular loops in *bmp10+10l* morphants (Figure5.6B', yellow asterisks, &C) compared to controls. The plexus length was not significantly altered in the morphants

(Figure5.6D). Although there was a tendency towards an increase, the number of leading sprouts in *bmp10/bmp10-l* double morphants was not significantly different from *control* morphants (Figure5.6E). These results suggested that Bmp10 may have overlapping roles with VEGF signaling in regulation of branch formation, but it is not likely to regulate plexus length and sprout regression.

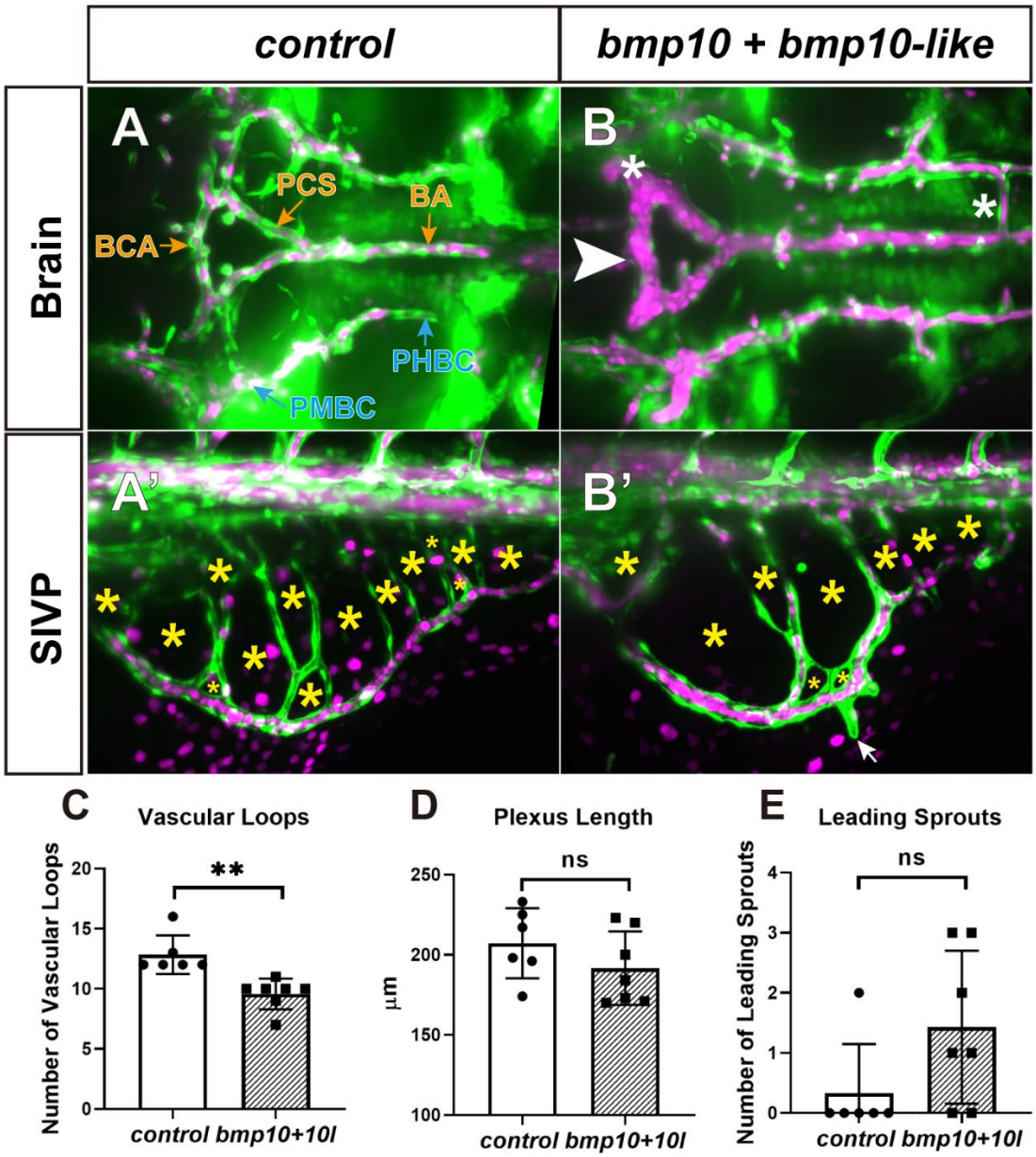

Figure5.6 Inhibition of *bmp10* and *bmp10-like* results in decreased vascular loops

(**A-B**) Embryos from *Tg(fli1a:egfp)^{y1};(gata1a:DsRED)^{sD2}* are injected with *control* or *bmp10* (15ng) + *bmp10-like* (3ng) morpholinos, and are imaged in both the cranial vessels and the SIVP at 72hpf. (**B**) The cranial vasculature in *bmp10* + *bmp10-l* morphants is enlarged in BCA and PCS, and develops AVMs (asterisks). (**C**) Knockdown of *bmp10+10l* reduces the number of vascular loops in the SIVP. (**D**) The plexus length of the SIVP is not altered in the absence of flow *bmp10+bmp10-l*. (**E**) The number of leading sprouts is not altered in *bmp10+bmp10-l* morphants. Unpaired t-test, n=6 or 7 from 2 replicates. **p<=0.01.

5.7 Overexpression of *bmpr2b* results in a shortened SIVP but does not cause ectopic leading sprouts

BMP signalling has been suggested to promote venous sprouting from the caudal vein plexus (CVP), showing ectopic hyper-sprouting of the ISVs when overexpressed Bmp2b ligand using *Tg(hsp70l:bmp2b)*^{fr13} line (Wiley *et al.*, 2011) (Figure5.7B). In addition, overexpression of *bmp2b* from 60hpf resulted in shortened SIVP with super-numerous branches (Wiley *et al.*, 2011), resembling phenotypes shown in DMH1-treated embryos (Figure5.3E &F). The authors also suggested that Bmp2b binds to Bmpr2b to transduce BMP signalling in the CVP. Given that *bmpr2b* expression is increased in the SIVP in the absence of flow (Figure5.2D), I hypothesised that blood flow inhibits *bmpr2b* during SIVP remodelling, and overexpression of *bmpr2b* causes vascular defects such as ectopic leading sprouts.

To conditionally overexpress Bmpr2b in the zebrafish larva, I generated a transgenic line *Tg(hsp70l:bmpr2b-v2a-GFP)*^{SH601} in which *bmpr2b* expression is driven by a heat-shock (HS) promoter *hsp70l.* Tagged GFP fused to Bmpr2b via a self-cleaving V2A peptide was used as an indicator of successful overexpression of *bmpr2b-v2a-GFP* element following heat shock induction. To verify the transgenic line was functional, embryos were heat-shocked at 1dpf and imaged at 2dpf in the CVP region (Figure5.7A) to compare the phenotypes showed in *Tg(hsp70l:bmp2b)*^{fr13} embryos (Wiley *et al.*, 2011). The blood vessels

were labelled with RFP tagged cell-junctional F-actin in endothelial cells using a *Tg(fli1a:AC-tagRFP)*^{SH511} line (Savage *et al.*, 2019).

Following out-crossing, half of the embryos carried the *bmpr2b-v2a-GFP* element while the other half did not, thus allowing these to be used as an internal control (HS-control). Following heat-shock, *bmpr2b* was strongly expressed in the somites as indicated by the GFP (Figure5.7E &E''). In addition, the GFP was co-localised with the RFP in the endothelial cells, suggesting that *bmpr2b* was likely overexpressed within the endothelial cells (Figure5.7E'', transverse cross section, white arrowheads). To clearly illustrate the spatial difference of the ISVs, the RFP channel was colour-coded based on z-stack distance (Figure5.7E' &E', white colour towards reader). Overexpression of *bmpr2b* resulted in ectopic sprouting from the CVP (Figure5.7E', yellow arrows), which was similar to but milder than the phenotype of *bmp2b* overexpression (Wiley *et al.*, 2011) (Figure5.7B &C). This milder phenotype might result from mosaic expression of *bmpr2b* at the time studied or from tight regulation of blood flow to suppress *bmpr2b* expression. These results suggested that the *Tg(hsp70l:bmpr2b-v2a-GFP)*^{SH601} line is capable of elevated transduction of BMP signalling in endothelial cells and induction of a BMP gain-of-function phenotype with veins.

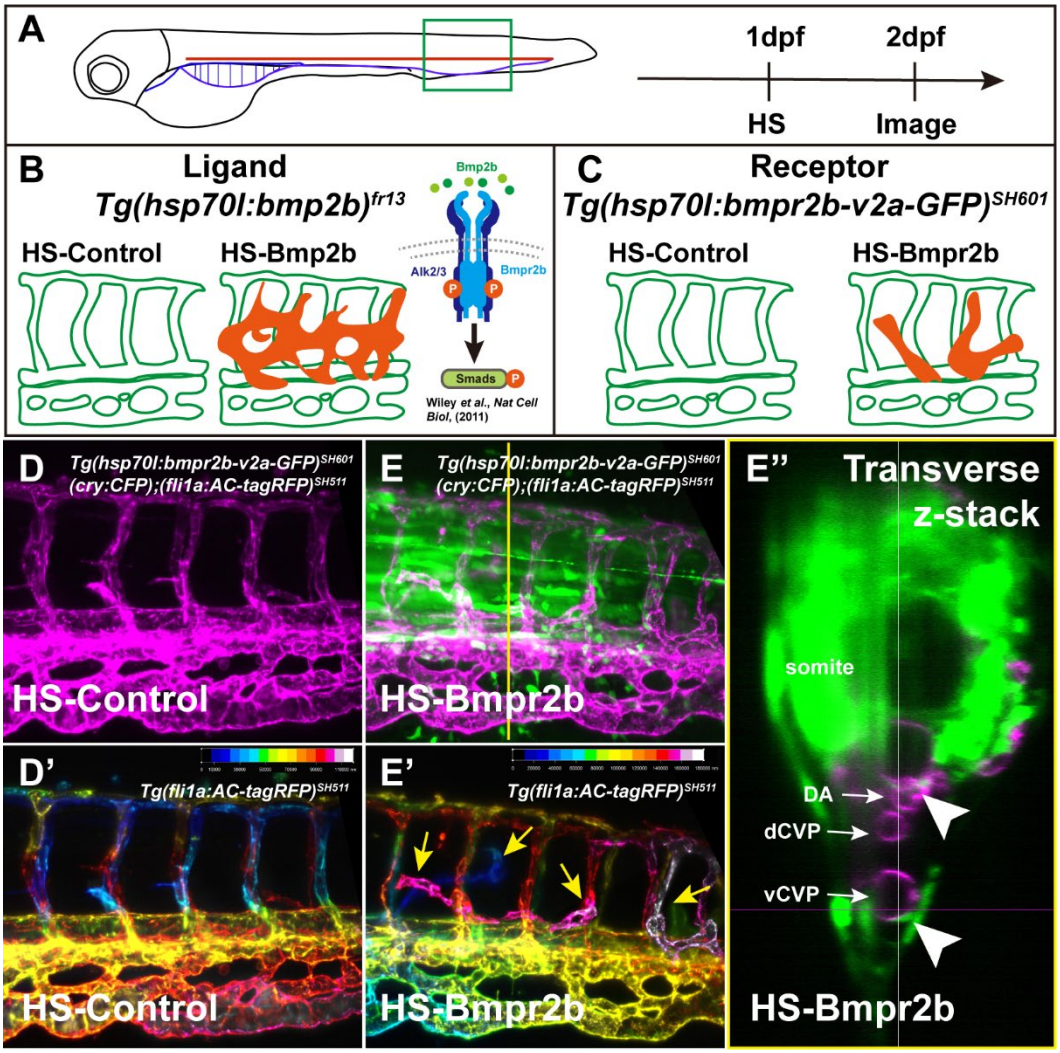

Figure5.7 Overexpression of *bmpr2b* results in ectopic sprouting from the CVP

(**A**) Embryos *from Tg(hsp70l:bmpr2b-v2a-GFP)^{SH601};(cry:CFP); (fli1:AC-tagRFP)^{SH511}* are heat-shocked at 1dpf and imaged in the CVP (green square) at 2dpf. (**B**) Schematics show that overexpression of ligand *bmp2b* results in drastic hyper-sprouting from the CVP (Wiley et al, 2011). (**C**) Schematics show that overexpression of receptor *bmpr2b* results in milder ectopic sprouting from the CVP. (**D** & **E**) Enforced *bmpr2b* (tagged GFP, cleaved off via v2a site) is expressed in somites and endothelial cells (white arrowheads). Transverse cross-section (yellow line in E) is shown in (**E''**). (**D'** & **E'**) RFP channels are colour-coded based on z-stack distance (scale: white towards reader). Ectopic sprouts of the ISVs are indicated by yellow arrows.

Next, I examined the role of *bmpr2b* during SIVP remodelling. Embryos from *Tg(hsp70l:bmpr2b-v2a-GFP)*^{SH601}*;(cryaa:CFP)* and *Tg(fli1:AC-tagRFP)*^{SH511} were heat-shocked at 48hpf, a few hours before the onset of the blood flow, to allow folding of the Bmpr2b protein (Figure5.8A). At 72hpf, compared to HS-Control (Figure5.8B), HS-Bmpr2b (indicated by GFP) was highly expressed in the yolk ball and in the skin of the zebrafish (Figure5.8C). The maximum intensity projection images omitted the details of endothelial expression due to bright GFP expression in the skin cells. Therefore, a single z-stack of the highlighted region (Figure5.8C) was shown and enlarged (Figure5.8C', white arrows) to demonstrate the expression of *bmpr2b-v2a-GFP* within the endothelial cells. The transverse cross-section of the single z-stack was also shown in Figure5.8C''. Downstream effector pSMAD was tested to confirm the activation of BMP signalling following heat shock (Figure5.13B). These data suggested that the expression of *bmpr2b* was also enforced in ECs within the SIVP.

Compared to HS-control, HS-Bmpr2b embryos exhibited a decrease in plexus length in the presence of flow (Figure5.8F & H). This phenotype was similar to but milder than that observed in embryos in which *bmp2b* was overexpressed as these displayed a complete failure of SIVP outgrowth (Wiley *et al.*, 2011). To examine the role of flow on *bmpr2b* regulation during SIVP remodelling, *bmpr2b* expression was enforced in *tnnt2a* morphants which also exhibited decreased plexus length (Figure5.8G & H). However, there was no

significant difference in the number of leading sprouts in the presence or absence of flow (Figure5.8I). Nor did they show a difference in the vessel diameter of the SIV in the presence of flow (Figure5.8J).

Collectively, these results showed that overexpression of *bmpr2b* leads to hyper-sprouting from the CVP but does not cause ectopic sprouts in the SIVP, suggesting that the role of BMP is context specific and functions differently among venous plexuses. HS-Bmpr2b embryos exhibited milder hyper-sprouting of the ISVs than those of HS-Bmp2b (Wiley *et al.*, 2011), suggesting that Bmp2b signalling is at least partially transduced via Bmpr2b, and other receptors might cooperate with Bmpr2b to be fully functional. More interestingly, overexpression of *bmpr2b* leads to a shortened SIVP, suggesting that *bmpr2b* is suppressed during SIVP ventral expansion.

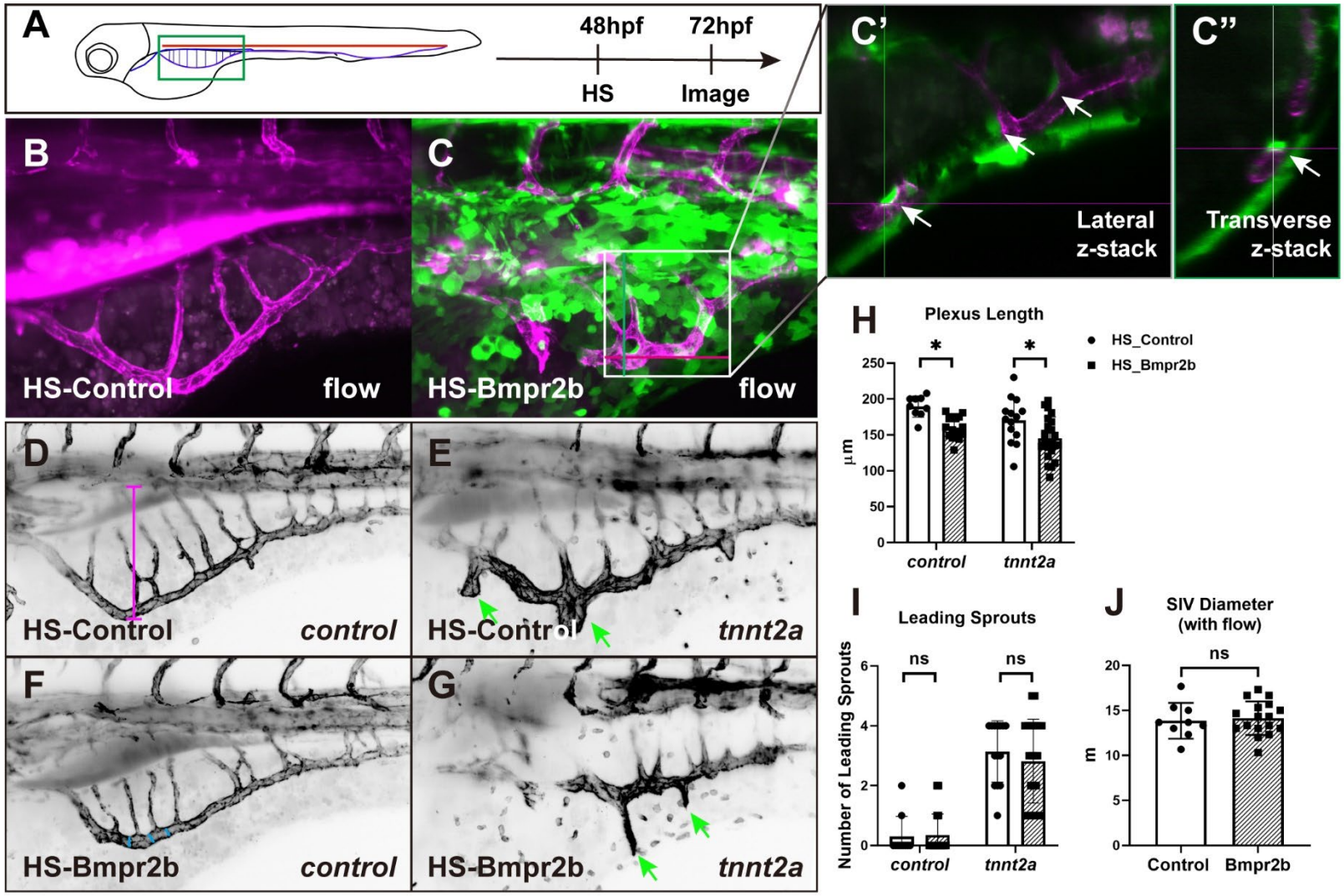
A
48hpf
72hpf
HS
Image
B
HS-Control
flow
C
HS-Bmpr2b
flow
C'
Lateral
z-stack
C"
Transverse
z-stack
D
HS-Control
control
E
HS-Control
tnnt2a
F
HS-Bmpr2b
control
G
HS-Bmpr2b
tnnt2a
H
Plexus Length
HS_Control
HS_Bmpr2b
µm
control
tnnt2a
I
Leading Sprouts
Number of Leading Sprouts
ns
control
tnnt2a
J
SIV Diameter
(with flow)
ns
Control
Bmpr2b

Figure5.8 Overexpression of *bmpr2b* results in shortened SIVP

(**A**) Embryos from outcross of *Tg(hsp70l:bmpr2b-v2a-GFP)^{SH601};(cry:CFP)* and *Tg(fli1a:AC-tagRFP)^{SH511}* are heat-shocked at 48pf and imaged in the SIVP (green square) at 72hpf. (**B** & **C**) Enforced *bmpr2b* (tagged GFP, cleaved off via v2a site) is expressed in the yolk ball and skin cells. The single z-stack (C') and transverse cross-section (C'') of the white square region in C are shown and GFP localises in endothelial cells (white arrowheads). (**D-G**) Embryos are injected with *control* or *tnnt2a* morpholino and only RFP channels (in grey) are shown to compare the phenotypes of the SIVP. Magenta line, plexus length; blue lines, vessel diameter; green arrows, leading sprouts. (**H**) The plexus length is decreased upon *bmpr2b* overexpression in the presence or absence of flow. (**I**) There is no significant difference in the number of leading sprouts when overexpresses *bmpr2b* in *control* or *tnnt2a* morphants compared to HS-Control. Two-way ANOVA, n=9 and17 in each group from 2 replicates. *p<=0.05. (**J**) The vessel diameter of the SIV is not altered in HS-Bmpr2b embryos compared to HS-Control. Unpaired t-test, HS-Control, n=9; HS-Bmpr2b, n=17; ns, no significance.

5.8 Overexpression of *bmp4* results in restriction of vessel diameter in the presence of flow

Although BMP2 and BMP4 have overlapping roles in blood vessels and are considered in the same subgroup, they can function differently based on context (Dyer *et al.*, 2014). In the zebrafish SIVP, knockdown of *bmp4* and overexpression of *bmp2b* exhibited similar reduction of plexus length (Goi and Childs, 2016; Wiley *et al.*, 2011), suggesting that manipulating the two ligands may lead to opposite results. Therefore, to investigate the role of Bmp4 in SIVP development, I generated a transgenic line *Tg(hsp70l:bmp4-v2a-GFP)*^{SH600} to conditionally overexpress *bmp4* ligand in the zebrafish larva. Tagged GFP (later cleaved via v2a site) is used as a reporter of successful overexpression of *bmp4-v2a-GFP* element under high temperature, as shown in Figure5.9B &D. The GFP was highly expressed in the somites as shown in transverse cross-section (Figure5.9D'', from yellow line in D). However, the GFP expression did not co-localise with the endothelial cells labelled with RFP (Figure5.9D', single z-stack of white square region in D), as previously demonstrated for *bmpr2b*. This is not unsurprising since bmp4 functions non-cell autonomously as a morphogen (Kishimoto *et al.*, 1997; Soh *et al.*, 2020).

Unlike overexpression of *bmp2b* or *bmpr2b*, enforcement of *bmp4* expression from 24hpf did not cause ectopic sprouting from the CVP

(Figure5.9B, yellow arrows), suggesting that *bmp4* signalling is not sufficient for sprouting from the CVP.

To examine whether *bmp4* was indeed overexpressed in the zebrafish larva, the embryos were heat-shocked from 48hpf, then fixed at different stages post-heat-shock and tested by *in situ* hybridisation for *bmp4*. *bmp4* was expressed in specific organs/tissues, such as the ear, the heart and the pectoral fins, in HS-Control embryos (Figure5.9E), while the expression was ubiquitous and darker in HS-Bmp4 embryos at 53hpf and 56hpf, and became more confined in somites at 72hpf. Immuno-staining of downstream effector pSMAD was tested to confirm the activation of BMP signalling following heat shock of *bmp4* (Figure5.13B). These data suggested that *bmp4* is indeed enforced in the heat-shock line and that GFP expression is localised in the same region as *bmp4* expression.

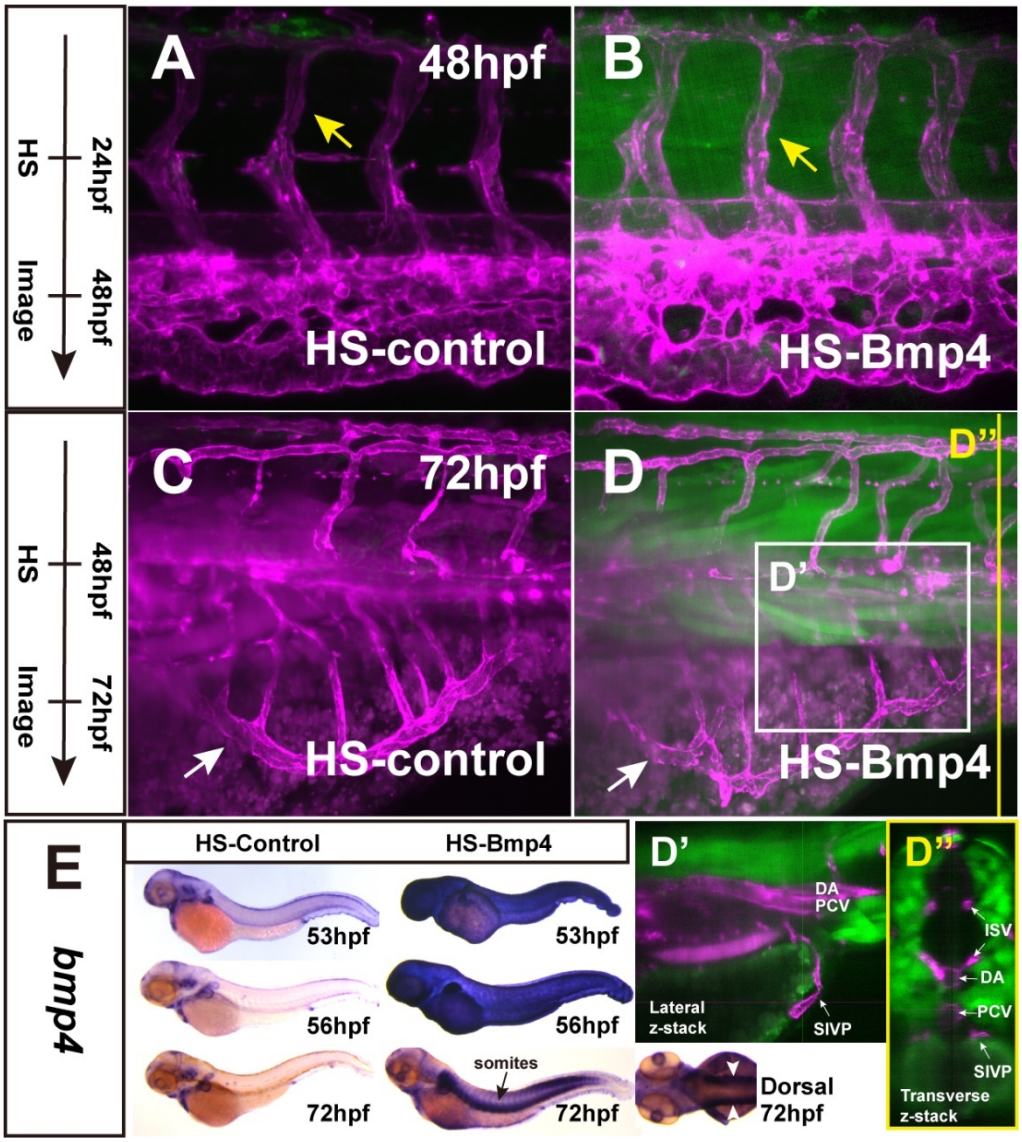

Figure5.9 Overexpression of *bmp4* does not cause ectopic sprouting from the CVP

(**A-B**) Embryos from *Tg(hsp70l:bmp4-v2a-GFP)^{SH600};(cry:CFP); (fli1a:AC-tagRFP)^{SH511}* are heat-shocked at 24hpf and imaged in the CVP at 48hpf. Compared to HS-Control, Bmp4 indicated by GFP is expressed in the somites after heat-shocked, however does not cause ectopic sprouting from the CVP (yellow arrows). (**C-D**) Embryos are heat-shocked at 48hpf and imaged in the SIVP at 72hpf. GFP is also expressed in the somites after heat-shocked but is not expressed within the ECs. Single z-stack from the white rectangle is shown in **D'** and transverse cross-section is shown in **D"**. (**E**) HS-Control and HS-Bmp4 embryos are tested by *in situ* hybridisation for *bmp4*. HS-Bmp4 embryos display ubiquitous and darker staining than that in HS-Controls at 53hpf and 56hpf, and show strong expression in the somites at 72hpf (Dorsal view, white arrowheads).

To examine the role of Bmp4 in SIVP remodelling in the presence or absence of flow, embryos from the heat-shock line were injected with *control* or *tnnt2a* morpholinos. Morphants were heat-shocked at 48hpf and imaged in the SIVP at 72hpf. Only RFP channels (inverted in grey) were shown for the clarity of the SIVP. Unlike overexpression of *bmp2b* (Wiley *et al.*, 2011) or *bmpr2b*, enforcement of *bmp4* expression did not shorten the plexus length of the SIVP, either in the presence or absence of flow (Figure5.10C-E). In addition, overexpression of *bmp4* did not alter the number of leading sprouts in both morphants (Figure5.10F). However, there was a significant decrease of vessel diameter in the SIV upon *bmp4* overexpression with flow (Figure5.10G), suggesting that *bmp4* is sufficient to restrict vessel diameter in the presence of flow.

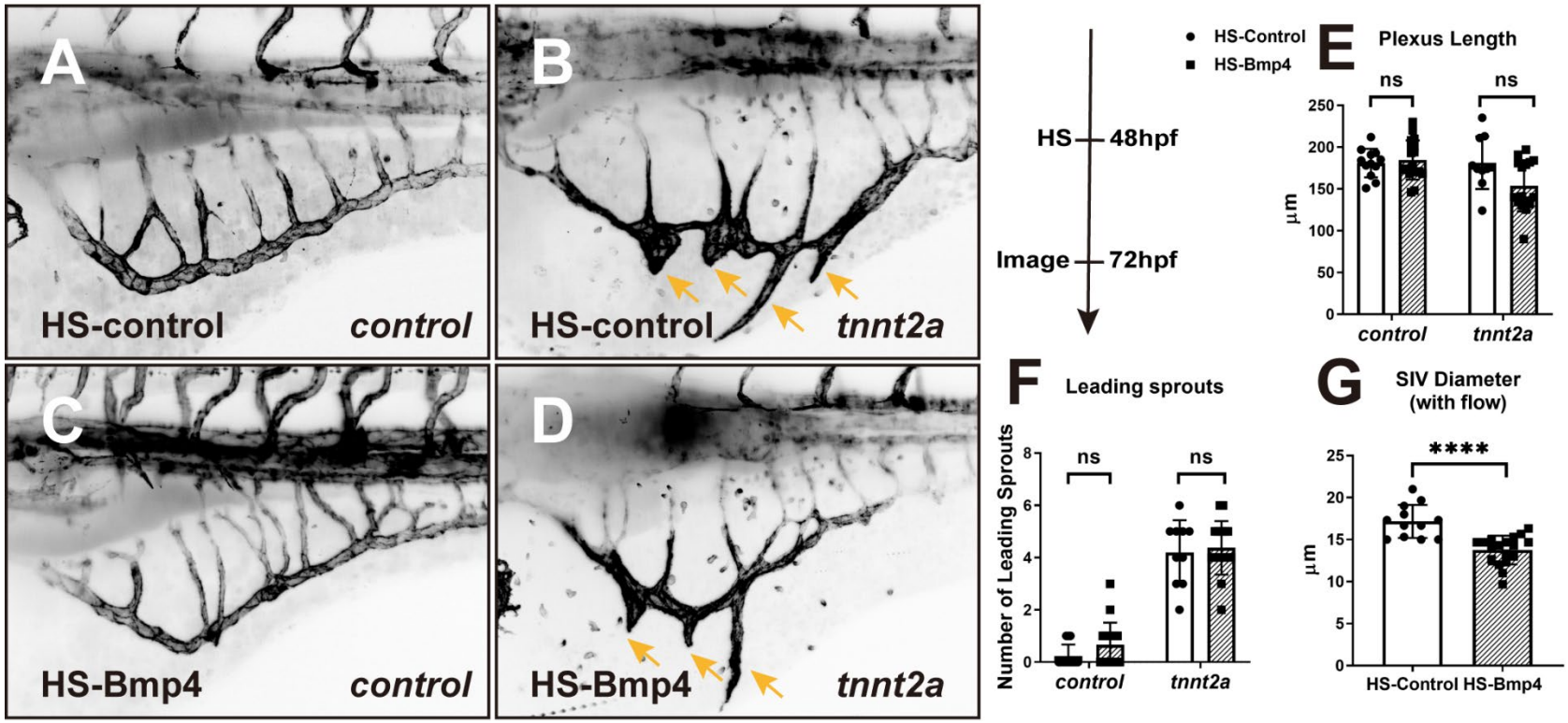

Figure5.10 Overexpression of *bmp4* restricts vessel diameter

(**A-D**) *Tg(hsp70l:bmp4-v2a-GFP)*^{SH600}*;(cry:CFP);(fli1a:AC-tagRFP)*^{SH511} embryos are injected with *control* or *tnnt2a* morpholino and are heat-shocked at 48pf and imaged in the SIVP at 72hpf. Only RFP channels (in grey) are shown to compare the phenotypes of the SIVP. Yellow arrows, leading sprouts. (**E & F**) The plexus length or the number of leading sprouts is not altered upon *bmp4* overexpression in the presence or absence of flow compared to HS-Control. Two-way ANOVA, n=12 or 18 each group from 3 replicates. ns, no significance. (**G**) The vessel diameter of the SIV is significantly decreased in HS-Bmp4 embryos compared to HS-Control. Unpaired t-test, HS-Control, n=12; HS-Bmpr2b, n=18, from 3 replicates; ****p<=0.0001.

5.9 Overexpression of *bmp4* rescues the enlarged vessel diameter present under low flow

Previously I have shown that *gata1a* morphants exhibited increase SIV diameter (Figure 3.12E) and that overexpression of *bmp4* restricted vessel diameter (Figure5.10G), therefore I asked whether overexpression of *bmp4* could rescue the enlarged vessel in *gata1a* morphants. Embryos from the heat-shock line *Tg(hsp70l:bmp4-v2a-GFP)^{SH600};(cry:CFP);(fli1a:AC-tagRFP)^{SH511}* were injected with *control* or *gata1a* morpholinos. Morphants were heat-shocked at 48hpf and imaged in the SIVP at 72hpf. Only RFP channels (inverted in grey) were shown to improve clarity of the SIVP (Figure5.11A-D).

Similar to previous observations, overexpression of *bmp4* resulted in a decrease in SIV diameter in the presence of normal flow. As expected, it also restricted the enlarged vessel diameter in majority of the *gata1a* morphants, showing a significant decrease in vessel diameter in *gata1a* morphants with HS-Bmp4 compared to those with HS-Control (Figure5.11E). On the other hand, there was no significant difference in plexus length or the number of leading sprouts following heat-shock in either morphant, suggesting that *bmp4* is sufficient to regulate vessel diameter but not other remodelling events in the SIVP.

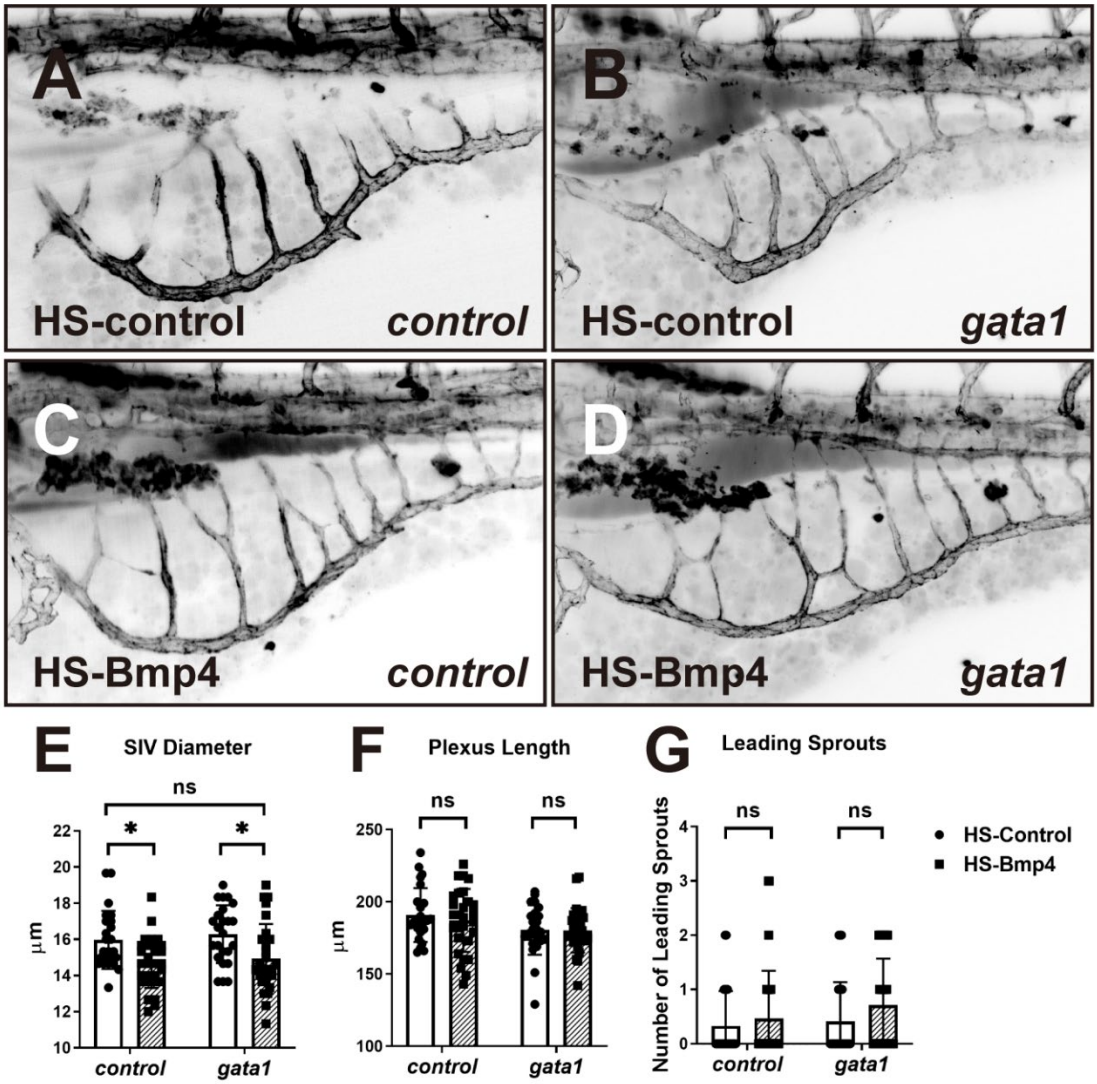

Figure5.11 Overexpression of *bmp4* rescues enlarged vessel diameter in *gata1a* morphants

(**A-D**) Embryos from *Tg(hsp70l:bmp4-v2a-GFP)^{SH600};(cry:CFP); (fli1a:AC-tagRFP)^{SH511}* are injected with *control* or *gata1a* morpholino and are heat-shocked at 48pf and imaged in the SIVP at 72hpf. Only RFP channels (in grey) are shown to compare the phenotypes of the SIVP. (**E**) The vessel diameter of the SIV is significantly decreased in HS-Bmp4 embryos compared to HS-Control, in both *control* and *gata1a* morphants. (**F**) The plexus length is not altered upon *bmp4* overexpression in both morphants. (**G**) There is no significant difference in the number of leading sprouts when overexpresses *bmp4* in *control* or *gata1a* morphants compared to HS-Control. Two-way ANOVA, n=24-28 in each group from 3 replicates. ns, no significance; *p<=0.05.

5.10 BMP signalling is pSmad1/5 independent during SIVP remodelling

Upon activation, BMP receptors phosphorylate downstream receptor-activated SMADs (R-SMADs), including SMAD1/5/8, which convey the signal from the membrane to the nucleus, where they activate transcription of target genes (Dyer *et al.*, 2014). To investigate whether BMP signalling is transduced via R-SMADs during SIVP development, whole mount immuno-histochemistry for pSMAD1/5 was performed. The technique has been difficult in zebrafish model due to fewer zebrafish specific antibodies and reduced optimisation of detection protocols. The aortic arches 1 (AA1) expresses *alk1* (Corti *et al.*, 2011) which activates pSMAD in the presence of flow (Laux *et al.*, 2013). Therefore, before analysing the expression of pSMADs in the SIVP, I tested whether the protocol used was applicable (see methods 2.2.1.25) and employed the expression of pSMADs in zebrafish AAs as an assessment (Figure5.12A). To outline the location of the endothelial nucleus, embryos from *Tg(fli1a:nls-mCherry)*^{SH370} were used.

Considering the dynamic expression of pSMADs and the continuous requirement of BMP signalling during SIVP development, embryos were fixed every 2 hours from 48hpf to 72hpf (13 time points in total) and processed for immuno-staining. The expression of pSMAD1/5 in the control AA1 and opercular artery (ORA) was co-localised with endothelial nucleus (RFP channel,

co-localisation shown as white colour in figures) at all time points tested, therefore only 72hpf was shown as a representative example (Figure5.12B). However, no pSMAD expression was detected in the absence of flow at all time points examined (Figure5.12B), suggesting that BMP signalling is activated by blood flow in AAs, consistent with previous reports (Corti *et al.*, 2011).

I also examined the expression of pSMADs in embryos treated with DMH1 or following overexpression of *bmpr2b* or *bmp4*. The corresponding controls (i.e. embryos treated with DMSO or HS-Controls) exhibited the same expression pattern as shown in the normal control (Figure5.12B). In the presence of flow, the expression of pSMADs in DMH1-treated embryos was substantially decreased (Figure5.12C, 'DMH1'), which was in line with its function as a BMP inhibitor (Hao *et al.*, 2010). Overexpression of *bmpr2b* led to significant increase of pSMAD expression in pharyngeal arches which were smaller in structure compared to HS-Controls (Figure5.12C, 'HS-Bmpr2b'). The co-localisation of pSMADs and EC nuclei was also detected in single z-stacks of the blood vessels (Figure5.12C, 'HS-Bmpr2b', yellow rectangle). Overexpression of *bmp4* also led to a stronger expression of pSMADs in ECs of AA1 and the ORA (Figure5.12C, 'HS-Bmp4'). In contrast, no pSMAD expression was observed in *tnnt2a* morphants of all groups, suggesting that pSMAD signalling was suppressed in the AAs in the absence of flow.

Collectively, these results showed that pSMAD expression decreases in

arteries when BMP signalling is inhibited and increases when overexpressed and that the immune-staining protocol is applicable and could be used to analyse pSMAD expression in the SIVP.

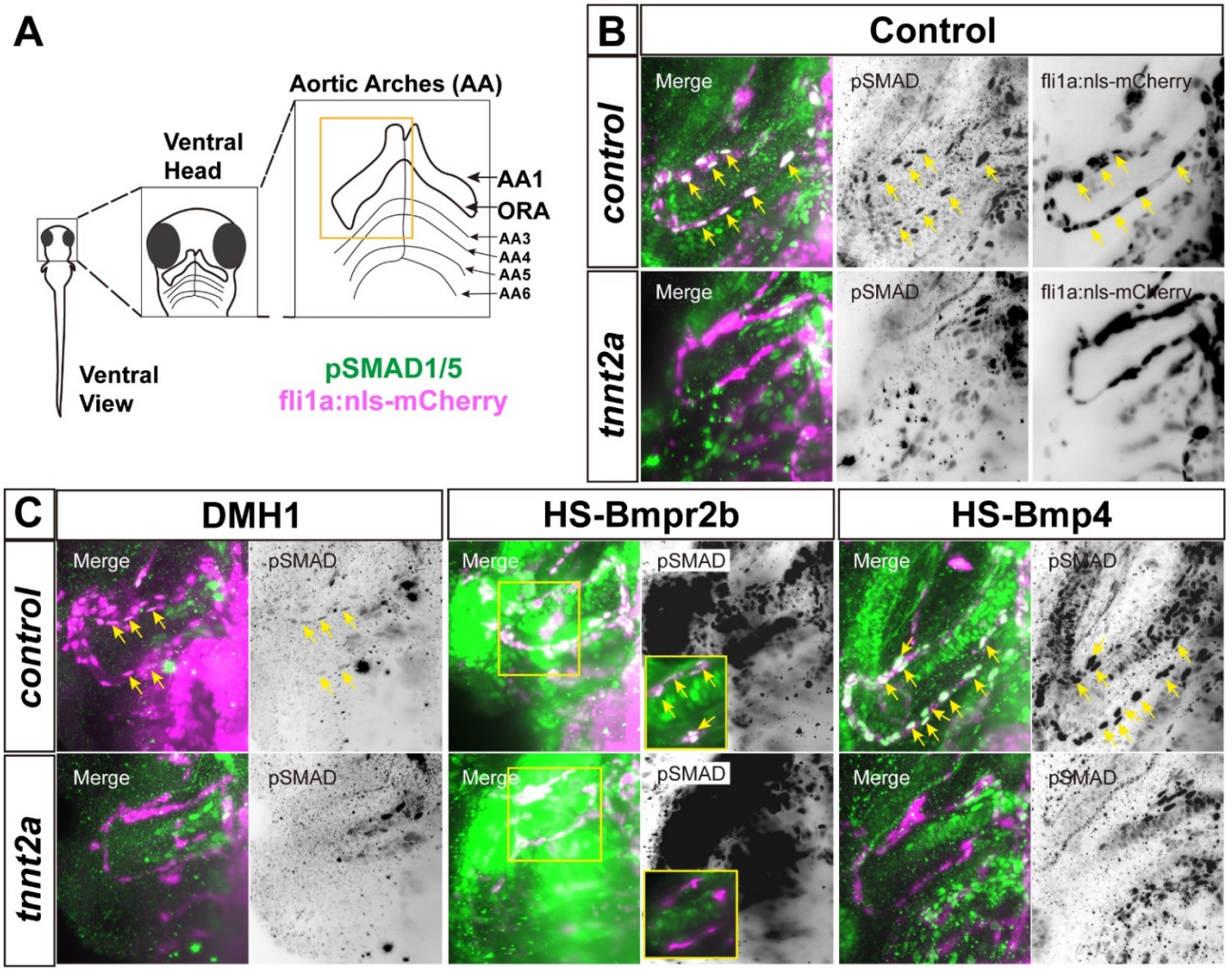
A
Aortic Arches (AA)
Ventral Head
AA1
ORA
AA3
AA4
AA5
AA6
Ventral View
pSMAD1/5
fli1a:nls-mCherry
B
Control
control
tnnt2a
Merge
pSMAD
fli1a:nls-mCherry
C
DMH1
HS-Bmpr2b
HS-Bmp4

Figure5.12 pSMAD1/5 expression is flow dependent in aortic arch

(**A**) Schematics show the position of AA1 and ORA in zebrafish. (**B-C**) Embryos from *Tg(fli1a:nls-mCherry)*^{SH370} are used. RFP-expressing endothelial cell nuclei are in magenta and pSMAD1/5 expression is in green. (**B**) Representative Control has been shown to indicate *control* morphants and those without treatment of DMH1 or HS-Bmpr2b or HS-BMP4 at 72hpf. pSMADs express in EC nuclei of the AA and ORA (yellow arrows) in the presence of flow but not in the absence of flow. (**C**) The expression of pSMADs (yellow arrows) is decreased in DMH1-treated embryos and increased in HS-Bmpr2b and HS-Bmp4 embryos in the presence of flow. No expression of pSMADs are detected in *tnnt2a* morphants. Yellow rectangle regions show the single z-stack from the maximum intensity projection images. AA, aortic arch; ORA, opercular artery.

Next, I analysed the expression of pSMAD during SIVP development from 48hpf to 72hpf. Using the same embryos that showed pSMAD1/5 expression in the AAs (Figure5.12), surprisingly, no expression was detected in the SIVP at all 13 time points (2hr interval from 48hpf to 72hpf) examined (Figure5.13A, only half of the time points showed due to space limitation), suggesting that BMP signalling was transduced in a pSMAD1/5 independent manner. Similarly, no expression of pSMAD1/5 was observed in DMH1-treated embryos (Figure5.13B, 'DMH1'). In addition, pSMADs were not present in the SIVP of *tnnt2a* morphants (Figure5.13A '*tnnt2a'* & B 'DMH1').

However, overexpression of BMP signalling via HS-Bmpr2b or HS-Bmp4 was sufficient to activate pSMAD expression in the SIVP in the presence of flow (Figure5.13B, 'HS-Bmpr2b' & 'HS-Bmp4'). The single z-stacks of the yellow rectangles were outlined to show the co-localisation of pSMADs and EC nuclei. In contrast, enforced BMP signalling failed to activate pSMAD expression in *tnnt2a* morphants. Collectively, these data suggest that BMP signalling functions via pSMAD1/5-independent pathways during SIVP remodelling, although activation of BMP signalling can induce pSMAD1/5 phosphorylation in ECs.

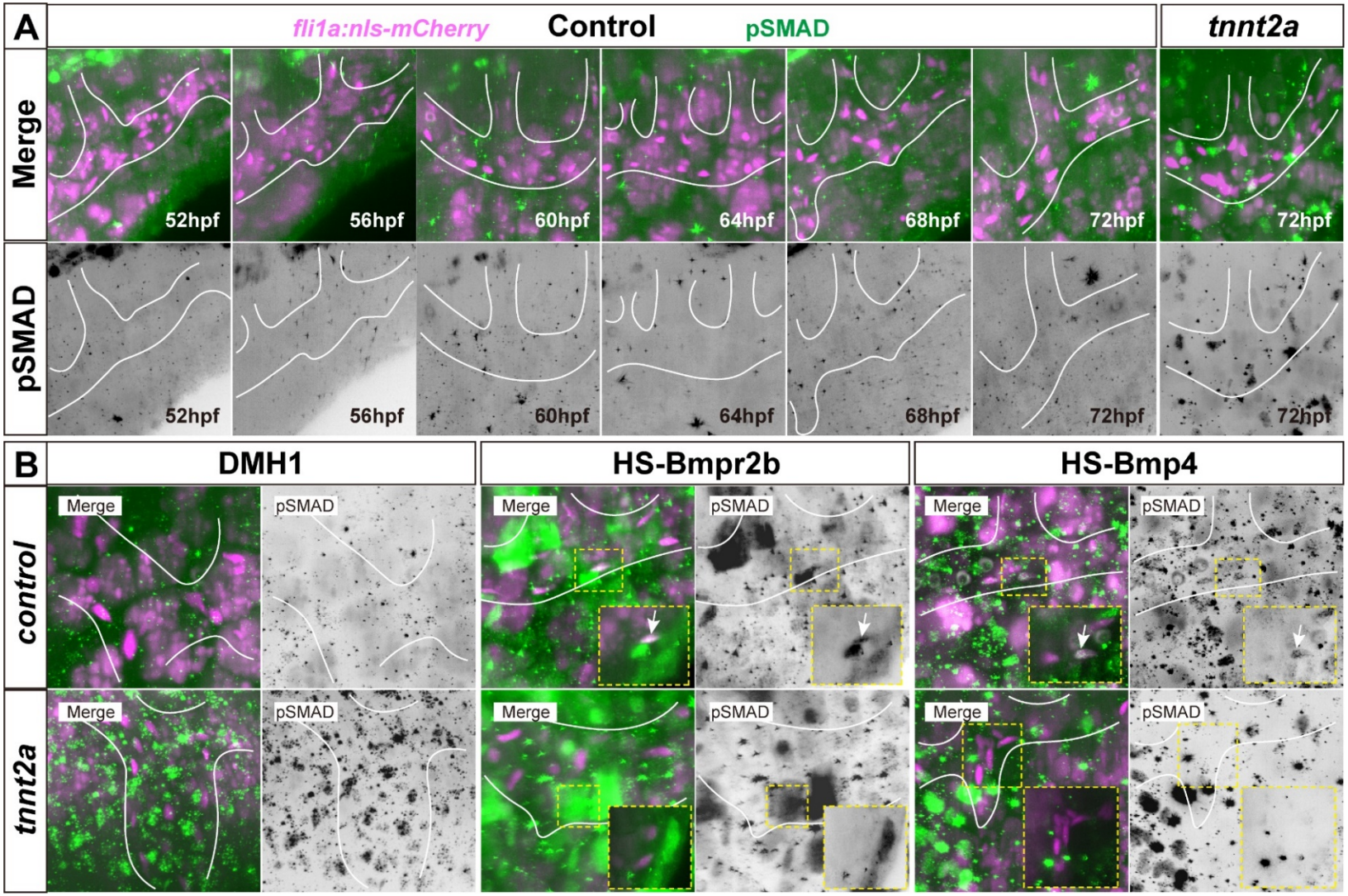
A
fli1a:nls-mCherry
Control
pSMAD
tnnt2a
Merge
pSMAD
52hpf
56hpf
60hpf
64hpf
68hpf
72hpf
72hpf
B
DMH1
HS-Bmpr2b
HS-Bmp4
control
tnnt2a
Merge
pSMAD

Figure5.13 BMP signalling is pSMAD1/5 independent during SIVP remodelling

(**A-B**) Embryos from *Tg(fli1a:nls-mCherry)*^{SH370} are used for immuno-staining of pSMAD1/5. RFP-expressing endothelial cell nuclei are in magenta and expression of pSMAD1/5 is in green. The SIVP is outlined in white. (**A**) Normal zebrafish embryos are fixed and stained every 2 hours from 48hpf to 72hpf (13 time points in total but only half of which are shown). No expression of pSMAD1/5 is detected int the SIVP at all time points tested in the presence or absence of flow. (**B**) The expression of pSMAD1/5 is not observed in DMH1-treated embryos but is increased in HS-Bmpr2b and HS-Bmp4 ECs in the presence of flow. No expression of pSMAD1/5 is detected in *tnnt2a* morphants. Yellow rectangle regions show the single z-stack from the maximum intensity projection images. White arrows indicate co-localisation of pSMAD1/5 and EC nuclei.

5.11 Discussion

In this chapter, I investigated the ligand/receptor expression patterns and the functions of several components of BMP signalling during SIVP remodelling, including *bmp10*, *bmp4, alk1*, and *bmpr2b.* Our data suggested a potential dispensable role of BMP signalling in sprout regression, although it is important in regulation of other remodelling events, such as branch formation and ventral expansion of the SIVP (Figure5.14). Here I summarise the key findings below:

1. *bmp10* is required for branch formation during SIVP development.

2. *bmp4* regulates SIV diameter and is sufficient to restrict enlarged vessel diameter caused by low flow.

3. *alk1* is expressed in the SIVP but may be dispensable for SIVP remodelling.

4. The expression of *bmpr2b* is increased in the leading sprouts in the absence of flow, however overexpression of *bmpr2b* fails to induce ectopic sprouts but is sufficient to inhibit ventral expansion of the SIVP.

5. BMP signalling is not transduced via Smad1/5 in the SIVP.

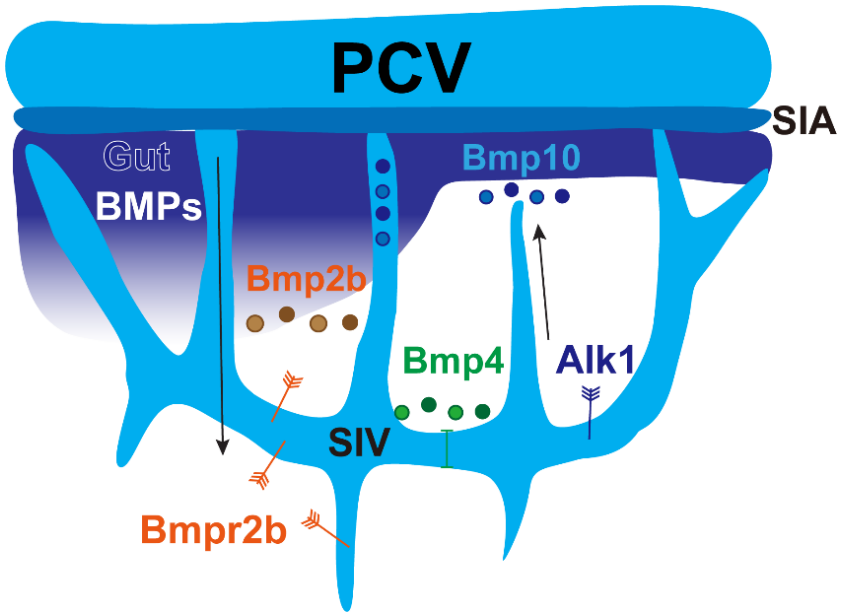

Figure5.14 The functions of BMP signalling pathways during SIVP remodelling

Schematic model shows the roles of BMP signalling pathways. The developing gut serves as a source of BMPs and Bmp10 is present in circulating blood flow (Laux *et al.*, 2013). Bmp2b inhibits ventral expansion of the SIVP via Bmpr2b; Bmp10/10-I binding to Alk1 may regulate the formation of the vertical branches (ICVs); Bmp4 is sufficient to restrict SIV diameter.

5.11.1.1 The potential dispensable role of BMP signalling in sprout regression

Treatment of DMH1 before the onset of flow leads to reduced SIVP expansion (Goi and Childs, 2016). In agreement with this, I have shown that treating embryos with DMH1 at different time points leads to distinct phenotypes, including failure of expansion of the SIV (24-72hpf) and disorganised branch

formation which lacks perfusion (24-48hpf) (Figure5.3C &E). The reduction in expansion was observed in the presence and absence of flow, indicating that BMP might serve as the flow-independent signal observed in cell trajectory analysis to induce EC ventral migration (Figure 3.7F). Interestingly, while ECs rapidly migrate ventrally from 48hpf to 72hpf (Figure 3.7B), DMH1 treatment during this period does not affect SIVP expansion (Figure5.4E). These observations suggest that ventral expansion of the SIVP may be pre-determined by BMP signalling during early stages (before onset of flow) and an adaptive flow-mediated mechanism subsequently fine-tunes the net distance of ECs to migrate. It has been demonstrated that the arteriovenous balance of the ISVs during secondary angiogenesis is pre-determined by an early heterogeneity in EC behaviour and Notch signalling in the primary ISVs, which leads to artery/vein-specific primary ISVs at a ratio of 60/40; subsequently, blood flow fine-tunes this ratio to approximately 50/50 (Geudens *et al.*, 2019). Whether such flow fine-tuned molecular-determined mechanism is present in other vascular beds remains to be determined.

Given that DMH1 inhibits BMP type I receptors (ALK1/2/3/6) and that only *alk1* expression is detected in ECs of the SIVP, I speculated that the DMH1-induced phenotype is mediated by *alk1*. However, knockdown of *alk1* and its ligand *bmp10+bmp10-like* did not phenocopy that in DMH1-treated embryos (Figure5.5D &Figure5.6E), suggesting a potential dispensable role of Bmp10-Alk1 signalling in sprout regression. BMP9/10-ALK1 signalling has been shown

to promote vascular remodelling and stabilisation via EC migration (Chen *et al.*, 2013; Corti *et al.*, 2011; Ricard *et al.*, 2012; Rochon *et al.*, 2016). *bmp10+bmp10-like* morphants displayed defects in branch formation, suggesting that *bmp10* is required for branch cell migration and vessel remodelling (Figure5.6C), although did not significantly increase sprout number. However, these findings need to be considered with caution because of potential sample bias due to high mortality and selection of embryos with flow in the SIVP. Future experiments may need to conditionally knockdown/delete *alk1* in SIVP ECs to investigate its functions in the SIVP. BMP2/4 and BMPR2 have been shown to promote angiogenic sprouting (Suzuki *et al.*, 2008; Wiley *et al.*, 2011). However, overexpression of *bmp4* or *bmpr2b* in the SIVP did not lead to ectopic sprouts (Figure5.8I & Figure5.10). Overall, manipulating BMP pathways including Bmp10-Alk1 (Figure5.5 & Figure5.6) and Bmp2/4-Bmpr2b signalling (Figure5.8 & Figure5.10) did not impair sprout regression. Our data implied a dispensable role of BMP signalling for sprout regression during SIVP remodelling.

This leaves the question as to what mechanism is underlying the DMH1-induced ectopic sprouts. BMP9 has been found to inhibit VEGF-induced angiogenesis (Scharpfenecker *et al.*, 2007) and co-receptor endoglin negatively regulates VEGF signalling in maintaining quiescence in ECs (Tual-Chalot *et al.*, 2020). Inhibition of BMP signalling with DMH1 may lead to increased sensitivity of ECs to VEGF in the SIVP, resulting in ectopic sprouts

which resembles overexpression of *vegfaa*$_{165}$ or *vegfc* (Figure4.4 & Figure4.7). However, DMH1-treated *tnnt2a* morphants displayed exacerbated ectopic sprouts (Figure5.4F), indicating that the inhibitory effects of DMH1 is flow independent, while enhanced VEGF signalling has no synergistic effects with blood flow in regulation of sprouts, thus there might be additional signals that contribute to this process. I did not investigate functions of *alk2* and *alk3a/b* during SIVP development, since their expression are not observed in ECs of the SIVP. However, their expression may have been at low levels not detectable by *in situ* hybridisation. It has been shown that ALK2 and ALK3, which likely in conjunction with BMPR2, prevent branch pruning in mouse retinal vessels (Lee *et al.*, 2017). It is possible that DMH1 inhibits Alk2 and Alk3 and therefore might inhibit sprout regression. Alternatively, given that *alk2* and *alk3* are expressed at regions where the intestine is formed (Figure 5.1G-L), DMH1 may affect the formation of the gut which could be the source of the BMP signalling, and subsequently affect SIVP remodelling. Although it is unlikely that ectopic sprouts were due to off-target effects of DMH1 since pSMAD1/5 expression is reduced following DMH1 treatment, I cannot exclude this possibility.

FLT4 has been shown to physically interacts with BMPR2 and facilitates endocytosis of BMPR2 to induce downstream effects (Hwangbo *et al.*, 2017). BMPR-mediated intracellular transactivation of VEGFR via c-Src has also been reported recently (Rezzola *et al.*, 2019). Given the overlapping functions of VEGF and BMP signalling in the SIVP, it is possible that such crosstalk is

present. In the previous chapter, I have shown that Flt4 could be activated under low flow and induces sprout regression (Figure 4.2 & Figure4.9E). Although increased expression of *bmpr2b* in the absence of flow (Figure5.2D) leads to speculation that *bmpr2b* promotes sprouting, the existence of crosstalk with VEGF may cause opposite effects such that transactivation of *flt4* induce sprout regression. This could potentially explain why overexpression of *bmpr2b* did not lead to ectopic sprouts (Figure5.8I).

Nonetheless, BMP signalling appears to be dispensable for sprout regression and my data suggests it has a multitude of roles in other remodelling events in the SIVP (Figure5.14). Overexpression of *bmpr2b* shortens the plexus length of the SIVP (Figure5.8H). Overexpression of *bmp2b* (Wiley *et al.*, 2011) or overexpression of Bmp2/4 antagonist *noggin3* (Hen *et al.*, 2015) also leads to a shortened SIVP, suggesting that the Bmp2b-Bmpr2b pathway regulates ventral expansion of the SIVP. While bmp4 morphants display failure of SIVP outgrowth (Goi and Childs, 2016), overexpression of *bmp4* at later stages does not affect the plexus length but restricts SIV diameter. Enhanced *bmp4* rescues the enlarged vessels induced by low flow-induced in *gata1a* morphants (Figure5.11). BMP4 signalling has been shown to induce vasoconstriction in diabetic patients via BMPR1a (ALK3) (Zhang *et al.*, 2014). Knockdown of *flt4* under low flow also restricts SIV diameter (Figure4.9F). Whether *bmp4* and *flt4* interacts in regulation of vascular diameter needs further investigation.

5.11.1.2 BMP signalling is not transduced via pSmad1/5 in the SIVP

BMP activity has been shown in the SIVP of *Tg(2xID1BRE:nls-mCherry)*^{ia17}, in which a BMP-responsive element (BRE) containing a 183bp cassette (-1046;-863) of the human *ID1* promoter induces expression of nuclear mCherry (Hen *et al.*, 2015; López-Rovira *et al.*, 2002; Schiavone *et al.*, 2014). However, I did not observe any GFP expression in the SIVP in another BRE line *Tg(bre:egfp)*^{pt510} (Korchynskyi and Ten Dijke, 2002; Laux *et al.*, 2011) (data not shown), which contains two regions of the mouse *Id1* promoter (-1052 to -1032; -1105 to -1080). ID1 is a downstream target of BMP and both of the *ID1* (*Id1)* promoter elements used in the two lines have been shown to be directly bound by SMAD1/5/8 and SMAD4 (Korchynskyi and Ten Dijke, 2002; López-Rovira *et al.*, 2002). Therefore, in theory the two lines reflect Smad activity in the zebrafish. The discrepancy of BRE expression in the SIVP may result from the different *ID1* promoter used (human versus mouse; different loci). Alternatively, it may reflect that different Smads are recruited in the SIVP.

In line with the observation of an absence of Smad activity in the SIVP from *Tg(bre:egfp)*^{pt510} embryos, our immunohistochemistry results show no pSMAD1/5 expression in the SIVP during remodelling (Figure5.13A). To ensure the absence of pSMAD signal was not due to technical problems, the expression of pSMAD in the aortic arch of the same embryos is evaluated as a positive control. I observed clear expression of pSMAD1/5 in AA1 which also

shows no GFP co-localisation following DMH1 treatment and strong GFP expression when *bmpr2b* or *bmp4* was overexpressed (Figure5.12). In addition, pSMAD1/5 expression was also detected in other organs which display well-known requirements for BMP signalling, such as heart, pectoral fin, pharyngeal arches, somites, and spinal cord (data not shown). Moreover, the pSMAD1/5 signal was detected in the SIVP when *bmpr2b* or *bmp4* expression was enforced (Figure5.13B). This suggests that although BMP signalling is not normally transduced via pSmad1/5 in the SIVP, these can be activated with exogenous BMP cues. Therefore, it is unlikely that the absence of pSMAD signal in the SIVP is due to a failure of antigen-retrieval or antibody penetrance. Other Smads which I have not tested, such as Smad8 or co-Smad4 might be required for the BMP cascade in the SIVP. Alternatively, ECs may engage non-Smad pathways or other TGF-β signalling in the SIVP. BMP2 induces cell polarisation and migration via PI3K-mediated cytoskeletal reorganisation (Hiepen *et al.*, 2014). BMP4 activates ERK1/2 to induce capillary sprouting from HUVEC spheroids (Zhou *et al.*, 2007). In the zebrafish caudal vein, Bmp2b combined with Bmpr2a/b activates R-Smad and Erk, leading to sprout migration and fusion (Wiley *et al.*, 2011). Erk has been shown to act as a specific effector of VEGF signalling during zebrafish ISV sprouting or lymphatic formation (Shin *et al.*, 2016a, 2016b). Given the overlapping functions of VEGF and BMP signalling during SIVP remodelling (e.g. ICV formation and vasoconstriction), it would be interesting to further investigate the role of Erk during SIVP

development.

Chapter 6 General discussion

6.1 Major findings

6.1.1.1 Model of flow sensitive SIVP development

The work presented in this thesis provides insight into the role of blood flow in endothelial cell polarisation and migration and the interaction of these cells with the VEGF and BMP signalling pathways during vessel remodelling (Figure 6.1). To study the cellular and genetic mechanisms underlying this process I have investigated the zebrafish SIVP, which is a vascular plexus that undergoes blood-flow dependent remodelling. During SIVP development, previous studies have reported the existence of leading sprouts comprised of two ECs (Hen *et al.*, 2015). My work has focused on furthering the understanding of how these leading sprouts remodel in response to blood flow and how loss of flow results in an increase in EC number in the leading sprouts. I show that blood flow is necessary for directed EC rearrangement and that the sprouts which contain an accumulation of ECs in the absence of flow do not form as a result of elevated proliferation but are rather due to impaired cell migration in the absence of cues provided by blood flow. I have also contributed to the general knowledge of vessel remodelling by firstly describing in detail the cellular behaviours during sprout regression. I propose a model, whereby blood flow instructs the polarisation and migration of ECs in the main vessel, followed by exposure of tip cells to blood flow which then triggers their subsequent migration towards the main vessel, leading to sprout regression. I have also

found that VEGF and BMP signalling are important for distinct aspects of SIVP development. In particular, the VEGF receptor *flt4* is required for sprout regression under low flow conditions. Since the SIVP has been a popular platform for drug screening and cancer models (Moshal *et al.*, 2011; Nicoli *et al.*, 2009; Nicoli and Presta, 2007), my work also suggests that blood flow and the timing of treatment are important factors to consider when using leading sprouts to evaluate drug efficacy.

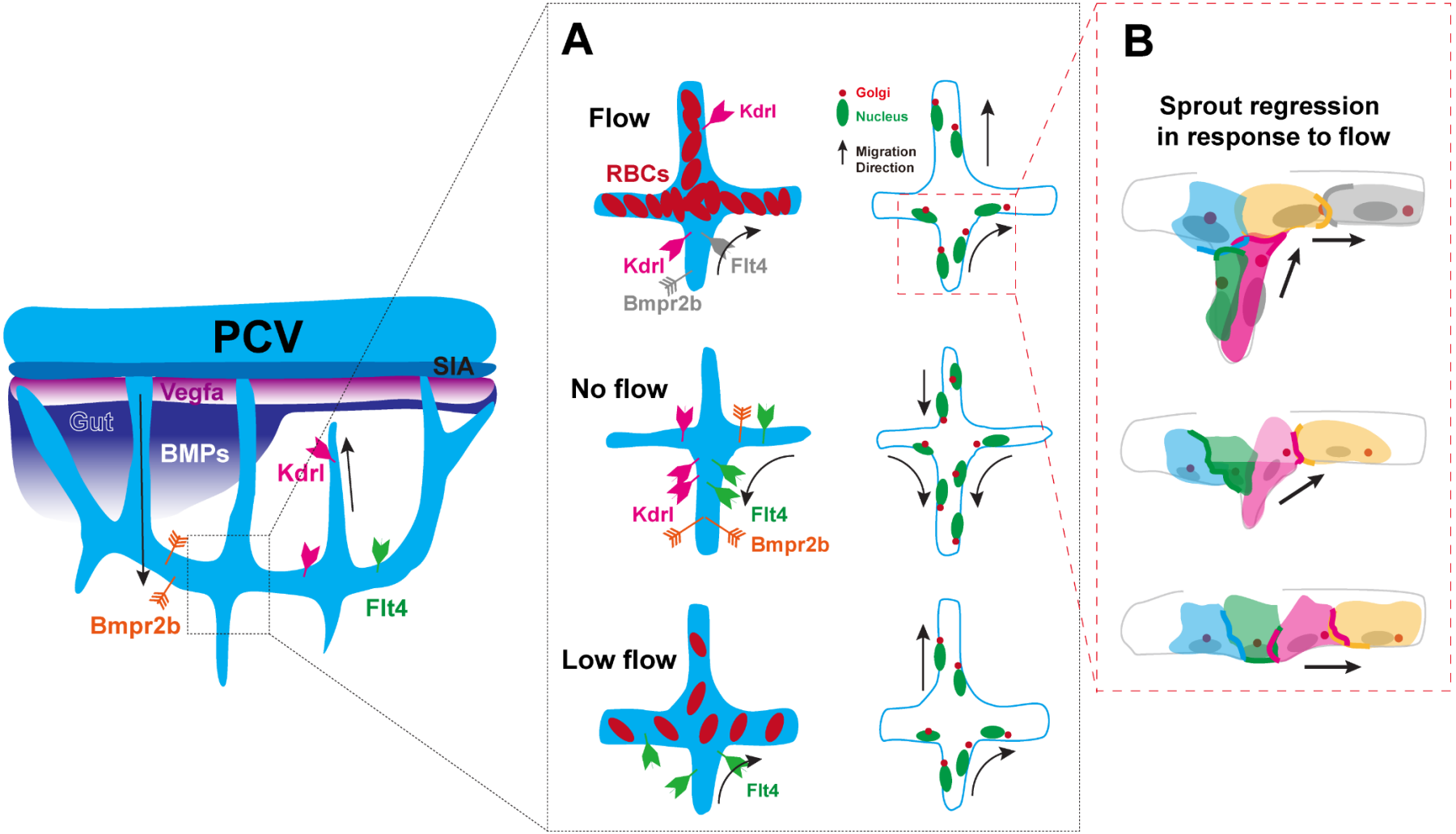
PCV
SIA
Vegfa
Gut
BMPs
Kdrl
Flt4
Bmpr2b
A
Flow
Kdrl
RBCs
Kdrl
Flt4
Bmpr2b
Golgi
Nucleus
Migration Direction
No flow
Kdrl
Flt4
Bmpr2b
Low flow
Flt4
B
Sprout regression in response to flow

Figure 6.1 Molecular and cellular mechanisms underlying SIVP sprout regression.

(**A**) Schematic illustrations depicting the cellular behaviours and molecular cues involved in SIVP sprout regression under different flow conditions, including in the presence and absence of flow and low flow. (**B**) Schematic illustrations depicting the cell coordination during sprout regression in response to flow. ECs (in grey and yellow) at the luminal surface migrate against flow and ECs (in green and pink) in the regressing sprout are pulled or use their neighbouring cells as migratory substrate via cell-cell junctions (thickened lines), followed by cell rearrangements that lead to sprout regression.

6.1.1.2 **Analysis methods**

Angiogenesis is often viewed as a binary process. Vessels are either actively undergoing angiogenesis or become quiescent with mural cell recruitment. Recently a concept has been proposed in which angiogenesis is a multistep event including sprouting, anastomosis, lumenisation and remodelling (Betz *et al.*, 2016). My results agree with this concept and provide a more nuanced understanding of angiogenesis, that these steps can be non-sequential and interlinked (sprouting and sprout regression in this case) and that not all events are required (non-anastomosed sprouts). With the help of high-resolution imaging technology, we are able to visualise these angiogenic events in more detail and in different vascular beds. However, how we turn such descriptive information into quantitative values is important in future analysis. It is my hope that the methods I employed in this thesis for cell tracking provides a new paradigm for measuring EC motility and behaviour *in vivo*. Previous studies, to my knowledge, usually only consider either cell migration trajectories in a small segment of vessel or the overall plexus expansion at individual timepoints. My results combine these two and reveal how ECs coordinate refinement of vessel segments while at the same time follow collective migration at a plexus level. In this case, for example, tip cells mostly undergo ventral migration, and together with other ECs drive SIVP expansion; they also display transient dorsal migration to undergo sprout regression in the meantime.

Furthermore, blood flow provides an additional horizontal force for these ECs to migrate and therefore while EC migration steps are variable, the final results of cell tracks are very different in the presence and absence of flow. Analysis of cell migration at both a single cell level and a plexus level provides a more comprehensive picture of how a vascular plexus develops *in vivo*. The Trackmate plugin in Fiji (ImageJ) provides an open and free source for tracing EC migration, yet it has limitations in accurate recognition of cells that are close to each other and manual correction is required. In this thesis I have only analysed cell tracks in 2 dimensions (x and y axis) and the depth (z axis) has not been quantified, due to computational difficulties with large datasets. Future analysis improvements will be required to improve imaging processing in large 4D data, including registration, segmentation and blob recognition.

6.2 Limitations and Future directions

6.2.1.1 **VEGF and BMP singling pathways during SIVP remodelling**

Inhibition of VEGF and BMP signalling at different time points suggest that these two pathways are critical for the initiation of SIVP development, while have more specific effects on certain parts of the plexus at later stages. Instead, the refinement of excessive branches (Lenard *et al.*, 2015) or sprouts is strongly influenced by flow. A model of SIVP development has been previously proposed whereby VEGF and BMP are required for dorsal and ventral migration of ECs,

respectively, and that retraction of leading sprouts is dependent on Notch and Flt1, which act as negative regulators of VEGF signalling (Hen *et al.*, 2015). The model implies that sprout regression is a result of anti-angiogenic sprouting via Notch and Flt1. Although my results go against the requirement of Notch and Flt1 in sprout regression, it appears that blood flow inhibits *flt4* expression during normal development, suggesting that flow suppresses VEGF-mediated angiogenesis. However, *flt4* is only required for sprout regression under *low flow* conditions. This observation suggests *flt4* may function as a mechano-sensor or mechano-transducer under low flow, however, further experiments are needed to test this hypothesis, which could include knocking down *gata1a* in *flt4* mutants, in a VE-cad-FRET background which indicates dynamics of pulling force on the cell junctions. I also lack firm evidence of which mechanoreceptors regulate sprout regression under normal flow conditions. Kdrl (VEGFR2) is a strong candidate since it is highly expressed in the SIVP and has been shown to facilitate mechano-transduction (Jin *et al.*, 2003; Tzima *et al.*, 2005). Alk1, Endoglin, and/or Bmpr2b may interact with VEGF receptors and regulate flow-mediated cell migration (Aspalter *et al.*, 2015; Hwangbo *et al.*, 2017; Jin *et al.*, 2017; Tual-Chalot *et al.*, 2020). I was unable to identify the potential mechanosensory/transducing functions of Vegfr2 or Alk1 because inhibition of these impairs blood circulation in the SIVP. Future experiments conditionally targeting theses receptors will be informative. Cell tracking analysis suggests a flow-independent cue for EC ventral migration. In line with

the model proposed by Hen *et al.*, my data suggests BMP signalling may represent such a signal. *bmpr2b* negatively regulates SIVP ventral expansion, however, which BMP ligand is required is unclear. Bmp2b or Bmp4 could be interesting candidates.

6.2.1.2 Cell junctional rearrangements may drive membrane retraction during sprout regression

While I suggest that when tip cells are exposed to blood flow, they migrate and retract their membrane into the main vessel, it is not clear how exactly the membrane retraction is achieved. My preliminary observations suggest that this may be facilitated by the actin cytoskeleton at the dorsal and/or ventral edges of cell junctions, which could provide a pulling force on the cells (Figure 6.2A). This resembles EC elongation during sprouting in which VE-cad regulates actin polymerisation at either end of the cell and drives cell extension (Paatero *et al.*, 2018; Sauteur *et al.*, 2014), but in a reverse mode. Alternatively, the tip cells anastomose with neighbouring SIV cells, driving EC migration towards each other, therefore causing the sprout to incorporate into the main vessel (Figure 6.2B). However, in the absence of flow, the distribution of junctional F actin is disorganised (Figure 6.2C & D), which may limit this process. Future experiments using junctional markers (e.g. ZO-1 and VE-cad) as well as actin markers, including lifeact and actin chromobodies as employed in this thesis, will be informative.

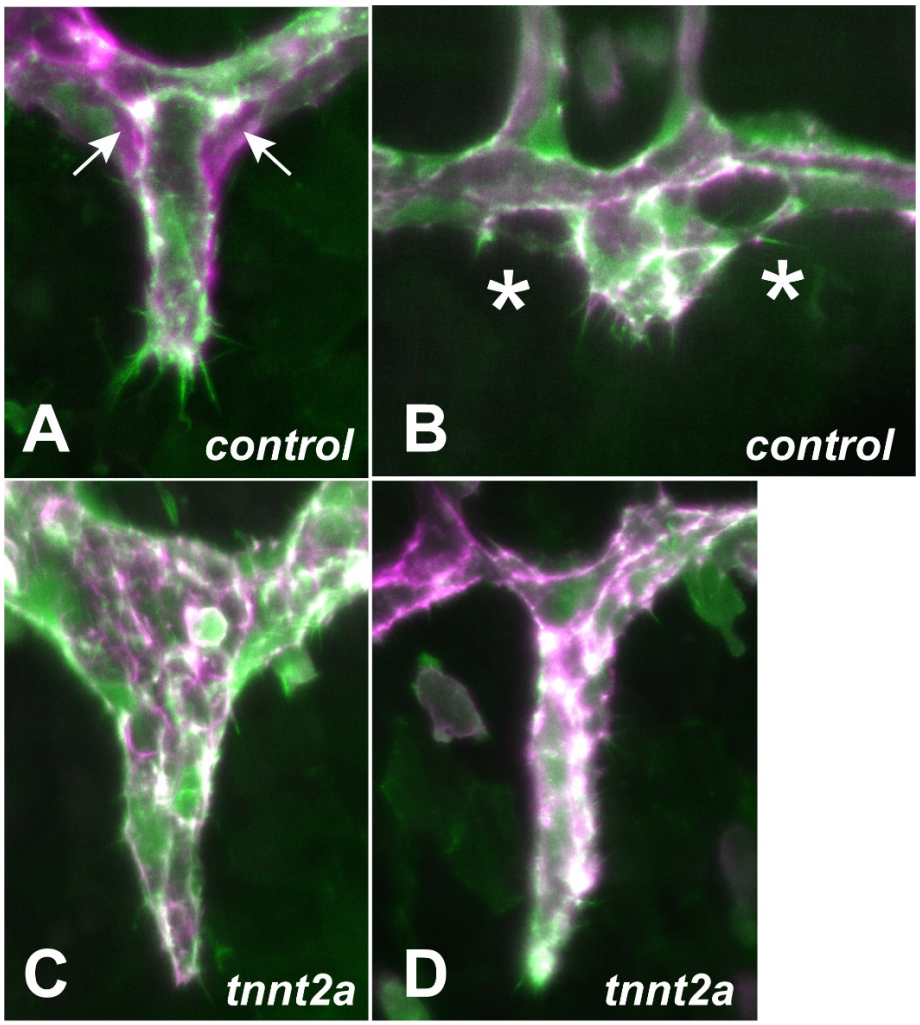

Figure 6.2 Distribution of F-actin at junctional edges during sprout regression

(**A-D**) Examples of leading sprouts in *control* or *tnnt2a* morphants from *Tg(fli1a:lifeact-mClover)*^{SH467}*;(fli1a:ACtagRFP)*^{SH511}*,* to show the regressing sprouts in the presence and absence of flow. (**A-B**) The retraction of cell membrane may facilitate by F-actin at the dorsal (white arrows) and/or ventral edges of cell junctions (A) or tip cells anastomosing with neighbouring SIV cells (B). (**C-D**) Still images show leading sprouts in the absence of flow, in which the distribution of junctional F actin is disorganised.

Chapter 7 Appendix

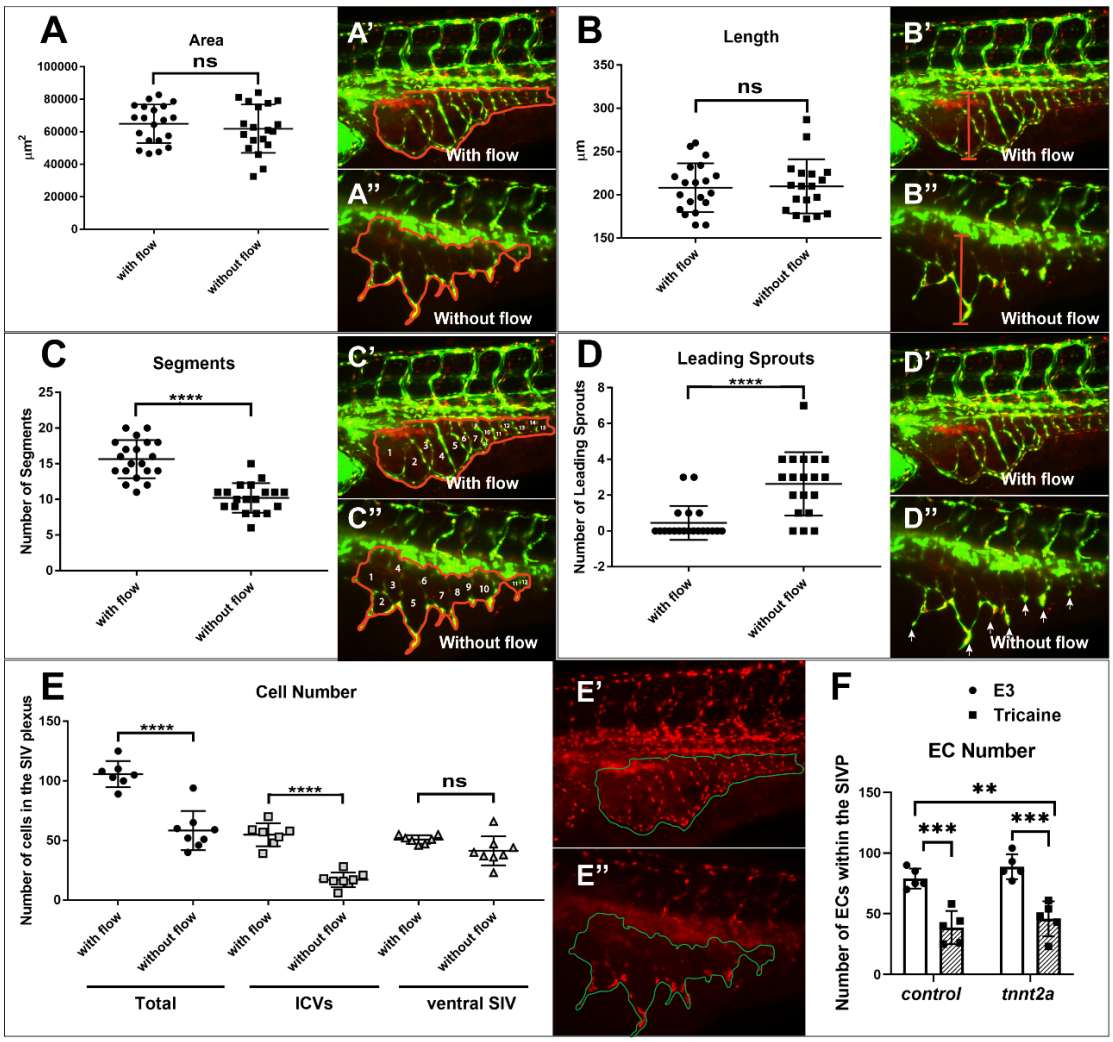

Figure 7.1 Embryos treated with tricaine display failure of sprout regression and reduced EC number.

Comparison of SIVP morphology at 72hpf in the presence (E3) or absence of blood flow (tricaine treatment). This figure is supplementary to Figure 3.2. (**A**) Measurement of area (A'& A'', circled areas) does not show significant difference. (**B**) Measurement of total length of the SIVP (B'& B'', vertical lines) does not show significant difference. (**C**) The number of vascular loops (C'& C'', white numbers) is significantly decreased in the absence of flow. (**D**) The number of leading sprouts (D'& D'', arrows) is increased in the absence of flow. (**E**) The total number of ECs (E'& E'', dots) in the SIVP is decreased in the absence of flow, due to a significant reduction of EC number in the ICVs (branches). E3, n=20; Tricaine, n=19; from three independent replicates. Unpaired t-test, ****p<=0.0001, ns, no significance. (**F**) Treatment of tricaine in *control* or *tnnt2a* morphants leads to decreased EC number, suggesting toxicity of tricaine in the SIVP. n=5 embryos from each group. Two-way ANOVA, *p<=0.05, ns, no significance.

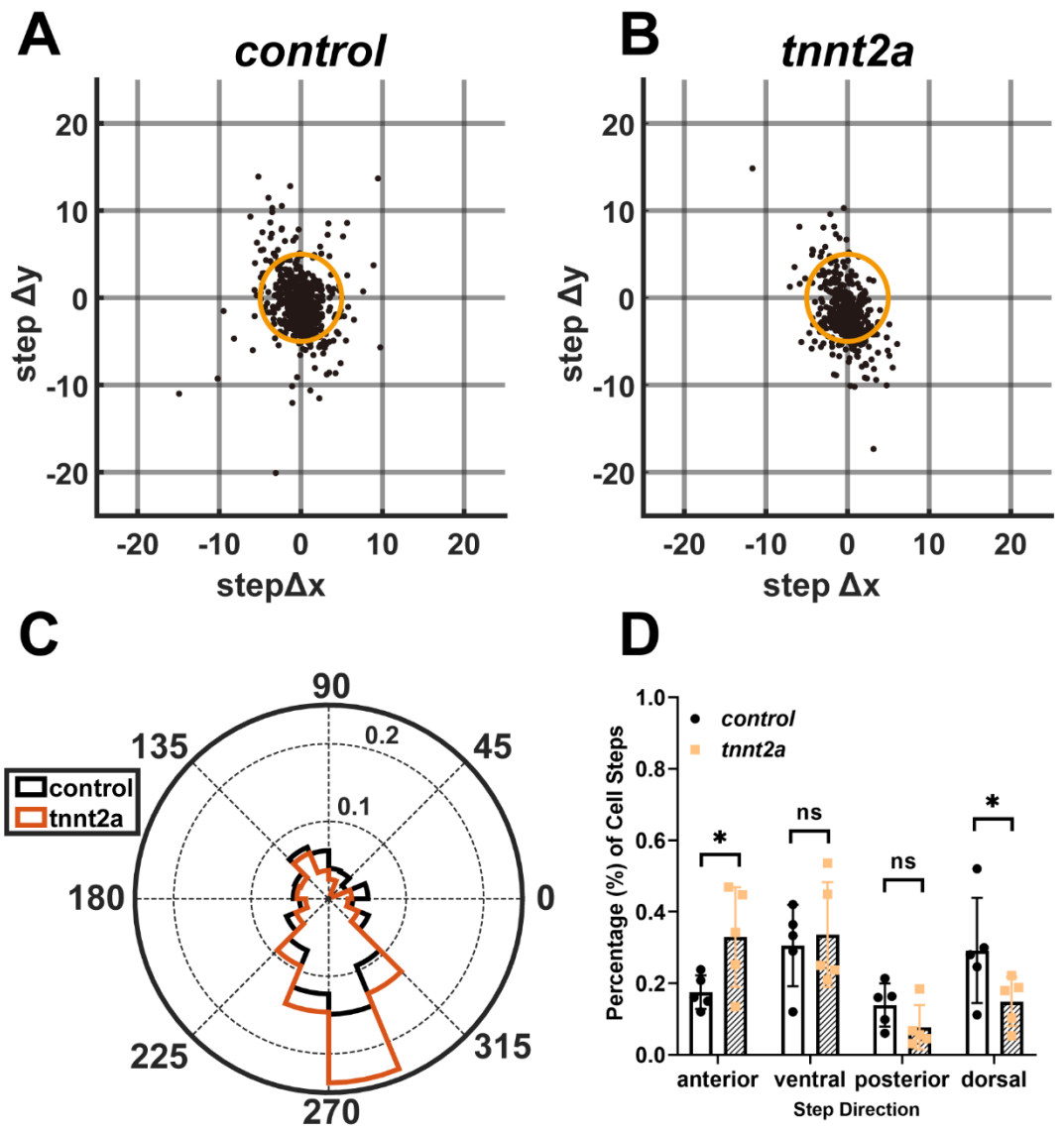

Figure 7.2 Blood flow regulates direction preference of EC migration during branch formation

(**A-B**) The coordinates of branch cell migration steps in the *control* or *tnnt2a* morphants are shown in scatter plot. The orange circle (radius = 5) in each plot is outlined as a reference for coordinate distribution. The steps are anisotropic yet favour in bottom-right in the absence of flow. (**C**) The angles of all branch cell migration steps are plotted in polar histogram. The length of each bar indicates the relative number of migration steps towards that direction (normalised to the total number of migration steps). The values in rose chart are grouped in bar chart in D for comparison. (**D**) There is a significant increase in anterior migration and a reduction in dorsal direction in the absence of flow. *control*, n=611 steps from 5 embryos; *tnnt2a*, n=830 steps from 5 embryos. Unpaired t-test, *p<=0.05.

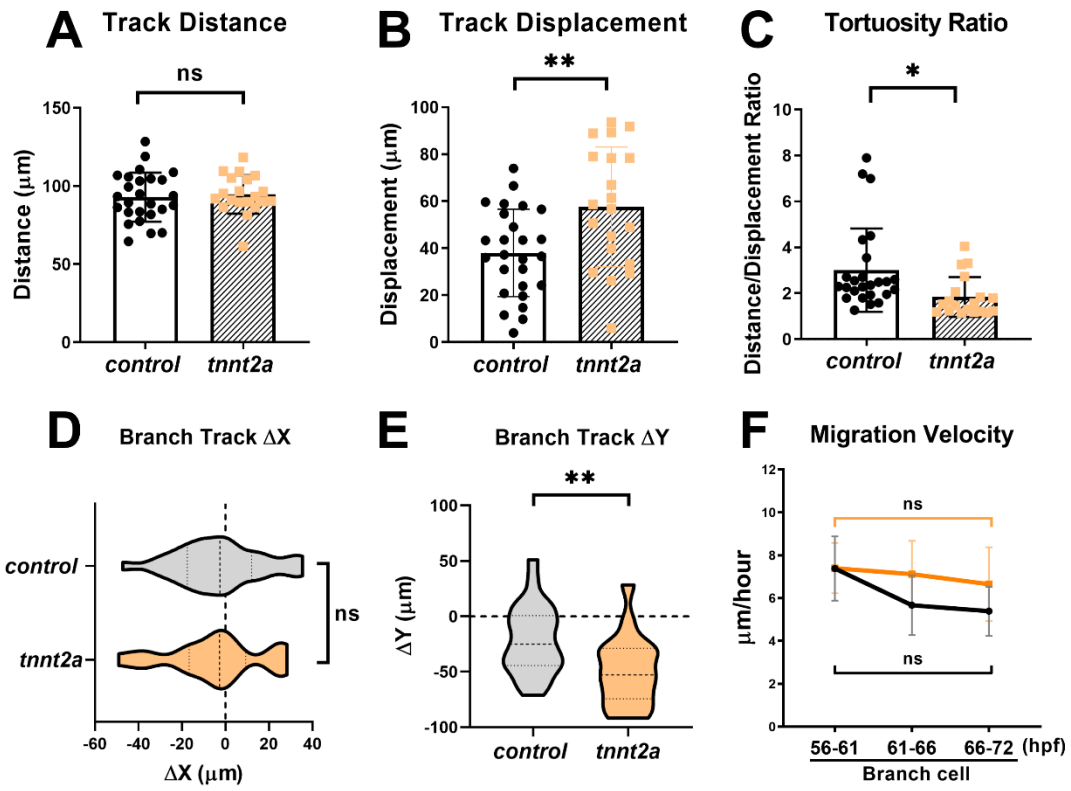

Figure 7.3 Branch cells migrate ventrally in the absence of flow

The track analysis of each track is quantified and compared between *control* (grey) and *tnnt2a* (orange) morphants. (**A**) The total distance does not significantly differ in branch cells of *control* (white bars) and *tnnt2a* (shaded bars) morphants. (**B-C**) Branch cell display significantly increased track displacement and reduced tortuosity ratio (distance/displacement ratio) in the absence of flow. (**D-E**) The track ΔX does not differ with/without flow, but there is a significant decrease in track ΔY in branch cells in the *tnnt2a* morphants, suggesting that branch cells migrate ventrally in the absence of flow. (**F**) The migration velocity of branch cells is not significantly different in the presence and absence of flow. *control*, n=26 tracks from 5 embryos; *tnnt2a*, n=20 tracks from 5 embryos. Unpaired t-test, *p<=0.05.

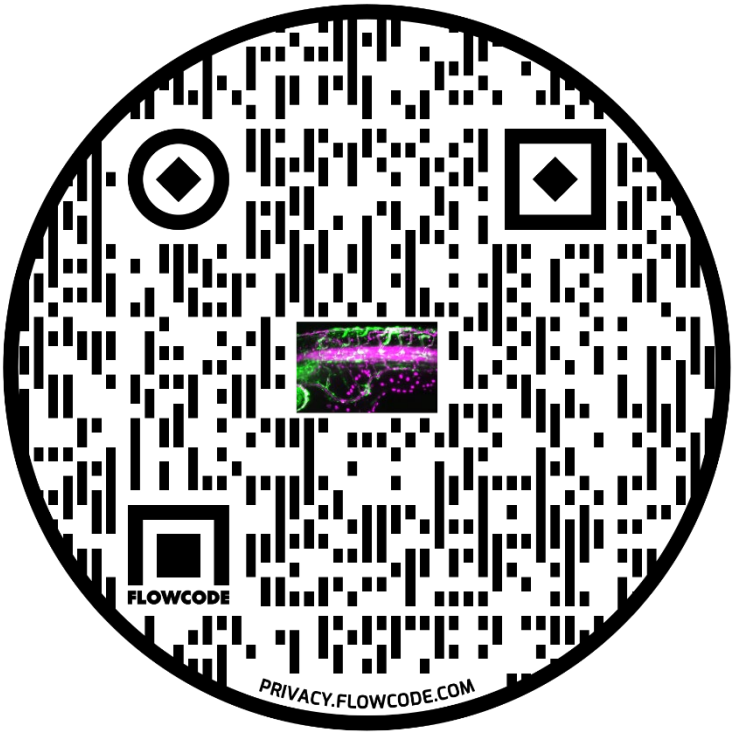

https://drive.google.com/file/d/1rH8NROz2HRYrzfSvjZlPn1ovwIeBvXmH/view

?usp=sharing

Movie 1 Blood flow perfuse the SIVP in an anterior-posterior manner

This movie corresponds to still images in Figure 3.1.
Time-lapse movie of *Tg(fli1a:egfp)*^{y1};*(gata1a:DsRED)*^{sD2} labelling endothelial cells in GFP and red blood cells in RFP. Images were taken at approximate 19 hours 5-minute intervals, starting at 53hpf. Z-series were flattened to 2D maximum intensity projections and presented in time series, 20 frames per second (fps). Arrows mark blood flow enters different segments of the SIVP.

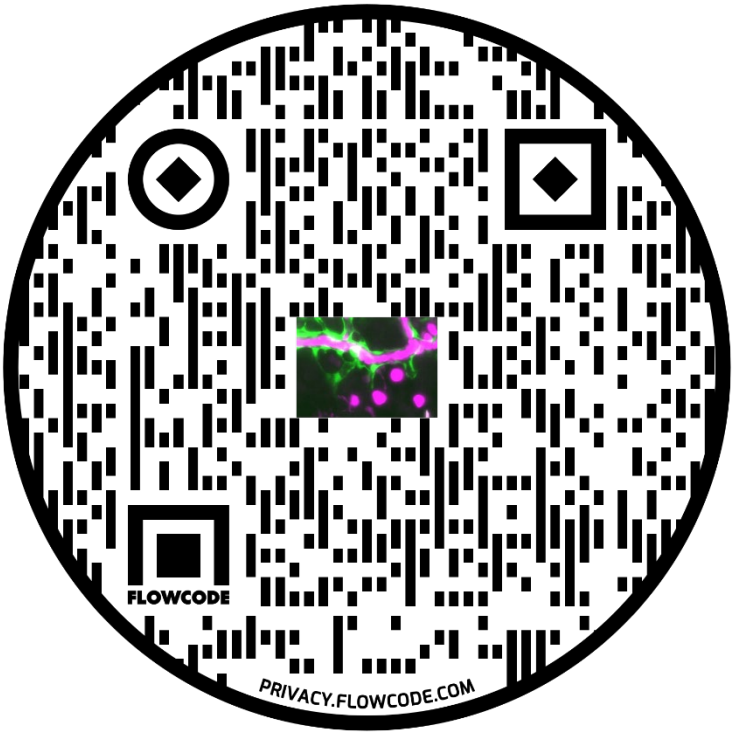

https://drive.google.com/file/d/1aPOR2B1vDP-NNt_7DJZySjAUnACnW8CW/view?usp=sharing

Movie 2 SIVP sprouts are free of flow during development

This movie corresponds to still images in Figure 3.1, zoomed in the sprouts. Time-lapse movie of *Tg(fli1a:egfp)*^{y1};*(gata1a:DsRED)*^{sD2} labelling endothelial cells in GFP and red blood cells in RFP. Images were taken at approximate 19 hours 5-minute intervals, starting at 53hpf. Z-series were flattened to 2D maximum intensity projections and presented in time series, 20 frames per second (fps). Arrowheads mark leading sprouts that are free of blood flow in the SIVP.

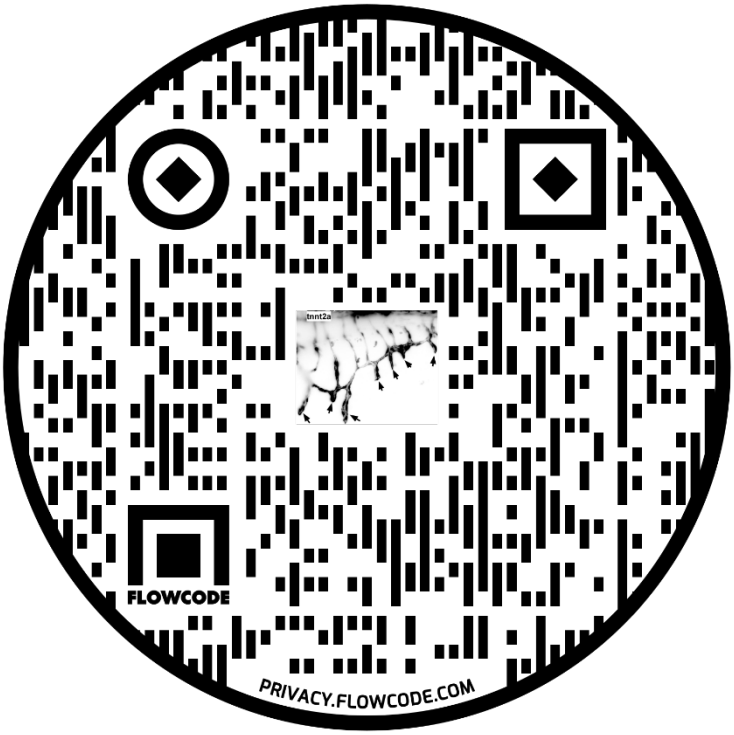

https://drive.google.com/file/d/1aXsNj5VXLBnthFYlCJs3nqUAih6ArkP1/view?

usp=sharing

Movie 3 Blood flow regulates leading sprout remodelling via regression

This movie corresponds to still images in Figure 3.4.
Time-lapse movie of *Tg(fli1a:egfp)*^{y1} *control* and *tnnt2a* morphants. Images were taken at approximate 14 hours 5-minute intervals and were down sampled to 30-minute interval in the movie, starting at 56hpf. Z-series were flattened to 2D maximum intensity projections and presented in time series, 3 frames per second (fps). Arrows mark leading sprouts undergoing regression in the presence of flow or failing to regress in the absence of flow.

https://drive.google.com/file/d/188kd7j1rtBmdH1hghG_xCHWhaYkCYsNO/view?usp=sharing

Movie 4 Cell migration trajectories in *control* morphants

This movie is supplementary to Figure 3.5, Figure 3.6, Figure 3.7.
Time-lapse movie of *Tg(fli1a:nls-mCherry)*^{SH370} overlaid with cell migration trajectories in *control* morphants. Images were taken at approximate 14 hours 30-minute interval, starting at 56hpf. Z-series were flattened to 2D maximum intensity projections and presented in time series, 5 frames per second (fps). Images were processed using TrackMate Plugin in Fiji (ImageJ). Orange, branch cells; blue, SIV cells; magenta, tip cells.

https://drive.google.com/file/d/145WeQX7fSpgDnv5Y3fY7m_9ehK_nX3Ck/view?usp=sharing

Movie 5 Cell migration trajectories in *tnnt2a* morphants

This movie is supplementary to Figure 3.5, Figure 3.6, Figure 3.7.
Time-lapse movie of *Tg(fli1a:nls-mCherry)*^{SH370} overlaid with cell migration trajectories in *tnnt2a* morphants. Images were taken at approximate 14 hours 30-minute interval, starting at 56hpf. Z-series were flattened to 2D maximum intensity projections and presented in time series, 5 frames per second (fps). Images were processed using TrackMate Plugin in Fiji (ImageJ). Orange, branch cells; blue, SIV cells; magenta, tip cells.

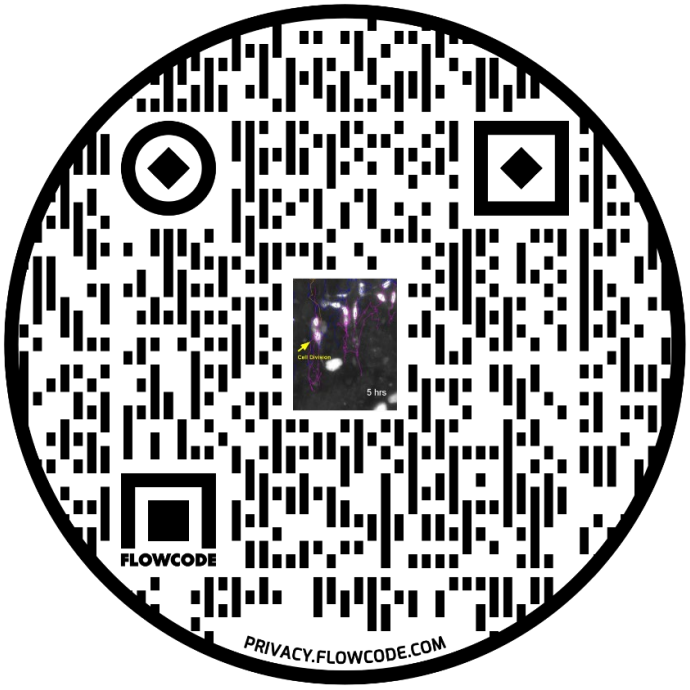

https://drive.google.com/file/d/1v7J25kF4LgV9R0K4kpEz-l1503Rj8T7u/view?usp=sharing

Movie 6 Daughter cells from the tip cells rapidly migrate towards SIV after cell division

This movie is supplementary to Figure 3.5A.
Time-lapse movie of *Tg(fli1a:nls-mCherry)*^{SH370} overlaid with cell migration trajectories. Tracking of proliferating tip cells shows that the one of the daughter cells of the tip cell migrate rapidly towards SIV after cell division, leaving only one pair of ECs within the sprout. Images were taken at approximate 14 hours 30-minute interval, starting at 56hpf. Z-series were flattened to 2D maximum intensity projections and presented in time series, 5 frames per second (fps). Images were processed using TrackMate Plugin in Fiji (ImageJ). Orange, branch cells; blue, SIV cells; magenta, tip cells.

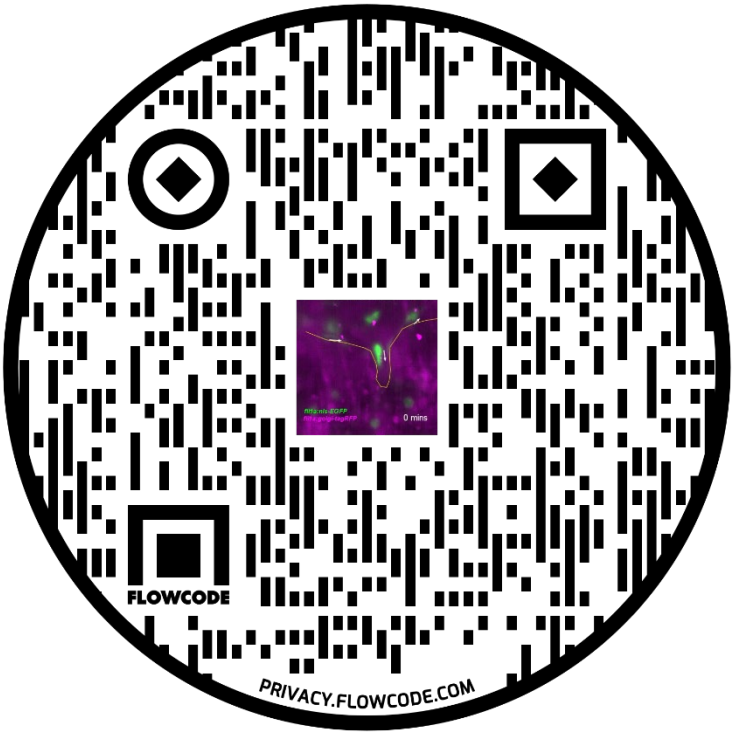

https://drive.google.com/file/d/1vb2OoW_XSZYZf3fWUzIEGlhuxfQvcAQm/view?usp=sharing

Movie 7 ECs polarise against blood flow during sprout regression

This movie corresponds to still images in Figure 3.8A-F.
Time-lapse movie of *Tg(fli1a:golgi-tagRFP);(cry:CFP)*^{SH529};*(fli1a:nls-GFP)*^{SH549} *control* morphants. Images were taken at approximate 20 hours 5-minute interval, starting at 56hpf. Z-series were flattened to 2D maximum intensity projections and presented in time series, 2 frames per second (fps). White arrows mark cell polarity indicated by the position of nucleus and Golgi apparatus. Yellow arrowheads mark the switch of cell polarity during sprout regression in the presence of flow.

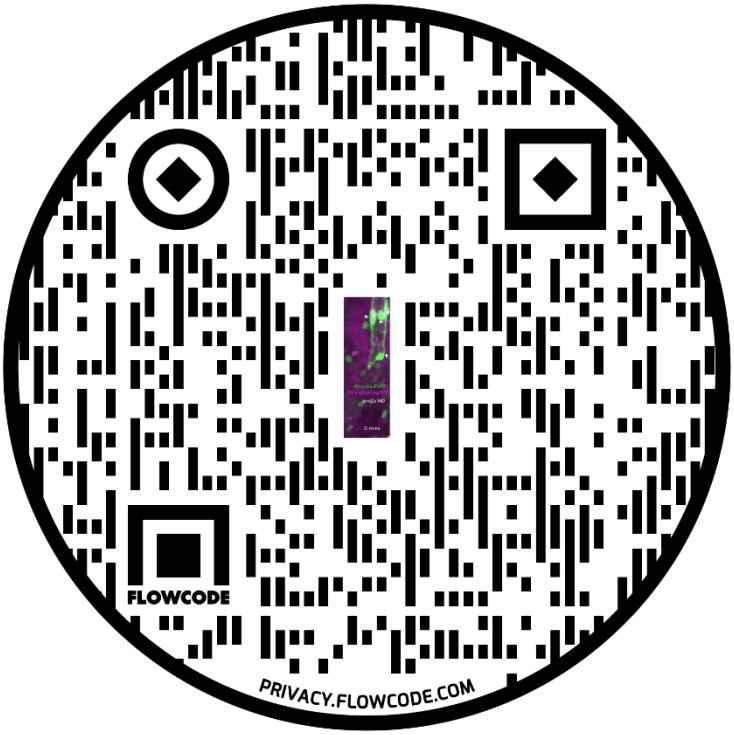

https://drive.google.com/file/d/182RAiiuODd8pNfKTnSYSIo6Q-PyIt-

ib/view?usp=sharing

Movie 8 Tip cells display disrupted polarisation in the absence of flow

This movie corresponds to still images in Figure 3.8a-f.
Time-lapse movie of *Tg(fli1a:golgi-tagRFP);(cry:CFP)*^{SH529};*(fli1a:nls-GFP)*^{SH549} *tnnt2a* morphants. Images were taken at approximate 16 hours 5-minute interval, starting at 56hpf. Z-series were flattened to 2D maximum intensity projections and presented in time series, 2 frames per second (fps). White arrows mark cell polarity indicated by the position of nucleus and Golgi apparatus.

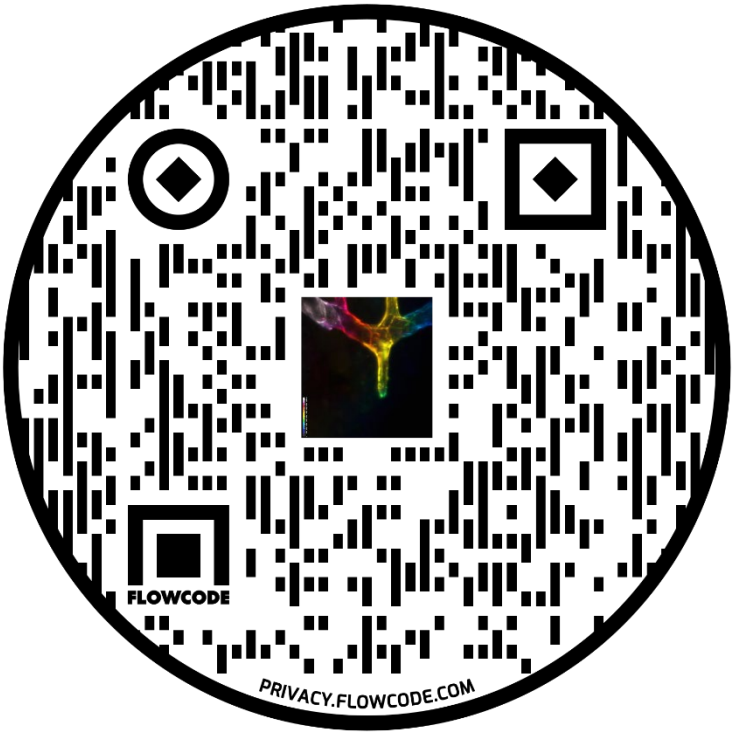

https://drive.google.com/file/d/1r96QKomhO8awFNSfWAxRZNJx1uPcFvEI/view?usp=sharing

Movie 9 Cell co-ordination during sprout regression

This movie corresponds to still images in Figure 3.10.
Time-lapse movie of *Tg(fli1a:egfp)*^{y1}*;(fli1a:AC-tagRFP)*^{SH511}. Images were taken at approximate 31 hours 5-minute interval, starting at 56hpf. Left: z-series were flattened to 2D maximum intensity projections and presented in time series, 2 frames per second (fps). Right: z-series were coloured coded in distance (white towards reader) and presented in time series at 2 fps.

Acknowledgement

I would like to begin by thanking Dr Robert Wilkinson for his outstanding mentorship throughout my PhD. He has not only been a great supervisor, but also a great mentor and friend. I thank him for always having an open door and putting up with all the silly questions, for patient bench supervision and saving me by lending all kinds of reagents (from his chaotic bench, magic!), for meticulous proof-reading for my reviews, posters, presentations and of course this thesis which without his guidance would not have been possible (and I believe he will cross/add some ‘THE’s when he reads this acknowledgement). I also thank his efforts for always trying to bring us together as a team, by pub crawling, hiking in the peak district, or just having fun playing guitar or decorating Christmas trees in the lab. I’m grateful for his encouragement and telling me to have faith in myself, and also harsh words sometimes to bring me back to the ground. May he be rewarded for the depth of his knowledge and the quality of his efforts.

I also thank Prof Paul Evans, for taking up the mess when things fell down, for letting me follow my instincts but also reminding me of the importance of practical hypothesis and measures. I also thank him for the daily online meetings during lockdowns due to Covid, to keep my sanity and normal daily routines.

I would like to thank my lab-mates/bubble-tea-gang members/drinking buddies, Dr Zhen Jiang and Dr Aaron Savage. For the fun we had, the stress

we shared, the critical discussions we had during lab meetings and the cheerful drinks we toasted in the pubs, the songs we sang in the Karaoke and the games we played on the trains, I wish nothing but all the best for your future.

I have the honour of working in a friendly and cooperative environment with many talented and fun people. I thank all PIs and members of the Chico, van Eeden and Noël groups and everyone else from the lovely C06 big family. A special thanks to Karishma (MATLAB coding, light-sheet talks and late night Katsus), Davide (best buddy, excellent cook, ~~coffee~~ espresso lover), Elizabeth (Fiji expert, outreaches, gothic queen), Rosemary (heart warmer, double sweet with Theo), Eleanor (the most supportive and go-to person in the lab), Karen (sassy mouth and soft heart), Philippa (a Disney princess), Chris (a symbol of 'British sarcasm' (in my eyes), great eyes for presentations), Rings, Matt, Julia, Ruth and Emma (laughs and deep conversations), Hannah (biker, 'I love COX2'), Deepak (shy but actually chatty), Ryan (knows everything with his headphones on) and Stone (the most curious person). Thank you for all the help, love, and happiness both in the lab and office over the past several years.

From my heart I thank my family, for always worrying me from million miles away but still support my decision of studying abroad. I also give my deepest thanks to Dr Yichen He, my partner in crime and friend for life, who puts up with all my hysterias and be the first person to cheer my success. Your support has been the only reason I have been able to complete this journey. This accomplishment is ours, not just mine. I have been very lucky to have you to

pursue both Master and PhD degree together in the same university. Thank you for always be there for the past seven years.

References

Adams, R.H., Alitalo, K., 2007. Molecular regulation of angiogenesis and lymphangiogenesis. Nat. Rev. Mol. Cell Biol. 8, 464–478.

Akimoto, S., Mitsumata, M., Sasaguri, T., Yoshida, Y., 2000. Laminar Shear Stress Inhibits Vascular Endothelial Cell Proliferation by Inducing Cyclin-Dependent Kinase Inhibitor p21. Circ. Res. 86, 185–190.

Ando, J., Yamamoto, K., 2013. Flow detection and calcium signalling in vascular endothelial cells. Cardiovasc. Res. 99, 260–268.

Ando, K., Fukuhara, S., Izumi, N., Nakajima, H., Fukui, H., Kelsh, R.N., Mochizuki, N., 2016. Clarification of mural cell coverage of vascular endothelial cells by live imaging of zebrafish. Development 143, 1328–1339.

Andres, A.C., Djonov, V., 2010. The mammary gland vasculature revisited. J. Mammary Gland Biol. Neoplasia 15, 319–328.

Arima, S., Nishiyama, K., Ko, T., Arima, Y., Hakozaki, Y., Sugihara, K., Koseki, H., Uchijima, Y., Kurihara, Y., Kurihara, H., 2011. Angiogenic morphogenesis driven by dynamic and heterogeneous collective endothelial cell movement. Development 138, 4763–4776.

Aspalter, I.M., Gordon, E., Dubrac, A., Ragab, A., Narloch, J., Vizán, P., Geudens, I., Collins, R.T., Franco, C.A., Abrahams, C.L., Thurston, G., Fruttiger, M., Rosewell, I., Eichmann, A., Gerhardt, H., 2015. Alk1 and Alk5 inhibition by Nrp1 controls vascular sprouting downstream of Notch. Nat. Commun. 6, 1–13.

Aydogan, V., Lenard, A., Denes, A.S., Sauteur, L., Belting, H., Affolter, M., 2015. Endothelial cell division in angiogenic sprouts of differing cellular architecture. Biol. Open 4, 1259–1269.

Baeyens, N., Bandyopadhyay, C., Coon, B.G., Yun, S., Schwartz, M.A., 2016a. Endothelial fluid shear stress sensing in vascular health and disease. J. Clin. Invest. 126, 821–828.

Baeyens, N., Larrivée, B., Ola, R., Hayward-piatkowskyi, B., Dubrac, A., 2016b. Defective fluid shear stress mechanotransduction mediates hereditary hemorrhagic telangiectasia (HHT). J. Cell Biol. 214, 807–816.

Baeyens, N., Nicoli, S., Coon, B.G., Ross, T.D., Van Den Dries, K., Han, J., Lauridsen, H.M., Mejean, C.O., Eichmann, A., Thomas, J.L., Humphrey, J.D., Schwartz, M.A., 2015. Vascular remodeling is governed by a vegfr3-dependent fluid shear stress set point. Elife 2015, 1–35.

Bahary, N., Goishi, K., Stuckenholz, C., Weber, G., LeBlanc, J., Schafer, C.A., Berman, S.S., Klagsbrun, M., Zon, L.I., 2007. Duplicate VegfA genes and orthologues of the KDR receptor tyrosine kinase family mediate vascular development in the zebrafish. Blood 110, 3627–3636.

Bentley, K., Franco, C.A., Philippides, A., Blanco, R., Dierkes, M., Gebala, V., Stanchi, F., Jones, M., Aspalter, I.M., Cagna, G., Weström, S.,

Claesson-Welsh, L., Vestweber, D., Gerhardt, H., 2014. The role of differential VE-cadherin dynamics in cell rearrangement during angiogenesis. Nat. Cell Biol. 16.

Berger, J., Currie, P.D., 2013. 503Unc, a Small and Muscle-Specific Zebrafish Promoter. Genesis 51, 443–447.

Betz, C., Lenard, A., Belting, H.-G., Affolter, M., 2016. Cell behaviors and dynamics during angiogenesis. Development 143, 2249–2260.

Blum, Y., Belting, H.G., Ellertsdottir, E., Herwig, L., Lüders, F., Affolter, M., 2008. Complex cell rearrangements during intersegmental vessel sprouting and vessel fusion in the zebrafish embryo. Dev. Biol. 316, 312–322.

Braun, A., Dang, K., Buslig, F., Baird, M.A., Davidson, M.W., Waterman, C.M., Myers, K.A., 2014. Rac1 and Aurora A regulate MCAK to polarize microtubule growth in migrating endothelial cells. J. Cell Biol. 206, 97–112.

Brown, M.A., Zhao, Q., Baker, K.A., Naik, C., Chen, C., Pukac, L., Singh, M., Tsareva, T., Parice, Y., Mahoney, A., Roschke, V., Sanya, I., Choe, S., 2005. Crystal structure of BMP-9 and functional interactions with pro-region and receptors. J. Biol. Chem. 280, 25111–25118.

Bryant, D.M., Datta, A., Rodríguez-Fraticelli, A.E., PeräCurrency Signnen, J., Martín-Belmonte, F., Mostov, K.E., 2010. A molecular network for de novo generation of the apical surface and lumen. Nat. Cell Biol. 12, 1035–1045.

Burrell, K., Agnihotri, S., Leung, M., Dacosta, R., Hill, R., Zadeh, G., 2013. A novel high-resolution in vivo imaging technique to study the dynamic response of intracranial structures to tumor growth and therapeutics. J. Vis. Exp. 1–12.

Bussmann, J., Bos, F.L., Urasaki, A., Kawakami, K., Duckers, H.J., Schulte-Merker, S., 2010. Arteries provide essential guidance cues for lymphatic endothelial cells in the zebrafish trunk. Development 137, 2653–2657.

Bussmann, J., Lawson, N., Zon, L., Schulte-Merker, S., Committee Zebrafish Nomenclature, 2008. Zebrafish VEGF receptors: A guideline to nomenclature. PLoS Genet. 4, 4–5.

Bussmann, J., Wolfe, S.A., Siekmann, A.F., 2011. Arterial-venous network formation during brain vascularization involves hemodynamic regulation of chemokine signaling. Development 138, 1717–1726.

Cao, J., Ehling, M., März, S., Seebach, J., Tarbashevich, K., Sixta, T., Pitulescu, M.E., Werner, A.C., Flach, B., Montanez, E., Raz, E., Adams, R.H., Schnittler, H., 2017. Polarized actin and VE-cadherin dynamics regulate junctional remodelling and cell migration during sprouting angiogenesis. Nat. Commun. 8, 1–20.

Carvalho, J.R., Fortunato, I.C., Fonseca, C.G., Pezzarossa, A., Barbacena, P., Dominguez-Cejudo, M.A., Vasconcelos, F.F., Santos, N.C.,

Carvalho, F.A., Franco, C.A., 2019. Non-canonical Wnt signaling regulates junctional mechanocoupling during angiogenic collective cell migration. Elife 8, 1–35.

Chan, Y.K., Kwok, H.H., Chan, L.S., Leung, K.S.Y., Shi, J., Mak, N.K., Wong, R.N.S., Yue, P.Y.K., 2012. An indirubin derivative, E804, exhibits potent angiosuppressive activity. Biochem. Pharmacol. 83, 598–607.

Chang, A.H., Raftrey, B.C., Amato, G.D., Surya, V.N., Poduri, A., Chen, H.I., Goldstone, A.B., Woo, J., Fuller, G.G., Dunn, A.R., Red-horse, K., 2017. DACH1 stimulates shear stress-guided endothelial cell migration and coronary artery growth through the CXCL12 – CXCR4 signaling axis. Genes Dev. 31, 1308–1324.

Chappell, J.C., Taylor, S.M., Ferrara, N., Bautch, V.L., 2009. Local Guidance of Emerging Vessel Sprouts Requires Soluble Flt-1. Dev. Cell 17, 377–386.

Chatzizisis, Y.S., Coskun, A.U., Jonas, M., Edelman, E.R., Feldman, C.L., Stone, P.H., 2007. Role of Endothelial Shear Stress in the Natural History of Coronary Atherosclerosis and Vascular Remodeling. Molecular, Cellular, and Vascular Behavior. J. Am. Coll. Cardiol. 49, 2379–2393.

Chen, H., Shi, S., Acosta, L., Li, W., Lu, J., Bao, S., Chen, Z., Yang, Z., Schneider, Mi.D., Chien, K.R., Conway, S.J., Yoder, M.C., Haneline, L.S., Franco, D., Shou, W., 2004. BMP-10 is essential for maintaining cardiac growth during murine cardiogenesis. Development 131, 2219–2231.

Chen, Hao, Ridgway, J.B., Sai, T., Lai, J., Warming, S., Chen, Hanying, Roose-Girma, M., Zhang, G., Shou, W., Yan, M., 2013. Context-dependent signaling defines roles of BMP9 and BMP10 in embryonic and postnatal development. Proc. Natl. Acad. Sci. U. S. A. 110, 11887–11892.

Chen, L.-J., Wang, W.-L., Chiu, J.-J., 2016. Vascular Endothelial Mechanosensors in Response to Fluid Shear Stress, in: Chien, S., Engler, A.J., Wang, Y.P. (Eds.), Molecular and Cellular Mechanobiology. Springer, pp. 29–57.

Chen, Q., Jiang, L., Li, C., Hu, D., Bu, J. wen, Cai, D., Du, J. lin, 2012. Haemodynamics-Driven Developmental Pruning of Brain Vasculature in Zebrafish. PLoS Biol. 10.

Chen, X., Gays, D., Milia, C., Santoro, M.M., 2017. Cilia Control Vascular Mural Cell Recruitment in Vertebrates. Cell Rep. 18, 1033–1047.

Chimote, G., Sreenivasan, J., Pawar, N., Subramanian, J., Sharma, S., Sivaramakrishnan, H., 2014. Comparison of effects of anti-angiogenic agents in the zebrafish efficacy–toxicity model for translational anti-angiogenic drug discovery. Drug Des. Devel. Ther. 8, 1107.

Cole, N.B., Smith, C.L., Sciaky, N., Terasaki, M., Edidin, M., Lippincott-Schwartz, J., 1996. Diffusional mobility of Golgi proteins in membranes of living cells. Science (80-.). 273, 797–801.

Conway, D.E., Breckenridge, M.T., Hinde, E., Gratton, E., Chen, C.S.,

Schwartz, M.A., 2013. Fluid shear stress on endothelial cells modulates mechanical tension across VE-cadherin and PECAM-1. Curr. Biol. 23, 1024–1030.

Coon, B.G., Baeyens, N., Han, J., Budatha, M., Ross, T.D., Fang, J.S., Yun, S., Thomas, J.L., Schwartz, M.A., 2015. Intramembrane binding of VE-cadherin to VEGFR2 and VEGFR3 assembles the endothelial mechanosensory complex. J. Cell Biol. 208.

Corti, P., Young, S., Chen, C.-Y., Patrick, M.J., Rochon, E.R., Pekkan, K., Roman, B.L., 2011. Interaction between alk1 and blood flow in the development of arteriovenous malformations. Development 138, 1573–1582.

Costa, G., Harrington, K.I., Lovegrove, H.E., Page, D.J., Chakravartula, S., Bentley, K., Herbert, S.P., 2016. Asymmetric division coordinates collective cell migration in angiogenesis. Nat. Cell Biol. 18, 1292–1301.

Covassin, L., Amigo, J., Suzuki, K., Teplyuk, V., Straubhaar, J., Lawson, N., 2006a. Global analysis of hematopoietic and vascular endothelial gene expression by tissue specific microarray profiling in zebrafish. Dev. Biol. 299, 551–562.

Covassin, L., Siekmann, A.F., Kacergis, M.C., Laver, E., Moore, J.C., Villefranc, J.A., Weinstein, B.M., Lawson, N.D., 2009. A genetic screen for vascular mutants in zebrafish reveals dynamic roles for Vegf/Plcg1 signaling during artery development. Dev. Biol. 329, 212–226.

Covassin, L., Villefranc, J., Kacergis, M., Weinstein, B., Lawson, N., 2006b. Distinct genetic interactions between multiple Vegf receptors are required for development of different blood vessel types in zebrafish. Proc. Natl. Acad. Sci. U. S. A. 103, 6554–6559.

David, L., Mallet, C., Keramidas, M., Lamandé, N., Gasc, J.M., Dupuis-Girod, S., Plauchu, H., Feige, J.J., Bailly, S., 2008. Bone morphogenetic protein-9 is a circulating vascular quiescence factor. Circ. Res. 102, 914–922.

De Jesus Perez, V.A., Alastalo, T.P., Wu, J.C., Axelrod, J.D., Cooke, J.P., Amieva, M., Rabinovitch, M., 2009. Bone morphogenetic protein 2 induces pulmonary angiogenesis via Wnt -β-catenin and Wnt - RhoA - Rac1 pathways. J. Cell Biol. 184, 83–99.

de Vinuesa, A.G., Abdelilah-Seyfried, S., Knaus, P., Zwijsen, A., Bailly, S., 2016. BMP signaling in vascular biology and dysfunction. Cytokine Growth Factor Rev. 27, 65–79.

Dick, A., Hild, M., Bauer, H., Imai, Y., Maifeld, H., Schier, A.F., Talbot, W.S., Bouwmeester, T., Hammerschmidt, M., 2000. Essential role of Bmp7 (snailhouse) and its prodomain in dorsoventral patterning of the zebrafish embryo. Development 127, 343–354.

Dimmeler, S., Assmus, B., Hermann, C., Haendeler, J., Zeiher, A.M., 1998. Fluid Shear Stress Stimulates Phosphorylation of Akt in Human

Endothelial Cells: Involvement in Suppression of Apoptosis. Circ. Res. 83, 334–341.

Drake, C.J., 2003. Embryonic and adult vasculogenesis. Birth Defects Res. Part C - Embryo Today Rev. 69, 73–82.

Dubrac, A., Genet, G., Ola, R., Zhang, F., Pibouin-Fragner, L., Han, J., Zhang, J., Thomas, J.L., Chedotal, A., Schwartz, M.A., Eichmann, A., 2016. Targeting NCK-Mediated Endothelial Cell Front-Rear Polarity Inhibits Neovascularization. Circulation 133, 409–421.

Dyer, L.A., Pi, X., Patterson, C., 2014. The role of BMPs in endothelial cell function and dysfunction. Trends Endocrinol. Metab. 25, 472–480.

Eichmann, A., Corbel, C., Jaffredo, T., Bréant, C., Joukov, V., Kumar, V., Alitalo, K., Le Douarin, N.M., 1998. Avian VEGF-C: Cloning, embryonic expression pattern and stimulation of the differentiation of VEGFR2-expressing endothelial cell precursors. Development 125, 743–752.

Ellertsdóttir, E., Lenard, A., Blum, Y., Krudewig, A., Herwig, L., Affolter, M., Belting, H.G., 2010. Vascular morphogenesis in the zebrafish embryo. Dev. Biol. 341, 56–65.

Elworthy, S., Lister, J.A., Carney, T.J., Raible, D.W., Kelsh, R.N., 2003. Transcriptional regulation of mitfa accounts for the sox10 requirement in zebrafish melanophore development. Development 130, 2809–2818.

Fantin, A., Vieira, J.M., Gestri, G., Denti, L., Schwarz, Q., Prykhozhij, S., Peri, F., Wilson, S.W., Ruhrberg, C., 2010. Tissue macrophages act as cellular chaperones for vascular anastomosis downstream of VEGF-mediated endothelial tip cell induction. Blood 116, 829–840.

Farooqui, R., Fenteany, G., 2005. Multiple rows of cells behind an epithelial wound edge extend cryptic lamellipodia to collectively drive cell sheet movement. J. Cell Sci. 118, 51–63.

Ferrara, N., Davis-Smyth, T., 1997. The Biology of Vascular Endothelial Growth Factor. Endorine Rev. 18, 4–25.

Finkenzeller, G., Hager, S., Stark, G.B., 2012. Effects of bone morphogenetic protein 2 on human umbilical vein endothelial cells. Microvasc. Res. 84, 81–85.

Flamme, I., Breier, G., 2002. The Role of Vascular Endothelial Growth Factors and Their Receptors During Embryonic Vascular Development, in: R.J., T. (Ed.), Assembly of the Vasculature and Its Regulation. Cardiovascular Molecular Morphogenesis. Birkhäuser, Boston, MA, p. 22.

Franco, C.A., Gerhardt, H., 2016. Blood flow boosts BMP signaling to keep vessels in shape. J. Biol. 214, 793–795.

Franco, C.A., Jones, M.L., Bernabeu, M.O., Geudens, I., Mathivet, T., Rosa, A., Lopes, F.M., Lima, A.P., Ragab, A., Collins, R.T., Phng, L.K., Coveney, P. V., Gerhardt, H., 2015. Dynamic Endothelial Cell Rearrangements Drive Developmental Vessel Regression. PLoS Biol. 13, 1–19.

Franco, C.A., Jones, M.L., Bernabeu, M.O., Vion, A.C., Barbacena, P.,

Fan, J., Mathivet, T., Fonseca, C.G., Ragab, A., Yamaguchi, T.P., Coveney, P. V., Lang, R.A., Gerhardt, H., 2016. Non-canonical wnt signalling modulates the endothelial shear stress flow sensor in vascular remodelling. Elife 5, 1–22.

Fujita, M., Cha, Y.R., Pham, V.N., Sakurai, A., Roman, B.L., Gutkind, J.S., Weinstein, B.M., 2011. Assembly and patterning of the vascular network of the vertebrate hindbrain. Development 138, 1705–1715.

Fukuhara, S., Zhang, J., Yuge, S., Ando, K., Wakayama, Y., Sakaue-Sawano, A., Miyawaki, A., Mochizuki, N., 2014. Visualizing the cell-cycle progression of endothelial cells in zebrafish. Dev. Biol. 393, 10–23.

Funahashi, Y., Shawber, C.J., Vorontchikhina, M., Sharma, A., Outtz, H.H., Kitajewski, J., 2010. Notch regulates the angiogenic response via induction of VEGFR-1. J. Angiogenes. Res. 2, 22–24.

Gaengel, K., Genové, G., Armulik, A., Betsholtz, C., 2009. Endothelial-mural cell signaling in vascular development and angiogenesis. Arterioscler. Thromb. Vasc. Biol. 29, 630–638.

Gaengel, K., Niaudet, C., Hagikura, K., Siemsen, B.L., Muhl, L., Hofmann, J.J., Ebarasi, L., Nyström, S., Rymo, S., Chen, L.L., Pang, M.F., Jin, Y., Raschperger, E., Roswall, P., Schulte, D., Benedito, R., Larsson, J., Hellström, M., Fuxe, J., Uhlén, P., Adams, R., Jakobsson, L., Majumdar, A., Vestweber, D., Uv, A., Betsholtz, C., 2012. The Sphingosine-1-Phosphate Receptor S1PR1 Restricts Sprouting Angiogenesis by Regulating the Interplay between VE-Cadherin and VEGFR2. Dev. Cell 23, 587–599.

Galloway, J.L., Wingert, R. a., Thisse, C., Thisse, B., Zon, L.I., 2005. Loss of Gata1 but not Gata2 converts erythropoiesis to myelopoiesis in zebrafish embryos. Dev. Cell 8, 109–116.

Garcia, M.D., Larina, I. V., 2014. Vascular development and hemodynamic force in the mouse yolk sac. Front. Physiol. 5 AUG, 1–10.

Gebala, V., Collins, R., Geudens, I., Phng, L.-K., Gerhardt, H., 2016. Blood flow drives lumen formation by inverse membrane blebbing during angiogenesis in vivo. Nat. Cell Biol. 18, 443–450.

Gerhardt, H., Golding, M., Fruttiger, M., Ruhrberg, C., Lundkvist, A., Abramsson, A., Jeltsch, M., Mitchell, C., Alitalo, K., Shima, D., Betsholtz, C., 2003. VEGF guides angiogenic sprouting utilizing endothelial tip cell filopodia. J. Cell Biol. 161, 1163–1177.

Gering, M., Patient, R., 2005. Hedgehog signaling is required for adult blood stem cell formation in zebrafish embryos. Dev. Cell 8, 389–400.

Geudens, I., Coxam, B., Alt, S., Gebala, V., Vion, A.C., Meier, K., Rosa, A., Gerhardt, H., 2019. Artery-vein specification in the zebrafish trunk is pre-patterned by heterogeneous Notch activity and balanced by flow-mediated fine-tuning. Dev. 146, 1–13.

Ghaffari, S., Leask, R.L., Jones, E.A. V, 2015. Flow dynamics control the location of sprouting and direct elongation during developmental

angiogenesis. Development 142, 4151 LP – 4157.

Goetz, J.G., Steed, E., Ferreira, R.R., Roth, S., Ramspacher, C., Boselli, F., Charvin, G., Liebling, M., Wyart, C., Schwab, Y., Vermot, J., 2014. Endothelial cilia mediate low flow sensing during zebrafish vascular development. Cell Rep. 6, 799–808.

Goi, M., Childs, S.J., 2016. Patterning mechanisms of the sub-intestinal venous plexus in zebrafish. Dev. Biol. 409, 114–128.

Goley, E.D., Welch, M.D., 2006. The ARP2/3 complex: an actin nucleator comes of age. Nat. Rev. Mol. Cell Biol. 7, 713–726.

Gore, A. V., Swift, M.R., Cha, Y.R., Lo, B., McKinney, M.C., Li, W., Castranova, D., Davis, A., Yoh-suke, M., Weinstein, B.M., 2011. Rspo1/wnt signaling promotes angiogenesis via vegfc/vegfr3. Development 138, 4875–4886.

Habeck, H., Odenthal, J., Walderich, B., Maischein, H.M., Bebber van, F., Busch-Nentwich, E., Dahm, R., Frohnh??fer, H.G., Geiger, H., Gilmour, D., Holley, S., Hooge, J., J??lich, D., Knaut, H., Maderspacher, F., Neumann, C., Nicolson, T., N??sslein-Volhard, C., Roehl, H., Sch??nberger, U., Seiler, C., S??llner, C., Sonawane, M., Wehner, A., Weiler, C., Hagner, U., Hennen, U., Kaps, C., Kirchner, A., Koblizek, T.I., Langheinrich, U., Metzger, C., Nordin, R., Pezzuti, M., Schlombs, K., deSantana-Stamm, J., Trowe, T., Vacun, G., Walker, A., Weiler, C., Schulte-Merker, S., 2002. Analysis of a zebrafish VEGF receptor mutant reveals specific disruption of angiogenesis. Curr. Biol. 12, 1405–1412.

Haeger, A., Wolf, K., Zegers, M.M., Friedl, P., 2015. Collective cell migration: Guidance principles and hierarchies. Trends Cell Biol. 25, 556–566.

Hamilton, N., Rutherford, H.A., Petts, J.J., Isles, H.M., Weber, T., Henneke, M., Gärtner, J., Dunning, M.J., Renshaw, S.A., 2020. The failure of microglia to digest developmental apoptotic cells contributes to the pathology of RNASET2-deficient leukoencephalopathy. Glia 68, 1531–1545.

Hansson, G.K., Schwartz, S.M., 1983. Evidence for cell death in the vascular endothelium in vivo and in vitro. Am. J. Pathol. 112, 278–286.

Hao, J., Ho, J.N., Lewis, J.A., Karim, K.A., Daniels, R.N., Gentry, P.R., Hopkins, C.R., Lindsley, C.W., Hong, C.C., 2010. In Vivo Structure Activity Relationship Study of Dorsomorphin Analogs Identifies Selective VEGF and BMP Inhibitors. ACS Chem Biol 5, 245–253.

Hartenstein, V., 2006. Blood cells and blood cell development in the animal kingdom. Annu. Rev. Cell Dev. Biol. 22, 677–712.

Hasan, S.S., Tsaryk, R., Lange, M., Wisniewski, L., Moore, J.C., Lawson, N.D., Wojciechowska, K., Schnittler, H., Siekmann, A.F., 2017. Endothelial Notch signalling limits angiogenesis via control of artery formation. Nat. Cell Biol. 19, 928–940.

Hayer, A., Shao, L., Chung, M., Joubert, L.M., Yang, H.W., Tsai, F.C.,

Bisaria, A., Betzig, E., Meyer, T., 2016. Engulfed cadherin fingers are polarized junctional structures between collectively migrating endothelial cells. Nat. Cell Biol. 18, 1311–1323.

Hazel, A.L., Pedley, T.J., 2000. Vascular Endothelial Cells Minimize the Total Force on Their Nuclei. Biophys. J. 78, 47–54.

Helker, C.S.M., Schuermann, A., Karpanen, T., Zeuschner, D., Belting, H.-G., Affolter, M., Schulte-Merker, S., Herzog, W., 2013. The zebrafish common cardinal veins develop by a novel mechanism: lumen ensheathment. Development 140, 2776–86.

Helker, C.S.M., Schuermann, A., Pollmann, C., Chng, S.C., Kiefer, F., Reversade, B., Herzog, W., 2015. The hormonal peptide Elabela guides angiob lasts to the midline during vasculogenesis. Elife 4, 1–13.

Hellström, M., Phng, L.K., Hofmann, J.J., Wallgard, E., Coultas, L., Lindblom, P., Alva, J., Nilsson, A.K., Karlsson, L., Gaiano, N., Yoon, K., Rossant, J., Iruela-Arispe, M.L., Kalén, M., Gerhardt, H., Betsholtz, C., 2007. Dll4 signalling through Notch1 regulates formation of tip cells during angiogenesis. Nature 445, 776–780.

Hen, G., Nicenboim, J., Mayseless, O., Asaf, L., Shin, M., Busolin, G., Hofi, R., Almog, G., Tiso, N., Lawson, N.D., Yaniv, K., 2015. Venous-derived angioblasts generate organ-specific vessels during embryonic development. Development 142, 4266–78.

Herbert, S.P., Huisken, J., Kim, T.N., Feldman, M.E., Houseman, B.T., Wang, R.A., Shokat, K.M., Stainier, D.Y.R., 2009. Selective Cell Sprouting : An Alternative Mode of Blood Vessel Formation. Science (80-.). 326, 294–298.

Herbert, S.P., Stainier, D.Y.R., 2011. Molecular control of endothelial cell behaviour during blood vessel morphogenesis. Nat. Rev. Mol. Cell Biol. 12, 551–64.

Herwig, L., Blum, Y., Krudewig, A., Ellertsdottir, E., Lenard, A., Belting, H.G., Affolter, M., 2011. Distinct cellular mechanisms of blood vessel fusion in the zebrafish embryo. Curr. Biol. 21, 1942–1948.

Hiepen, C., Benn, A., Denkis, A., Lukonin, I., Weise, C., Boergermann, J.H., Knaus, P., 2014. BMP2-induced chemotaxis requires PI3K p55γ/p110α-dependent phosphatidylinositol (3,4,5)-triphosphate production and LL5 recruitment at the cytocortex. BMC Biol. 12, 1–17.

Hikita, T., Mirzapourshafiyi, F., Barbacena, P., Riddell, M., Pasha, A., Li, M., Kawamura, T., Brandes, R.P., Hirose, T., Ohno, S., Gerhardt, H., Matsuda, M., Franco, C.A., Nakayama, M., 2018. PAR-3 controls endothelial planar polarity and vascular inflammation under laminar flow. EMBO Rep. 19, 1–19.

Hogan, B., Bos, F.L., Bussmann, J., Witte, M., Chi, N.C., Duckers, H.J., Schulte-Merker, S., 2009a. Ccbe1 is required for embryonic lymphangiogenesis and venous sprouting. Nat. Genet. 41, 396–398.

Hogan, B., Herpers, R., Witte, M., Heloterä, H., Alitalo, K., Duckers,

H.J., Schulte-Merker, S., 2009b. Vegfc/Flt4 signalling is suppressed by Dll4 in developing zebrafish intersegmental arteries. Development 136, 4001–4009.

Huang, Y., Goel, S., Duda, D.G., Fukumura, D., Jain, R.K., 2013. Vascular Normalization as an Emerging Strategy to Enhance Cancer Immunotherapy. Am. Assoc. Cancer Res. 22, 2943–2949.

Hughes, S., Chan-Ling, T., 2000. Roles of endothelial cell migration and apoptosis in vascular remodeling during development of the central nervous system. Microcirculation 7, 317–333.

Hwangbo, C., Lee, H.W., Kang, H., Ju, H., Wiley, D.S., Papangeli, I., Han, J., Kim, J.D., Dunworth, W.P., Hu, X., Lee, S., El-Hely, O., Sofer, A., Pak, B., Peterson, L., Comhair, S., Hwang, E.M., Park, J.Y., Thomas, J.L., Bautch, V.L., Erzurum, S.C., Chun, H.J., Jin, S.W., 2017. Modulation of Endothelial Bone Morphogenetic Protein Receptor Type 2 Activity by Vascular Endothelial Growth Factor Receptor 3 in Pulmonary Arterial Hypertension. Circulation 135, 2288–2298.

Inoue, D., Wittbrodt, J., 2011. One for all-a highly efficient and versatile method for fluorescent immunostaining in fish embryos. PLoS One 6, 1–7.

Isogai, S., Horiguchi, M., Weinstein, B.M., 2001. The Vascular Anatomy of the Developing Zebrafish: An Atlas of Embryonic and Early Larval Development. Dev. Biol. 230, 278–301.

Isogai, S., Lawson, N.D., Torrealday, S., Horiguchi, M., Weinstein, B.M., 2003. Angiogenic network formation in the developing vertebrate trunk. Development 130, 5281–5290.

Jakobsson, L., Franco, C.A., Bentley, K., Collins, R.T., Ponsioen, B., Aspalter, I.M., Rosewell, I., Busse, M., Thurston, G., Medvinsky, A., Schulte-Merker, S., Gerhardt, H., 2010. Endothelial cells dynamically compete for the tip cell position during angiogenic sprouting. Nat. Cell Biol. 12, 943–953.

Jin, S.-W., Beis, D., Mitchell, T., Chen, J.-N., Stainier, D., 2005. Cellular and molecular analyses of vascular tube and lumen formation in zebrafish. Development 132, 5199–209.

Jin, Y., Muhl, L., Burmakin, M., Wang, Y., Duchez, A.C., Betsholtz, C., Arthur, H.M., Jakobsson, L., 2017. Endoglin prevents vascular malformation by regulating flow-induced cell migration and specification through VEGFR2 signalling. Nat. Cell Biol. 19, 639–652.

Jin, Z.-G., Ueba, H., Tanimoto, T., Lungu, A.O., Frame, M.D., Berk, B.C., 2003. Ligand-Independent Activation of Vascular Endothelial Growth Factor Receptor 2 by Fluid Shear Stress Regulates Activation of Endothelial Nitric Oxide Synthase. Circ. Res. 93, 354–363.

Jones, E., 2011. The initiation of blood flow and flow induced events in early vascular development. Semin. Cell Dev. Biol. 22, 1028–1035.

Jones, E., le Noble, F., Eichmann, A., 2006. What determines blood vessel structure? Genetic prespecification vs. hemodynamics. Physiology

21, 388–95.

Jung, B., Obinata, H., Galvani, S., Mendelson, K., Ding, B. Sen, Skoura, A., Kinzel, B., Brinkmann, V., Rafii, S., Evans, T., Hla, T., 2012. Flow-Regulated Endothelial S1P Receptor-1 Signaling Sustains Vascular Development. Dev. Cell 23, 600–610.

Kamei, M., Saunders, W.B., Bayless, K.J., Dye, L., Davis, G.E., Weinstein, B.M., 2006. Endothelial tubes assemble from intracellular vacuoles in vivo. Nature 442, 453–456.

Karaman, S., Leppänen, V.M., Alitalo, K., 2018. Vascular endothelial growth factor signaling in development and disease. Dev. 145, 1–8.

Karthik, S., Djukic, T., Kim, J.D., Zuber, B., Makanya, A., Odriozola, A., Hlushchuk, R., Filipovic, N., Jin, S.W., Djonov, V., 2018. Synergistic interaction of sprouting and intussusceptive angiogenesis during zebrafish caudal vein plexus development. Sci. Rep. 8, 1–15.

Khalil, A.A., Friedl, P., 2010. Determinants of leader cells in collective cell migration. Integr. Biol. 2, 568–574.

Kimura, E., Isogai, S., Hitomi, J., 2015. Integration of vascular systems between the brain and spinal cord in zebrafish. Dev. Biol. 406, 40–51.

Kirmizitas, A., Meiklejohn, S., Ciau-Uitz, A., Stephenson, R., Patient, R., 2017. Dissecting BMP signaling input into the gene regulatory networks driving specification of the blood stem cell lineage. Proc. Natl. Acad. Sci. U. S. A. 114, 5814–5821.

Kishimoto, Y., Lee, K.H., Zon, L., Hammerschmidt, M., Schulte-Merker, S., 1997. The molecular nature of zebrafish swirl: BMP2 function is essential during early dorsoventral patterning. Development 124, 4457–4466.

Kochhan, E., Lenard, A., Ellertsdottir, E., Herwig, L., Affolter, M., Belting, H.G., Siekmann, A.F., 2013. Blood Flow Changes Coincide with Cellular Rearrangements during Blood Vessel Pruning in Zebrafish Embryos. PLoS One 8, 1–7.

Koenig, A.L., Baltrunaite, K., Bower, N.I., Rossi, A., Stainier, D.Y.R., Hogan, B.M., Sumanas, S., 2016. Vegfa signaling promotes zebrafish intestinal vasculature development through endothelial cell migration from the posterior cardinal vein. Dev. Biol. 411, 115–127.

Kohli, V., Schumacher, J.A., Desai, S.P., Rehn, K., Sumanas, S., 2013. Arterial and Venous Progenitors of the Major Axial Vessels Originate at Distinct Locations. Dev. Cell 25, 196–206.

Korchynskyi, O., Ten Dijke, P., 2002. Identification and functional characterization of distinct critically important bone morphogenetic protein-specific response elements in the Id1 promoter. J. Biol. Chem. 277, 4883–4891.

Korn, C., Augustin, H.G., 2015. Mechanisms of Vessel Pruning and Regression. Dev. Cell 34, 5–17.

Korn, C., Scholz, B., Hu, J., Srivastava, K., JessicaWojtarowicz,

Arnsperger, T., Adams, R.H., Boutros, M., Augustin, H.G., Augustin, I., Wojtarowicz, J., Arnsperger, T., Adams, R.H., Boutros, M., Augustin, H.G., Augustin, I., 2014. Endothelial cell-derived non-canonical Wnt ligands control vascular pruning in angiogenesis. Oncol. Rep. 141, 1757–1766.

Krueger, J., Liu, D., Scholz, K., Zimmer, A., Shi, Y., Klein, C., Siekmann, A., Schulte-Merker, S., Cudmore, M., Ahmed, A., le Noble, F., 2011. Flt1 acts as a negative regulator of tip cell formation and branching morphogenesis in the zebrafish embryo. Development 138, 2111–20.

Kuo, M.W., Wang, C.H., Wu, H.C., Chang, S.J., Chuang, Y.J., 2011. Soluble THSD7A is an N-glycoprotein that promotes endothelial cell migration and tube formation in angiogenesis. PLoS One 6.

Kwan, K.M., Fujimoto, E., Grabher, C., Mangum, B.D., Hardy, M.E., Campbell, D.S., Parant, J.M., Yost, H.J., Kanki, J.P., Chien, C. Bin, 2007. The Tol2kit: A multisite gateway-based construction Kit for Tol2 transposon transgenesis constructs. Dev. Dyn. 236, 3088–3099.

Kwon, H.B., Wang, S., Helker, C.S., Rasouli, S.J., Maischein, H.M., Offermanns, S., Herzog, W., Stainier, D.Y., 2016. In vivo modulation of endothelial polarization by Apelin receptor signalling. Nat. Commun. 7, 11805.

Lacaud, G., Kouskoff, V., 2017. Hemangioblast, hemogenic endothelium, and primitive versus definitive hematopoiesis. Exp. Hematol. 49, 19–24.

Ladwein, M., Rottner, K., 2008. On the Rho'd : The regulation of membrane protrusions by Rho-GTPases. FEBS Lett. 582, 2066–2074.

Lanahan, A., Zhang, X., Fantin, A., Zhuang, Z., Rivera-Molina, F., Speichinger, K., Prahst, C., Zhang, J., Wang, Y., Davis, G., Toomre, D., Ruhrberg, C., Simons, M., 2013. The Neuropilin 1 Cytoplasmic Domain Is Required for VEGF-A-Dependent Arteriogenesis. Dev. Cell 25, 156–168.

Larson, J.D., Wadman, S.A., Chen, E., Kerley, L., Clark, K.J., Eide, M., Lippert, S., Nasevicius, A., Ekker, S.C., Hackeff, P.B., Essner, J.J., 2004. Expression of VE-cadherin in zebrafish embryos: A new tool to evaluate vascular development. Dev. Dyn. 231, 204–213.

Laux, D.W., Febbo, J.A., Roman, B.L., 2011. Dynamic analysis of BMP-responsive smad activity in live zebrafish embryos. Dev. Dyn. 240, 682–694.

Laux, D.W., Young, S., Donovan, J.P., Mansfield, C.J., Upton2, P.D., Roman, B.L., 2013. Circulating Bmp10 acts through endothelial Alk1 to mediate flow-dependent arterial quiescence. Development 140, 3403–3412.

Laviña, B., Castro, M., Niaudet, C., Cruys, B., Álvarez-Aznar, A., Carmeliet, P., Bentley, K., Brakebusch, C., Betsholtz, C., Gaengel, K., 2018. Defective endothelial cell migration in the absence of Cdc42 leads to capillary-venous malformations. Dev. 145, 1–20.

Lawson, N.D., Vogel, A.M., Weinstein, B.M., 2002. Sonic hedgehog

and vascular endothelial growth factor act upstream of the Notch pathway during arterial endothelial differentiation. Dev. Cell 3, 127–136.

Lawson, N.D., Weinstein, B.M., 2002a. In Vivo Imaging of Embryonic Vascular Development Using Transgenic Zebrafish. Dev. Biol. 248, 307–318.

Lawson, N.D., Weinstein, B.M., 2002b. Arteries and veins: making a difference with zebrafish. Nat. Rev. Genet. 3, 674–682.

le Noble, F., Moyon, D., Pardanaud, L., Yuan, L., Djonov, V., Matthijsen, R., Bréant, C., Fleury, V., Eichmann, A., Le, N.F., Moyon, D., Pardanaud, L., Yuan, L., Djonov, V., Matthijsen, R., Breant, C., Fleury, V., Eichmann, A., 2004. Flow regulates arterial-venous differentiation in the chick embryo yolk sac. Development 131, 361–375.

Lee, H.-W., Chong, D.C., Ola, R., Dunworth, W.P., Meadows, S., Ka, J., Kaartinen, V.M., Qyang, Y., Cleaver, O., Bautch, V.L., Eichmann, A., Jin, S.-W., 2017. Alk2/ACVR1 and Alk3/BMPR1A Provide Essential Function for Bone Morphogenetic Protein–Induced Retinal Angiogenesis. Arterioscler. Thromb. Vasc. Biol. ATVBAHA.116.308422.

Lee, P., Goishi, K., Davidson, A.J., Mannix, R., Zon, L., Klagsbrun, M., 2002. Neuropilin-1 is required for vascular development and is a mediator of VEGF-dependent angiogenesis in zebrafish. Proc. Natl. Acad. Sci. U. S. A. 99, 10470–10475.

Lenard, A., Daetwyler, S., Betz, C., Ellertsdottir, E., Belting, H.G., Huisken, J., Affolter, M., 2015. Endothelial Cell Self-fusion during Vascular Pruning. PLoS Biol. 13, 1–25.

Lenard, A., Ellertsdottir, E., Herwig, L., Krudewig, A., Sauteur, L., Belting, H.G., Affolter, M., 2013. In vivo analysis reveals a highly stereotypic morphogenetic pathway of vascular anastomosis. Dev. Cell 25, 492–506.

Leslie, J.D., Ariza-McNaughton, L., Bermange, A.L., McAdow, R., Johnson, S.L., Lewis, J., 2007. Endothelial signalling by the Notch ligand Delta-like 4 restricts angiogenesis. Development 134, 839–844.

Liang, D., Chang, J.R., Chin, A.J., Smith, A., Kelly, C., Weinberg, E.S., Ge, R., 2001. The role of vascular endothelial growth factor (VEGF) in vasculogenesis, angiogenesis, and hematopoiesis in zebrafish development. Mech. Dev. 108, 29–43.

Lin, K., Hsu, P., Chen, B.P., Yuan, S., Usami, S., John, Y., Li, Y., Chien, S., 2000. Molecular mechanism of endothelial growth arrest by laminar shear stress. PNAS 97, 9385–9389.

Liu, C.H., Wang, Z., Sun, Y., Chen, J., 2017. Animal models of ocular angiogenesis: From development to pathologies. FASEB J. 31, 4665–4681.

Lizama, C.O., Zovein, A.C., 2013. Polarizing pathways: balancing endothelial polarity, permeability, and lumen formation. Exp Cell Res 319, 1247–1254.

Lobov, I., Cheung, E., Wudali, R., Cao, J., Halasz, G., Wei, Y.,

Economides, A., Lin, H.C., Papadopoulos, N., Yancopoulos, G.D., Wiegand, S.J., 2011. The DII4/notch pathway controls postangiogenic blood vessel remodeling and regression by modulating vasoconstriction and blood flow. Blood 117, 6728–6737.

Lobov, I., Rao, S., Carroll, T.J., Vallance, J.E., Ito, M., Ondr, J.K., Kurup, S., Glass, D. a, Patel, M.S., Shu, W., Morrisey, E.E., McMahon, A.P., Karsenty, G., Lang, R. a, 2005. WNT7b mediates macrophage-induced programmed cell death in patterning of the vasculature. Nature 437, 417–421.

Lobov, I., Renard, R.A., Papadopoulos, N., Gale, N.W., Thurston, G., Yancopoulos, G.D., Wiegand, S.J., 2007. Delta-like ligand 4 (DII4) is induced by VEGF as a negative regulator of angiogenic sprouting. Proc. Natl. Acad. Sci. U. S. A. 104, 3219–3224.

López-Rovira, T., Chalaux, E., Massagué, J., Rosa, J.L., Ventura, F., 2002. Direct binding of Smad1 and Smad4 to two distinct motifs mediates bone morphogenetic protein-specific transcriptional activation of Id1 gene. J. Biol. Chem. 277, 3176–3185.

Lowe, D.G., 2004. Distinctive Image Features from Scale-Invariant Keypoints David. Int. J. Comput. Vis. 60, 91–110.

Lowery, J.W., de Caestecker, M.P., 2010. BMP signaling in vascular development and disease. Cytokine Growth Factor Rev. 21, 287–298.

Lucitti, J.L., Jones, E.A. V, Huang, C., Chen, J., Fraser, S.E., Dickinson, M.E., 2007. Vascular remodeling of the mouse yolk sac requires hemodynamic force. Development 134, 3317 LP – 3326.

Makanya, A.N., Hlushchuk, R., Djonov, V.G., 2009. Intussusceptive angiogenesis and its role in vascular morphogenesis, patterning, and remodeling. Angiogenesis 12, 113–123.

Martin, M., Veloso, A., Wu, J., Katrukha, E.A., Akhmanova, A., 2018. Control of endothelial cell polarity and sprouting angiogenesis by noncentrosomal microtubules. Elife 7, 1–37.

Matthews, M., Varga, Z.M., 2012. Anesthesia and euthanasia in zebrafish. ILAR J. 53, 192–204.

Miller, A.F., Harvey, S.A.K., Thies, R.S., Olson, M.S., 2000. Bone Morphogenetic Protein-9:AN AUTOCRINE/PARACRINE CYTOKINE IN THE LIVER. Biol. Chem. 275, 17937–17945.

Miriyala, S., Nieto, M.C.G., Mingone, C., Smith, D., Dikalov, S., Harrison, D.G., Jo, H., 2006. Bone morphogenic protein-4 induces hypertension in mice: Role of noggin, vascular NADPH oxidases, and impaired vasorelaxation. Circulation 113, 2818–2825.

Monteiro, R., van Dinther, M., Bakkers, J., Wilkinson, R., Patient, R., ten Dijke, P., Mummery, C., 2008. Two novel type II receptors mediate BMP signalling and are required to establish left-right asymmetry in zebrafish. Dev. Biol. 315, 55–71.

Moshal, K.S., Ferri-Lagneau, K.F., Haider, J., Pardhanani, P., Leung,

T.C., 2011. Discriminating different cancer cells using a zebrafish in vivo assay. Cancers (Basel). 3, 4102–4113.

Mukouyama, Y.S., Gerber, H.P., Ferrara, N., Gu, C., Anderson, D.J., 2005. Peripheral nerve-derived VEGF promotes arterial differentiation via neuropilin 1-mediated positive feedback. Development 132, 941–952.

Nakajima, H., Yamamoto, K., Agarwala, S., Terai, K., Fukui, H., Fukuhara, S., Ando, K., Miyazaki, T., Yokota, Y., Schmelzer, E., Belting, H.-G., Affolter, M., Lecaudey, V., Mochizuki, N., 2017. Flow-Dependent Endothelial YAP Regulation Contributes to Vessel Maintenance. Dev. Cell 40, 523–536.

Neal, A., Nornes, S., Wallace, M.D., Payne, S., Chouliaras, K., Wilkinson, R., Liu, K., Sholapurka, R., Ratnayaka, I., Bond, G., Bou-Gharios, G., Chico, T., Val, S. De, 2017. Vein Identity Requires BMP Signalling Through Alk3. unpublished.

Neto, F., Klaus-Bergmann, A., Ong, Y.T., Alt, S., Vion, A.C., Szymborska, A., Carvalho, J.R., Hollfinger, I., Bartels-Klein, E., Franco, C.A., Potente, M., Gerhardt, H., 2018. YAP and TAZ regulate adherens junction dynamics and endothelial cell distribution during vascular development. Elife 7, 1–30.

Neuhaus, H., Rosen, V., Thies, R.S., 1999. Heart specific expression of mouse BMP-10 a novel member of the TGF-β superfamily. Mech. Dev. 80, 181–184.

Nicenboim, J., Malkinson, G., Lupo, T., Asaf, L., Sela, Y., Mayseless, O., Gibbs-Bar, L., Senderovich, N., Hashimshony, T., Shin, M., Jerafi-Vider, A., Avraham-Davidi, I., Krupalnik, V., Hofi, R., Almog, G., Astin, J.W., Golani, O., Ben-Dor, S., Crosier, P.S., Herzog, W., Lawson, N.D., Hanna, J.H., Yanai, I., Yaniv, K., 2015. Lymphatic vessels arise from specialized angioblasts within a venous niche. Nature 522, 56–61.

Nicoli, S., De Sena, G., Presta, M., 2009. Fibroblast growth factor 2-induced angiogenesis in zebrafish: The zebrafish yolk membrane (ZFYM) angiogenesis assay. J. Cell. Mol. Med. 13, 2061–2068.

Nicoli, S., Presta, M., 2007. The zebrafish/tumor xenograft angiogenesis assay. Nat. Protoc. 2, 2918–2923.

Nicoli, S., Ribatti, D., Cotelli, F., Presta, M., 2007. Mammalian tumor xenografts induce neovascularization in zebrafish embryos. Cancer Res. 67, 2927–2931.

Nilsson, I., Bahram, F., Li, X., Gualandi, L., Koch, S., Jarvius, M., Söderberg, O., Anisimov, A., Kholová, I., Pytowski, B., Baldwin, M., Ylä-Herttuala, S., Alitalo, K., Kreuger, J., Claesson-Welsh, L., 2010. VEGF receptor 2/-3 heterodimers detected in situ by proximity ligation on angiogenic sprouts. EMBO J. 29, 1377–1388.

Nohata, N., Uchida, Y., Stratman, A.N., Adams, R.H., Zheng, Y., Weinstein, B.M., Mukouyama, Y.S., Gutkind, J.S., 2016. Temporal-specific roles of Rac1 during vascular development and retinal angiogenesis. Dev.

Biol. 411, 183–194.

Nolan-Stevaux, O., Zhong, W., Culp, S., Shaffer, K., Hoover, J., Wickramasinghe, D., Ruefli-Brasse, A., 2012. Endoglin Requirement for BMP9 Signaling in Endothelial Cells Reveals New Mechanism of Action for Selective Anti-Endoglin Antibodies. PLoS One 7.

Oh, S.P., Seki, T., Goss, K.A., Imamura, T., Yi, Y., Donahoe, P.K., Li, L., Miyazono, K., Ten Dijke, P., Kim, S., Li, E., 2000. Activin receptor-like kinase 1 modulates transforming growth factor-β1 signaling in the regulation of angiogenesis. Proc. Natl. Acad. Sci. U. S. A. 97, 2626–2631.

Paatero, I., Sauteur, L., Lee, M., Lagendijk, A.K., Heutschi, D., Wiesner, C., Guzmán, C., Bieli, D., Hogan, B.M., Affolter, M., Belting, H.G., 2018. Junction-based lamellipodia drive endothelial cell rearrangements in vivo via a VE-cadherin-F-actin based oscillatory cell-cell interaction. Nat. Commun. 9.

Panza, P., Maier, J., Schmees, C., Rothbauer, U., Söllner, C., 2015. Live imaging of endogenous protein dynamics in zebrafish using chromobodies. Dev. 142, 1879–1884.

Park, J.E., Chen, H.H., Winer, J., Houck, K.A., Ferrara, N., 1994. Potentiation of vascular endothelial growth factor bioactivity, in vitro and in vivo, and high affinity binding to flt-1 but not to flk-l/kdr. J. Biol. Chem. 269, 25646–25654.

Patel-Hett, S., D'Amore, P.A., 2011. Signal transduction in vasculogenesis and developmental angiogenesis. Int. J. Dev. Biol. 55, 353–369.

Pelton, J.C., Wright, C.E., Leitges, M., Bautch, V.L., 2014. Multiple endothelial cells constitute the tip of developing blood vessels and polarize to promote lumen formation. Development 141, 4121–6.

Phng, L.-K., Potente, M., Leslie, J.D., Babbage, J., Nyqvist, D., Lobov, I., Ondr, J.K., Rao, S., Lang, R.A., Thurston, G., Gerhardt, H., 2009. Nrarp Coordinates Endothelial Notch and Wnt Signaling to Control Vessel Density in Angiogenesis. Dev. Cell 16, 70–82.

Phng, L.-K., Stanchi, F., Gerhardt, H., 2013. Filopodia are dispensable for endothelial tip cell guidance. Development 140, 4031–4040.

Poduri, A., Chang, A.H., Raftrey, B., Rhee, S., Van, M., Red-Horse, K., 2017. Endothelial cells respond to the direction of mechanical stimuli through SMAD signaling to regulate coronary artery size. Dev. 144, 3241–3252.

Quillien, A., Moore, J.C., Shin, M., Siekmann, A.F., Smith, T., Pan, L.Y., Moens, C.B., Parsons, M.J., Lawson, N.D., 2014. Distinct Notch signaling outputs pattern the developing arterial system. Development 141, 1544–1552.

Raghunath, M., Sy Wong, Y., Farooq, M., Ge, R., 2009. Pharmacologically induced angiogenesis in transgenic zebrafish. Biochem. Biophys. Res. Commun. 378, 766–771.

Rao, S., Lobov, I.B., Vallance, J.E., Tsujikawa, K., Shiojima, I., Akunuru, S., Walsh, K., Benjamin, L.E., Lang, R.A., 2007. Obligatory participation of macrophages in an angiopoietin 2- mediated cell death switch. Development 134, 4449–4458.

Reischauer, S., Stone, O.A., Villasenor, A., Chi, N., Jin, S.W., Martin, M., Lee, M.T., Fukuda, N., Marass, M., Witty, A., Fiddes, I., Kuo, T., Chung, W.S., Salek, S., Lerrigo, R., Alsio, J., Luo, S., Tworus, D., Augustine, S.M., Mucenieks, S., Nystedt, B., Giraldez, A.J., Schroth, G.P., Andersson, O., Stainier, D.Y.R., 2016. Cloche is a bHLH-PAS transcription factor that drives haemato-vascular specification. Nature 535, 294–298.

Rezzola, S., Di Somma, M., Corsini, M., Leali, D., Ravelli, C., Polli, V.A.B., Grillo, E., Presta, M., Mitola, S., 2019. VEGFR2 activation mediates the pro-angiogenic activity of BMP4. Angiogenesis 22, 521–533.

Ribatti, D., 2010. The chick embryo chorioallantoic membrane as an in vivo assay to study antiangiogenesis. Pharmaceuticals 3, 482–513.

Ricard, N., Ciais, D., Levet, S., Subileau, M., Mallet, C., Zimmers, T.A., Lee, S.J., Bidart, M., Feige, J.J., Bailly, S., 2012. BMP9 and BMP10 are critical for postnatal retinal vascular remodeling. Blood 119, 6162–6171.

Robinson, C.J., Stringer, S.E., 2001. The splice variants of vascular endothelial growth factor (VEGF) and their receptors. J. Cell Sci. 114, 853–865.

Rochon, E.R., Menon, P.G., Roman, B.L., 2016. Alk1 controls arterial endothelial cell migration in lumenized vessels. Development 143, 2593–2602.

Roman, B.L., Pham, V.N., Lawson, N.D., Kulik, M., Childs, S., Lekven, A.C., Garrity, D.M., Moon, R.T., Fishman, M.C., Lechleider, R.J., Wienstein, B.M., 2002. Disruption of acvrl1 increases endothelial cell number in zebrafish cranial vessels. Development 129, 3009–3019.

Rosen, J.N., Sweeney, M.F., Mably, J.D., 2009. Microinjection of zebrafish embryos to analyze gene function. J. Vis. Exp. 1–5.

Rossi, A., Gauvrit, S., Marass, M., Pan, L., Moens, C.B., Stainier, D.Y.R., 2016. Regulation of Vegf signaling by natural and synthetic ligands. Blood.

Sakao, S., Taraseviciene‐Stewart, L., Lee, J.D., Wood, K., Cool, C.D., Voelkel, N.F., 2005. Initial apoptosis is followed by increased proliferation of apoptosis‐resistant endothelial cells. FASEB J. 19, 1178–1180.

Sato, Y., Lansford, R., 2013. Transgenesis and imaging in birds, and available transgenic reporter lines. Dev. Growth Differ. 55, 406–421.

Sauteur, L., Krudewig, A., Herwig, L., Ehrenfeuchter, N., Lenard, A., Affolter, M., Belting, H.G., 2014. Cdh5/VE-cadherin promotes endothelial cell interface elongation via cortical actin polymerization during angiogenic sprouting. Cell Rep. 9, 504–513.

Savage, A.M., Kurusamy, S., Chen, Y., Jiang, Z., Chhabria, K.,

MacDonald, R.B., Kim, H.R., Wilson, H.L., van Eeden, F.J.M., Armesilla, A.L., Chico, T.J.A., Wilkinson, R.N., 2019. tmem33 is essential for VEGF-mediated endothelial calcium oscillations and angiogenesis. Nat. Commun. 10, 1–15.

Scharpfenecker, M., van Dinther, M., Liu, Z., van Bezooijen, R.L., Zhao, Q., Pukac, L., Löwik, C.W.G.M., ten Dijke, P., 2007. BMP-9 signals via ALK1 and inhibits bFGF-induced endothelial cell proliferation and VEGF-stimulated angiogenesis. J. Cell Sci. 120, 964–972.

Schiavone, M., Rampazzo, E., Casari, A., Battilana, G., Persano, L., Moro, E., Liu, S., Leach, S.D., Tiso, N., Argenton, F., 2014. Zebrafish reporter lines reveal in vivo signaling pathway activities involved in pancreatic cancer. DMM Dis. Model. Mech. 7, 883–894.

Schuermann, A., Helker, C.S.M., Herzog, W., 2014. Angiogenesis in zebrafish, in: Seminars in Cell and Developmental Biology. Elsevier Ltd, pp. 106–114.

Sehnert, A.J., Huq, A., Weinstein, B.M., Walker, C., Fishman, M., Stainier, D.Y.R., 2002. Cardiac troponin T is essential in sarcomere assembly and cardiac contractility. Nat. Genet. 31, 106–110.

Seiler, C., Abrams, J., Pack, M., 2010. Characterization of zebrafish intestinal smooth muscle development using a novel sm22α-b promoter. Dev. Dyn. 239, 2806–2812.

Senger, D.R., Connolly, D.T., Van De Water, L., Feder, J., Dvorak, H.F., 1990. Purification and NH2-Terminal Amino Acid Sequence of Guinea Pig Tumor-secreted Vascular Permeability Factor. Cancer Res. 50, 1774–1778.

Shalaby, F., Rossant, J., Yamaguchi, T.P., Gertsensteln, M., Wu, X.-F., Breitman, M.L., Schuh, A.C., 1995. Failure of blood-island formation and vasculogenesis in Flk-1-deficient mice. Nature 376, 62–66.

Shin, M., Beane, T., Quillien, A., Male, I., Zhu, L.J., Lawson, N.D., 2016a. Vegfa signals through ERK to promote angiogenesis, but not artery differentiation. Development dev.137919.

Shin, M., Male, I., Beane, T.J., Villefranc, J.A., Kok, F.O., Zhu, L.J., Lawson, N.D., 2016b. Vegfc acts through ERK to induce sprouting and differentiation of trunk lymphatic progenitors. Development dev.137901.

Sid, H., Schusser, B., 2018. Applications of gene editing in chickens: A new era is on the Horizon. Front. Genet. 9, 1–12.

Siekmann, A.F., Affolter, M., Belting, H.G., 2013. The tip cell concept 10 years after: New players tune in for a common theme. Exp. Cell Res. 319, 1255–1263.

Siekmann, A.F., Lawson, N.D., 2007. Notch signalling limits angiogenic cell behaviour in developing zebrafish arteries. Nature 445, 781–784.

Simons, M., Alitalo, K., Annex, B.H., Augustin, H.G., Beam, C., Berk, B.C., Byzova, T., Carmeliet, P., Chilian, W., Cooke, J.P., Davis, G.E.,

Eichmann, A., Iruela-Arispe, M.L., Keshet, E., Sinusas, A.J., Ruhrberg, C., Woo, Y.J., Dimmeler, S., 2015. State-of-the-art methods for evaluation of angiogenesis and tissue vascularization: A scientific statement from The American Heart Association, Circulation Research.

Simons, M., Gordon, E., Claesson-Welsh, L., 2016. Mechanisms and regulation of endothelial VEGF receptor signalling. Nat. Rev. Mol. Cell Biol. 17, 311–325.

Soh, G.H., Pomreinke, A.P., Müller, P., 2020. Integration of Nodal and BMP Signaling by Mutual Signaling Effector Antagonism. Cell Rep. 31.

Souilhol, C., Serbanovic-Canic, J., Fragiadaki, M., Chico, T.J., Ridger, V., Roddie, H., Evans, P.C., 2020. Endothelial responses to shear stress in atherosclerosis: a novel role for developmental genes. Nat. Rev. Cardiol. 17, 52–63.

Stainier, D., Fouquet, B., Chen, J.N., Warren, K.S., Weinstein, B.M., Meiler, S.E., Mohideen, M. a, Neuhauss, S.C., Solnica-Krezel, L., Schier, a F., Zwartkruis, F., Stemple, D.L., Malicki, J., Driever, W., Fishman, M.C., 1996. Mutations affecting the formation and function of the cardiovascular system in the zebrafish embryo. Development 123, 285–292.

Stainier, D., Raz, E., Lawson, N.D., Ekker, S.C., Burdine, R.D., Eisen, J.S., Ingham, P.W., Schulte-Merker, S., Yelon, D., Weinstein, B.M., Mullins, M.C., Wilson, S.W., Ramakrishnan, L., Amacher, S.L., Neuhauss, S.C.F., Meng, A., Mochizuki, N., Panula, P., Moens, C.B., 2017. Guidelines for morpholino use in zebrafish. PLoS Genet. 13, 6–10.

Stainier, D., Weinstein, B.M., Detrich, H.W., Zon, L.I., Fishman, M.C., 1995. Cloche, an Early Acting Zebrafish Gene, Is Required By Both the Endothelial and Hematopoietic Lineages. Development 121, 3141–3150.

Stratman, A.N., Pezoa, S.A., Farrelly, O.M., Castranova, D., Dye, L.E., Butler, M.G., Sidik, H., Talbot, W.S., Weinstein, B.M., 2017. Interactions between mural cells and endothelial cells stabilize the developing zebrafish dorsal aorta. Development 144, 115–127.

Strilić, B., Eglinger, J., Krieg, M., Zeeb, M., Axnick, J., Babál, P., Müller, D.J., Lammert, E., 2010. Electrostatic cell-surface repulsion initiates lumen formation in developing blood vessels. Curr. Biol. 20, 2003–2009.

Strilić, B., Kučera, T., Eglinger, J., Hughes, M.R., McNagny, K.M., Tsukita, S., Dejana, E., Ferrara, N., Lammert, E., 2009. The Molecular Basis of Vascular Lumen Formation in the Developing Mouse Aorta. Dev. Cell 17, 505–515.

Stryker, Z.I., Rajabi, M., Davis, P.J., Shaker A., M., 2019. Evaluation of Angiogenesis Assays. biomedicines 7, 1–13.

Sugden, W.W., Meissner, R., Aegerter-Wilmsen, T., Tsaryk, R., Leonard, E. V., Bussmann, J., Hamm, M.J., Herzog, W., Jin, Y., Jakobsson, L., Denz, C., Siekmann, A.F., 2017. Endoglin controls blood vessel diameter through endothelial cell shape changes in response to haemodynamic cues. Nat. Cell Biol. 19.

Sumanas, S., Lin, S., 2006. Ets1-related protein is a key regulator of vasculogenesis in zebrafish. PLoS Biol. 4, 0060–0069.

Suzuki, Y., Montagne, K., Nishihara, A., Watabe, T., Miyazono, K., 2008. BMPs promote proliferation and migration of endothelial cells via stimulation of VEGF-A/VEGFR2 and angiopoietin-1/Tie2 signalling. J. Biochem. 143, 199–206.

Suzuki, Y., Ohga, N., Morishita, Y., Hida, K., Miyazono, K., Watabe, T., 2010. BMP-9 induces proliferation of multiple types of endothelial cells in vitro and in vivo. J. Cell Sci. 123, 1684–1692.

Szymczak, A.L., Workman, C.J., Wang, Y., Vignali, K.M., Dilioglou, S., Vanin, E.F., Vignali, D.A.A., 2004. Correction of multi-gene deficiency in vivo using a single “self-cleaving” 2A peptide-based retroviral vector. Nat. Biotechnol. 22, 589–594.

Takahashi, T., Yamaguchi, S., Chida, K., Shibuya, M., 2001. A single autophosphorylation site on KDR/Flk-1 is essential for VEGF-A-dependent activation of PLC-γ and DNA synthesis in vascular endothelial cells. EMBO J. 20, 2768–2778.

Tardy, Y., Resnick, N., Nagel, T., Gimbrone, M.A., Dewey, C.F., 1997. Shear stress gradients remodel endothelial monolayers in vitro via a cell proliferation-migration-loss cycle. Arterioscler. Thromb. Vasc. Biol. 17, 3102–3106.

Thalgott, J.H., Dos-Santos-Luis, D., Hosman, A.E., Martin, S., Lamandé, N., Bracquart, D., Srun, S., Galaris, G., De Boer, H.C., Tual-Chalot, S., Kroon, S., Arthur, H.M., Cao, Y., Snijder, R.J., Disch, F., Mager, J.J., Rabelink, T.J., Mummery, C.L., Raymond, K., Lebrin, F., 2018. Decreased expression of vascular endothelial growth factor receptor 1 contributes to the pathogenesis of hereditary hemorrhagic telangiectasia type 2. Circulation 138, 2698–2712.

Tinevez, J.Y., Perry, N., Schindelin, J., Hoopes, G.M., Reynolds, G.D., Laplantine, E., Bednarek, S.Y., Shorte, S.L., Eliceiri, K.W., 2017. TrackMate: An open and extensible platform for single-particle tracking. Methods 115, 80–90.

Tkachenko, E., Gutierrez, E., Saikin, S.K., Fogelstrand, P., Kim, C., Groisman, A., Ginsberg, M.H., 2013. The nucleus of endothelial cell as a sensor of blood flow direction. Biol. Open 2, 1007–1012.

Torres-Vázquez, J., Gitler, A.D., Fraser, S.D., Berk, J.D., Pham, V.N., Fishman, M.C., Childs, S., Epstein, J.A., Weinstein, B.M., 2004. Semaphorin-plexin signaling guides patterning of the developing vasculature. Dev. Cell 7, 117–123.

Traver, D., Paw, B.H., Poss, K.D., Penberthy, W.T., Lin, S., Zon, L.I., 2003. Transplantation and in vivo imaging of multilineage engraftment in zebrafish bloodless mutants. Nat. Immunol. 4, 1238–1246.

Tual-Chalot, S., Garcia-Collado, M., Redgrave, R.E., Singh, E., Davison, B., Park, C., Lin, H., Luli, S., Jin, Y., Wang, Y., Lawrie, A.,

Jakobsson, L., Arthur, H.M., 2020. Loss of endothelial endoglin promotes high-output heart failure through peripheral arteriovenous shunting driven by VEGF signaling. Circ. Res. 126, 243–257.

Tzima, E., Irani-Tehrani, M., Kiosses, W.B., Dejana, E., Schultz, D.A., Engelhardt, B., Cao, G., DeLisser, H., Schwartz, M.A., 2005. A mechanosensory complex that mediates the endothelial cell response to fluid shear stress. Nature 437, 426–431.

Ubezio, B., Blanco, R.A., Geudens, I., Stanchi, F., Mathivet, T., Jones, M.L., Ragab, A., Bentley, K., Gerhardt, H., 2016. Synchronization of endothelial Dll4-Notch dynamics switch blood vessels from branching to expansion. Elife 5.

Udan, R.S., Vadakkan, T.J., Dickinson, M.E., 2013. Dynamic responses of endothelial cells to changes in blood flow during vascular remodeling of the mouse yolk sac. Development 140, 4041–4050.

Van Der Stoel, M., Schimmel, L., Nawaz, K., Van Stalborch, A.M., De Haan, A., Klaus-Bergmann, A., Valent, E.T., Koenis, D.S., Van Nieuw Amerongen, G.P., De Vries, C.J., De Waard, V., Gloerich, M., Van Buul, J.D., Huveneers, S., 2020. DLC1 is a direct target of activated YAP/TAZ that drives collective migration and sprouting angiogenesis. J. Cell Sci. 133.

Villefranc, J.A., Amigo, J., Lawson, N.D., 2007. Gateway compatible vectors for analysis of gene function in the zebrafish. Dev. Dyn. 236, 3077–3087.

Vogrin, A.J., Bower, N.I., Gunzburg, M.J., Roufail, S., Okuda, K.S., Paterson, S., Headey, S.J., Stacker, S.A., Hogan, B.M., Achen, M.G., 2019. Evolutionary Differences in the Vegf/Vegfr Code Reveal Organotypic Roles for the Endothelial Cell Receptor Kdr in Developmental Lymphangiogenesis. Cell Rep. 28, 2023-2036.e4.

Wakayama, Y., Fukuhara, S., Ando, K., Matsuda, M., Mochizuki, N., 2015. Cdc42 mediates Bmp-Induced sprouting angiogenesis through Fmnl3-driven assembly of endothelial filopodia in zebrafish. Dev. Cell 32, 109–122.

Wang, K.C., Yeh, Y.T., Nguyen, P., Limqueco, E., Lopez, J., Thorossian, S., Guan, K.L., Li, Y.S.J., Chien, S., 2016. Flow-dependent YAP/TAZ activities regulate endothelial phenotypes and atherosclerosis. Proc. Natl. Acad. Sci. U. S. A. 113, 11525–11530.

Wang, L., Luo, J.-Y., Li, B., Tian, X.Y., Chen, L.-J., Huang, Yuhong, Liu, J., Deng, D., Lau, C.W., Wan, S., Ai, D., Mak, K.-L.K., Tong, K.K., Kwan, K.M., Wang, N., Chiu, J.-J., Zhu, Y., Huang, Yu, 2016. Integrin-YAP/TAZ-JNK cascade mediates atheroprotective effect of unidirectional shear flow. Nature 540, 579–582.

Wang, R.N., Green, J., Wang, Z., Deng, Y., Qiao, M., Peabody, M., Zhang, Q., Ye, J., Yan, Z., Denduluri, S., Idowu, O., Li, M., Shen, C., Hu, A., Haydon, R.C., Kang, R., Mok, J., Lee, M.J., Luu, H.L., Shi, L.L., 2014. Bone Morphogenetic Protein (BMP) signaling in development and human

diseases. Genes Dis. 1, 87–105.

Wang, Y., Kaiser, M.S., Larson, J.D., Nasevicius, A., Clark, K.J., Wadman, S.A., Roberg-perez, S.E., Ekker, S.C., Hackett, P.B., Mcgrail, M., Essner, J.J., 2010. Moesin1 and Ve-cadherin are required in endothelial cells during in vivo tubulogenesis. Development 137, 3119–3128.

Warboys, C.M., Amini, N., De Luca, A., Evans, P.C., 2011. The role of blood flow in determining the sites of atherosclerotic plaques. F1000 Med. Rep. 3, 1–8.

Weijts, B., Gutierrez, E., Saikin, S.K., Ablooglu, A.J., Traver, D., Groisman, A., Tkachenko, E., Jolla, L., Jolla, L., Jolla, L., 2016. Blood flow directs arterial-venous remodeling through Notch activation and endothelial cell migration .

Whitesell, T.R., Kennedy, R.M., Carter, A.D., Rollins, E.L., Georgijevic, S., Santoro, M.M., Childs, S.J., 2014. An α-smooth muscle actin (acta2/αsma) zebrafish transgenic line marking vascular mural cells and visceral smooth muscle cells. PLoS One 9, 1–10.

Wild, R., Klems, A., Takamiya, M., Hayashi, Y., Strähle, U., Ando, K., 2017. Neuronal sFlt1 and Vegfaa determine venous sprouting and spinal cord vascularization. Nat. Commun. 8.

Wiley, D.M., Kim, J.-D., Hao, J., Hong, C.C., Bautch, V.L., Jin, S.-W., 2011. Distinct signalling pathways regulate sprouting angiogenesis from the dorsal aorta and the axial vein. Nat. Cell Biol. 13, 686–92.

Wilkinson, R.N., Koudijs, M.J., Patient, R.K., Ingham, P.W., Schulte-Merker, S., Van Eeden, F.J.M., 2012. Hedgehog signaling via a calcitonin receptor-like receptor can induce arterial differentiation independently of VEGF signaling in zebrafish. Blood 120, 477–488.

Wooderchak-Donahue, W.L., McDonald, J., O'Fallon, B., Upton, P.D., Li, W., Roman, B.L., Young, S., Plant, P., Fülöp, G.T., Langa, C., Morrell, N.W., Botella, L.M., Bernabeu, C., Stevenson, D.A., Runo, J.R., Bayrak-Toydemir, P., 2013. BMP9 mutations cause a vascular-anomaly syndrome with phenotypic overlap with hereditary hemorrhagic telangiectasia. Am. J. Hum. Genet. 93, 530–537.

Wozney, J.M., Rosen, V., Celeste, A.J., Mitsock, L.M., Whitters, M.J., Kriz, R.W., Hewick, R.M., Wang, E.A., 1988. Novel regulators of bone formation: Molecular clones and activities. Science (80-.). 242, 1525–1534.

Wu, R.S., Lam, I.I., Clay, H., Duong, D.N., Deo, R.C., Coughlin, S.R., 2018. A Rapid Method for Directed Gene Knockout for Screening in G0 Zebrafish. Dev. Cell 46, 112-125.e4.

Xu, C., Hasan, S.S., Schmidt, I., Rocha, S.F., Pitulescu, M.E., Bussmann, J., Meyen, D., Raz, E., Adams, R.H., Siekmann, A.F., 2014. Arteries are formed by vein-derived endothelial tip cells. Nat. Commun. 5.

Xu, J., Zhu, D., Sonoda, S., He, S., Spee, C., Ryan, S.J., Hinton, D.R., 2012. Over-expression of BMP4 inhibits experimental choroidal neovascularization by modulating VEGF and MMP-9. Angiogenesis 15,

213–227.

Yaniv, K., Isogai, S., Castranova, D., Dye, L., Hitomi, J., Weinstein, B.M., 2006. Live imaging of lymphatic development in the zebrafish. Nat. Med. 12, 711–716.

Yokota, Y., Nakajima, H., Wakayama, Y., Muto, A., Kawakami, K., Fukuhara, S., Mochizuki, N., 2015. Endothelial Ca2+ oscillations reflect VEGFR signaling-regulated angiogenic capacity in vivo. Elife 4, 1–26.

You, L., Lin, F., Lee, C.T., Demayo, F.J., 2005. Suppression of Notch signalling by the COUP-TFII transcription factor regulates vein identity. Nature 435, 98–104.

Yu, J.A., Castranova, D., Pham, V.N., Weinstein, B.M., 2015. Single-cell analysis of endothelial morphogenesis in vivo. Development 142, 2951–2961.

Yurdagul, A., Finney, A., Woolard, M.D., Orr, A.W., 2016. The Arterial Microenvironment: The Where and Why of Atherosclerosis. Biochem. J 473, 1281–1295.

Zahra, F.T., Sajib, M.S., Ichiyama, Y., Akwii, R.G., Tullar, P.E., Cobos, C., Minchew, S.A., Doçi, C.L., Zheng, Y., Kubota, Y., Gutkind, J.S., Mikelis, C.M., 2019. Endothelial RhoA GTPase is essential for in vitro endothelial functions but dispensable for physiological in vivo angiogenesis. Sci. Rep. 9, 1–15.

Zanin, R., Pegoraro, S., Ros, G., Ciani, Y., Piazza, S., Bossi, F., Bulla, R., Zennaro, C., Tonon, F., Lazarevic, D., Stupka, E., Sgarra, R., Manfioletti, G., 2019. HMGA1 promotes breast cancer angiogenesis supporting the stability, nuclear localization and transcriptional activity of FOXM1. J. Exp. Clin. Cancer Res. 38, 1–23.

Zeng, G., Taylor, S.M., McColm, J.R., Kappas, N.C., Kearney, J.B., Williams, L.H., Hartnett, M.E., Bautch, V.L., 2007. Orientation of endothelial cell division is regulated by VEGF signaling during blood vessel formation. Blood 109, 1345–1352.

Zhang, J., Gao, B., Zhang, W., Qian, Z., Xiang, Y., 2018. Monitoring antiangiogenesis of bevacizumab in zebrafish. Drug Des. Devel. Ther. 12, 2423–2430.

Zhang, Y., Liu, J., Tian, X.Y., Wong, W.T., Chen, Y., Wang, L., Luo, J., Cheang, W.S., Lau, C.W., Kwan, K.M., Wang, N., Yao, X., Huang, Y., 2014. Inhibition of bone morphogenic protein 4 restores endothelial function in db/db diabetic mice. Arterioscler. Thromb. Vasc. Biol. 34, 152–159.

Zhang, Y., Xu, B., Chen, Q., Yan, Y., Du, J., Du, X., 2018. Apoptosis of Endothelial Cells Contributes to Brain Vessel Pruning of Zebrafish During Development. Front. Mol. Neurosci. 11, 222.

Zhang, Y.E., 2009. Non-Smad pathways in TGF-β signaling. Cell Res. 19, 128–139.

Zhong, T.P., Rosenberg, M., Mohideen, M.-A.P.K., Weinstein, B.,

Fishman, M.C., 2000. gridlock, an HLH gene required for assembly of the aorta in zebrafish. Science (80-.). 287, 1820–1824.

Zhou, J., Lee, P., Tsai, C., Lee, C., Yang, T., Chuang, H., Lin, W., Ting-Er, L., Seh Hong, L., Shu-Yi, W., Yuh-LIen, C., Shu, C., Jeng-Jiann, C., 2012. Force-specific activation of Smad1/5 regulates vascular endothelial cell cycle progression in response to disturbed flow. PNAS 109, 7770–7775.

Zhou, Q., Heinke, J., Vargas, A., Winnik, S., Krauss, T., Bode, C., Patterson, C., Moser, M., 2007. ERK signaling is a central regulator for BMP-4 dependent capillary sprouting. Cardiovasc. Res. 76, 390–399.

Zhou, Q., Perovic, T., Fechner, I., Edgar, L.T., Hoskins, P.R., Gerhardt, H., Krüger, T., Bernabeu, M.O., 2020. Association between erythrocyte dynamics and vessel remodelling in developmental vascular networks. bioRxiv.